University of Nottingham
UK | CHINA | MALAYSIA

Exploring the Potential Role of Endothelial ZEB1 in Developmental and Pathological Angiogenesis

Kathryn Rebecca Green BSc MRes

A thesis submitted to the University of Nottingham
for the degree of Doctor of Philosophy (PhD)

Supervisors: Dr. Andrew V Benest, Prof. David O Bates
& Dr. Alan McIntyre

May 2025

Abstract

Angiogenesis, the process by which new blood vessels are generated from the pre-existing vasculature, relies on morphological changes in the endothelial cells (ECs) that line all blood vessels, termed the vascular endothelium. During development, angiogenesis is crucial to accommodate tissue growth; however, post-development, the endothelium exists within a quiescent state characterized by limited proliferation, reduced metabolism, and controlled permeability. This transition between angiogenesis and quiescence is tightly regulated to ensure efficient vascular development and subsequent homeostasis. Dysregulation of this process is implicated in multiple diseases, so understanding the transcriptional mechanisms behind these processes is important.

Recent work suggests that transcription factors involved in epithelial-to-mesenchymal transition (EMT) may play a role in the regulation of phenotypic switching within the endothelium. Among these transcription factors, ZEB1, which functions as both a transcriptional repressor and activator, has been identified as a potential regulator of the switch between quiescence and angiogenesis. This thesis investigates the potential role of endothelial ZEB1, through in vitro assays and transcriptomic analysis, in combination with in vivo models of developmental angiogenesis, as well as models of pathological angiogenesis and vascular disease.

Unlike other EMT transcription factors, ZEB1 expression was found to be enriched within confluent ECs. RNA-Seq analysis identified differentially expressed genes resulting from ZEB1 knockdown, which, alongside ZEB1 ChIP-Seq, revealed genes that are directly bound and regulated by ZEB1. Further analysis of these genes identified enriched biological processes such as cell adhesion and response to inflammation. In vivo, the loss of endothelial ZEB1 during developmental angiogenesis resulted in reduced progression of the angiogenic front and alterations in vascular network structure. In a pathological model of wet age-related macular degeneration, however, loss of endothelial ZEB1 caused an increase in neovascular lesion size and leakage. In a peripheral artery disease model, endothelial ZEB1 knockout had no impact on blood flow recovery but did lead to alternative vessel remodeling in both ischemic and non-ischemic limbs. In summary, these findings indicate that loss of endothelial ZEB1 impacts vascular development and disease.

This research therefore suggests that ZEB1 plays a role in the regulation of the quiescent-angiogenic switch

Acknowledgments

Firstly, I would like to thank my supervisors, Andy, Dave and Alan for their support, advice, and guidance throughout my project. Andy, thank you for your contribution, guidance and insights into my doctoral journey which allowed me to grow as a researcher. Thank you also for allowing me to have the opportunity to complete and present research at international conferences across the world.

I am thankful to everyone within TVBL for being such lovely and inspiring people who I am grateful to have met, presented to and worked alongside. I would like to express my gratitude to Dr. Kenton Arkil, Professor Lucy Donaldson, and Dr. Dan Booth for their invaluable advice during lab meetings. Thank you also to the BBSRC DTP team, for their guidance and support, with special thanks to Sandra for all your help.

To my lab mates, past and present, Zarah, Joe, Nada, Charles, Jade and Nick, thank you for everything. You are all so incredibly talented and it has been a pleasure to work with you. Special thanks to Dr Nick Beazley-Long for your guidance and encouragement, especially during my first BSU studies. I am very grateful for the mentorship and advice during the early phases of my PhD. A big thanks to Joe for all your help understanding and preparing the RNA and ChIP-Seq data with such patience and clarity; especially dealing with the repetitive basic questions such as 'so what is a Log2 fold change again!?'. Nada, your dedication is inspiring, I am so glad to see you believe in yourself more and more every day. And Zarah, thank you for being such a great friend during this entire PhD journey, from the late-night confocal help to eye dissections, along with endless cups of tea and sitting outside A floor showers whilst I stunk of BME. The experience would not have been the same without you and I am grateful we were in this together.

Special thanks to Dr Joanna Kalucka for allowing me to work within her lab at Aarhus University, and to BMVBS for the funding. My gratitude is extended to the entire lab for the warmest of welcomes, the best 26th birthday, as well as for all their technical expertise, scientific knowledge and never-ending supply of bread and cake. Dr Julie Christensen, thank you for your help setting up the CRISPR experiments, and Olivia thank you for your

help with everything, including the 80+ plates of 1000s of spheroids. The experience was beyond amazing. And to Ibrahim, Olivia and Joe, for taking me out dancing! Mange Tak!

To all my friends and colleagues in the BDI and beyond, I cannot thank you enough. Zarah, Eva, Pippa, Grace, Michaela and George, please know my liver may never recover from the hours spent in another, and my dignity may be lost forever in the karaoke booths, but the memories I will cherish always. Thank you all so much for your encouragement and support with any science-related question I threw at you, along with all the frequent Portland trips. You're all excellent scientists and wonderful friends.

I'd also like to thank all my friends and family outside of science for their never-ending support, and for putting up with my endless science focused conversations. To my UoB friends for all the podcast length voice notes and to my friends back home for the hours spent in the pub explaining why an experiment hasn't worked, again. I am grateful to always have you guys in my corner, cheering me on in whatever I do. I would not have been able to keep myself grounded if it was not for you all. And special thanks to my wonderful colleagues at Helios Medical Communications, notably Sim, Kathryn, Tess and Leah, for all your support, belief and encouragement.

A huge thank you to my Mum and Dad, for their constant love and always believing in me. Dad, thank you for all your encouragement, as well as your help with basic chemistry questions. Mum, thank you for always being there for me, providing me with plenty of tea, cake, gin and wine. To my entire family, my brothers, aunts, uncles, cousins, as well as my gained family, Caroline, Steve, Emily, Tim and Isaac, thank you for always being interested and supportive. A special thanks to my Auntie Betty and Uncle Geoff, for letting me live with them during my PIP, and completely spoiling me with home cooked meals and packed lunches.

Finally, to Elliott, I cannot thank you enough for all your love, support and understanding during this experience. Thank you for all the weekend trips to weigh mice (often twice), the late nights, long days, always listening to me, looking after me and for keeping me smiling. Thank you for always being by my side and always believing in me.

Publications, Presentations, Grants and Awards

Publications

Green KR, Beazley-Long N, Lynch AP, Allen CL, Bates DO, Benest AV. Quantification of Angiogenesis in Laser Choroidal Neovascularization. Methods Mol Biol. 2022;2441:223-231.

Tabrizi ZB, **Green KR**, Lynch AP, Ahmed NS, Beazley-Long N, Benest AV. Simple Gene Knockdown in Endothelial Cells Using Short Interfering RNA Oligonucleotides. Methods Mol Biol. 2022;2441:251-255.

Presentations and Abstracts

Center of Membrane Proteins and Receptors (COMPARE) University of Nottingham and University of Birmingham Early Career Researcher (ECR) symposium 2021 – Invited speaker – 'Exploring the role of endothelial ZEB1 in a mouse model of Age-related Macular Degeneration'.

Joint British Microvascular and Vascular Biology Society (BMVBS) and German Society for Microcirculation and Vascular Biology (GfMVB) in Berlin, Germany 2022 – Abstract and Poster Presentation – 'Loss of endothelial ZEB1 results in increased choroidal neovascularization without an increase in inflammation'.

International Vascular Biology meeting in Oakland, CA 2022 – Abstract and Poster Presentation – 'ZEB1 is involved in the maintenance of endothelial quiescence'.

73rd Annual Conference of the BMVBS in Edinburgh, Scotland 2023 – Abstract and Oral Presentation – 'Knockout of endothelial ZEB1 results in inefficient developmental angiogenesis and reduced vessel sprouting'.

Grants

- BBSRC *in vivo* support funding (£2000)
- BMVBS Student Assistance Scheme (SAS), 2022
- University of Nottingham School of Medicine Support Grant
- Researcher Academy Conference Travel and Training Fund
- BMVBS SAS, 2023
- BMVBS Laboratory Travel Grant – to complete research at Aarhus University

Awards

- School of Medicine Impact Forum – 3rd place poster prize
- School of Medicine Sue Watson Event – 2nd place oral presentation prize
- UoN Tri-campus award for Commitment to Enhancing Research Culture and Environment 2023 – Team award as Chair of the ECR Society

Declarations

I, Kathryn Rebecca Green, confirm that the work presented in this thesis was carried out in accordance with the requirements of the University's Regulations and Codes of Practice for Research Degree Programs and that is has not been submitted for any other academic award. I confirm that the work demonstrated in this thesis are my own. Where information has been derived from other sources, I confirm this has been indicated in the thesis.

SIGNED……..

DATE……13.05.25……..

Abbreviations

α-SMA – α Smooth Muscle Actin

AMD – Age-Related Macular Degeneration

ANOVA – Analysis of Variance

Ang – Angiopoietin

ATP – Adenosine Triphosphate

BCA – Bicinchoninic Acid

BBB – Blood Brain Barrier

BMP – Bone Morphogenetic Protein

BSA – Bovine Serum Albumin

cDNA – Copy DNA

CD – Cluster of Differentiation

CDC42 – Cell Division Control Protein 42

ChIP – Chromatin Immunoprecipitation

CNV – Choroidal Neovascularization

CoIP – Co-Immunoprecipitation

CRISPR – Clustered Regularly Interspaced Short Palindrome Repeats

CtBP – C Terminal Binding Protein

CXCL – Chemokine (C-X-C motif) Ligand

CXCR – Chemokine (C-X-C motif) Receptor

DAPI – 4',6-Diamidino-2-phenylindole

DEG – Differentially Expressed Gene

DNA – Deoxyribonucleic Acid

DLL4 – Delta-like Canonical Notch Ligand 4

DR – Diabetic Retinopathy

ECs – Endothelial Cells

ECM – Extracellular Matrix

E-CAD – Epithelial Cadherin

EMT – Epithelial to Mesenchymal Transition

EndoMT – Endothelial to Mesenchymal Transition

EPCAM – Epithelial Cell Adhesion Molecule

ERG – ETS Related Gene

ERK – Extracellular Signal-Related Kinase

ETS – Erythroblast Transformation Specific

FGF – Fibroblast Growth Factor

FGFR – FGF Receptor

FFA – Fundus Fluorescein Angiography

FITC – Fluorescein Isothiocyanate

FOX – Forkhead Box

GAPDH – Glyceraldehyde-3-Phosphate Dehydrogenase

GO – Gene Ontology

HIF – Hypoxia Inducible Factor

HLI – Hind Limb Ischemia

HUVECs – Human Umbilical Vein Endothelial Cells

IGF – Insulin Growth Factor

IGFR – IGF Receptor

ICAM – Intracellular Adhesion Molecule

IFN – Interferon

iECKO – Inducible Endothelial Cell Knockout

i.p. – Intraperitoneal

KLF – Krüppel-Like Factor

KD – Knockdown

KEGG – Kyoto Encyclopedia of Genes and Genomes

KO – Knockout

LAMC2 – Laminin Subunit Gamma 2

MACS – Magnetic Activated Cell Sorting

miRNA – Micro RNA

MMPs – Matrix Metalloproteases

mRNA – Messenger RNA

MTT – 3-(4,5-Dimethylthiazol-2-yl)-2,5-diphenyl Tetrazolium Bromide

NOS – Nitric Oxide Synthase

NR2F2 – Nuclear Receptor Subfamily 2 Group F Member 2

Nrp – Neuropilin

NSC – Non Silencing Control

Ns – Not Significant

OCT – Optimal Cutting Temperature Compound

ORA – Over Representation Analysis

OXPHOS – Oxidative Phosphorylation

PAD – Peripheral Artery Disease

P1 – Postnatal Day 1

PFA – Paraformaldehyde

PBS – Phosphate Buffered Saline

PBS-X – PBS with Triton-X

PCR – Polymerase Chain Reaction

PECAM – Platelet and Endothelial Cell Adhesion Molecule

PHDs – Prolyl Hydroxylase Domain

PlGF – Placenta Growth Factor

PDGF – Platelet-Derived Growth Factor

PDGFR – Platelet-Derived Growth Factor Receptor

PMSF – Phenylmethylsulfonylfluoride

PPAP – Phosphofructokinase-2/fructose-2,6-bisphosphatase 3

RIPA – Radioimmunoprecipitation Assay Buffer

RNA – Ribonucleic Acid

ROCK – Rho Associated Coiled-Coil Containing Protein Kinase

ROS – Reactive Oxygen Species

Seq – Sequencing

shRNA – Small Hairpin RNA

siRNA – Short Interfering RNA

SRSF – Serine and Arginine Rich Splicing Factor

SRPK – SRSF Protein Kinase

TGF-β – Transforming Growth Factor β

TGFβR2 – TGFβ Receptor 2

TBST – TBS with Tween-20

TNF-α – Tumor Necrosis Factor α

VCAD – Vascular Endothelial Cadherin

VEGF – Vascular Endothelial Growth Factor

VEGFR – VEGF Receptor

VE-PTP – Vascular Endothelial Protein Tyrosine Phosphatase

VPF – Vascular Permeability Factor

vSMCs – Vascular Smooth Muscle Cells

vWF – von Willebrand Factor

Wnt – Wingless-Related Integration Site

WT – Wild Type

YAP – Yes1 Associated Transcriptional Regulator

ZEB1 – Zinc Finger E-box Binding Homeobox 1

Contents

List of figures:

List of tables:

Chapter 1:

Introduction

1 Introduction

1.1 The Vasculature

Blood vessels are essential for the transport of cells, solutes and gasses throughout the body. The mature vasculature is a closed tubular system of branched hierarchical vessels that form a network consisting of capillaries, arteries, arterioles, veins and venules (Figure 1.1). Arteries and arterioles travel away from the heart, delivering blood into capillary networks within organs and tissues. Venules and subsequent veins then collect the blood from the capillary beds to be returned to the heart, whereas lymphatic system returns excessive fluid from the capillary network back into circulation (Adams & Alitalo, 2007). In order to constantly support and supply the demands of the tissue, the vasculature remains dynamic, both in terms of its function but also the phenotype of its component cells. The importance of a functional vascular network that has the ability to respond to stimuli is evident due to the extensive variety of diseases that occur as result of flaws in the vasculature (Carmeliet, 2003).

1.1.1 Structure and function of the endothelium

Although blood vessels vary in their properties, they all contain a lumen lined by a monolayer of endothelial cells, termed the vascular endothelium (Galley & Webster, 2004). Endothelial cells (ECs) are polarised so that different regions of the cell membrane interact with different environments. The abluminal region of the cell interacts with the basement membrane, a highly structured extracellular matrix composed of proteoglycans, proteins and glycoproteins (Leclech et al., 2021). Whereas at the opposite pole, the luminal side is coated in a specialised glycocalyx and interacts directly with the contents of the vessel (Pries et al., 2000). The endothelium establishes a selective barrier between the tissue and the contents of the blood. Key components of this barrier include adherens junctions and tight junctions, both of which are important for maintaining specific vessel properties and vascular homeostasis.

Adherens junctions are formed by transmembrane proteins called cadherins. Vascular endothelial cadherin (VE-cadherin), a primary component of these adherens junctions, form calcium dependent, homophilic interactions between endothelial cells. The

intracellular component of VE-cadherin interacts with other proteins such as β-catenin, which in turn interact with the cytoskeleton (Claesson-Welsh et al., 2021). In response to permeability factors, VE-cadherin can be phosphorylated, regulating the structure of these adherens junctions and therefore the permeability of the vessel (Orsenigo et al., 2012). Tight junctions instead are composed of claudins, JAMs and occludins which exist in complexes with intracellular scaffolding proteins. The composition and abundance of these tight junction complexes influences the barrier tightness and permeability (Claesson-Welsh et al., 2021). Changes in both junction types are coordinated to ensure vascular homeostasis is maintained (Taddei et al., 2008; Tornavaca et al., 2015).

The endothelium is heterogeneous across different vascular beds within different organs and tissues. This refers to the large variation and diversity of molecular characteristics between ECs depending on their environmental context and requirements (Aird, 2007). A clear illustration of this would be the variations between tissues with distinctly different functions. For example, the endothelium within the brain forms a specialised blood brain barrier (BBB) that lines cerebral blood vessels. This is an essential protective barrier that strictly regulates the passage of substances between the contents of the blood and cellular components of the brain, crucially regulating the diffusion of ions and nutrients whilst restricting the passage of potentially harmful molecules (Daneman & Prat, 2015). Structurally the endothelium within the BBB therefore has high expression of junction and barrier proteins such as JAMs, Occludins, Claudins and Cadherins, along with a vast network of support cells such as pericytes (Kadry et al., 2020). Whereas the endothelium within the glomerulus of the kidney has different functions, whereby they form a crucial component of the renal filtration barrier. These endothelial cells display unique characteristics such as fenestrations and a specialised glycocalyx which facilitate the filtration process (Fogo & Kon, 2010). These two contrasting examples highlight the tissue specific characteristics of the endothelium, and the importance of these characteristics for the function of the entire organ. Hence, endothelium heterogeneity and functionality is a crucial part of all aspects of physiology.

What was first simply labelled as either veins or arteries by Hippocrates has now drastically expanded to the heterogenous system that is known today (Aird, 2007). Within

the last decade, advances in single cell transcriptomics have provided in-depth information surrounding the inventory of endothelial cells within specific organ systems, as well as in health and disease. Kalucka et al published the first murine endothelial cell transcriptomic atlas, which further revolutionised the way endothelial heterogeneity was understood. This atlas not only identified heterogeneity between organs, but also intra-tissue heterogeneity within organs, identifying multiple endothelial subtypes with distinct transcriptomic profiles and characteristics which translate to organ function. This work includes findings such as the specific expression of vascular barrier integrity genes within gut and small intestine ECs, which agree with previous reports that highlight their importance within the blood-gut barrier (Kalucka et al., 2020; Spadoni et al., 2015). As well as this, specific EC subclusters were identified within vascular beds, such as the lung which had separate artery, vein and lymphatics EC clusters, along with two distinct capillary clusters, which demonstrated the large amount of heterogeneity even within organs (Kalucka et al., 2020). The same single cell transcriptomics analysis has been applied to a multitude of diseases and morbidities including cancer (Zhang et al., 2023) and obesity (Bondareva et al., 2022), which have all identified distinct changes in endothelial transcriptomic profile, with multiple subtypes of diseased endothelial cells contributing to the pathology (Becker et al., 2023). Hence, a deeper comprehension of the endothelium holds significant importance for both normal physiological development and the advancement of pathological diseases, ultimately leading to enhanced approaches in disease treatment.

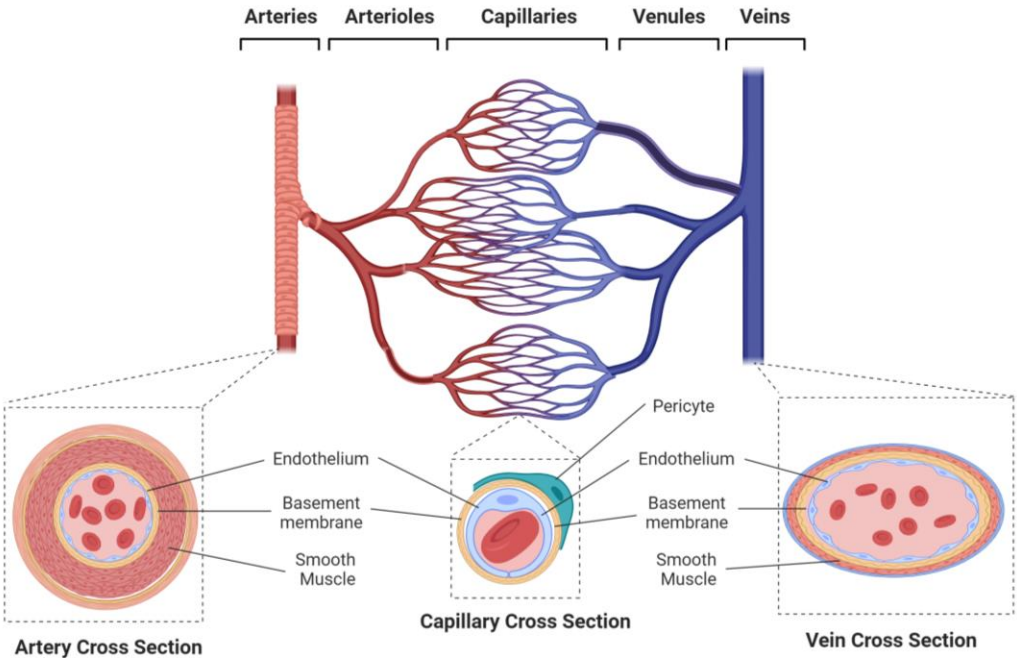

Figure 1.1 Schematic of the vascular system. *The vascular system is a hierarchical network of arteries, arterioles, capillaries, venules and veins. Arteries carry blood away from the heart towards capillary beds which are the primary site of gaseous and nutrient exchange, with veins carrying blood back to the heart. All vessels are lined by endothelial cells, hence termed the endothelium, which lies on a basement membrane. Pericytes coat capillaries whereas larger vessels are coated in smooth muscle cells. Created with biorender.*

1.1.2 Vasculogenesis

During early embryonic development, the first endothelial cells, and hence blood vessels, are formed *de novo* via a process termed vasculogenesis. In this process, endothelial progenitor cells known as angioblasts, migrate and associate into clusters to form blood islands that surround haematopoietic precursors which will eventually differentiate into components of the blood. This process of blood island formation drives the creation of the primitive vascular network. The remodelling of this network along with the differentiation and recruitment of mural support cells occurs gradually until a hierarchical network is generated containing arteries, veins and capilaries (Risau & Flamme, 1995).

1.1.3 Angiogenesis

Once vasculogenesis has generated the initial plexus, the expansion of the network occurs as a result of angiogenesis. Angiogenesis is that process in which new blood vessels are generated from the pre-existing vasculature (Carmeliet, 2003). Angiogenesis is essential in development and growth as the vasculature is required to expand to meet the needs of the growing tissue. However, it is also important post-development in processes such as wound healing and exercise (DiPietro, 2016; Ross et al., 2023). Much of the early research into angiogenesis was focused on tumours after Judah Folkman proposed tumour angiogenesis as a targetable process in treatment of cancers (Folkman, 1971). Since then, the process of angiogenesis has been well researched is now understood to be a highly coordinated series of events that can vary depending on the context of angiogenic initiation (Eelen et al., 2020; Liu et al., 2023).

Broadly, angiogenesis can be split into two major types: sprouting angiogenesis and intussusceptive angiogenesis. The initial reports of angiogenic sprouts were seen in embryological development studies. Early microscopy studies within the tail of frog larva revealed blood vessels sent out sprouts from already present vessels (Clark, 1918), and later in avian studies, angiogenic tip cells were first defined (Kurz et al., 1996). Continued research allowed for these tip cells to be further characterised in the angiogenic vessels within the developing mouse retina. This study described tip cells as specialised migratory endothelial cells defined by actin filopodia extension (Gerhardt et al., 2003; Ruhrberg et al., 2002) s. Whereas, intussusceptive angiogenesis was characterized in studies of the developing rat lung, where small holes within the vasculature were observed instead of capillary sprouts. These holes lead to the expansion of the network by driving capillary replication and remodeling (Caduff et al., 1986).

The process of sprouting angiogenesis has been well defined to occur through multiple steps (Figure 1.2). The initiation of angiogenesis is a result of the release of pro-angiogenic signaling molecules which act upon the endothelium. The stimulated endothelial cells then begin to change morphology, becoming more motile and invasive (Eilken & Adams, 2010). A sprout is then formed from existing vessels, which branch outwards towards the location of the stimulus. These branches form a lumen and eventually connect in a process

termed anastomosis, allowing blood flow through the nascent vessel (Potente et al., 2011). Generally, the term angiogenesis is used to describe neovascularization in the microvasculature and capillaries. Whereas the term arteriogenesis describes the collateral formation of larger arteriole vessels as a result of an occlusion to the blood supply (Scholz et al., 2001). Arteriolargenesis is where these microvessels are converted into muscle coated micro vessels by the recruitment of smooth muscle cells (Benest et al., 2008).

1.1.4 Pro-angiogenic signalling mechanisms

1.1.4.1 VEGF

The stimulation of angiogenesis requires an increase in pro-angiogenic cytokines and stimuli. The most well studied of these is Vascular Endothelial Growth Factor A (VEGF-A). VEGF was initially identified as Vascular Permeability Factor (VPF) in the research of tumours in 1983. Senger et al classified this secreted protein as VPF due to its ability to increase the vascular permeability of tumour associated blood vessels (Senger et al., 1983). Not long after, another group identified and purified a novel growth factor specific for its mitogenic effect on endothelial cells, hence terming it VEGF (Ferrara & Henzel, 1989). Purification and subsequent protein sequancing of Sengers VPF confirmed that VPF and VEGF were in fact the same protein and hence VEGF was understood to be a potent angiogenic and vascular permeability associated cytokine (Senger et al., 1990).

Further work has identified multiple members of the VEGF family of growth factors, VEGF-A, VEGF-B (Olofsson et al., 1996), VEGF-C (Joukov et al., 1996), VEGF-D (Achen et al., 1998), VEGF-E (viral VEGF) (Meyer et al., 1999), and Placenta growth factor (PlGF) (Maglione et al., 1991). The other VEGF family members have proven to have a variety of distinctive roles, with VEGF-B implicated in early embryogenesis and development, and VEGF-C and D involved in regulating lymphangiogenesis (Ferrara et al., 2003; Shibuya, 2006). VEGF molecules act by binding to VEGF receptors (VEGFR), which are classical receptor tyrosine kinases expressed on the surface of ECs. Likewise, to VEGF, there are multiple VEGFRs; VEGFR1 (also known as Flt-1) and VEGFR2 (also known as KDR) are primarily expressed on blood vascular endothelial cells (Shibuya, 2006). VEGFR3 is primarily expressed on lymphatic endothelial cells (Kaipatnen et al., 1995) and was once believed to be a receptor that is specific to lymphatic ECs; however, it has since been identified as being expressed

in blood ECs, specifically on tip and stalk cells during sprouting angiogenesis and vessel fusion (Tammela et al., 2008), suggesting its role is not purely associated with lymphatics.

Numerous isoforms of VEGF-A have been identified with varying bioavailability and function. The isoforms differ in length owing to alternative splicing and are designated VEGFxxx, where xxx represents the amino acid number within the protein sequence and hence, the protein size (Ferrara et al., 2003). $VEGF_{165}$ is the predominant isoform; it is secreted however a fraction remains bound to the cell surface and extracellular matrix (Park et al., 1993). The smaller $VEGF_{121}$ does not bind heparin and hence is a freely diffusible protein. Whereas the larger isoforms, such as $VEGF_{189}$ and $VEGF_{206}$ bind to heparin with high affinity, sequestering their location to the extracellular matrix (Ferrara et al., 2003; Houck et al., 1992). Another isoform of VEGF-A has been identified that arises from alternative splicing of exon 8, which was discovered by Bates et al. This isoform, designated VEGF-A_{xxx}b, was shown to have anti-angiogenic properties comparison to its pro-angiogenic alternative splice variant, VEGF-A_{xxx}a (Bates et al., 2002). This highlights how alternative splicing can not only affect the bioavailability of VEGF, but also regulate its pro-angiogenic activity.

VEGF-A specifically binds to VEGFR1 and VEGFR2 but can also bind to neuropilin family members and heparan sulfate proteoglycans (HSPGs), both of which are able to modulate signal transduction activity and hence are known as co-receptors (Simons et al., 2016). VEGFR1 has a greater affinity for VEGF-A, around 10 times greater than VEGFR-2; however, the tyrosine kinase activity was observed to be 10-fold higher in VEGF-A binding to VEGFR2, compared to VEGFR1 (Sawano et al., 1996). VEGFR1 knockout mice are embryonic lethal at around embryonic day 8.5 owing to an overgrowth of vascular endothelial cells, resulting in disorganised vessels, generating an inadequate vascular network (Fong et al., 1995). This formation of a disordered network as a response to VEGFR1 KO suggested VEGFR1 may have roles in the regulation of VEGFR2-driven angiogenesis, specifically within embryo vascular development. This hypothesis was supported by the fact VEGFR2 KO mice in contrast display no formation of blood vessels and subsequently die around embryonic day 9 (Sakurai et al., 2005). Taken together, these two studies suggest opposing roles for these two receptors in order to generate a

structured blood vessel network. Interestingly, mice lacking the intracellular kinase domain of VEGFR1 had no observed phenotype which provided strong evidence that VEGFR1s role in regulating angiogenesis and vessel formation is independent of its tyrosine kinase activity (Hiratsuka et al., 1998) . This therefore describes a system by which VEGFR1 regulates angiogenesis by competing with VEGFR2 in binding VEGF-A. Further to this, VEGFR1 has been identified as having a soluble isoform which when expressed acts to inhibit angiogenesis by sequestering available VEGF-A (Kendall & Thomas, 1993; Shibuya, 2006). This information together indicates that the activation of VEGFR2 is the primary driver of angiogenic signaling within ECs, whereas VEGFR1 plays a regulatory role.

Within fully developed adults VEGFR3 is commonly restricted to the lymphatic endothelium, however during development it is present on all endothelial cells. Deletion or inhibition of VEGFR3 resulted in decreased angiogenic sprouting, branching and proliferation within the mouse retinal microvasculature. Not only this, activation of VEGFR3 was able to sustain angiogenesis during VEGFR2 inhibition (Tammela et al., 2008). This therefore suggests it is not only VEGFR2 that promotes angiogenesis signaling within ECs, but also VEGFR3. More recently a study was conducted by Karaman et al that investigated the interplay between VEGFR1, VEGFR2 and VEGFR3 in vascular development using endothelial specific knockout models, where the knockout was induced at different time points postnatally. This identified that the vascular regression caused by VEGFR2 KO was tissue specific, with only some vascular beds being affected, including the retina. This team therefore suggested that VEGFR1 and VEGFR3 alone could promote vessel survival. The team also identified that VEGFR3, although primarily expressed in lymphatic vessels, was able to attenuate VEGFR2 signaling on blood endothelial cells as well as promote EC survival when VEGFR2 was lost (Karaman et al., 2022). This research therefore highlights the dynamic interplay between VEGFR1 2 and 3, as well as organ specificity and developmental time points specifically.

1.1.4.2 FGF

Fibroblasts growth factors (FGF) have also been identified in the initiation and regulation of angiogenesis. Basic FGF (bFGF, also known as FGF-2) was initially identified as a proangiogenic factor capable of stimulating endothelial cells in an autocrine and paracrine

fashion (Montesano et al., 1986). Upon stimulation of endothelial cells, bFGF was capable of inducing both proliferation and migration, along with the expression of growth factors and proteases that promote angiogenesis (Seghezzi et al., 1998). Due to its pro-angiogenic role, much of the research on bFGF has focused on its inhibition as a form of anti-angiogenic therapy. However more recently, bFGF was identified as a modulator for VEGFR1 splicing in endothelial cells via the activation of spliceosome constituents SRSF1/SRPK1 (Jia et al., 2021). This finding provided a link between bFGF and VEGFR signalling within angiogenesis.

1.1.4.3 CXCR4/CXCL12

Although chemokines have diverse roles in inflammatory processes, there have been distinct roles for chemokines identified in angiogenesis. A noteworthy example is the chemokine receptor CXCR4 and its ligand CXCL12. Microarray analysis of tip cells to identify tip cell associated genes identified CXCR4 as having enriched expression within EC tip cells (Strasser et al., 2010). CXCR4 was also observed to be expressed in developing vascular endothelial cells as mice lacking CXCR4 die *in utero* due to defective vascular development (Tachibana et al., 1998). This phenotype was replicated in endothelial specific CXCR4 KO mice (Ara et al., 2005), highlighting the endothelial specific activity of CXCR4. Inhibition of CXCR4 *in vivo* using inhibitors or anti-CXCR4 antibodies resulted in a dramatic change in tip cell morphology and patterning, along with a reduction in vascular density and a reduction in filopodia number (Strasser et al., 2010). These results therefore suggest that CXCR4 mediates tip cell morphology and branching in sprouting angiogenesis.

1.1.5 Regulation of angiogenic processes

1.1.5.1 Tip Cell Selection

During development and growth, expanding tissues must generate a vascular network to ensure a sufficient supply of oxygen. As the tissue expands, hypoxia occurs within the tissue, triggering hypoxia signaling which activates transcription factors such as hypoxia-inducible factors (HIF). In normal oxygen conditions prolyl hydroxylase (PHD) enzymes hydroxylate HIFs, which causes the binding of the von-Hippel-Lindau E3 ubiquitin ligase. This allows for the ubiquitination of HIF proteins, targeting them for degradation by the proteasome. However, in low oxygen conditions the enzymatic activity of PHDs is

inhibited, which as a result stabilizes HIF proteins. This allows them to activate hypoxic response genes, including pro-angiogenic factors for example VEGF-A which is activated by HIF-1α (Krock et al., 2011; Liu et al., 1995).

In the developing mouse retina, sprouting angiogenesis requires a gradient of pro-angiogenic cytokines such as VEGF, which are released by astrocytes within the growing avascular regions to guide tip cell migration (Gerhardt et al., 2003; Ruhrberg et al., 2002). This results in a tip cell being selected that begins to break away from the basement membrane and migrate outwards to initiate the formation of a sprout. Importantly, not all ECs react in the same way to this angiogenic stimulation, as this would result in severe disruption to the network. Instead, only the tip cells respond to VEGF-A by migrating towards the VEGF-A stimulus, whereas the stalk cells respond differently to VEGF-A via increased proliferation (Gerhardt et al., 2003).

This process of tip cell selection was assumed to be highly regulated. Although Gerhardt et al identified that tip and stalk cells responded differently to pro-angiogenic VEGF-A, it was not until a few years later that the Notch signalling to its Delta-like-4 (DLL4) ligand was identified as a mechanism of tip-stalk selection. In response to VEGF-A, it was determined that all ECs upregulated DLL4 expression, but tip cells appear to express significantly more DLL4 compared to stalk cells (Lobov et al., 2007). This higher expression of Dll4 activates Notch signaling in adjacent ECs which acts to inhibit the tip cell phenotype. Without this interaction between DLL4 on tip cells and Notch on stalk cells, an increase in tip cell number, EC proliferation and tip cell markers is observed within the developing mouse retina (Hellström et al., 2007; Suchting et al., 2007), indicative of unregulated tip cell/stalk selection. Conversely, the Notch ligand Jagged1 has been identified as having higher expression in stalk cells. Endothelial specific KO of Jagged1 within the developing mouse retina significantly reduced angiogenic sprouting, whereas overexpression significantly increased sprouting (Benedito et al., 2009). Therefore, this signaling between Notch and Jagged1 on stalk cells is observed as being regulatory of the stalk cell phenotype.

In 2010, Jakobsson et al linked this tip stalk regulation by Notch and Dll4 with the expression of VEGFR2 and VEGFR1, providing an explanation as to why these two EC

subtypes respond differently to VEGF-A. It has previously been noted that *in vitro*, DLL4 activation of Notch was observed to downregulate VEGFR2 and hence modulate the cellular response to VEGF-A (Williams et al., 2006). But by using computational modeling and mosaic spouting assays *in vivo*, it was determined that tip cells express significantly higher levels of VEGFR2 and lower levels of VEGFR1, in comparison to stalk cells (Jakobsson et al., 2010). The balance between pro-angiogenic VEGFR2 signaling and the angio-regulatory binding of VEGF-A to VEGFR1 is therefore able to manipulate the EC response to VEGF. This dynamic expression of VEGFR1 and 2 was observed to be regulated by active NOTCH signaling within stalk cells, and time lapse microscopy identified that shuffling of tip and stalk phenotype occurs constantly (Jakobsson et al., 2010). Therefore, the Notch/DLL4 and Notch/Jagged 1 signaling between ECs is essential for the correct ratio of tip and stalk cells via the regulation of VEGFR2/VEGFR1 expression.

1.1.5.2 Breakdown of the extracellular matrix

In order for tip cells to migrate and the trailing stalk cells to proliferate, ECs must actively modulate their local environment. This primarily involves the breakdown of extracellular matrix (ECM) proteins and basement membrane so that ECs can freely migrate and proliferate to undergo angiogenesis (Eelen et al., 2020). The degradation of the basement membrane is mediated by matrix metalloproteases (MMPs) that are increased in expression and secreted by tip cells. VEGF-A stimulation of ECs *in vitro* has been determined to increase the expression of multiple MMPs, including MMP-1, -3, -7, -8, -9, -10, -13 and -19. Although these proteases are thought to have varying roles, MMP-10 was identified as being a major regulator of EC migration, as knockdown of MMP-10 by siRNA inhibited VEGF induced migration *in vitro* and *in vivo* (Heo et al., 2010). *In vivo* studies have also highlighted the importance of MMPs in sprouting angiogenesis, with deletion of MMP-2 observed to reduce retinal angiogenesis in mice (Ohno-Matsui et al., 2003). Along with a passive role in modulating the external environment of ECs to allow for migration, MMPs play a more active role in angiogenesis as they are able to release pro-angiogenic cytokines that are sequestered within the ECM such as VEGF, bGFG and TGF-β (Wang & Khalil, 2018).

1.1.5.3 Tip Cell Guidance

A gradient of pro-angiogenic cytokines, including VEGF, is essential for tip cell guidance of the angiogenic sprout. Within the developing retina, the release of heparan sulphate bound VEGF-A_{165} from astrocytes of avascular regions serves as a chemo-attractive signal that induces EC activation and migration (Gerhardt et al., 2003; Ruhrberg et al., 2002). VEGF is able to trigger migratory behavior in tip cells via Cdc42 regulation of filopodia formation and Rac1 induction of lamellipodia (De Smet et al., 2009). But as for the actual guidance of this migration, ECs are observed to follow similar signaling pathways that axons display in the formation of neuronal networks such as the use of ROBO guidance receptors and Netrins (Potente et al., 2011). An identified mediator of tip cell guidance is Neuropilin-1 (Nrp-1), a transmembrane Semaphorin receptor which is also capable of binding VEGF-A. Nrp-1 knockout mice show no changes in EC proliferation but displayed irregular EC migration and tip guidance during sprouting. Using a model of angiogenesis in the neonatal hind brain, the team described the sprouts as 'blind-ended', as tip cells were unable to form an efficient vascular network due to the lack of sprout direction (Gerhardt et al., 2004). Interestingly, Phng et al identified that filopodia formation was not required for EC guidance, despite previous reports highlighting their importance in migration (Phng et al., 2013). The guidance of endothelial tip cells remains incompletely elucidated.

1.1.5.4 Lumen formation and anastomosis

The proliferation of stalk cells promotes the sprout extension but to form a functional vessel with blood flow the sprout is required to form a lumen and anastomose to create a closed network. In doing so, tip cells are required to lose their highly migratory phenotype, and stalk cells are required to reduce their level of proliferation. Instead, ECs form strong junctional connections to each other, regain apical-basal polarity and regenerate and attach to the basal lamina (Adams & Alitalo, 2007). Vessel anastomosis is the process in which two tip cells interact with each other to form a complete vessel. Macrophages have been identified as facilitators of this process by interacting with tip cells and their filopodia, however anastomosis can occur without the presence of macrophages, suggesting their role is purely facilitatory (Fantin et al., 2010). Live imaging techniques have also identified that multiple filopodia connections occur before the upregulation of

major cell adhesion molecules such as VE-Cadherin that allow the two ended vessels to fuse (Lenard et al., 2013).

A number of mechanisms of lumen formation have been proposed; these include wapping, budding, cavitation, cell hollowing, cord hollowing and membrane invagination (reviewed in Ghasemi Nasab et al 2022). Wrapping involves polarisation and elongation of ectodermal cells, wedge-shaped cell formation, and neural plate fusion. Budding involves polarised epithelial cells elongating and forming lumens through bud gyration. Cavitation forms lumens via apoptosis of inner cells in dense cell masses, driven by extracellular matrix signaling and loss of cell attachment. Cell hollowing generates intracellular lumens via vacuole fusion within single cells. Cord hollowing creates lumens between endothelial cells in cell cords without apoptosis. Finally, membrane invagination expands pre-formed lumens into neighboring cells (Ghasemi Nasab et al., 2022).

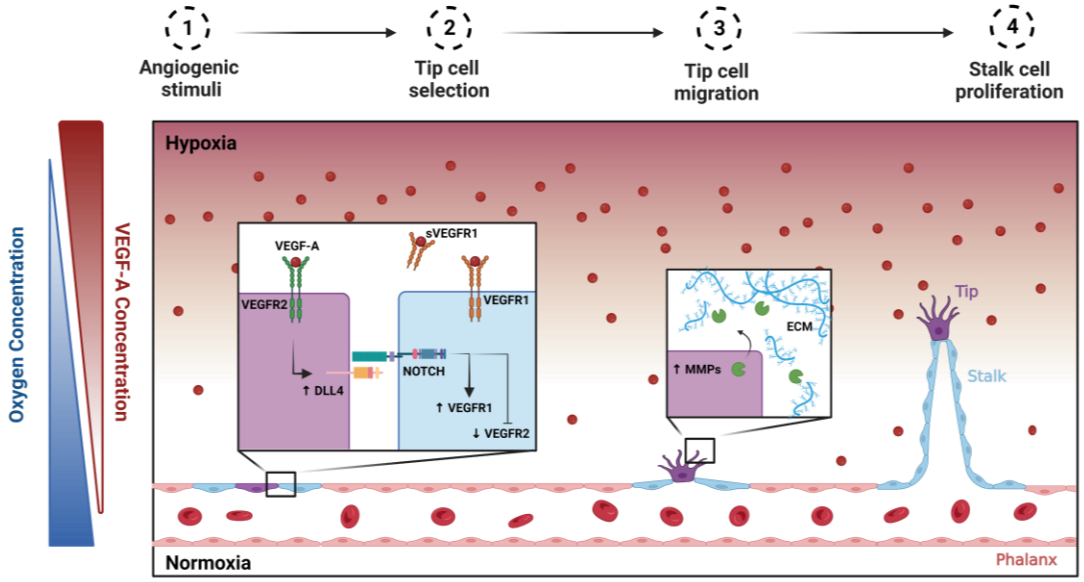

Figure 1.2 Schematic diagram of sprouting angiogenesis. *In low oxygen conditions hypoxia signalling tiggers the expression and release of pro-angiogenic signalling molecules such as VEGF-A. VEGF-A binds to VEGFR2 receptors on ECs which triggers the angiogenic process. Initially a tip cell is selected as a result of initial VEGFR2 activation inducing DLL4 expression and NOTCH activation on adjacent ECs. This NOTCH signalling triggers the upregulation of VEGFR1 and downregulation of VEGFR2 in stalk cells to modulate their response to VEGF-A. The tip cell releases MMPs to break down the ECM and migrates towards the higher concentrations of VEGF-A within the hypoxic stimulus. The stalk cells proliferate behind, creating an angiogenic sprout. Created with biorender. Created with biorender.*

1.1.6 Vessel Regression and Maturation

1.1.6.1 Mural Cell Recruitment

Nascent vessels are required to undergo phases of regression, remodelling and maturation in order to generate a plexus that efficiently meets the demand on the surrounding tissue. In the early stages of vessel maturation, ECs begin to recruit mural support cells such as pericytes and vascular smooth muscle cells (vSMCs) (Adams & Alitalo, 2007; Fruttiger, 2007). The secretion of Platelet Derived Growth Factor B (PDGFB) by maturing ECs acts on PDGF Receptor β (PDGFβ) on mural cells which initiates the recruitment to the maturing vasculature (Hellström et al., 1999). This communication between ECs and mural cells also occurs in the opposite direction, with mural cells releasing Ang1 which acts upon Tie2 receptor on endothelial cells (Suri et al., 1996).

Pericytes are support cells that are major components of the neuro vascular unit which connects components of the vascular system and nervous system; however they are also present within other non-neuronal regions of the vasculature. They were first identified by Rouget in 1874 (Rouget, 1874), in which he termed them Rouget cells, but later Zimmermann defined these vascular support cells as pericytes (Zimmermann, 1923). High resolution imaging along with pericyte labelling techniques have demonstrated that pericytes surround capillary ECs (Hartmann et al., 2015; Mizutani et al., 2022). The recruitment of pericytes by endothelial PDGFB has proven to be essential in blood vessel maturation, as PDGFB or PDGFRβ deficient mice leads to an absence of pericytes within the vasculature. Although no differences were observed in vessel density, length or branching, pericyte deficient mice had increased vascular leakage and endothelial hyperplasia causing defects in the overall vascular morphology of the blood brain barrier (Daneman et al., 2010; Hellström et al., 2001). Pericytes are thought to also play a role in regulating vascular contractility, however this is debated among the literature and likely context and tissue dependent (Fernández-Klett et al., 2010; Hill et al., 2015). Not only this, pericytes have also been identified as being sources of pro-survival signals for endothelial cells, with the ability to impact the cell cycle and angiogenic sprouting (Durham et al., 2014). Interestingly, Eiken et al demonstrated that pericytes express VEGFR1 which leads to the spatial restriction of VEGF signaling and therefore promotes endothelial sprouting

(Eilken et al., 2017). The role of pericytes is therefore diverse, from vessel maturation and stabilisation, but also regulation of angiogenic sprouting.

During vessel maturation, the network begins to form a hierarchy which requires the recruitment of vSMCs to larger vessels. Similarly to pericytes, these vSMCs wrap around nascent vessels however unlike pericytes, the basement membrane of ECM proteins separates ECs from vSMCs (Gaengel et al., 2009). The recruitment of vSMCs is an essential part of vascular development, with mutations that lead to a loss of this process resulting in early embryonic lethality. An example of which is the endothelial specific deletion of LKB1, which resulted in a loss of TGFβ mediated vSMC recruitment and lethality at E12.5 (Londesborough et al., 2008). It has also been demonstrated in mouse embryos that hemodynamic force regulates the recruitment of vSMCs, as reduced blood flow reduced the vSMCs recruitment. In reduced flow embryos, an increase in expression of Semaphorin3a, 3f and 3g was noted, along with a decrease in FOXC2 and HEY1, which could be involved in regulating the response to flow and hence vSMC recruitment (Padget et al., 2019). More recently, communication between ECs and vSMCs via extracellular vesicles (EVs) was identified, with miR-539 secreted by EC EVs and miR-582 secreted by vSMCs EVS, providing a further mechanism for EC to vSMC communication (Fontaine et al., 2022).

1.1.6.2 Vessel Regression and Pruning

The regression and remodelling phases of plexus generation require coordinated signalling between pro- and anti-angiogenic factors which result in the elimination of vessels, otherwise known as vessel pruning (Adams & Alitalo, 2007). This process has been extensively studied in the neonatal mouse retina, due to the fact the development of the vasculature occurs postnatally, and so different stages of vascular development can be observed. The retinal vasculature also goes through multiple phases of remodelling; the first being the regression of the hyaloid vessels that were present within the early development of eye, which are eventually replaced by the retinal vasculature. Whereas the second stage of regression occurs in order to prune the newly formed vascular network and generate a stable plexus (Fruttiger, 2007). Vessel stability has been observed to be controlled by numerous factors, including astrocyte derived VEGF, as astrocyte

specific deletion of VEGF resulted in vessel regression (Scott et al., 2010). Notch signalling has also been identified in the regulation of vessel stability in angiogenesis. The activation of DLL4/Notch in stalk cells induced expression of Nrarp (Notch-regulated ankyrin repeat protein) which promoted Wnt signalling via Lef1, and that loss of either Nrarp or Lef1 resulted in vessel regression (Phng et al., 2009). EC KO of Wnt secretion factor Evi was also found to induce vessel regression in both the neonatal retina and tumour angiogenesis (Korn et al., 2014). This research highlights the balance of multiple pro-survival signals in the generation of a new vascular network.

Vessel pruning can occur via either migration and re-localisation (Ishida et al., 2003), or selective apoptosis of endothelial cells (Hughes & Chan-Ling, 2000), with both of these processes aided by leukocytes. Apoptosis, a form of programmed cell death, occurs as a result of decreased EC survival factors, such as VEGF, and increased pro-apoptotic signals. Although originally believed to play a major role in vessel pruning, the exact role of apoptosis in angiogenesis and vascular plexus remodelling remains a topic of debate within the literature. Using EC specific deletion of apoptosis effector proteins BAK and BAX, Watson et al demonstrated that apoptosis is not required for vessel pruning, however it does remove non-perfused vessel segments. Apoptosis is also determined to influence EC number during angiogenesis and vessel maturation, which results in an increase in capillary diameter (Watson et al., 2016). Whereas within the hyaloid vasculature, apoptosis regulated by ANG2 is required for hyaloid vessel regression, a process which requires macrophages (Rao et al., 2007). Key proteins have been identified by transcriptomic analysis, such FGD5 as a novel driver of vascular pruning via angiogenesis, with loss and gain of function studies revealing FGD5 inhibits neovascularisation and promotes apoptosis induced vaso-obilteration via p53 (C. Cheng et al., 2012). Interestingly, endothelial specific loss of Caspase 8, a key mediator in apoptosis, results in reduced angiogenesis and EC proliferation, along with destabilisation of VE-cadherin and EC junctions (Tisch et al., 2019). This suggests that apoptosis factors may not only facilitate the pruning of the network but also the initial angiogenic generation of the vasculature. Therefore, the requirement for apoptosis within angiogenesis and vascular remodelling is evident, but the exact regulation and roles of angiogenesis is likely to be context specific.

As well as the previously mentioned hypoxia induction of VEGF-A inducing angiogenesis, oxygen sensing pathways have also been identified as key regulators of vessel pruning. As the tissue becomes vascularised and oxygen availability increases, the release of pro-angiogenic signals reduces, leading to a switch to vessel maturation and pruning (Adams & Alitalo, 2007). Von Hippel-Lindau is an essential regulator of HIF-1α, with its activation in normoxic conditions leading to HIF-1α degradation (Maxwell et al., 1999). In VHL syndrome a mutation within VHL results in an increase in susceptibility to certain tumors, as well as the growth of benign neoplasms called hemangioblastomas that contain highly proliferative endothelial cells (Kanno et al., 2009). In VHL mutant mice, vascular abnormalities were identified, with defects in arterial and venous branching and maturation at later developmental stages (Arreola et al., 2018). Oxygen sensing is also mediated by prolyl hydroxylase domain proteins (PHDs), with PHD2 deficient mice observed to have defective vascular pruning. This was initially believed to be due to the increased VEGF-A release by astrocytes with active HIF signaling, however treatment with anti-VEGF agents did not reverse the phenotype, indicating other mechanisms must also be involved (Duan & Fong, 2019).

1.1.6.3 Arteriovenous differentiation

Arteriovenous differentiation is the process by which newly developed vessels differentiate into either arteries or veins and is essential for the formation of a hierarchical network (Corada et al., 2014). Arteries gain further vSMC coverage which increases their contractability to cope with the increased shear stress, whereas veins are under less pressure and are required to develop valves to ensure the flow of blood is unidirectional (Adams & Alitalo, 2007). Arterial differentiation has been identified as being regulated by VEGF signalling and Notch signalling, many of this research originally demonstrated in zebrafish. Loss of Notch signalling led to defects in arterial venous differentiation and loss of arterial markers, indicating Notch signalling was essential for arterial differentiation (Lawson et al., 2001). Over expression of VEGF resulted in the expansion of arterial markers and the downregulation of venous markers. From this work it was identified that low levels of VEGF-A promote EC survival, whereas high levels promote arterial differentiation and inhibit venous differentiation (Casie Chetty et al., 2017). Whereas venous differentiation is regulated by the suppression of Notch signalling by the

transcription factor COUP-TFII (also known as Nr2f2). COUP-TFII has been identified as a venous specific transcription factor, and loss of COUP-TFII resulted in an increase in arterial gene expression and characteristics, whereas ectopic expression of COUP-TFII led to fusion of veins and arteries within the embryo (You et al., 2005). Interestingly it appears that this control of arterial venous fate by COUP-TFII is linked to the cell cycle, with COUP-TFII binding to multiple vein-specific enhancers which are close to actively expressed cell cycle genes (Sissaoui et al., 2020). Proliferating endothelial cells have also been observed to express venous markers (McDonald et al., 2018), further supporting the link between cell cycle and venous fate.

1.1.7 Endothelial quiescence and the angiogenic switch

Once angiogenesis has occurred and new vessels begin to stabilise, endothelial cells enter a state of quiescence in which they no longer proliferate or migrate. These ECs regain apical basal polarity and are held within an intact monolayer in a network of vessels, often descried as phalanx cells, due to their similarities to Greek military formations (Mazzone et al., 2009). In healthy adults, the majority of endothelial cells remain in this quiescent state as the vasculature has matured and adapted to the tissue it serves. This reduced proliferation observed within the quiescent endothelium has been observed in a study which demonstrated that ECs have a half-life of approximately 6 years (Bergmann et al., 2015). But despite this reduced activity, quiescent ECs are still constantly sensing and monitoring external signals and retain the ability to switch to towards an activated angiogenic state should the tissue require it, hence remaining entirely plastic (Potente et al., 2011; Ricard et al., 2021). Many of the signalling mechanisms involved in angiogenesis are also implicated in vascular maintenance and EC quiescence. Because of this, the multiple signalling pathways that govern this quiescence and the switch towards angiogenesis are tightly regulated. As such, a loss or dysregulation of this quiescence is a hallmark for angiogenic disease (Carmeliet, 2003).

1.1.7.1 Signalling pathways regulating quiescence

Although a prominent pro-angiogenic factor, the balance of VEGF-A signalling has proven to be highly important in the control of EC survival and quiescence. It has been demonstrated that ECs have autocrine VEGF-A signalling, which is essential for vascular

homeostasis. Endothelial specific deletion of VEGF resulted in sudden death in around half of mice by 25 weeks of age, suggesting that paracrine VEGF alone was unable to compensate for this loss (Lee et al., 2007a). The stimulation of quiescent ECs by VEGF-A has proven to be important in the maintenance of fenestrated vessels. This has been observed in the glomerulus of the kidney, whereby heterozygous deletion of VEGF-A resulted in reduced fenestrations and endothelial swelling (Eremina et al., 2003). Whereas in the pulmonary vasculature, which contains no fenestrations, inhibition of VEGF signalling by VEGFR2 inhibitors resulted in pruning of the vasculature (Kasahara et al., 2000). This therefore demonstrates that VEGF is required for vascular maintenance in a tissue specific manner.

Likewise, FGF ligands have been implicated angiogenesis but also maintenance of the vasculature. By activating the down regulation of TGFβ signalling within ECs, bFGF promotes endothelial identify by inhibition of TGFβ mediated mesenchymal gene activation (Chen et al., 2012). An example of an endothelial gene regulated by FGF signalling within ECs is VEGFR2, as ECs lacking FGF demonstrated a reduced response to VEGF-A due to the down regulation of VEGFR2 (Murakami et al., 2011). FGF signalling has also been demonstrated to play a role in sensing shear stress in the quiescent endothelium. Syndecan 4, a key modulator of bFGF signalling, is part of the complex pathway that senses shear stress (Baeyens et al., 2014), suggesting that bFGF may be influencing this process. This has been observed in disease, with loss of FGF signalling in areas of shear stress associated within an increase in atherosclerosis (Chen et al., 2015).

Angiopoietins (ANGs) are a family of secreted signalling molecules, made up of ANG1, ANG2, ANG3 and ANG4. Unlike VEGF and FGF, the angiopoietins have roles specifically to quiescence. ANG1 binds to its receptor TIE2 expressed on ECs (Suri et al., 1996). The phosphorylation of TIE2 is observed throughout the quiescent vasculature (Wong et al., 1997). This phosphorylation activates pro-survival pathways via Akt and the upregulation surviving, which inhibits EC apoptosis (Papapetropoulos et al., 2000). This activated Akt signalling by TIE2 is also able to regulate Notch signalling in quiescent endothelial cells via the activation of the transcription factor ERG. The mediation of ANG1 signalling by ERG was demonstrated to be required for vessel stabilisation in the neonatal mouse retina

(Shah et al., 2017). However, ANG2 is also able to bind the TIE2 receptor, acting as an agonist and competing with ANG1. This binding of ANG2 to TIE2 has been demonstrated to deactivate quiescence signalling during hypoxia and inflammation, resulting in the activation of the endothelium and loss of quiescence (Fiedler et al., 2006; Maisonpierre et al., 1997).

Transforming growth factor β (TGFβ) signaling has been implicated in the control of EC behavior and vascular development. Although deletion of endothelial TGFβ receptor 2 (TGFβR2) in adult mice, or inhibition in zebrafish, had no effect on the vasculature (Park et al., 2008), it has proven to be crucial in development, with deletion of endothelial TGFβR2 in development results in embryonic lethality due to failures in cerebrovascular development (Nguyen et al., 2011). TGFβ signaling is associated with endothelial to mesenchymal transition (EndoMT), a process in which endothelial cells adopt a mesenchymal phenotype, and hence within quiescent endothelial cells, TGFβ signaling is inhibited via multiple methods (Alvandi & Bischoff, 2021). ERK1/2 activation in ECs has been identified as being a key pathway in inhibiting TGFβ signaling, as disruption of ERK1/2 in ECs in mice resulted in EndoMT via the activation of TGFβ signaling (Ricard et al., 2019). Upstream of ERK1/2, the disruption of FGF signaling was also identified as increasing the expression of TGFβ ligands and activation of TGFβ signaling in ECs, leading to EndoMT(Chen et al., 2012). The inhibition of TGFβ signaling was also identified by Schlereth et al in the transcriptomic and epigenetic analysis of endothelial quiescence within the lung endothelium. This revealed a loss of DNA methylation within TGFβ family signaling genes, SMAD6 and SMAD7, that was observed within the quiescent ECs (Schlereth et al., 2018). This inhibition of TGFβ signaling in the quiescent endothelium is therefore important in maintaining endothelial quiescence and vascular homeostasis, as without this regulation vascular defects result in diseases such a pulmonary hypertension (Alvandi & Bischoff, 2021).

1.1.7.2 Endothelial cell metabolism in the quiescence-angiogenic switch

It is essential that metabolism of endothelial cells adapts depending on whether they're existing within an activated angiogenic state, or a quiescent state. The process of angiogenesis implicates a rapid change in EC behavior and morphology and for this to

occur, ECs must display a highly dynamic and adaptive metabolism in order to keep up with the high energy demand (Eelen et al., 2018). Research has identified that angiogenic ECs primarily rely on glycolysis to generate ATP, with the glycolytic flux observed as being 200-fold higher than that of oxidative phosphorylation. This increase in glycolysis is in response to the rapid increase in ATP required for the angiogenic processes of migration and proliferation to occur (De Bock et al., 2013). In a short period of time, glycolysis can quickly generate larger amounts of ATP, in comparison to the alternative oxidative phosphorylation (OXPHOS) metabolism. This fast generation of ATP is essential for cytoskeletal remodeling within tip cells, and quick cell cycle progression in the proliferative stalk cells (De Bock et al., 2013; Draoui et al., 2017). The importance of quiescent ECs altering their metabolism during the switch to angiogenesis was highlighted in research by De Bock et al, in which it was identified that inhibiting or silencing the major glycolytic enzyme Phosphofructokinase-2/fructose-2,6-bisphosphatase 3 (PFKFB3) had major impacts on angiogenesis. This glycolytic inhibition reduced not only the proliferation of ECs, but also affected cytoskeleton remodeling which proved to be essential for the formation of filopodia and lamellipodia. As a result, EC KO of PFKFB3 *in vivo* resulted in reduced vascular sprouting and vascular defects, which were observed within the neonatal mouse retina (De Bock et al., 2013). However, there is also evidence to suggest that OXPHOS metabolism is also increased during angiogenesis, as inhibition of OXPHOS metabolism reduced tumor angiogenesis (Coutelle et al., 2014). This indicates that angiogenesis requires a general increase in multiple forms of ATP generating metabolic pathways and methods. With this increasing evidence of the importance of metabolism during the quiescent-angiogenic switch, it is becoming clear that endothelial metabolism may not just be a consequence of angiogenic activation but also a key driver of this phenotypic switch (Eelen et al., 2018).

Quiescent endothelial cells on the other hand have a significantly reduced energy demand, requiring around a third of that of angiogenic endothelial cells (Coutelle et al., 2014). Because of this metabolic pathways that drive ATP pathways are reduced; with this coupling of metabolism to growth state being central to vascular function in development and homeostasis (Li et al., 2019). Despite this reduced energy demand, and the abundance of oxygen available, quiescent ECs *in vitro* still generate 85% of their ATP via glycolysis,

which was identified in capillary, arteriole, venous and lymphatic endothelial cells (De Bock et al., 2013). The preference for anerobic respiration, even within quiescent ECs that are not migrating towards low oxygen areas, is likely to preserve oxygen for perivascular cells within the environment of the supplied tissues. This poses the question of how ECs regulate the metabolic switch between quiescent and angiogenic ECs. Wilhelm et al identified that the transcription factor FOXO1 plays an integral part in the regulation of EC metabolism within the quiescent endothelium. Over expression of FOXO1 within ECs resulted in a robust decrease in both glycolytic metabolism and OXPHOS metabolism, suggesting FOXO1 is a significant regulator of EC metabolism (Wilhelm et al., 2016). This alteration of metabolism by FOXO1 in turn impacted angiogenesis, with EC specific FOXO1 gain of function mice displaying reduced angiogenic sprouting in response to decreased metabolism. Conversely, EC FOXO1 KO displayed hyperproliferation as a result of ECs inability to enter the reduced metabolic state within quiescence (Wilhelm et al., 2016). However, as well as a general reduction in EC metabolism, the metabolic profile of quiescent ECs also varies significantly compared to angiogenic ECs. Kalucka et al identified that quiescent endothelial cells have a 3-fold increase in fatty acid oxidation metabolism, compared to proliferating ECs, however this increase was to support redox homeostasis and not energy production (Kalucka et al., 2018). Whereas inhibition of FAO in angiogenic endothelial cells did not impact energy production or redox homeostasis, but instead impacted the production of nucleotides required for DNA synthesis and hence EC proliferation, resulting in vascular sprouting defects due to the reduced proliferation (Schoors et al., 2015). As well as this contrast, inhibition of FAO within the quiescent endothelium resulted in endothelial dysfunction as observed by increase leukocyte infiltration and increased barrier permeability (Kalucka et al., 2018). This therefore provided a further link as to the importance of metabolic activity in regulating the properties of a quiescent endothelium. The metabolic activity within quiescent ECs is therefore strictly regulated to ensure ECs remain in a low energy demanding state, with appropriate barrier properties, unless the switch to angiogenesis is required (Eelen et al., 2018). The importance of the metabolic changes implicated within and driving the quiescent-angiogenic are therefore evident.

1.1.7.3 Transcriptional regulation

The molecular mechanisms that govern endothelial quiescence and the angiogenic switch are underpinned by cellular signalling as well as transcriptional control. As previously mentioned FOXO1 was identified as an impactful promoter of endothelial quiescence via the regulation of endothelial metabolism. FOXO1 global knockout mice do not survive post embryonic day 11 due to impaired vascular development (Hosaka et al., 2004), and this is phenocopied within EC specific FOXO1 KO mice (Dharaneeswaran et al., 2014), highlighting it is within the transcriptional control of ECs specifically that FOXO1 is having an impact. Mechanistically this reduction in metabolism and EC proliferation was achieved by the suppression of the transcription factor MYC (Wilhelm et al., 2016), suggesting FOXO1 is a key regulator of endothelial quiescence. But despite this evidence, FOXO1 has also been implicated within angiogenic processes, suggesting its role is not completely clear cut. During sprouting angiogenesis, hypoxia induced activation of the Hippo pathway member MST1 was identified as regulating the nuclear import of FOXO1 in angiogenic tip cells within the neonatal mouse retina (Kim et al., 2019). This nuclear import and activation of FOXO1 by MST1 was identified as being crucial for EC polarisation in sprouting angiogenesis, with EC specific MST1 KO resulting in the same vascular defects observed previously in EC specific KO of FOXO1 (Kim et al., 2019; Wilhelm et al., 2016). This therefore indicates that FOXO1 may have roles in both the control of endothelial quiescence and the control of angiogenic processes.

The ETS family of transcription factors have been strongly identified as master regulators of EC development due to their direct regulation of genes involved in EC identity (De Val et al., 2008). A prominent endothelial transcription factor within this family is the ETS Related Gene (ERG), a transcription factor that is highly expressed in ECs within the majority of adult tissues (Shah et al., 2017). ERG has been identified as directly binding to promotors and regulating the expression of key genes regulating the quiescent vascular barrier, including VE-Cadherin (Birdsey et al., 2008), and Claudin-5 (Yuan et al., 2012). Indeed, overexpression of ERG *in vivo* reduces the permeability of VEGF-induced neovessels, by the upregulation of these barrier proteins (Birdsey et al., 2015). Constitutive endothelial-specific deletion of ERG results in embryonic lethality due to vascular defects, while inducible endothelial-specific knockout of ERG leads to impaired

vascular development, as demonstrated in the neonatal mouse retina. Not only this, depletion of endothelial specific ERG leads to defective pathological angiogenesis in tumours, as a consequence of increased vascular instability due to a loss of Wnt/β-catenin and VE-cadherin signaling (Birdsey et al., 2015). ERG has also been implicated within the repression of inflammation, with ERG expression being downregulated in response to pro-inflammatory stimuli such as TNF-α. Likewise over-expression of ERG reduces the response to inflammation by repressing the expression of pro-inflammatory markers such as ICAM-1 and VCAM (Sperone et al., 2011). This therefore indicates that ERG plays a crucial role in the regulation of key endothelial genes and is implicated in both physiological angiogenesis, pathological angiogenesis and vascular homeostasis. But despite ERGs major roles within the endothelium, knockout of other individual ETS family transcription factors appear to have little effect on vascular development, likely due to redundancy and compensation among this transcription factor family (De Val & Black, 2009).

1.2 Vascular Disease and Endothelial Dysfunction

Although loss of quiescence and activation of the endothelium is required for response to certain stimuli such as inflammation, aberrant endothelial activation can result in disease. Because of this, the molecular control of the quiescent endothelium and the regulation of the angiogenic switch it required to be strictly maintained. Dysregulation of endothelial quiescence results in disruption to vascular homeostasis, which is a feature in almost every disease, due to the nature of the endothelium being present in almost all tissues (Rajendran et al., 2013). Not only this, disruption to endothelial quiescence and the angiogenic switch directly results in diseases of the vasculature (Carmeliet, 2003). A schematic of this quiescent-activated switch is observed in Figure 1.3.

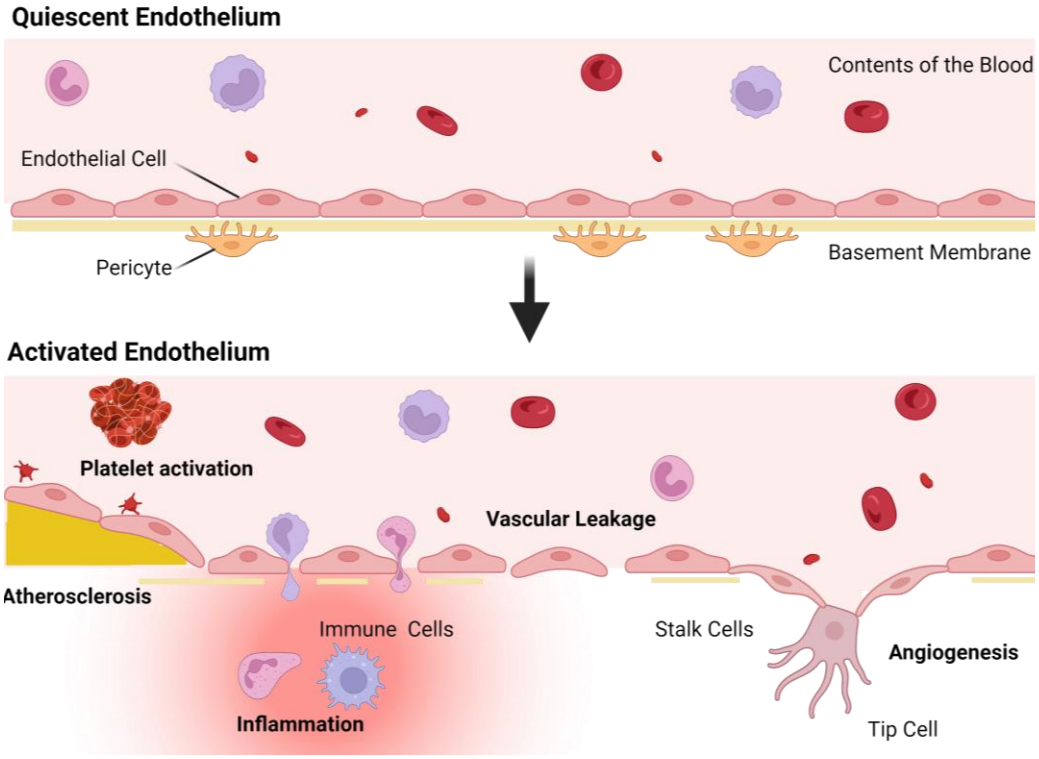

Figure 1.3 Schematic illustrating the differences between a quiescent and activated endothelium. *In the fully developed adult almost all ECs exist within a state of quiescence, however they retain the ability to react to appropriate stimuli and become activated when needed e.g. angiogenesis in wound repair and responses to inflammation. This switch between a quiescence and activated endothelium is highly regulated and loss of this regulation can result in a loss of quiescence and aberrant EC activation which is a hallmark of multiple diseases and a trigger for vascular disease. Created with biorender.*

1.2.1 Neovascular eye disease

A loss of endothelial quiescence has been heavily implicated in neovascular eye disease (Dreyfuss et al., 2015). An example of such disease is wet age-related macular degeneration (wAMD, sometimes termed neovascular AMD or nAMD). AMD is the leading cause of vision loss in developed countries in those aged over 60 (Wong et al., 2014). In wAMD unwanted angiogenesis occurs within the highly fenestrated choroidal vessels in the posterior eye segment, resulting in inflammation and angiogenesis in a process called choroidal neovascularisation (CNV). The neovessels generated as a result of this

angiogenesis are fragile and leaky, resulting in increased retinal damage and increased immune cell activation and infiltration due to upregulation of pro-inflammatory markers (Yeo et al., 2019).

Numerous mechanisms have been identified that trigger and impact the progression of AMD which involve changes to the retinal pigmented epithelium (RPE). The RPE consists of polarized epithelial cells which sit on the Bruchs membrane, together forming the outer blood retinal barrier (Strauss, 2005). It has numerous functions, including removal metabolites produced by the photoreceptors within the retina and the secretion of VEGF to maintain the health of the choriocapilaries (Datta et al., 2017). As the RPE ages and begins to senesce, metabolites accumulate on the Bruchs membrane, leading to the formation of vitreous warts which damage the retina and impact its blood supply. The senescence of the RPE also leads to the accumulation of VEGF, produced by immune cells. Other factors can also impact the RPE resulting in its dysfunction, such as oxidative stress owing to the retina having a high rate of oxygen consumption, and inflammation. Together these factors can promote RPE dysfunction, resulting in rupture of the Bruchs membrane and neovascularisation (Datta et al., 2017; Deng et al., 2022).

Another form of neovascular eye disease is Diabetic Retinopathy (DR), which has two stages: non-proliferative DR and proliferative DR, the latter considered as a more advanced stage of DR. Pro-longed hyperglycemia in diabetes results in microvascular damage, primarily as a result of elevated oxidative stress due to the increase in radical oxygen species from the increased glucose metabolism (Fowler, 2008). In non-proliferative DR this endothelial cell dysfunction initially causes blood flow changes and loss of pericytes, which leads to structural changes to the vascular network that are associated with microaneurysm formation. Impairment of the inner blood retinal barrier also occurs due to the thickening of the basement membrane and endothelial cell apoptosis (Ejaz, 2008). These changes result in capillary occlusion, hypoxia and subsequent release of VEGF which increases vascular permeability (Huang et al., 2015). In proliferative DR, neovascularisation occurs which can cause vision loss as a result of vitreous hemorrhage of the nascent vessels (Wang & Lo, 2018).

Based on VEGFs involvement in vascular leakage permeability and neovascularisation, along with the increase in VEGF expression within the aqueous humour in wAMD and DR patients (Zhou et al., 2020), the standard treatment for both conditions is the administration of VEGF inhibitors, such as bevacizumb and ranibizumab via intravitreal injection (Fogli et al., 2018). However, the estimated range of patients that have suboptimal or inadequate responses to anti-VEGF therapy is between 10-50% (Bontzos et al., 2020; Cobos et al., 2018; Heier et al., 2012; Kitchens et al., 2013; Krebs et al., 2013; Otsuji et al., 2013). This indicates alternative mechanisms are driving wAMD (Fernández-Robredo et al., 2014; Krebs et al., 2013). Ang/Tie signaling pathway has also been considered as a therapeutic target within wAMD patients due to its role in regulating vascular integrity. Targeting negative regulators of this pathway may therefore prevent neovascularisation and induce normalization within the choriocapillaris. Indeed ANG2, the agonist of the pro-normalisation ANG1, has been identified as elevated within the aqueous humour of AMD patients, with its expression level correlated with disease progression (Ng et al., 2017). Promoting Tie-2 signaling via inhibition of VE-PTP, a negative regulator of Tie-2, suppresses ocular neovascularisation and stabilises choroidal vessels, as well as retinal vessels in a model of diabetic retinopathy (Shen et al., 2014). As a result of these findings, drugs targeting the Ang/Tie pathway are currently in clinical trials for various angiogenic diseases (Akwii & Mikelis, 2021). Faricimab, a humanized antibody which simultaneously binds VEGF-A and Ang-2 showed positive outcomes in clinical trials and has since has been approved for use in the USA, UK and EU for both neovascular AMD and DR (Panos et al., 2023).

TGF-β has also been identified as a possible mechanistic driver of wAMD. The levels of TGF-β within the aqueous humour of wAMD patients were determined to be elevated, indicating TGF-β signaling is involved in the progression of wAMD (Tosi et al., 2017). Not only this, TGF-β levels remained elevated even after routine anti-VEGF therapy, which suggests this mechanism occurs independently of VEGF (Tosi et al., 2017). Increased expression of TGF-β was also observed within a laser CNV mouse model of wAMD, providing further evidence for its involvement. In the same study, inhibition of TGF-β reduced CNV lesion size, providing support for alternative treatments to be developed which target TGF-β signaling (Wang et al., 2017). Interestingly, these inhibitors also

impacted VEGF and TNF-α expression within these lesions, indicating that the mechanism may not be totally independent of VEGF.

1.2.2 Cardiovascular disease

In cardiovascular diseases the endothelial layer can become dysfunctional due to a loss of quiescence and vascular homeostasis, resulting in oxidative stress, inflammation and elevated cholesterol levels. This dysfunction leads to reduced nitric oxide production, impaired vasodilation, increased permeability, and a pro-inflammatory state (Gimbrone & García-Cardeña, 2016). This results in CVD progression, contributing to the development of a number of linked conditions including hypertension, coronary artery disease, peripheral artery disease and stroke (Castro-Ferreira et al., 2018).

Peripheral artery disease (PAD) is a common pathology within CVD which affects the lower limbs due to a narrowing of the larger vessels that supply them. This is commonly caused by atherosclerosis; a buildup of fatty deposits, cholesterol, and inflammatory cells on the inner walls of arteries, leading to narrowing and reduced blood flow (Libby et al., 2019). As a result of the blockage, the lower limb becomes progressively ischaemic, causing pain. Hypoxia within the limb induces pro-angiogenic signalling to promote collateral vessel formation and revascularisation of the affected area, resorting blood and oxygen supply. However, in PAD patients the insufficient collateral vessel formation results in prolonged tissue ischaemia, and if not treated leads to critical limb ischaemia and eventually gangrene which regurly results in limb amputation (Morley et al., 2018). Although angiogenesis occurs within the hypoxic tissue, the major collateral vessel formation is primarily driven by arteriogenesis in response to the increase in shear stress as a result of arteriole blockage (Pipp et al., 2004). The initial EC dysfunction resulting in vessel occlusion, along with the inability of PAD patients to form stable collateral vessels suggest that there may be dysregulation in EC quiescence and vessel normalisation.

1.2.3 Tumour angiogenesis

It is noteworthy that a lot of the literature surrounding angiogenesis within disease is focused on tumour angiogenesis. The high energy demanding nature of a tumour requires a great supply of oxygen and nutrients, which in turn rapidly drives angiogenesis (Hanahan & Weinberg, 2011). The natural quiescence of the endothelium is lost within a tumour,

generating a hyper-angiogenic morphology, in an attempt to satisfy the needs of the growing tumour (Hanahan & Folkman, 1996). However, the vessels generated by tumour angiogenesis are structurally abnormal, and therefore this affects their functionality. There is a clear absence of a normal EC phenotype, resulting in poorly connected ECs which do not appear to have a cobblestone-like appearance, and often have a disrupted monolayer. The aberrant vessels produced are irregular, wide and highly leaky. The outcome of this is abnormal perfusion, allowing platelets to accumulate, which causes flawed delivery of metabolites and oxygen (Potente et al., 2011). Tumour angiogenesis is therefore a phenomenon by which loss of vessel quiescence and normalisation regulation aids disease progression. However, the fact cancers are genetically unstable and abnormal in every sense of cellular behavior, make it complicated to draw firm conclusions on angiogenesis alone, when a multitude of different tumour and environmental factors come into play. This must be taken into consideration when discussing angiogenesis in both cancerous and non-cancerous conditions.

In summary, vascular diseases and pathologies often occur as a result of a phenotypic switch within the ECs that support that tissue. This is observed directly within vascular diseases such as PAD and wAMD, but also indirectly such as in tumour angiogenesis. Understanding the events that result in EC phenotypic switching is therefore crucial for our understanding of disease.

1.3 Endothelial to mesenchymal transition

Epithelial to mesenchymal transition (EMT) is a well-studied process of cellular state transition, defined as the phenotypic transition of epithelial cells into a mesenchymal phenotype. It is implicated within biological processes as well as pathophsyiological processes such as cancer. The EMT that occurs within cancers plays an important role in tumour initiation, invasion and metastasis, as originally normal epithelial cells begin to adopt a mesenchymal phenotype, resulting in them becoming highly invasive and eventually metastatic. However, EMT is also a physiological process that occurs within embryonic development and is essential for multiple processes, including (Brabletz et al., 2018; Kalluri & Weinberg, 2009).

A rapidly emerging area of vascular research has been focused on the process of endothelial to mesenchymal transition (EndoMT). Like EMT, EndoMT involves the transition of a type of cell (endohtelail cells in he case of EndoMT) into mesenchymal cells. During this process, the endothelial cells begin to lose their characteristics including a loss of polarity, cell-cell junctions and cobble stone like appearance. Instead, there is a gain of mesenchymal properties, resulting in a phenotype that is more invasive and migratory, with an elongated cellular structure (Piera-Velazquez & Jimenez, 2019). At a molecular level there is an observed loss of expression of key endothelial genes such as vWF, CD31/PECAM1 and VE-Cadherin, whilst a gain of mesenchymal marker genes such as N-cadherin, fibronectin and α-SMA (Piera-Velazquez & Jimenez, 2012).

1.3.1 EndoMT in physiology

EndoMT has been identified as being essential within physiological development of the heart and cardiac valves. In early embryonic development, it has been reported that endothelial cells lining the endocardium within the atrioventricular canal gave rise to mesenchymal heart cushion cells that contribute to valve tissue formation (Eisenberg & Markwald, 1995; Kinsella & Fitzharris, 1980). EndoMT was also demonstrated to take place within pulmonary vascular remodeling and intimal thickening, as immunolabeling techniques within the chick embryo identified mesenchymal cells that had arisen from the endothelium (Arciniegas et al., 2005). Since these discoveries, there have been various propositions of EndoMT playing physiological roles within development. For example, there are some suggestions that pericytes and other mural support cells arise from the endothelium and hence are created as a result of EndoMT (Armulik et al., 2005). Advanced lineage tracing techniques in mice have identified that smooth muscle cells within the pulmonary vasculature have originated from ECs (Lee et al., 2023), providing evidence of EndoMT and supporting earlier reports. There have also been reports that have identified an intermediatory state between endothelial and mesenchymal phenotypes, termed partial EndoMT, in which molecular characteristics of both cell types are observed. This has brought about the theory that angiogenesis is an EndoMT-like event due to the phenotypic transition from a quiescent phalanx cell to an elongated migratory tip cell with mesenchymal properties (Figure 1.4) (Fang et al., 2021a; Welch-Reardon et al., 2015). During sprouting angiogenesis ECs undergo morphological changes which are similar to

those that are observed in EMT, such as increased motility (Jakobsson et al., 2010), destabilisation of cell-cell junctions (Bentley et al., 2014) and increased expression and release of ECM degradation proteases (Del Toro et al., 2010). These similarities within the two processes henceforth support this theory. In addition to this, studies which have explored the effect of known EMT driving transcription factors have provided evidence for their role in angiogenesis. For example, knock out of Slug, a prominent EMT promoting transcription factor that has also been linked to EndoMT, resulted in inhibition of sprouting angiogenesis *in vitro* and *in vivo* (Welch-Reardon et al., 2014). This therefore provides further evidence that angiogenesis could be a partial EndoMT-like event.

1.3.2 EndoMT in pathology

EndoMT has also been implicated in multiple disease scenarios and hence has been a topic for research in the generation of new therapeutic targets. For example, post-myocardial infarction, EndoMT is induced by activated Wnt signaling in ECs. This resulted in the generation of SMA^+ mesenchymal cells that were determined to be derived from ECs via lineage tracing. It was concluded that this induction of EndoMT played a role in the generation of mesenchymal cells that take part in tissue repair post myocardial infarction (Aisagbonhi et al., 2011). EndoMT has also been implicated in renal fibrosis, with research into Alport syndrome demonstrating that 30-50% of fibroblasts within the fibrotic kidney also expressed endothelial markers. This suggested these fibroblasts had an endothelial origin, which was confirmed by linage tracing (Zeisberg et al., 2008). This was also observed within diabetic nephropathy induced renal fibrosis (Li et al., 2009). EndoMT has also been observed within other fibrotic conditions cardiac fibrosis observed within heart failure. In a mouse model of cardiac fibrosis, lineage tracing also identified fibroblasts had an endothelial cell origin, and that this induction of EndoMT was induced by TGFβ (Zeisberg et al., 2007). Together, this indicates that the EndoMT within fibrosis is not tissue or disease specific, but instead a general hallmark of the fibrotic process. Within pulmonary hypertension it has been revealed that EndoMT contributes to the accumulation of α-smooth muscle actin-expressing mesenchymal-like cells that contribute to the pathophysiology of the disease. This was demonstrated within rat models of PAH and the transcription factor TWIST, a known EMT regulator was identified as a molecular promotor of EndoMT (Ranchoux et al., 2015). This was also demonstrated in recent

lineage tracing experiments which also identified that BMP signaling activated ZEB1, another prominent EMT transcription factor, however unlike TWIST, ZEB1 suppressed EndoMT in pulmonary hypertension (Lee et al., 2023). This demonstrates that the drivers of EndoMT are not fully understood and suggests that EndoMT may have dissimilar activators and repressors to EMT.

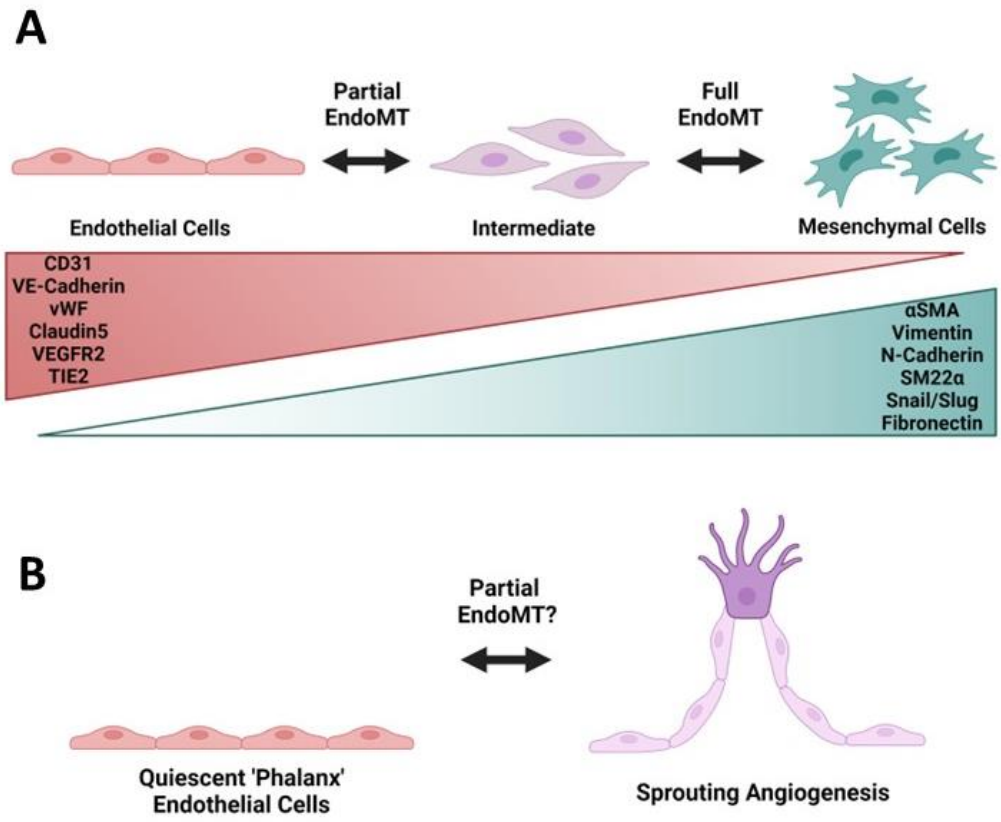

Figure 1.4 The process of EndoMT and possible similarities to sprouting angiogenesis. (A) *Endothelial to Mesenchymal Transition (EndoMT) is a process whereby ECs lose their identity and their EC specific markers and begin to gain a more mesenchymal phenotype with mesenchymal markers. This can be full EndoMT, in which ECs differentiate fully into mesenchymal cells such as fibroblasts, or partial EndoMT where cells have an intermediatory phenotype with both EC markers and mesenchymal markers.* ***(B)*** *Angiogenesis has been described as an EndoMT like event due to the phenotypic change between quiescent phlanax ECs and angiogenic sprouting ECs resembling partial EndoMT. Created with biorender.*

1.4 ZEB1

1.4.1 Structure and function

The Zinc finger E-box binding homebox 1 (ZEB1/Def1/ZFH/TCF8, but hereby known as ZEB1) was first identified in *Drosophila melanogaster* as the homologue zfh-1 in 1991 (Fortini et al., 1991). Not long after, a research group focusing on development of chick embryos identified ZEB1 as a nuclear factor expressed in multiple early development cell types that was capable of binding transcriptomic enhancers (Funahashi et al., 1993; Funahashi et al., 1991). Since then, ZEB1 has been identified as a prominent transcription factor that utilises C2H2 zinc finger motifs to bind CAGGTA/G E-box-like elements within target genes. The ZEB1 gene is located on Chr10p11.22. The protein consists of 1117 amino acids and is made up of a central homologous structural homeodomain (Vandewalle et al., 2009). The homeodomain family of proteins is a large group of transcription factors that contain a global domain called a homeodomain which is around 60 amino acids in length and normally functions as a DNA-binding domain. They were originally discovered in *Drosophila melanogaster* and found to have important roles in regulating axial patterning, segment identity and embryogenesis (Banerjee-Basu & Baxevanis, 2001). Since then, over 129 homeodomains have been identified in humans, separated into multiple subclasses based on structure and function, with ZEB1 belonging to the zinc finger sub class (Bürglin & Affolter, 2016).

However, in ZEB1 this central homeodomain does not bind DNA. Instead, DNA binding is achieved through two zinc finger domains; one based in the C terminal, and one based on the N terminal (Vandewalle et al., 2009). ZEB1 is also able to interact with protein binding partners via its interaction domains including C terminal binding protein (CtBP) interaction domain, Smad interaction domain and CAF/p300 binding domain (Figure 1.5) (Wu et al., 2020). ZEB2 has also been identified and although slightly larger shares a similar structure to ZEB1, hence both belonging within the ZEB homeobox family of transcription factors (Verschueren et al., 1999).

ZEB1 has been recurrently identified as a transcription factor that is capable of both transcriptional activation and repression. On a molecular level, the function of ZEB1 depends on the interaction of its binding partners. Postigo and Dean first identified the

ability of ZEB1 to act as a transcriptional repressor occurred through binding to CtBP, which acted as a co-repressor (Postigo & Dean, 1999). Since this, the transcriptional repressor activity of ZEB1 has been extensively highlighted throughout the literature, resulting in ZEB1 often be referred to a transcriptional repressor, despite it having known roles in transcriptional activation (Caramel et al., 2018; Postigo et al., 2003). Whereas the binding of co-activators to ZEB1 such as p300, Smads, CAF and YAP, have been identified as promoting gene transcription (Guo et al., 2022; Wu et al., 2020).

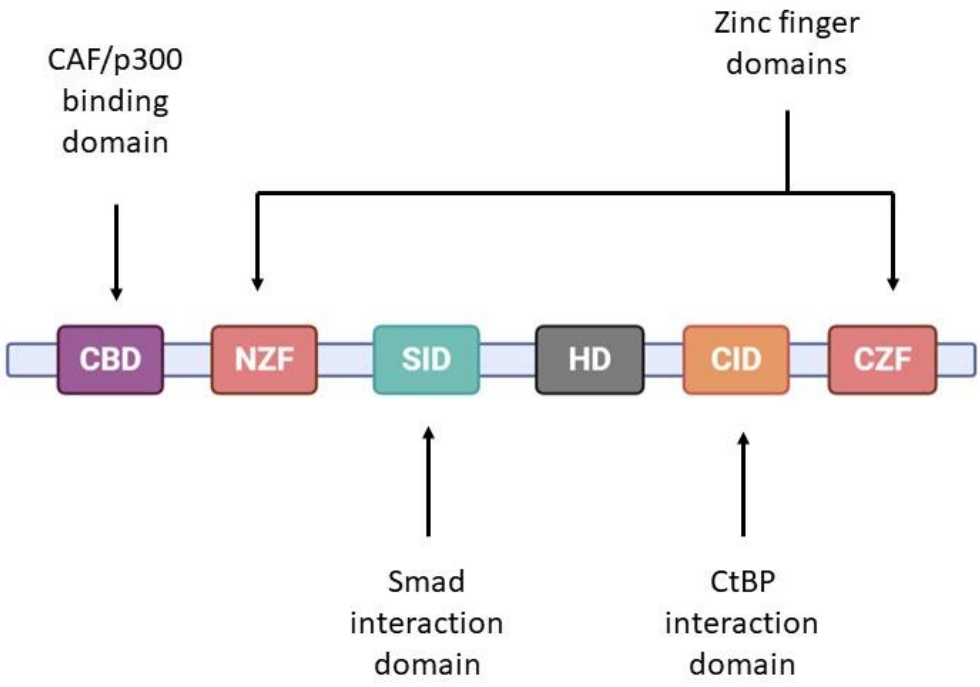

Figure 1.5 Schematic diagram of ZEB1. *The structure of ZEB1 contains two DNA binding zinc finger domains, one N terminal (NZF) and one C terminal (CZF). There is a central homeodomain (HD), along with three regulatory/interaction domains: CAF/p300 binding domain (CBD), a Smad interaction domain (SID) and a C terminal binding protein (CtBP) interaction domain (CID), all of which have known roles in modifying ZEB1s regulation of transcription. Created with biorender.*

1.4.2 Known roles of ZEB1

During embryonic development, ZEB1 has been identified as controlling the expression of key regulatory genes in processes such as differentiation. After the initial work in identifying ZEB1 in chick embryos by Funahashi et al, ZEB1 knockout mice were generated (Takagi et al., 1998). Although homozygous deletion of ZEB1 results in a litter that develops to term, none survive postnatally, with caesarean section at embryonic day 18.5 identifying pups that were unable to respire, resulting in death. The defects that occurred as a result of ZEB1 KO include severe T cell deficiency, along with multiple skeletal patterning abnormalities such as craniofacial abnormalities of neural crest origin, bone fusions within long bones and ribs, as well as hyperplasia of intervertebral discs (Takagi et al., 1998). This research therefore highlights the essential role within skeletal patterning, but also indicated a role within T cell development. Notably, Takagi et al also reports that ZEB1 KO embryos display internal bleeding. Although they did not expand on this further, this does suggest an impact on the vascular system.

A significant proportion of the literature places ZEB1 as a key regulatory of epithelial to mesenchymal transition (EMT) (Brabletz et al., 2018; Kalluri & Weinberg, 2009). ZEB1 has been implicated in EMT via the direct repression of multiple epithelial genes, including CDH1 (E-Cadherin), in which ZEB1 directly binds to the E-box located at the CDH1 promotor (Onder et al., 2008; Sánchez-Tilló et al., 2010). Forced expression of ZEB1 is sufficient to downregulate E-cadherin and induce EMT within a breast cancer model (Eger et al., 2005). Interestingly there is some contrasting evidence for this, as Sánchez-Tilló et al showed that this repression was observed to be independent of CtBP co-repressor activity, indicating that ZEB1 may be capable of transcriptional repression without the need for CtBP. ZEB1 has also been implicated in EMT via the up-regulation of mesenchymal genes within glioblastoma in response to TGFβ stimulation and interaction with phosphorylated Smad2 (Joseph et al., 2014). This therefore indicates that the promotion of EMT can occur both via the transcriptional repression and activation functions of ZEB1.

The expression of ZEB1 within multiple cancers has been associated with higher levels of disease progression and metastasis due to its role in promoting EMT. In colorectal cancer

ZEB1 was found to promote a loss of cell polarity by suppressing Lgl2, resulting in increased metastasis (Spaderna et al., 2008). This phenotypic modulation by ZEB1 has also been described as an enhancer of cancer cell plasticity, allowing for the constant adaptations under the changing conditions of the tumor microenvironment, as well as metastasis to secondary sites (Drápela et al., 2020; Zhang et al., 2015). Although EMT can exist as a complete process in which epithelial cells fully transition to mesenchymal cells, there is evidence to suggest that partial EMT results in a stem-cell like hyperplastic state. This was first observed in epithelial cells that were induced in culture to stimulate EMT which showed that not only do they express mesenchymal markers but also stem-cell markers (Mani et al., 2008). ZEB1 has been identified as being part of a feedback group with miR-200 family members that drives cellular plasticity (Brabletz & Brabletz, 2010; Liu et al., 2014). This has been observed within the context of pancreatic cancer, whereby depletion of ZEB1 within a pancreatic cancer mouse model resulted in a reduction in stemness, colonization and plasticity of tumor cells, which in-turn reduced disease progression and metastasis (Krebs et al., 2017). This promotion of stemness via feedback loops is also observed in other cancers. This includes breast cancer, whereby a feedback loop between ZEB1 and CD44 actively induces EMT and orchestrates stemness (Preca et al., 2015). This evidence further highlights the ability of ZEB1 to not only promote EMT, but also stemness, leading to an increase in cell plasticity. In summary, ZEB1, either alone or together with other EMT driving transcription factors such as ZEB2, Slug and Snail, actively promotes cancer progression via EMT, cell plasticity and therapy resistance.

There is also evidence to suggest ZEB1 has functions beyond EMT, including regulation of cell cycle and proliferation. Mouse embryonic fibroblasts from ZEB1 KO mice were found to undergo early senescence in comparison to WT controls. The group found that ZEB1 was able to manipulate cell cycle progression by the repression of cyclin dependent kinase inhibitors CDKN1A and INK4B, hence a loss of ZEB1 induced the expression of these inhibitors which indued senescence (Liu et al., 2008, 2014). Although these data were only observed within mouse embryonic fibroblasts, a recent publication using single cell RNA-seq data of human knee cartilage in the study of osteoarthritis identified a senescent cell population that was driven by ZEB1 expression (Swahn et al., 2023). Interestingly, ZEB1 expression in MDA-MB-231 breast cancer cells was identified as being responsible for the

upregulation of VGEF-A. This determined to directly promote tumour angiogenesis and disease progression, with ZEB1 expression being directly correlated to VEGF-A and CD31 expression in breast cancer tissues (Liu et al., 2016). This therefore provides evidence that within cancer cells, ZEB1 is able to promote the expression of pro-angiogenic cytokines.

1.4.3 Regulation of ZEB1 expression and activity

TGFβ has been well characterised as a promotor of EMT, as well as a regulator of ZEB1 expression. Within NMuMG cells (mouse mammary gland epithelial cells), TGFβ was found to upregulate the expression of ZEB1, which in-turn downregulated epithelial splicing regulatory protein 2 (ESRP2) (Horiguchi et al., 2012a). This upregulation of ZEB1 by TGFβ has also been observed within glioblastoma, with ZEB1 determined as being responsible for the expression of genes that result in increased migration and invasion within the disease (Joseph et al., 2014). Interestingly, TGFβ has not only been found to regulate ZEB1 expression but has also been demonstrated as having a direct impact on its sub-cellular localization. In lung adenocarcinoma, TGFβ was found to induce the nuclear import of ZEB1 which in-turn induced EMT. Prior to nuclear translocation via TGFβR2 activation, ZEB1 was shown to bind free actin and RhoA within the cytoplasm, which actively inhibited actin polymerization and blocking cell migration (Guo et al., 2022). This identified a new contrasting role for ZEB1 in inhibiting an EMT driven process such as migration, a process which is regulated by TGFβ stimulation.

The expression of ZEB1 has also been found to be regulated by other signaling pathways. Within glioblastoma, Wnt/β-catenin signaling was identified as driving EMT via the upregulation of ZEB1 expression (Kahlert et al., 2012). Interestingly within MCF10A epithelial cells expressing a constitutively active subunit NFκB, elevated expression of ZEB1 was identified along with an EMT phenotype and reduced E-cadherin expression (Chua et al., 2007). This study also identified that ZEB1 KD via siRNA reduced the number of viable cells, providing further evidence that ZEB1 is required for cell cycle progression. Finally, in renal cell carcinoma HIF-1α was observed to repress E-Cadherin expression via the increased expression ZEB1 (Krishnamachary et al., 2006), indicating ZEB1 expression is regulated by hypoxia signaling.

Another method of post-translational regulation of ZEB1 is ubiquitin targeted degradation. Siah, a ubiquitin ligase, has been identified as a regulator of ZEB1 degradation via the proteasome; with the downregulation of Siah observed within EMT, resulting in an increase in ZEB1 expression and hence EMT (Chen et al., 2014). It has also been observed that in the absence of Caspase-8-associated protein 2 (FLASH), the half-life of ZEB1 decreases from 3 hours to 1 hour, indicating that FLASH protects ZEB1 from proteasomal degradation and in-turn promotes EMT (Abshire et al., 2016). The ubiquitin targeting of ZEB1 degradation has also been determined to be regulated by the balancing of the E3 ubiquitin ligase TRIM26 and the deubiquitinating enzyme USP39 (Li et al., 2016). This indicates that a balance of factors promotes ZEB1 protein stability, which can be dependent on the cell system.

ZEB1 also has multiple phosphorylation sites which have been identified as modulators for its activity (Llorens et al., 2016; Park et al., 2022). In early identification and study of these phosphorylation sites, it was identified that ZEB1 was differentially phosphorylated in different cell types (Costantino et al., 2002). It was later identified that increased phosphorylation of sites near the C terminal zing finger domain by IGFR1/MEK/ERK signaling inhibited transcriptional repression activity of ZEB1. Interestingly, this research also identified that ZEB1s subcellular localisation could also be regulated by phosphorylation of different residues (Llorens et al., 2016). This therefore suggests that the function of ZEB1 as a transcriptional repressor, along with its subcellular localization, can be modified by phosphorylation.

As previously mentioned, ZEB1 can interact with a variety of co-activators and co-repressors which modulate its activity. This includes the previously described CtBP, a co-repressor in the negative regulation of CDH1 expression (Eger et al., 2005; Postigo & Dean, 1999). This complex with CtBP has also been found to repress the expression of several other genes, including Bcl6 in B cell lymphoma (Papadopoulou et al., 2010). Although, CtBP independent repression activity of ZEB1 has been identified (Sánchez-Tilló et al., 2010), including the recruitment of NuRD/CHD4 complex to the C terminal zinc finger domain which represses the expression of TBC122b, miR-200c and miR-141. This suppression of TBC122b resulted in the degradation of E-cadherin (Manshouri et al.,

2019), suggesting that ZEB1 is able to suppress E-cadherin and promote EMT via numerous mechanisms. The interaction of ZEB1 with transcriptional activators has also been well reported, primarily within the context of TGFβ signaling, but also via other mechanisms. ZEB1 is able to interact with phosphorylated Smads to induce expression to TGFβ responsive genes via its Smad interaction domain. On top of this, TGFβ is able to activate and recruit pCAF and p300, which are able to bind and activate ZEB1 via its CAF/p300 binding domain (Postigo et al., 2003), indicating that TGFβ modulation of ZEB1 activity can occur through multiple mechanisms. Finally, in breast cancer ZEB1 has been identified as being a binding partner of the transcriptional co-regulator YAP to promote transcriptional activation of genes associated with therapy resistance and metastasis (Lehmann et al., 2016). This complex of both ZEB1 and YAP together was identified as being able to target TEAD-binding sites via ChIP-Seq (Feldker et al., 2020), which further highlights the importance of binding partners in modulating ZEB1 expression.

1.4.4 Endothelial ZEB1

Within the literature, there have been a small number of reports that have explored the role of ZEB1 within endothelial cells. In the commencement of the research presented in this thesis, the literature was primarily focused on two separate areas of research: ZEB1 in cornea endothelial cells and ZEB1 in tumour angiogenesis. Since the work in this thesis was initiated, there have been a couple of more recent publications which present conflicting reports for the role of endothelial ZEB1.

1.4.4.1 ZEB1 in Corneal Neovascularisation

The link between ZEB1 and endothelial cells was first identified within the context of Posterior polymorphous corneal dystrophy (PPCD). Within humans it has been identified that roughly half of PPCD patients had heterozygous frameshift and nonsense mutations within the ZEB1 gene. PPCD is a rare disease of the cornea, in which overgrowth of corneal endothelial cells and aberrant endothelial basement membrane is observed, indicating that ZEB1 may play a role in endothelial basement membrane organisation (Krafchak et al., 2005; Liskova et al., 2007). As a direct result of these findings, ZEB1 mutant mice, originally developed by Takagi et al, have been identified as a model to study PPCD in the attempt to develop therapeutic strategies (Liu et al., 2009).

The cornea is an avascular tissue, but despite this neovascularisation of the cornea can occur from the pericorneal plexus, leading to corneal neovascular disease (Chang et al., 2012). In a more recent publication using an alkali burn model of corneal neovascularisation, ZEB1-/+ mice displayed less severe angiogenesis and lymphangiogenesis compared to ZEB1+/+ controls (Jin et al., 2020). What is important to note is that within these studies, the transgenic mice used are global heterozygous ZEB1 KO mice. The team determined that ZEB1 expression was significantly reduced in the ZEB1+/- mice, however this global KO still means that ZEB1 expression will be reduced in other cell types. Hence, the effect observed within these studies may not be completely due to loss of endothelial ZEB1, and instead a loss of ZEB1 in other cell types. However, Jin et al did assess the level of ZEB1 expression within vascular ECs of alkali induced neovascular lesions, which revealed a significant increase in ZEB1 expression in comparison to the vascular ECs within PBS treated controls (Jin et al., 2020). This therefore provides an indication that endothelial ZEB1 specifically is increased in expression within newly formed vasculature. The team also found that ZEB1 KD by shRNA induced senescence within retinal microvascular endothelial cells, and that ZEB1-CtBP inhibitors could functionally inactivate ZEB1 in a similar way (Jin et al., 2020). These results suggest that ZEB1 plays a role in angiogenesis and neovascularisation.

1.4.4.2 ZEB1 in tumour angiogenesis

Earlier studies identified ZEB1, historically known as TCF8, as a contributer to tumour angiogenesis. For instance ZEB1 upregulated VEGF-A in breast cancer cells (Liu et al., 2016). Inuzuka et al extended this by showing that ZEB1+/- knockout mice developed larger melanoma tumours, attributed to increased angiogenesis (Inuzuka et al., 2009). However, because this was a global heterozygous knockout, effects in non-endothelial cells could not be ruled out. Supporting this, ZEB1 knockdown in HUVECs enhanced angiogenesis and reduced cell adhesion, suggesting that endothelial ZEB1 may maintain vascular quiescence (Inuzuka et al., 2009).

More recently, the role of endothelial ZEB1 was explored in tumour angiogenesis using an inducible endothelial specific ZEB1 KO mouse model. From this it was identified that EC ZEB1 KO reduced tumour growth and decreased the amount of tumour angiogenesis (Fu

et al., 2020). This is contrasting to research published by Inuzuka et al; however, this work was achieved using a global knockout, which may explain the differences in results. Not only this, Fu et al showed that vascular ZEB1 expression levels were high in various tumours and that knocking out ZEB1 induced vessel normalisation within tumours, which aided chemotherapy delivery (Fu et al., 2020). This evidence is similar to what Jin et al, 2020, observed within corneal neovascularisation, where ZEB1 expression is associated with recently developed vessels, as tumours are very angiogenic tissues.

1.4.4.3 ZEB1 in osteogenesis linked angiogenesis

Interestingly, in a separate publication the same team also found that endothelial ZEB1 is essential for angiogenesis driven osteogenesis in development. Endothelial ZEB1 expression was found to be associated with CD31 high Endomucin high endothelial cells, known for their role in coupling angiogenesis to osteogenesis. Not only this, deletion of endothelial ZEB1 specifically impaired blood vessel formation and reduced osteogenesis as a result (Fu et al., 2020). This work is supported by the fact ZEB1 global knockout results in neonatal lethality, with a major affect being skeletal abnormalities (Takagi et al., 1998). This therefore suggests that endothelial ZEB1 is playing a crucial role in the angiogenesis which drives osteogenesis. The observed association of ZEB1 with angiogenesis is similar to what is observed to Jin et al in corneal neovascularisation, but this time providing evidence within a developmental model, instead of a disease model.

1.4.4.4 ZEB1 in vascular quiescence

A recent publication found a completely contrasting role for endothelial ZEB1 by inducing vascular quiescence. The team found that deletion of endothelial ZEB1 resulted in delayed quiescence entry and severe vascular deformities within the developing retinal vasculature. ZEB1 represses Wif1 expression which in turn allows for activation of Wnt/β-catenin that causes the increased expression of the quiescence regulator FOXO1 (Yu et al., 2022). This is in complete contrast to what was observed by Fu et al in their tumor angiogenesis publication, where supplementary analysis of EC ZEB1 KO revealed no significant difference in the development of the retinal vasculature (Fu et al., 2020). This provides further conflicting evidence of the role of endothelial ZEB1.

1.5 Summary, Aims and Hypothesis

The vascular endothelium is a heterogenous tissue which plays a pivotal role in maintaining vascular integrity and regulating vascular homeostasis. Within development, as well as growth and repair, angiogenesis is required to create a vascular network which is able to supply and adapt to the needs of the surrounding tissue. However post-development, it is essential that the endothelium exists within a quiescent state, but importantly retains the ability to respond appropriately to pro-angiogenic stimuli. Dysregulation of the switch between quiescent and angiogenic ECs is a hallmark for vascular disease and has been implicated in multiple other pathologies. The control of this phenotypic switch between quiescent and angiogenic endothelial cells is therefore crucial but despite this, the transcriptional and molecular control of this phenotypic switch remains not fully elucidated. With EndoMT emerging as a similar phenotypic switching event that occurs within ECs, there has been an increase in the focus on transcription factors known to drive trans differentiation-like events, such as EMT. Along with other EMT promoting transcription factors, ZEB1 has been implicated in the transcriptional control of ECs, however the literature remains conflicted.

The aim of this thesis is to identify the role of endothelial ZEB1 within physiological and pathological angiogenesis. I set out to test the hypothesis that loss of endothelial ZEB1 impacts the ability of the vasculature to undergo quiescent-angiogenic phenotypic switching. In order to test this hypothesis, I will achieve the following aims:

1. Observe *in vitro* the transcriptomic differences in confluent (quiescent) and subconfluent (proliferating) Human Umbilical Vein Endothelial Cells using RNA-Seq
2. Determine how ZEB1 affects the transcriptome of confluent Human Umbilical Vein Endothelial Cells using RNA-Seq and ChIP-Seq
3. Assess if loss of ZEB1 affects the angiogenic processes using *in vitro* angiogenic assays
4. Determine whether EC specific KO of ZEB1 altered the physiological angiogenesis using the neonatal retina as a model for developmental angiogenesis

5. Establish if loss of EC ZEB1 affects the development of neovascular lesions and vascular leakage within a mouse model of wAMD
6. Establish whether loss of EC ZEB1 affects the blood flow recovery and collateral vessel formation in a mouse model of PAD

Chapter 2:

Materials and Methods

2 Materials and Methods

2.1 Cell culture

Human Umbilical Vein Endothelial Cells (HUVECs) from pooled donors were purchased from Promocell. Unless stated otherwise, this was the case for all HUVEC data presented within this thesis. For experiments in section 3.3.8-11 (ZEB1 CRISPR KO with MTT, migration assay and sprouting assay), HUVECs were isolated in house from single donors by Bettina Hansen, Aarhus Univeristy.

2.1.1 Maintenance and Routine Subculture

HUVECs were cultured in Endothelial Cell Growth Medium (promocell) with 2% Endothelial Growth Supplements (promocell) at 37°C and 5% CO^2. Cells were passaged upon reaching 80-90% confluency by washing with sterile PBS before detaching using Trypsin/EDTA at a ratio of 0.04%/0.03% respectively. Cells were centrifuged at 100xG to pellet before being resuspended in complete media and seeded into new flasks. Cells were never split greater than 1/5 to ensure confluency never fell below 40%. Cells were regularly checked to ensure they maintained endothelial cell cobblestone morphology and only passages 2 – 7 were used for experiments.

2.1.2 Cell Counting

Post detachment using Trypsin, the cell pellet was resuspended in 10mL complete media. 10µL cell suspension was loaded onto a haemocytometer and cells counted by taking an average number of cells within 4 squares. The number of cells per mL was then calculated using the following equation:

$$\text{Cells per mL} = \text{Average number of cells counted x } 10^4$$

2.1.3 Cryopreserving Cells

Post detachment using Trypsin, cells were counted as described above. Cells were then centrifuged at 100xG for 5 minutes, supernatant discarded and resuspended in freezing media (complete media supplemented with 10% DMSO (Sigma)) at a volume of 1 x 10^6 per mL. The suspension was then aliquoted to ensure 1 x 10^6 cells were added to each cryovial

before placing in an isopropanol filled Mr Frosty overnight at -80°C. Cryopreserved cells were then stored long-term in liquid nitrogen.

2.1.4 Thawing Cryopreserved Cells

Cryovials containing 1 x 10^6 cryopreserved cells per vial were removed from liquid nitrogen and rapidly warmed to 37°C in a water bath for approximately 2 minutes. Each cryovial was added to one T75 flask containing complete media, pre-warmed to 37°C. Cells were allowed to adhere overnight and media changed the following day to remove any unrevived cells and DMSO.

2.1.5 Confluent vs Sub-confluent experiments

HUVECs were seeded at different densities by increasing the surface area for growth whilst maintaining the same number of cells. 1 x 10^6 were seeded into a 60mm diameter dish for the confluent condition compared to 1 x 10^6 being split over four 60mm diameter dishes for the sub-confluent condition. Cells were allowed to adhere overnight, and appropriate confluency was confirmed by observing the cells down the microscope before protein or RNA extraction took place. Subconfluent HUVECs covered approximately 40% of the surface area of the dish, whereas confluent endothelial cells resemble an intact monolayer that completely covers the dish. An image of confluent and subconfluent HUVECs can be observed in Figure 2.1.

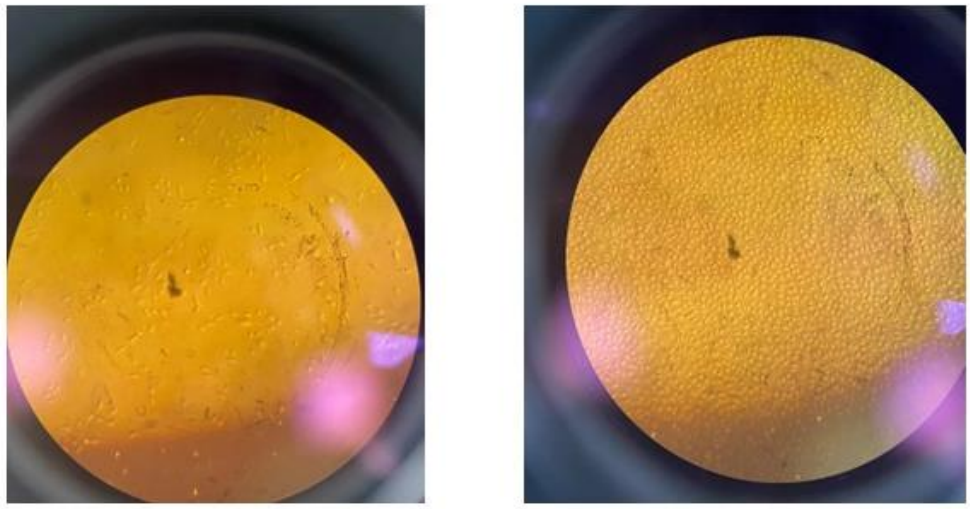

Figure 2.1 Subconfluent and confluent HUVECs
Confluent and Subconfluent HUVECs in culture imaged using an iPhone camera looking down a Nikon microscope at 20x magnification

2.1.6 Transient gene knockdown using siRNA

HUVECs were seeded into 60mm diameter dishes with approximately 1 million cells per dish and allowed to adhere overnight to ensure 100% confluency. Cells were transfected with 200nM pooled siRNA directed towards ZEB1 (siRNA ID s229972, Thermo Fischer) or ON-TARGET plus Non-targeting control Pool (Non-silencing control (NSC), DharmaconTM Reagents) using PromoFectin-HUVEC (promocell) and Opti-MEM (Gibco) and incubated for 4 hours. Transfection media was then replaced with complete media and cells incubated for 48 hours for RNA extraction or 72 hours for protein extraction.

2.1.7 CRISPR Cas9 KO of ZEB1

HUVECS were isolated from donated umbilical veins from single donors using CD31 microbead selection by Bettina Hansen, Aarhus Univeristy. HUVECs isolated this way were seeded into 0.1% gelatine coated vessels but otherwise were cultured as stated previously. To achieve ZEB1 KO, 150,000 cells from a single donor were centrifuged at

100xG and resuspended in a 20µL mixture of 6µg recombinant Cas9 (Invitrogen), 6ug single guide RNA (Synthego) against ZEB1 or control, in OptiMEM media. HUVECs were then nucleofected using the LONZA 4D-Nucleofector Core unit using the primary cell P3 setting with a pulse code of CM138. Cells were then plated in 0.1% gelatine coated 6-well plate for knockout confirmation and propagation.

2.1.8 MTT Assay – Metabolism and Viability

HUVECs were seeded 18,750 cells per well of a 96 well plate. 24-, 48-, 72- and 96-hours post-plating, 12.5µL of 3-(4,5-dimethylthiazol-2-yl)-2,5-diphenyl tetrazolium bromide (MTT) at 0.5mg/mL, placed on an orbital shaker for 3 minutes before being incubated at 37°C + 5% CO^2 for 4 hours. Post incubation, all the media was removed and 100µL DMSO was added to each well to solubilise the formazan product. The plate was briefly shaken on an orbital shaker before incubating overnight at 37°C + 5% CO^2. The absorbance of the solution was then measured at 570nm using a plate reader. Four technical repeats were used for each condition.

2.1.9 Scratch Assay

HUVECs were seeded at a density of 42,500 cells per well of a 24 well plate and allowed to grow for at least 6 days to allow a stable monolayer to form. 4 hours prior to scratch, cell media was replaced with 1% serum media along with 5µg/mL mitomycin C to inhibit proliferation. A vertical scratch was created with a pipette tip. Images of the scratch were taken at 0, 4, 6, 18, 24 and 32 hours were then imaged using an Olympus EP50 with digital camera attachment. 3 wells were generated per condition to create 3 technical repeats. Scratch closure was analysed by measuring the negative space using image J.

2.1.10 Sprouting Assay

A HUVEC cell suspension was counted and 750,000 cells per condition were centrifuged at 1,100 RPM before being resuspended in 15mL of basal Endothelial Cells Growth Media. 3.75mL 1% methylcellulose (Sigma) was added to the cell suspension before being transferred to a reagent reservoir. Using a multi-channel pipette, this total mixture (18.75mL) was pipetted into 25µL droplets on the bottom of a low adherent 10cm dishes, giving rise to around 10 dishes per condition. These plates were then placed upside down in the incubator overnight at 37°C to allow spheroid formation.

The following day spheroids were harvested by gently pipetting 10mL 10% FBS in PBS over the spheroids before collecting them in a 50mL tube. The spheroids were centrifuged for 5 minutes at 300xG with no brake, followed by 3 minutes at 500xG with no brake. The supernatant was discarded, and the pelleted spheroids were gently resuspended in 1.5mL 5mg/mL Fibrinogen (Sigma) in basal Endothelial Cell Growth Media. 0.9 units of Thrombin (Sigma) (9µL) were added to the spheroids before quickly transferring to across 3 wells of a 24-well plate. The fibrinogen was allowed to solidify at 37°C for 20 minutes before adding 500µL Endothelial Cell Growth Media with 1% growth supplements.

Spheroids were then imaged using an Olympus EP50 with digital camera attachment at 24h and 48h post seeding into the fibrinogen gel. At least 10 spheroids were analysed per well, and at least 3 wells were analysed per condition generating 3 technical repeats. Images were analysed on image J to determine sprout number, sprout length and branching number.

2.2 Inducible endothelial cell (iECKO) knockout mouse model

C57BL/6 ZEB1$^{fl/fl}$ cdh5 Cre-ERT2 mice were bred in house within the University of Nottingham Biological Support Unit. ZEB1$^{fl/fl}$ were received from Thomas Brabletz (S. Brabletz et al., 2017), and cdh5 Cre-ERT2 were received from Ralf Adams (Sörensen et al., 2009). All experimental animals were treated in accordance with the Animal (Scientific Procedures) Act of 1986 (ASPA) under the authority of the Home Office. The experiments within this thesis were either performed under the UK Home Office License PPL PE6932817F or PPL P3E735452 held by Professor David O Bates. All *in vivo* experiments were performed on mixed gender mice and all animals were genotyped by Transnetyx Inc. ZEB1$^{fl/fl}$ cdh5 Cre-ERT2$^{+/-}$ and ZEB1$^{fl/fl}$ cdh5 Cre-ERT2$^{-/-}$ animals were bred to create a mixed litter of ZEB1$^{fl/fl}$ cdh5 Cre-ERT2$^{+/-}$ and ZEB1$^{fl/fl}$ cdh5 Cre-ERT2$^{-/-}$ for studies. All decisions regarding animal health and welfare from *in vivo* work within this thesis were done under the guidance and supervision of Named Animal Care and Welfare Officers (NACWO) as well as the Named Veterinary Surgeon (NVS).

2.2.1 Tamoxifen induction of endothelial cell ZEB1 knock out in adult mice

100mg Tamoxifen (Sigma) was added to 1mL 100% ethanol (Thermo) and heated gently to 37°C until fully dissolved before the addition of 9mL sterile sunflower oil in a class 2 safety cabinet.

To induce genetic recombination, both ZEB1$^{fl/fl}$ cdh5 Cre-ERT2$^{+/-}$ and ZEB1$^{fl/fl}$ cdh5 Cre-ERT2$^{-/-}$ adult mice between 8-12 weeks of age received a daily dose of Tamoxifen at 1mg/25g via intraperitoneal (i.p.) injection on 5 consecutive days to induce endothelial ZEB1 knock out in the ZEB1$^{fl/fl}$ cdh5 Cre-ERT2$^{+/-}$ mice and ZEB1$^{fl/fl}$ cdh5 Cre-ERT2$^{-/-}$ are control animals due to having no Cre recombinase expression and therefore no genetic KO via recombination. Animals were welfare checked and weighed in the days prior to dosing to ensure there were no signs of ill health. Animals were also weighed, and welfare checked each morning prior to dosing, monitored for at least 1-hour post-dosing and welfare checked at least 5 hours post-dosing to ensure no adverse effects occurred. Daily welfare checks were stopped 24 hours after the last dose, providing there were no health concerns and reduced to twice a week. Any animals which showed signs of adverse effects, pain or ill health were closely monitored along with advice from a NACWO or NVS. Animals which continued to show signs of ill health or had lost >20% of their body weight from the start of the study were culled by schedule 1 cervical dislocation method.

2.2.2 Endothelial Cell Isolation from Lung Tissue

Primary murine endothelial cells from were isolated from both ZEB1$^{fl/fl}$ cdh5 Cre-ERT2$^{+/-}$ and ZEB1$^{fl/fl}$ cdh5 Cre-ERT2$^{-/-}$ adult mice that had been dosed as described previously.

2.2.2.1 Lung Dissection and Digestion

Mice were culled by cervical dislocation and death confirmed by permanent disruption of blood flow. Lung dissociation and EC isolation was achieved using the lung dissociation kit from Miltenyi. Whole lungs were dissected and washed in iced cold PBS 4-5 times until all blood was removed. The lungs were then transferred into basal endothelial cell media (Promocell), minced with scissors into small pieces before being digested in lung dissociation kit enzyme mix (Miltenyi) at 37°C for around 2 hours with regular agitation to aid digestion. The cell suspension was then placed through a 30µL and 70µL smart strainer (Miltenyi) along with 2.5mL PEB cell sorting buffer to generate a single cell suspension.

2.2.2.2 CD31 Magnetic Cell Sorting

The total cells in suspension were counted using a haemocytometer as described above. 10% of the total cells were removed and centrifuged at 300xG, supernatant discarded, and pellet stored at -80°C ready for RNA extraction for the input fraction. The remaining cells

were centrifuged at 100xG, supernatant discarded, and the pellet resuspended in 10µL CD31 microbeads (miltenyi) and 90µL PEB sorting buffer per 10^7 cells before being added to an end-to-end rotator for 30 minutes at 4°C. The labelled cells were then centrifuged at 100xG at 4°C, resuspended in 500µL PEB per 107 cells ready for magnetic cell sorting.

The labelled cell suspension was added directly to LS columns on miltenyi magnets that had been pre-primed with 3mL PEB. The LS columns were washed 3 times with 3mL PEB and the total flow through kept as the CD31- fraction. The column was then removed from the magnet, 3mL PEB added, and the plunger firmly applied to remove the CD31+ cells from the column and into the eluted fraction. Both the CD31- and CD31+ fractions were then centrifuged at 300xG, supernatant discarded, and cell pellet stored at -80°C ready for RNA or Protein extraction.

2.3 Neonate Dosing and Developmental angiogenesis

$ZEB1^{fl/fl}$ cdh5 $Cre\text{-}ERT2^{+/-}$ and $ZEB1^{fl/fl}$ cdh5 $Cre\text{-}ERT2^{-/-}$ adult mice were crossed to create a mixed litter of $ZEB1^{fl/fl}$ cdh5 $Cre\text{-}ERT2^{+/-}$ and $ZEB1^{fl/fl}$ cdh5 $Cre\text{-}ERT2^{-/-}$ pups (Figure 2.2 A). All pups from each litter used within the study were taken forward for dosing.

2.3.1 Neonate Dosing

Tamoxifen was made up as previously described. Animals born on postnatal day 0 were dosed with 50µg Tamoxifen in 5µL sunflower oil via i.p. injection using a 27G insulin needle on postnatal days 1, 2 and 3. Animals were constantly monitored for at least 1-hour post-dosing and checked throughout the day every 1-2 hours to ensure no adverse reaction had taken place. Prior to dosing each morning, the pups were physically monitored and checked for signs of ill health along with being weighed to ensure significant weight gain. On postnatal day 4 the pups were weighed once in the morning to ensure significant weight gain and monitored twice again throughout the day for signs of ill health. On postnatal day 5, the pups were culled by cervical dislocation before tissue dissection for downstream analysis (Figure 2.2 B).

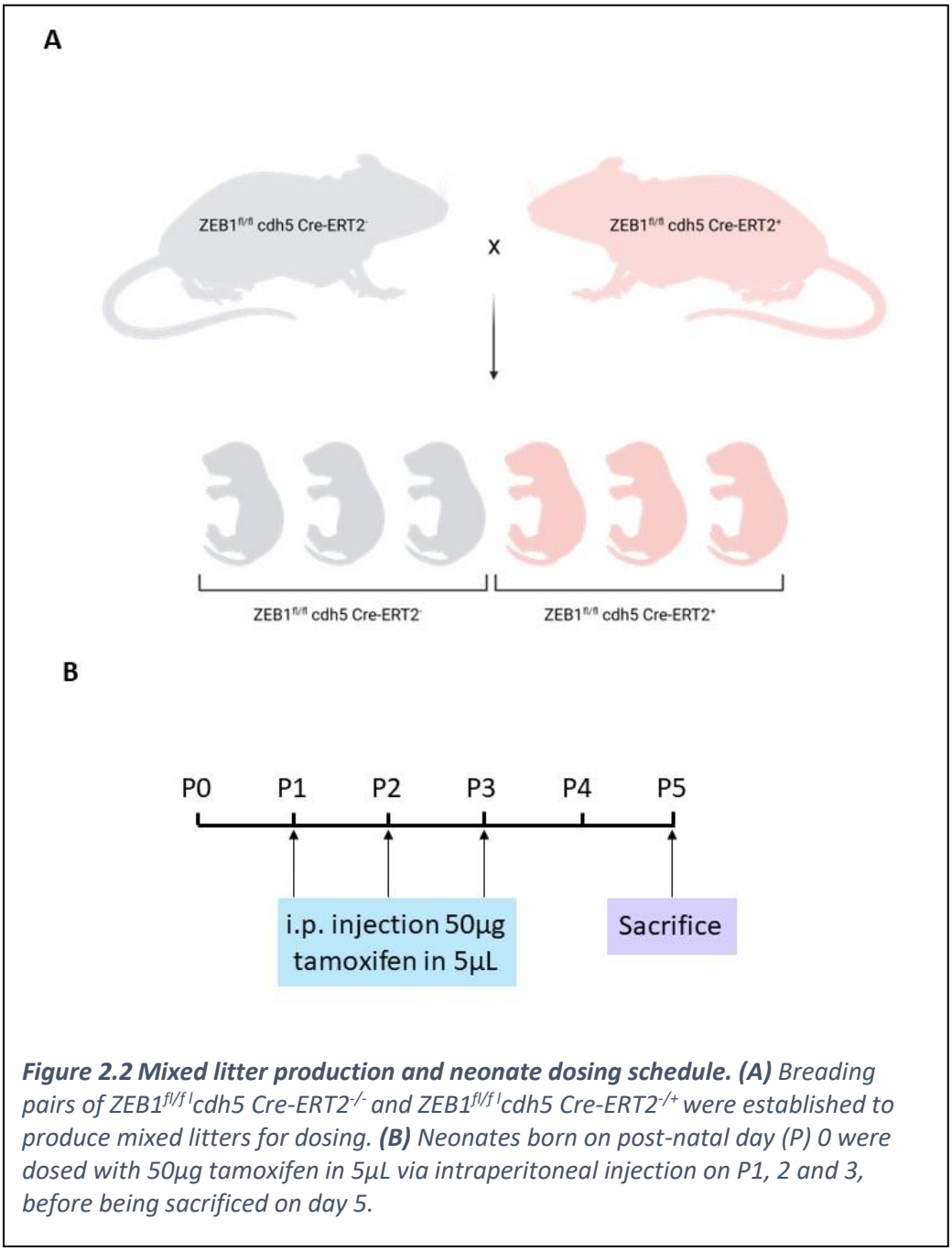

Figure 2.2 Mixed litter production and neonate dosing schedule. (A) *Breading pairs of ZEB1$^{fl/fl}$cdh5 Cre-ERT2$^{-/-}$ and ZEB1$^{fl/fl}$cdh5 Cre-ERT2$^{-/+}$ were established to produce mixed litters for dosing.* ***(B)*** *Neonates born on post-natal day (P) 0 were dosed with 50µg tamoxifen in 5µL via intraperitoneal injection on P1, 2 and 3, before being sacrificed on day 5.*

2.3.2 Adverse effects

A few neonate mice experience adverse effects due to the tamoxifen dosing. These include lack of weight gain, loss of pink colour, fluid build-up around injection site, rejection by the mother and lack of milk spot, indicating insufficient feeding. Under the guidance of a NACWO, these animals were culled immediately by cervical dislocation. A

small number of neonates were found dead the next morning after dosing. Often these deaths were within the pre-weaning mortality rate of the litter or had occurred due to cannibalism by the mother. Any deaths that were beyond the normal pre-weaning mortality rate for the mouse strain were reported to the Home Office.

2.3.3 Neonate Eye Dissection

Both eyes were dissected by the removal of skin covering the eye socket using fine forceps and scissors. Each eye was pierced through the cornea with a 25G needle before being fixed whole in 4% PFA at room temperature for 1-2 hours. Following fixation, eyes were washed twice in PBS before being dissected using a Leica dissection microscope. The cornea and iris were removed using forceps and scissors before removing lens along with the sclera from the back of the eye to leave only the retina. The retina was then petaled and placed into an individual well of a 96 well plate.

2.3.4 Immunofluorescent staining of the neonate retina

Retinas were washed in PBS every 15 minutes for 2 hours with rocking before blocking in 0.22um filter sterilised 4% Bovine Serum Albumin (BSA) and 0.5% Triton-X in PBS for 2 hours. Retinas were subsequently incubated for 48 hours with rocking at 4°C in primary antibodies (listed in table Table 3) in 4% BSA and 0.5% Triton-X in PBS.

Following primary antibody incubation, retinas were washed in 0.5% Triton-X in PBS every 30 minutes on rocking platform for 4 hours. Secondary antibodies (listed in table Table 3) along with DAPI 1:1000 in 4% BSA and 0.5% Triton-X in PBS were added and incubated for 48 hours on a rocking platform at 4°C.

Retinas were washed 0.5% Triton in PBS every 30 minutes for 4 hours before being washed in PBS twice. The retinas were then mounted into glass slides with Fluorshield mounting medium (Thermo), topped with a coverslip and sealed using clear nail varnish at room temperature.

2.3.5 Imaging and analysis of the neonate retina

Stained retinae were subsequently imaged on a confocal microscope using 0.5µm Z stacking. Images were exported as LIF files and imported into Image J for image analysis using maximum projection images. Vascular extension, which is the percentage of vascular

front progression towards the retinal periphery, was calculated as described in Figure 2.3 whereby the angiogenic front progression length was divided by the total retina length.

To quantify changes in the vascular network structure, two regions were focused on in the angiogenic retina (Figure 2.4): the angiogenic front (Figure 2.4 B) and the central plexus (Figure 2.4 C). The CD31+ area was calculated as a percentage from these specific regions. The vasculature was manually skeletonised (Figure 2.5) to determine average vessel length in µm as well as vessel node (how many times one vessel contacts another, examples included in Figure 2.5 C, D and E). Vascular density is described as the amount of individual vessel segments per mm^2 retina whereas branch point density per mm^2 was quantified as described in Figure 2.5. Along the angiogenic front, tip cells were counted and displayed as tip cells per mm^2 angiogenic front (Figure 2.6). Finally, endothelial cell number was determined by the number of ERG+ nuclei per mm^2 retina, along with ERG% staining and average nuclei size. Analysis methods were obtained and adapted from Fantin, 2022 (Fantin, 2022).

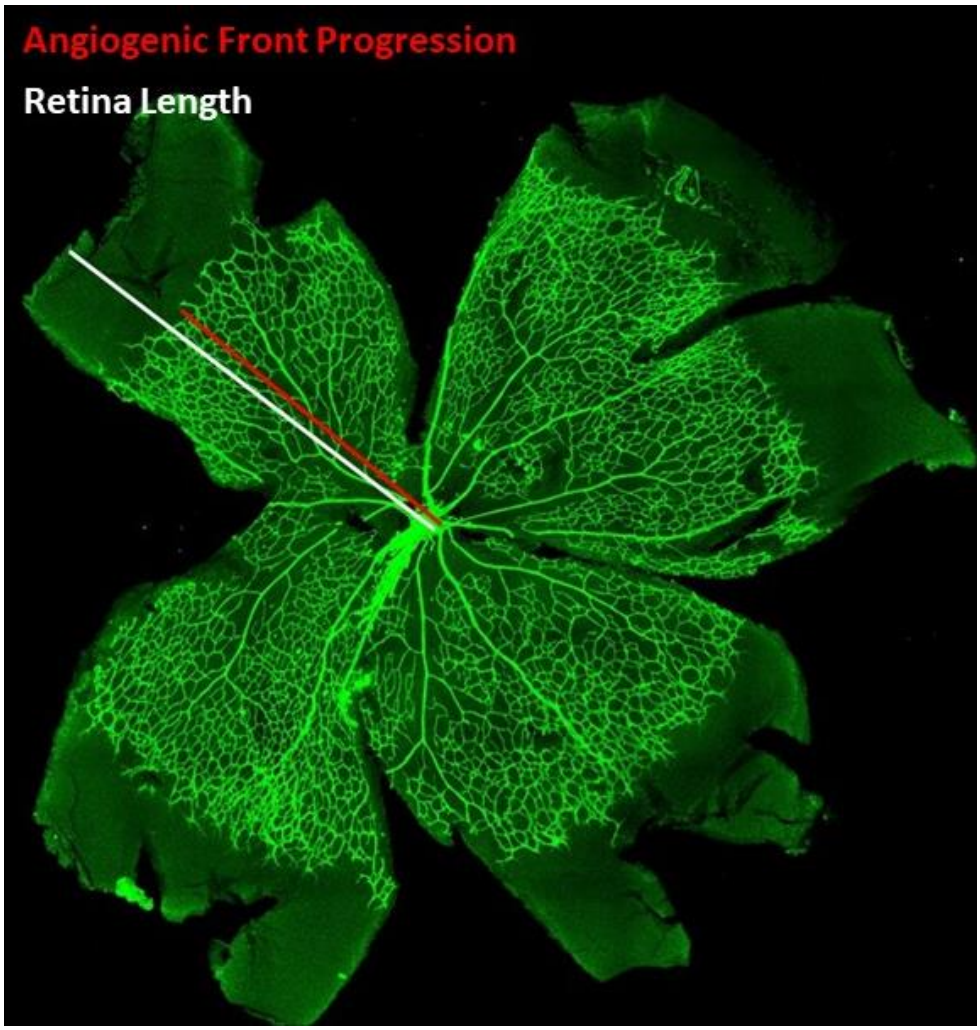

Figure 2.3 Method of vascular extension analysis. *Dissected P5 retina which was flat mount stained for CD31 and imaged on a confocal microscope at 10x magnification. Analysis was done using Image J. Firstly using the line tool was used to calculate the white 'retina length line' length. Secondly it was used to calculate the red angiogenic front progression line. Both originating at the optic nerve point. The percentage of angiogenic front progression was therefore calculated from these lengths.*

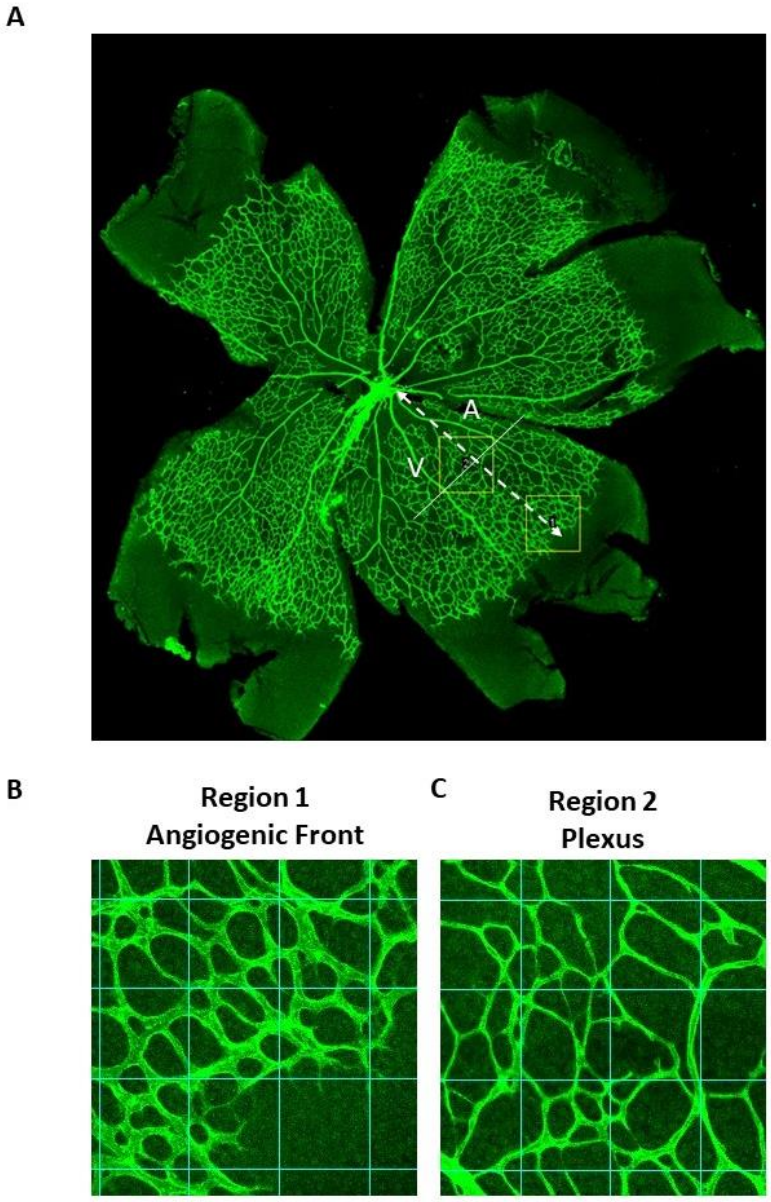

Figure 2.4 Method of isolating regions of the vasculature for structure analysis. ***(A)*** *Dissected P5 retina which was flat mount stained for CD31 and imaged on a confocal microscope at 10x magnification. The angiogenic front is determined at the very edge of the developing plexus as it meets the avascularised area, labelled box 1.* ***(B)*** *Zoomed in gridded version of the angiogenic font.* ***(C)*** *Corresponds to a gridded version of box 2 in image* ***(A)*** *which is selected further back in the developing plexus, roughly equidistant from the angiogenic front and the optic nerve, as well as equidistant from nearby major vessels A (artery) and V (vein).*

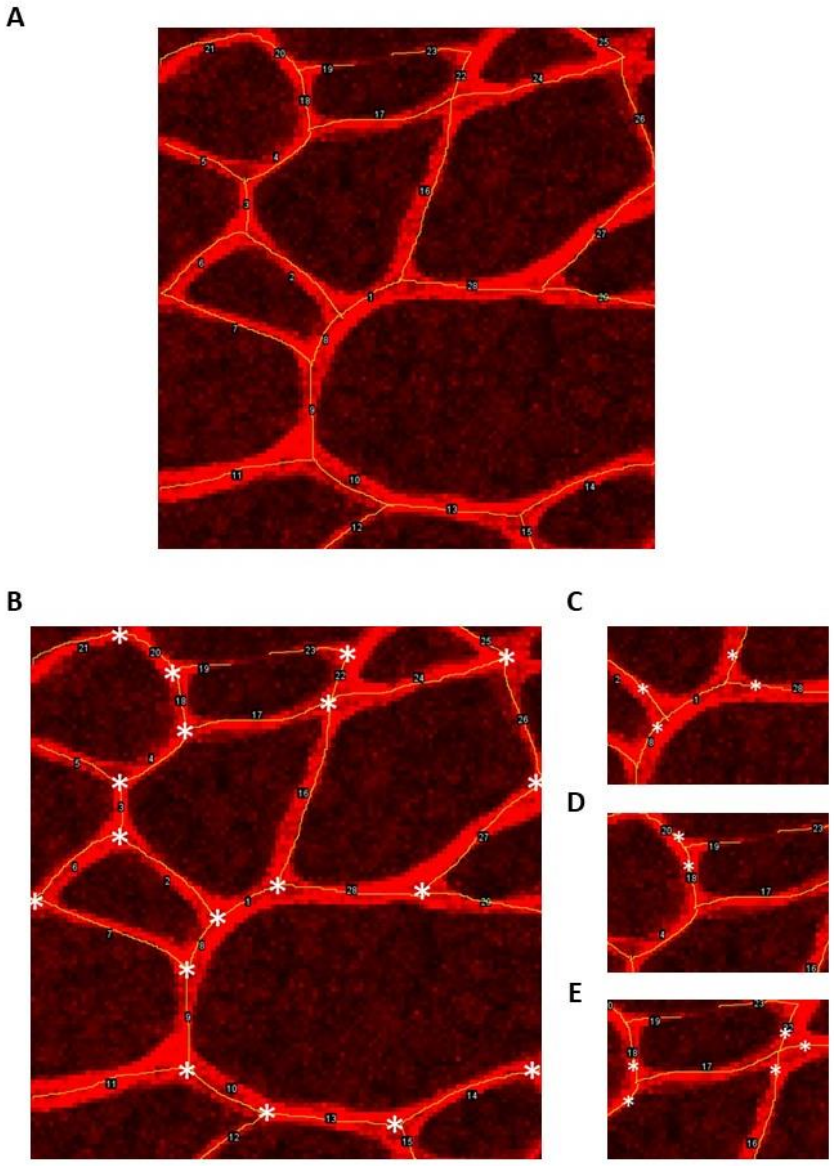

Figure 2.5 Method of skeletonization the vascular network for vessel density, length, node and branch point analysis. (A) *Dissected P5 retina which was flat mount stained for CD31 (now shown in red) and imaged on a confocal microscope at 10x magnification. The network is skeletonised using the free hand line tool on image J, with each vessel segment corresponding to one line. This allows for the measurement of segment length (µm) and vascular density (segment length per mm^2)* ***(B)*** *Branch points are highlighted with a white asterix in order to calculate branch points per mm^2* ***(C)*** *Vessel segment with a node of 4. Vessel segment 1 is attatched to 4 vessels, noted with an asterix. (D) Vessel with a node of 2. Vessel segment 19 is attatched to 2 vessels, noted with an asterix. (E) Vessel with a node of 5. Vessel segment 17 is attatched to 5 vessels, noted with an asterix.*

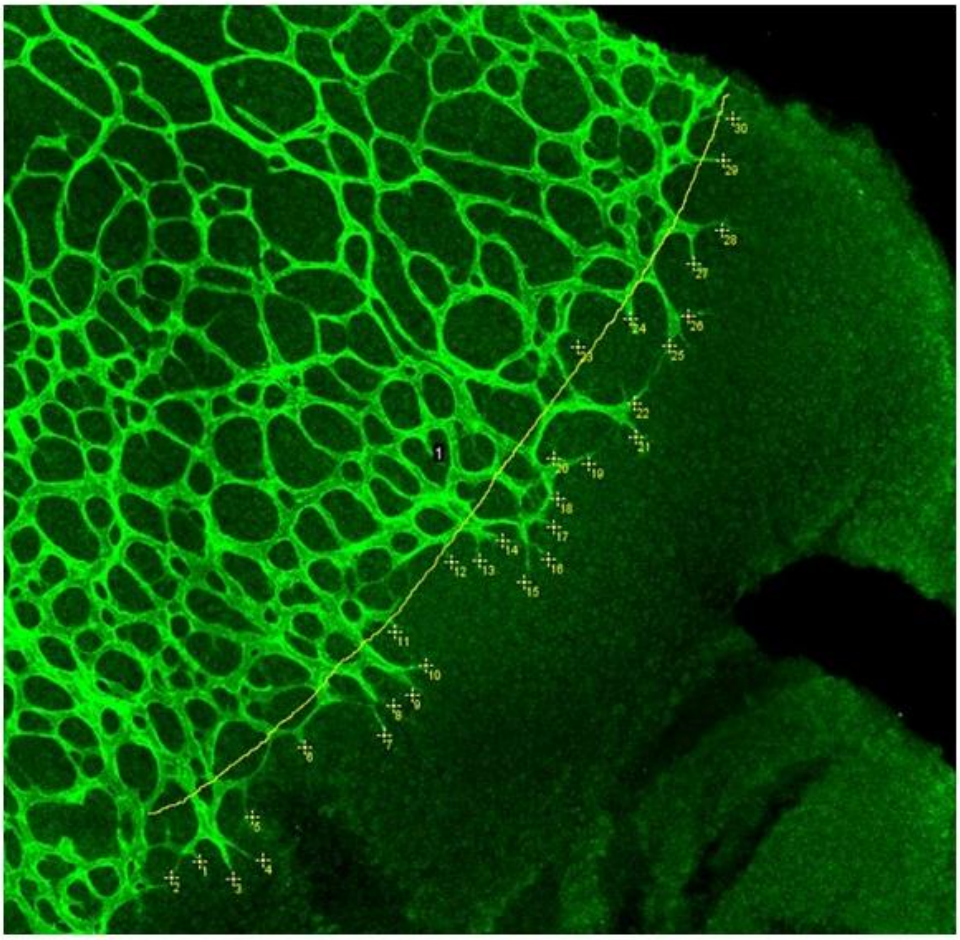

Figure 2.6 Analysis method for calculating tip cell number. *CD31 stained retinal flat mount was imaged on a confocal microscope at 10x magnification and analysed using Image J. Using the free hand line tool, the length of the vascular front was determined, noted as line 1. Individual tip cells were then counted to display tip cells per mm of vascular front.*

2.4 Laser-Induced Choroidal Neovascularization (CNV)

The study timeline can be seen in Figure 2.7. Mixed litters of *ZEB1$^{fl/fl}$cdh5 Cre-ERT2^{+}* and *ZEB1$^{fl/fl}$cdh5 Cre-ERT2^{-}* mice grew until they reached around 8-10 weeks of age. At this time, they both underwent tamoxifen administration via intraperitoneal injection for 5 consecutive days, receiving a dose of 40mg/kg in sunflower oil (described in section 2.2.1). Following dosing, *ZEB1$^{fl/fl}$cdh5 Cre-ERT2^{+}* and *ZEB1$^{fl/f}$ cdh5 Cre-ERT2^{-}* mice are referred to as ZEB1^{iECKO} and control respectively. Post-dosing, the mice underwent a break week in which no further procedures occurred.

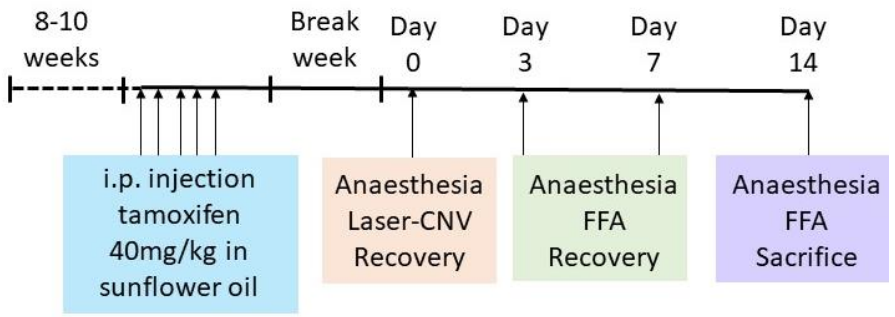

Figure 2.7 A study timeline for ZEB1^{iECKO} and control mice undergoing laser-CNV. *ZEB1$^{fl/fl}$cdh5CRE-ERT2^{+} and ZEB1$^{fl/fl}$cdh5CRE-ERT2^{-} mice are grown until approximately 8-10 weeks of age before receiving daily doses of 40mg/kg tamoxifen in sunflower oil over 5 consecutive days (after which CRE-ERT^{+} and CRE-ERT2^{-} are known as ZEB1^{iECKO} and control respectively). After a break week, mice are anaesthetised before being lasered and recovered on day 9. On days 3, 7 and 14 mice are anaesthetised in order to undergo fundus fluoresceine angiography (FFA) before being recovered, accept from day 14 when mice are sacrificed, and tissue sent for downstream analysis.*

2.4.1 Induction of Anaesthesia

On day 0, anaesthetics were made up by adding 0.125mL ketamine (Ketastet, Zoetis, 100mg/ml stock) and 0.147mL medetomidine (Sedastart, Animalcare Limited, 1mg/mL stock) to 0.728mL sterile water. Mice were weighed before being anaesthetised by i.p. injection of the anaesthetic mix. 100µL of anaesthetic was administered per 25g body weight, which worked out to be the body weight x4 in µL. Once a negative pedal and eye

reflex test confirmed loss of reflexes, the mouse was prepared for laser induction. Whilst under anaesthesia the animal was kept warm using heated pads and the animal's welfare was constantly monitored along with the depth of anaesthesia by the pedal and reflex.

2.4.2 Laser Induction

For laser induction, the Micron IVTM ophthalmoscope (Pheonix Technology Group Inc.) along with the Meridian Merilas Green laser photocoagulator (532nm, class 3b) attachment was used. Prior to induction, the laser wavelength, time and spot size were set to 450mW, 130ms and 50µm.

Unless there were abnormalities, the right eye was always lasered. On two occasions the left eye was lasered due to the mice having an abnormal white right eye. The eye to be lasered was prepared by topically applying one drop of 5% phenylephrine hydrochloride and 0.8% tropicamide to dilate the pupils. Once the pupil had fully dilated, Viscotears was applied to both eyes to allow for easy imaging and to prevent the drying and irritation of the eyes under anaesthetic.

The animal was transferred to the warmed imaging cradle set up with the Micron IVTM ophthalmoscope (Pheonix Technology Group Inc.) with the Meridian Merilas Green laser photocoagulator (532nm, class 3b) attachment. The animal was positioned, and image focused so that the back of the eye was clearly visible on the computer screen and the image centred on the optic disk. Using the guide laser, four laser burns were created approximately equal distance from the optic nerve as well as each other, and between the major vessels within the retina (Figure 2.8 A and B).

2.4.3 Anaesthetic Recovery

For anaesthetic reversal 200µL Atipamezole (Sedastop, Animalcare Limited, 5mg/mL) was diluted in 800µL sterile saline. Mice were injected with 200µL of this 1mg/mL Sedastop in saline via i.p injection, placed in a warmed recovery cage and welfare monitored to ensure timely recovery from the anaesthesia. Mice were monitored within 6 hours of gaining their righting reflex, as well as a full welfare and eye check 24 hours post anaesthesia to ensure appropriate recovery. Animals were closely monitored throughout the remainder of the study.

2.4.4 Fundus Fluorescein Angiography

On days 3, 7 and 14 post-lasering the lasered mice underwent Fundus Fluorescein Angiography (FFA) to observe lesion leakage which is achieved under general anaesthetic. Mice were anaesthetised as previously described in section 2.4.1. Once anaesthesia is achieved one drop of 5% phenylephrine hydrochloride and 0.8% tropicamide is applied topically on the lasered eye in order to dilate the pupil. Once the pupil had fully dilated, Viscotears was applied to both eyes to allow for easy imaging and to prevent the drying and irritation of the eyes under anaesthetic.

The mouse was transferred to the warmed imaging cradle set up with the Micron IVTM ophthalmoscope (Pheonix Technology Group Inc.). The animal was positioned with the lens focused so that the back of the eye was clearly visible on the computer screen to check that there were no abnormalities. The animal then received an i.p. injection of 200µL 10% Sodium Fluorescein whilst the barrier and excitation filters on the Micron were changed to the FITC channel to observe the fluoresceine leakage. Approximately 3 minutes after i.p. injection, images of the lesions were captured using the Micron program (Figure 2.8 C). Lesion size was measured and analysed by drawing round the lesions and measuring their area FIJI. Merged lesions were made note of. Because these were uncommon, they were removed from the analysis.

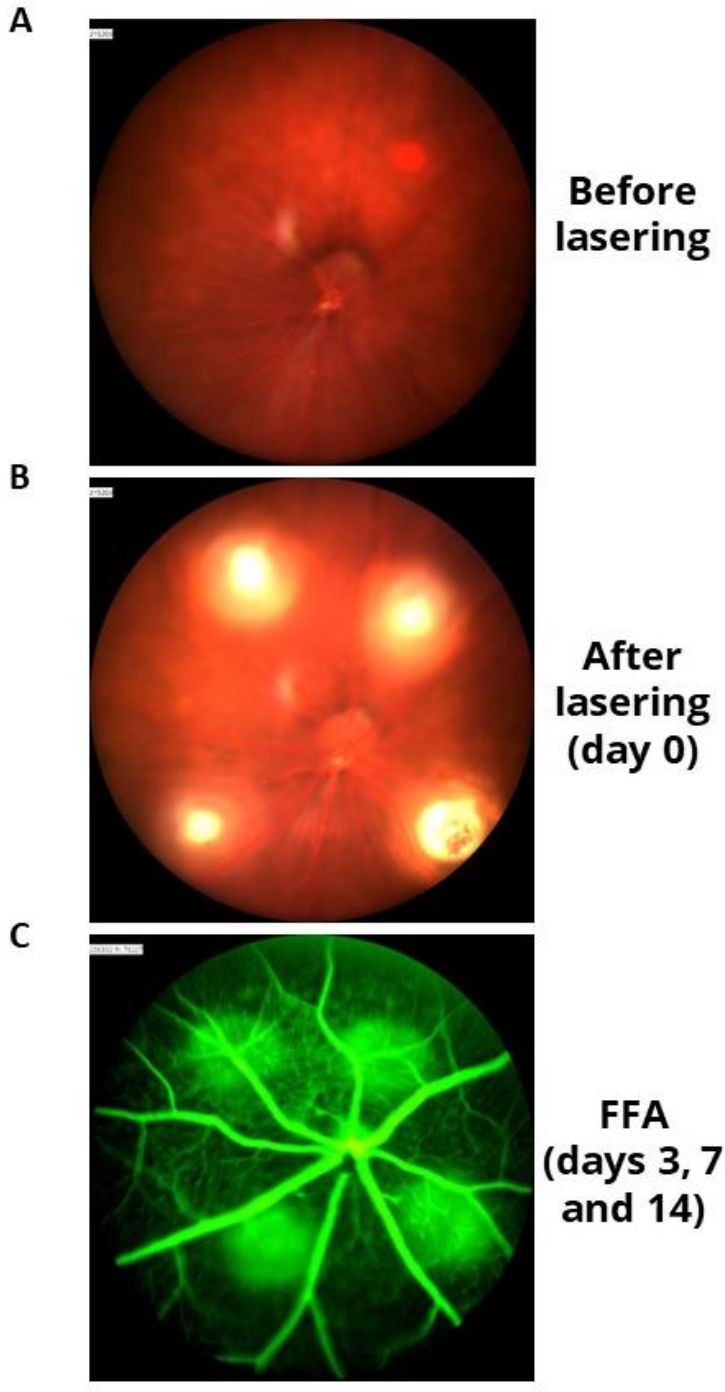

Figure 2.8 Images taken using the Micron IV™ ophthalmoscope (Pheonix Technology Group Inc.). *Images taken using the Micron IV™ ophthalmoscope* ***(A)*** *before lasering,* ***(B)*** *immediately after lasering and* ***(C)*** *fundus fluoresceine angiography (FFA) images take in the days that follow lasering.*

2.4.5 Adverse effects

A small minority of mice experienced adverse effects during initial studies involving tamoxifen dosed mice followed by anaesthesia using Medetomidine and Ketamine. These mice appeared to show signs of ill health 24 hours post anaesthetic recovery from the first instant of anaesthesia. These mice were either culled by schedule 1 cervical dislocation or found dead and reported to the home office. On post-mortem examination these mice had pale kidneys along with a full and inflamed bladder, as well as crystals in the bladder (identified by Dr Nick-Beazley Long). From this, the decision was taken to introduce a break week between tamoxifen dosing and any form of anaesthesia. Since then, there have been no adverse effects of this kind.

2.4.6 Staining of whole-mount choroids

On day 14 post-lasering, mice were culled via cervical dislocation and death confirmed by the permanent disruption of blood flow before tissue taken for staining and further analysis.

2.4.6.1 Dissection and Fixation

The lasered eye was removed and fixed whole in room temperature 4% PFA for one hour. The eyes were washed twice with PBS before being dissected using a dissection microscope (Leica) and dissection tools. Any fatty or connective tissue behind the eye was gently removed before piercing the cornea to allow removal of the cornea and iris using scissors. The choroid was then petalled to allow for flat mounting and the retina removed. The choroid was then stored in PBS until staining.

2.4.6.2 Staining of Choroid Flat Mounts

Choroids were washed in PBS every 15 minutes for 2 hours with rocking before blocking in 0.22µm filter sterilised 4% Bovine Serum Albumin (BSA) and 0.5% Triton-X in PBS for 2h. Choroids were subsequently incubated for 48 hours at 4°C with rocking in primary antibodies (listed in table Table 3) in 4% BSA and 0.5% Triton-X in PBS.

Following primary antibody incubation, choroids were washed in 0.5% Triton-X in PBS every 30 minutes on rocking platform for 4 hours. Secondary antibodies Anti-Rat Alexa Fluor 488 and Anti-Rabbit Alexa Fluor 555 were diluted in 1:500 along with DAPI 1:1000 in

4% BSA and 0.5% Triton-X in PBS were added and incubated for 48 hours on a rocking platform overnight at 4°C.

Choroids were washed 0.5% Triton in PBS every 30 minutes for 4 hours at room temperature before being washed in PBS twice. Choroids were then mounted into glass slides with Fluorshield mounting medium (Thermo), topped with a coverslip and sealed using clear nail varnish. Slides were then stored at 4°C. Lesions were imaged using a Leica TCS SPE Confocal Microscope. An 8x8 tilescan of the Choroid was taken at 20x magnification. CD31 lesion size as well as CD45 inflammation intensity within the lesion was analysed using image J by drawing round the lesions.

2.5 Hind Limb Ischaemia surgery (HLI)

The HLI method used within this thesis from of a protocol published by Bhalla et al (Bhalla et al., 2022). A full study timeline along with images of the surgery can be seen in Figure 2.9.

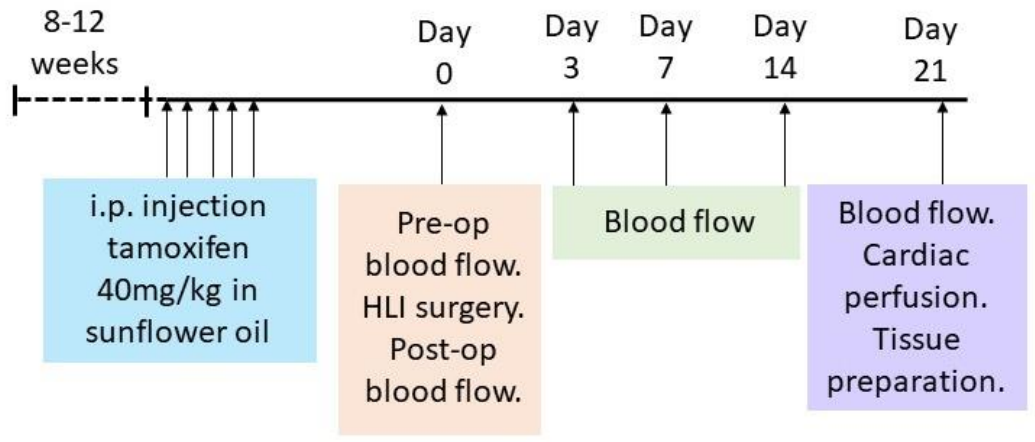

Figure 2.9 A study timeline for ZEB1^{iECKO} and control mice undergoing HLI. *ZEB1$^{fl/fl}$cdh5CRE-ERT2$^{+/-}$ and ZEB1$^{fl/fl}$cdh5CRE-ERT2$^{-/-}$ mice are grown until approximately 8-12 weeks of age before receiving daily doses of 40mg/kg tamoxifen in sunflower oil over 5 consecutive days (after which CRE-ERT^{+} and CRE-ERT2^{-} are known as ZEB1^{iECKO} and control respectively). Mice are anaesthetised before pre-operative blood flow measurements, followed by surgery and post op blood flow measurements. On days 3, 7, 14 and 21 mice are anaesthetised in order to undergo blood flow imaging. On day 21 the mice are perfused fixed, and tissue prepared for staining.*

2.5.1 HLI surgery

Mixed litters of *ZEB1$^{fl/fl}$cdh5 Cre-ERT2^{+}* and *ZEB1$^{fl/fl}$cdh5 Cre-ERT2^{-}* mice were grown until they reached around 8-12 weeks of age. At this time, both groups underwent tamoxifen administration via intraperitoneal injection for 5 consecutive days, receiving a dose of 40mg/kg in sunflower oil (described in section 2.2.1). Following dosing, *ZEB1$^{fl/fl}$cdh5 Cre-ERT2$^{-/+}$* and *ZEB1$^{fl/fl}$cdh5 Cre-ERT2$^{-/-}$* mice are referred to as ZEB1^{iECKO} and control respectively.

Post-tamoxifen dosing, all mice were checked to ensure no signs of ill health before undergoing HLI surgery. All surgeries were performed start to finish by either Dr Sohni Ria Bhalla or Dr Mussarat Wahid. ZEB1^{iECKO} and control mice were placed under general anaesthesia via gaseous 2% isoflurane (100%, w/w, IsoFlo ®) in 100% oxygen at a flow rate of 2L/minute. Pre-operative blood flow to both paws was then determined by using the laser speckle imaging system (FLPI-2, Moors Instruments). Before commencing the surgery, the withdrawal reflexes were tested to confirm no response and throughout the surgery the body temperature of the mouse was monitored and controlled via a rectal probe and heat mat (Harved Apparatus).

All mice received pre-operative analgesic by the subcutaneous injection of 0.05mg/kg buprenorphine (Animalcare Group) diluted in sterile saline (0.9% NaCl). Preparation of the left hind limb surgical area was achieved by application of hair removal cream (Nair) before being sterilised using the hydrex derma spray (Scientific Laboratory Supplies). The mouse was then placed on the surgical platform with the left hind paw taped into position and covered in a surgical drape to leave only the surgical area exposed.

After depilation and sterilisation of the surgical site, an incision was made between the knee and the abdomen, and the femoral artery was exposed. Two individual sutures were placed around the femoral artery, the first being placed above the superficial epigastric artery, and the second being placed below the epigastric artery and the saphenous artery, followed by electrocoagulation of the femoral artery using a cauterizer (Wuhan Spring Scenery Medical Instrument Co Ltd, Evergreen). Images of the surgery process can be observed in Figure 2.9, taken from (Bhalla et al., 2022)

Post-surgery animals were closely monitored to ensure they recovered well. Animals were allowed to recover in a pre-warmed post-operative cage with fresh bedding and mash. For the first few hours' post-surgery the animals were observed to ensure they recovered from the anaesthesia well and showed no signs of pain or suffering. For the immediate 7 days post-surgery, the weights as well as general health and wellbeing of the animals were monitored twice a day, along with the surgery site, paws and tail to ensure there were no adverse effects. The welfare checks were reduced to weekly after this period unless there was cause for concern.

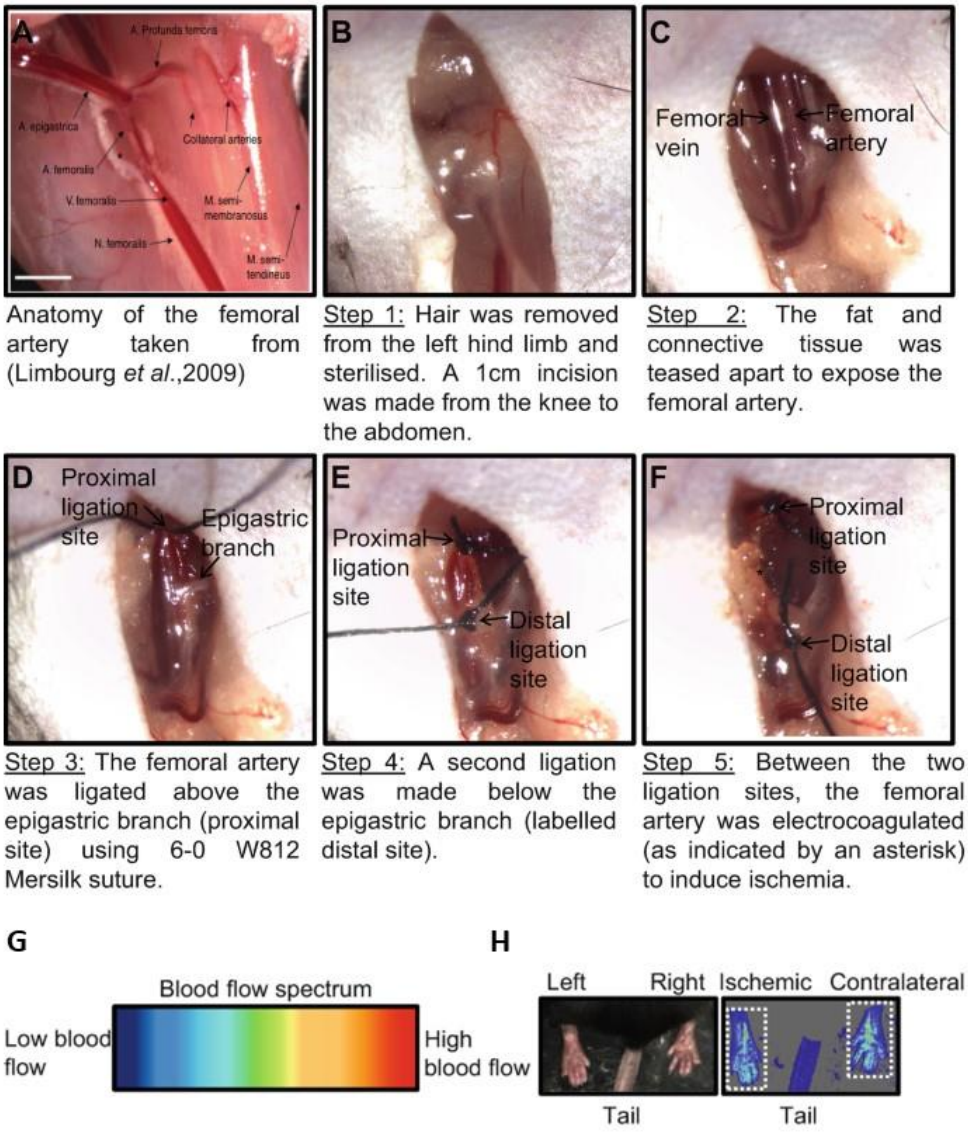

Anatomy of the femoral artery taken from (Limbourg *et al*.,2009)

Step 1: Hair was removed from the left hind limb and sterilised. A 1cm incision was made from the knee to the abdomen.

Step 2: The fat and connective tissue was teased apart to expose the femoral artery.

Step 3: The femoral artery was ligated above the epigastric branch (proximal site) using 6-0 W812 Mersilk suture.

Step 4: A second ligation was made below the epigastric branch (labelled distal site).

Step 5: Between the two ligation sites, the femoral artery was electrocoagulated (as indicated by an asterisk) to induce ischemia.

Figure 2.10 HLI surgery and blood flow speckle intensity images, taken from (Bhalla et al 2021). (A) – (F) *images of HLI surgery taken from Bhalla et al, except for (A) taken from Limbourg et al 2009.* ***(G)*** *The level of blood flow is representative of the intensity of the spectrum.* ***(H)*** *Example of blood flow images pre-surgery, with the white box indicating the region of interest (ROI) used to calculate blood flow via speckle intensity. Post-surgery the left paw will become ischaemic.*

2.5.2 Measurement of blood flow

All blood flow measurements and subsequent analysis were performed by Dr Nick Beazley-Long. Blood flow measurements of the hindlimb paws were performed on days 3, 7, 14 and 21 post surgery. Prior to imaging all animals were welfare checked. Mice were anaesthetised with 2% Isoflurane (100% w/w, IsoFlo®) in 100% oxygen at a flow rate of 2L/minute. Withdrawal reflexes were tested using the toe pinching and eye twitching reflex to confirm stable anaesthesia before being transferred to the heat pad and imager. Blood flow images were taken using the Moors Laser Speckle Imaging System. To determine blood flow, the speckle intensity within the region of interest was measured and calculated by the Moors Instrument Analysis software. Animals were allowed to recover from anaesthetic in a pre-warmed cage before being transferred back to its home cage once a full recovery was observed.

2.5.3 Euthanasia via Cardiac Perfusion

Immediately after imaging on day 21, the mice were not allowed to recover from anaesthia. Animals received an i.p. injection of 1mg/kg medetomidine and 75mg/kg ketamine. 3-4 minutes post i.p. injection the animal was removed from the isoflurane nose cone and depth of anaesthesia was tested for by the toe pinching and eye twitching reflex. Once stable anaesthia was confirmed, the chest cavity of the animal was opened using scissors and held by gripped forceps. The left ventricle was pierced using a 30G needle attatched to a syringe with 25mL PBS. Immediately after this the vena cava was cut using scissors and the 25mL PBS slowly pushed through into the heart of the mouse. More PBS was added to the syringe until the PBS exiting from the mouse ran clear. This was then followed by 25mL paraformaldehyde. Cardiac perfusion was performed by either the author or Dr Nick Beazley-Long (see COVID statement in section 7.7.1).

Both hind legs were removed from the carcass and gastrocnemius muscle dissected and fixed in 4% PFA overnight. The following day the muscle was washed 3-4 times with PBS before being stored in 30% sucrose overnight for cryoprotection. The following day the muscle was removed from the sucrose and embedded in optimal cutting temperature compound (OCT, Labtech) and immediately stored at -80°C.

2.5.4 Sectioning of gastrocnemius muscle

Gastrocnemius muscle embedded in OCT was removed from the -80°C and immediately placed into the cryostat chamber held at -20°C for approximately 30 minutes. The muscle was mounted onto the chuck to ensure transverse sections were to be produced. Multiple 16μm sections were generated on each superfrost plus slide (Thermo Scientific) from different regions along the muscle. Slides were stored at -20°C or immediately taken for staining.

2.5.5 Immunofluorescence staining of gastrocnemius muscle

Before staining the muscle, sections were drawn around using a hydrophobic PAP pen (Scientific Laboratory Supplies). All staining steps were performed in a dark staining tray with humidity. The sections were dehydrated by washing each section with PBS 3 times for 5 minutes. Sections were blocked and permeabilised using filter sterilised 4% BSA and 0.5% Triton-X in PBS for 2h at 4°C. Primary antibodies were then diluted according to Table 3 in filter sterilised 4% BSA and 0.5% Triton-X in PBS and incubated at 4°C overnight. The following day the sections were washed in PBS 3 times for 5 minutes before being incubated in secondary antibody diluted in filter sterilised 4% BSA and 0.5% Triton-X in PBS according to Table 3 along with DAPI (1:1000) overnight at 4°C. The following day the sections were washed with PBS 3 times for 5 minutes before removal of all PBS using the edge of a kimtech wipe. Coverslips were mounted onto the sectioned with Fluorshield mounting medium (Thermo) and sealed using clear nail varnish at room temperature in the stain tray without humidity for 20 minutes. Slides were then stored at 4°C or imaged immediately.

2.5.6 Confocal microscopy and image analysis of gastrocnemius muscle

Immunofluorescent stained gastrocnemius muscle slides were imaged using the Leica TCS SPE Confocal Microscope at 20x magnification. For each gastrocnemius muscle (both contralateral and ischaemic) 4 sections were taken, and a 3*3 tile scan was taken of each section for analysis. Quantification of staining was achieved using Image J. Measurements of both staining area and number of stained structures were quantified and normalised to muscle fibre area.

2.6 Protein based assays

Protein was extracted from cultured primary endothelial cells. Cells for experiments were seeded into 6cm diameter dishes for protein extraction at the experiment's end point.

2.6.1 Cell Lysis

Cultured cells were removed from the incubator and immediately placed on ice. Media was removed before two PBS washes with ice cold PBS. 150µL RIPA buffer (Thermo) supplemented with Protease and Phosphatase cocktail inhibitors (Roche) was added to each 60mm diameter dish, unless stated otherwise. The cells were the lysed via scrapping with the RIPA buffer on ice for approximately 5 minutes before being transferred into an Eppendorf tube and incubated on ice for 30 minutes. The lysate was then centrifuged at 16,000 x g at 4°C for 20 minutes to pellet cellular debris. The remaining supernatant was then stored at -80°C.

2.6.2 Protein quantification

The protein concentration of cell lysates was determined via Pierce BCA assay (Thermo). A range of protein standards were made by serial dilution of BSA in PBS within a range of 2000µg/mL and 0µg/mL. Cell lysates were diluted between 1:5-1:10 in RIPA buffer to ensure they fell within the linear range of the standards. BCA working reagent was prepared using a 50:1 ratio of reagent A and reagent B respectively. 200µL of BCA working reagent plus 25µL of either sample or standard was placed in one well of a 96 well plate. Three technical repeats were set up per sample or standard. The plate was incubated at 37°C before absorbance being read at 562nm using a plate reader (BMG LABTECH). The blank reading was subtracted from all readings. The protein concentration of the samples was determined from the standard curve calculated from the protein standards and their absorbances using Microsoft Excel™.

2.6.3 SDS-PAGE

Samples were diluted with PBS according to the BSA results previously to ensure they were all at the same concentration before the addition of 4x Laemelli buffer (BioRad) that was supplemented with Beta-mercaptoethanol. Samples were heated to 95°C for 8 minutes followed by sonicating for 15 minutes using a water bath sonicator filled with ice and

water. Samples were briefly centrifuged before 10-50µg of protein from each sample was loaded onto a pre-cast 5-20% gradient gel (BioRad) along with 2µL precision plus protein ladder (BioRad). The gel was run at 80V for approximately 2.5 hours at room temperature in TGS running buffer (25nM tris-base, 190nM glycine and 0.1% SDS, pH adjusted to 8.3).

2.6.4 Transfer and Blocking

The proteins were transferred onto a nitrocellulose membrane using the trans-blot turbo transfer system (BioRad). This was achieved using the mixed molecular weight pre-setting and using trans-blot turbo transfer buffer (BioRad) supplemented with 20% ethanol. The membrane was then blocked in 5% BSA (Sigma-Aldich) in TBST (Tris buffered saline with 0.1% tween-20) for 1.5 hours at room temperature on an orbital shaker.

2.6.5 Western Blotting

Primary antibodies were made up in 1% BSA in TBST according to Table 3 before being added to the membrane in a 50mL falcon and incubated overnight rolling at 4°C. The following day the membrane was washed with TBST three times for 10 minutes. Secondary antibodies with fluorescent conjugates were made up in 1% TBST according to table Table 3 before being added to the membrane and incubating for 1 hour, rolling at room temperature in darkness. This was followed by three 10-minute TBST washes in darkness before the membrane was imaged using the Licor Odyssey imaging system.

2.6.6 Stripping and re-probing

Nitrocellulose membrane that had already been probed was stripped of its bound antibodies by the addition of 0.4M NaOH (Sigma Aldrich) for 5 minutes on an orbital shaker, before two washes in TBST to remove any excess NaOH. The membrane was re-blocked in 5% BSA in TBS-t before the addition of primary antibodies as described above to probe for another protein.

2.7 RNA based assays

RNA was isolated from both *in vitro* cultured primary endothelial cells and *ex-vivo* extracted lung tissue. Cultured endothelial cells were washed with sterile PBS before detaching using Trypsin/EDTA at a ratio of 0.04%/0.03% and pelleted at 200xG ready for

RNA extraction. Unless stated otherwise, all *ex-vivo* RNA extraction occurred on cells extracted via magnetic cell sorting before being pelleted at 200xG.

2.7.1 RNA extraction

All RNA extraction was achieved using the QIAGEN RNeasy kit unless stated otherwise. The cell pellet was resuspended in 350µL RLT buffer along with 350µL 70% ethanol before being transferred into a QI-shredder column. The column was centrifuged at 8000xG for 15 seconds and the flow through discarded. The column was washed by the addition of 700µL RW1 buffer, centrifuged at 8000xG for 15 seconds and flow through discarded. 500µL RPE buffer was added to the column before being centrifuged at 8000xG for 15 seconds and flow through discarded, before this step being repeated again for a longer centrifuged time of 2 minutes. The membrane was dried by further centrifugation of the column alone with no buffer additions at 16,000xG for 1 minute. To elute the RNA, 30µL RNAase free water was added directly to the column before being centrifuged at 8000xG for 1 minute. The concentration and quality of the eluted RNA was then determined by NanoDrop™ (ThermoFisher Scientific). All RNA was stored at -80°C.

2.7.2 DNAse treatment

RNA was DNAse treated using the Promega RQ1 RNase-Free DNase kit. Unless stated otherwise, 2µg RNA along with 2µL DNAse buffer and 2µL DNAse made up to a total volume of 18µL with RNAse free water was incubated in a thermocycler at 37°C for 30 minutes. 2µL DNAse stop solution was added followed by incubation in a thermocycler at 65°C for 10 minutes.

2.7.3 cDNA synthesis

2µg DNAase treated RNA in 20µL total volume was taken forward for reverse transcription using the Takara PrimeScript RT Master Mix kit. Unless stated otherwise, µL of master mix was added to the 2µg DNAse treated RNA before being incubated in a thermocycler for 37°C for 15 minutes, followed by 85°C for 5 seconds. cDNA was stored at -20°C.

2.7.4 Digital Droplet PCR (ddPCR)

Between 50ng-320ng cDNA was taken forward for digital droplet PCR. Each reaction was set up with either 2x digital droplet master mix or 4x digital droplet master mix (BioRad),

along with 10x TaqMan probe listed in table Table 1, and made up with water to make a final reaction volume of 25µL. Droplets were generated using the droplet generator (BioRad) with 70µL droplet generator oil (BioRad). The samples were then placed in a thermocycler for 10 minutes at °C, followed by 40 cycles of 30s and 95°C and 1 minute of 60°C, finally followed by 98°C for 10 minutes as a final extension. Droplets were read using the QX100 Droplet Reader (BioRad).

Table 1 ddPCR probes

Probe Target	Supplier
ZEB1 (Human)	Thermo Fisher
TBP (Human)	Thermo Fisher
ZEB1 (Mouse)	Thermo Fisher
CD31 (Mouse)	Thermo Fisher
GAPDH (Mouse)	Thermo Fisher

2.7.5 RNA sequencing

Untreated RNA was sequenced using Illumina sequencing by Novogene. Analysis of the raw data was all performed by Jospeh Horder unless stated otherwise. To check the quality of the FASTQ files and identify adaptors, FASTQC program was used. The Cutadapt program was used to trim illumine universal adaptors for both forward and reverse strands. Bases with a quality of less than 20 were removed. Alignment of the trimmed reads to the human genome GRCh38 was performed using STAR, followed by the featuredCounts package to quantify the reads to the gene. The read counts were normalise and differential expression analysis was achieved using DESeq2. Genes with an adjusted p value smaller than 0.05 were considered significant.

Overrepresentation analysis to identify significant gene ontology (GO) terms biological processes, molecular functions and cellular components, along with Kyoto Encyclopaedia of Genes and Genomes (KEGG) significant pathway analysis (performed by the author). Figures were generated using GraphPad prism (performed by the author).

2.7.5.1 Analysis of publicly available data sets

Publicly available data sets were identified using Gene Expression Omnibus. Data were pre-filtered using an adjusted p-value threshold of Adjp > 0.05. Log2 fold changes (L2FC) were subsequently retained for analysis (data extracted by Dr Michaela Griffin). Pathway enrichment was performed using CytoScape to conduct global pathway analysis, facilitating the identification of key biological processes and molecular networks.

2.8 Chromatin Immunoprecipitation (ChIP)

ChIP was achieved using the Active Motif ChIP-IT High Sensitivity kit. Unless otherwise stated, the buffers are provided in the kit and the makeup of all buffers are stated in Table 2. HUVECs between passages 2-7 were plated in 150mm dishes with 20mL complete media and allowed to grow until they had reached 100% confluency before being taken forward for ChIP.

2.8.1 Cell Fixation

Cells were fixed by adding 2mL Complete Cell Fixation Solution directly to the culture media of each 150 mm diameter dish and rocked gently at room temperature for 15 minutes. To stop the fixation 1.1mL Stop Solution was added directly to each dish and rocked at room temperature for 5 minutes. Cells were detached from the dish by scraping with a rubber policeman before being pelleted by centrifuging at 1,250xG at 4°C for 3 minutes. The supernatant was discarded, leaving the pellet to be resuspended in 10mL ice cold PBS Wash Buffer before centrifugation at 1,250xG at 4°C twice. The cell pellet was then kept on ice.

2.8.2 Chromatin Preparation

The cell pellet was resuspended in 5mL Chromatin Prep Buffer with 5µL Protease Inhibition Cocktail and 5µL 100mM PMSF before being incubated on ice for 10 minutes. Cell lysis was achieved by transferring the pellet to a chilled dounce homogeniser and completing 30 strokes before being centrifuged at 1,250xG for 3 minutes at 4°C. The pellet was then resuspended in 500µL ChIP buffer with 5µL Protease inhibitor cocktail and 5µL 100mM PMSF before being incubated on ice for 10 minutes and proceeding to chromatin shearing.

2.8.3 Chromatin Shearing via Sonication

Chromatin was sheared using the Bioruptor® Cooled Sonicator (Diagenode) at 4°C for 35 rounds of 30 seconds on and 30 seconds off. Chromatin was then centrifuged at 16,000xG at 4°C for 2 minutes to pellet cellular debris. 25µL of the remaining supernatant was then taken to assess chromatin preparation and shearing whilst the remaining chromatin was stored at -80°C.

2.8.4 DNA gel to Monitor Chromatin Preparation and Shearing

175µL TE buffer at pH 8.0 and 1µL RNAse A was added to the 25µL sheared chromatin before being incubated in a thermocycler at 37°C for 1 hour. 2µL of Proteinase K was then added before being incubated in a thermocycler at 37°C for 2 hours. The chromatin mixture is then transferred to a new Eppendorf tube along with 83µL Precipitation Buffer, 2µL Carrier and 750µL absolute ethanol before being stored at -80°C overnight to precipitate the DNA.

The following day the sample was centrifuged at 16,000xG for 15 minutes at 4°C to pellet the DNA before discarding the supernatant and air drying the pellet for 10-15 minutes. The DNA pellet was then resuspended in 25µL DNA purification elution buffer, incubated at room temperature for 10 minutes and vortexed to ensure the pellet is completely resuspended in solution. The concentration of the DNA was then analysed by absorbance at 260nm via nanodrop.

500ng of input DNA was mixed with 1µL 500mM NaCl and adjusted to 10µL with sterile water before being placed in a thermocycler at 100 °C for 20 minutes, followed by 50°C for 5 minutes. Samples were mixed with gel loading buffer before being loaded onto a 2% agarose gel with ethidium bromide (Sigma) and ran at 120V for 5-10 minutes. The gel was imaged using gel imager (Licor).

2.8.5 Immunoprecipitation of Chromatin

Each immunoprecipitation reaction was set up with 4µg ZEB1 primary antibody (Proteintech) or 4µg rabbit IgG control, 5µL protease inhibitor cocktail, 5µL Blocker Mix, approximately 10µg sheared chromatin and topped up to 200µL with ChIP buffer. This reaction mixture was placed in an end-to-end rotator overnight at 4°C.

Protein G agarose beads were pre-washed by mixing equal amounts of TE pH 8.0 buffer to beads and centrifuging at 1,250xG to pellet beads and remove supernatant. This process was repeated twice. 30µL of Protein G beads were added to each immunoprecipitation reaction and placed in and end-to-end rotator for 3 hours at 4°C. 600µL ChIP buffer was added to the immunoprecipitation reaction before adding the entire contents to a ChIP filtration column. Flow through was allowed to occur by gravity and was discarded. The columns were then washed with 900µL Wash Buffer AM1 for a total of 5 times before being centrifuged at 1250xG for 3 minutes to remove residual wash buffer. The sample was eluted by adding 50µL 37°C Elution Buffer AM4 to the column, incubated at room temperature for 5 minutes before being centrifuged at 1250xG for 3 minutes and then taken for DNA purification.

2.8.6 DNA purification

2µL of Proteinase K was added to the eluted ChIP DNA and placed in a thermocycler for 30 minutes at 55°C followed by 2 hours at 80°C. To confirm the pH of each sample was correct, 500µL DNA purification buffer and 5µL 3M Sodium Acetate was added to each sample and the correct pH was confirmed by a bright yellow colour.

Each sample was added to a DNA purification column before being centrifuged at 1250xG rpm for 1 minute and the flow through discarded. 750µL DNA Purification Wash Buffer (80% Ethanol) was added to each column before being centrifuged at 1250xG for one minuet then two minutes to dry the membrane and flow through discarded. The purified DNA was then eluted from the column by adding 36µL of DNA Purification Elution Buffer pre-warmed to 37°C directly to the column and centrifuging at 1250xG for 1 minute.

2.8.7 ChIP sequencing

Purified ChIP DNA was sent to Novogene for Illumina sequencing. Unless stated otherwise, analysis of the raw data files was all completed by Joseph Horder using R studio. To check the quality of the FASTQ files and identify adaptors, FASTQC program was used. The Cutadapt program was used to trim illumine universal adaptors for both forward and reverse strands. Bases with a quality of less than 20 were removed and the minimum read length set to 1. Bowtie2-build was used to index human genome GRCh38 followed by Bowtie2 to align samples to this genome. SAM files were converted to BAM files using the

Samtools program. The Sambamba markup program was used to sort and filter duplicate reads followed by Sambamba view to remove unmapped and multi-mapped reads. Reads aligned against known blacklist regions of the genome were removed using Bedtools intersect.

The ENCODE analysis pipeline was followed with a less stringent -p 1e-3 significance cut off to handle replicates within the IDR program. The MACS2 program was used for peak calling on individual ZEB1 replicates against the combined control replicates. The quality of the ChIP-Seq analysis was determined by the ChIPQC program. The two replicates with the highest read within the peaks percentage calculated by ChIPQC were used as the IDR program takes only 2 replicates. The IDR program was run with default settings to identify reproducible peaks and peaks passing the IDR cut off of 0.05 were identified. Peaks were annotated to genes by the ChIP seeker R package with promotor regions defined as 1000bp up or downstream of the transcription start site. Motif enrichment analysis was performed using HOMER.

The annotated ChIP-Seq genes and the RNA-Seq differentially expressed genes were cross referenced in R studio. Overrepresentation analysis to identify significant gene ontology (GO) terms biological processes, molecular functions and cellular components, along with Kyoto Encyclopaedia of Genes and Genomes (KEGG) significant pathway analysis (performed by the author). Figures were generated using GraphPad prism (performed by the author).

2.9 Statistical analysis

All statistical analysis, unless stated otherwise, were performed using Graph Pad Prism 10 software. Specific statistical analyses methods are mentioned for each individual experiment within its figure legends. A p value smaller than 0.05 was considered significant. Biological repeats are noted within each figure legend as n.

2.10 List of Buffers

Table 2 List of Buffers

Buffer Name	Method	Buffer Contents
PEB Buffer – 50mL	Magnetic Cell Sorting – Section 2.2.2	0.5g BSA, 200µL 500mM EDTA, 50mL PBS
Complete Cell Fixation Solution – 2.5mL	ChIP using Active Motif ChIP-IT High Sensitivity Kit – Section 2.8	180µL Fixation Buffer (provided), 750µL 37% formaldehyde, 1.57mL sterile water
PBS Wash Buffer – 25mL	ChIP using Active Motif ChIP-IT High Sensitivity Kit – Section 2.8	2.5mL 10x PBS (provided), 1.25mL Detergent (provided), 21.25mL sterile water
DNA Purification Wash Buffer (80% Ethanol) – 50mL	ChIP using Active Motif ChIP-IT High Sensitivity Kit – Section 2.8	40mL 100% Ethanol and 10mL DNA Purification Buffer

2.11 Antibodies and stains

Table 3 A list of antibodies and stains along with their uses and dilutions

Target	Primary/ Secondary	Dilution	Animal/ Conjugate	Supplier	Use
Isolectin B4 (iB4)	Stain (Primary)	1:100	Streptavidin	Sigma Aldrich	HLI staining
Alpha Smooth Muscle Actin	Primary	1:100	Cy3	Sigma Aldrich	HLI staining
mCD45	Primary	1:100	Goat	R&D Systems	HLI staining and whole mount choroid staining
mCD31	Primary	1:100	Rat	BD Bioscience	Whole mount retina staining and whole mount choroid staining

ERG	Primary	1:100	Rabbit	Abcam	Whole mount retina staining
Streptavidin 488	Secondary	1:500	Alexa Fluor 488	Invitrogen	HLI staining
Anti-rat 488	Secondary	1:500	Alexa Fluor 488	Invitrogen	Whole mount retina staining
Anti-goat 555	Secondary	1:500	Alexa Fluor 555	Invitrogen	HLI staining and whole mount choroid staining
Anti-rabbit 555	Secondary	1:500	Alexa Fluor 555	Invitrogen	Whole mount retina staining
ZEB1	Primary	1:1000	Rabbit	Proteintech	Western Blot, ChIP
FOXO1	Primary	1:1000	Rabbit	Cell Signalling	Western Blot
PFKFB3	Primary	1:1000	Rabbit	Cell Signalling	Western Blot
VECAD	Primary	1:1000	Rabbit	Abcam	Western Blot
Phosphor-VECAD (pY321)	Primary	1:1000	Rabbit	Sigma Aldrich	Western Blot
Slug	Primary	1:1000	Rabbit	Abcam	Western Blot
β actin	Primary	1:1000	Mouse	Santa Cruz	
Vinculin	Primary	1:5000	Rabbit	Cell Signalling	Western Blot
IRDye® 800CW Goat anti-Rabbit	Secondary	1:5000	IRDye® 800CW	LI-COR	Western Blot
IRDye® 680CW Goat anti-Mouse	Secondary	1:5000	IRDye® 680CW	LI-COR	Western Blot

Chapter 3:

Identification of ZEB1 as a regulator of endothelial cell gene transcription *in vitro*

3 Identification of ZEB1 as a regulator of endothelial cell gene transcription *in vitro*

3.1 Introduction

Resting endothelial cells (ECs) under physiological conditions are mostly in a quiescent state. This state is represented as a structured monolayer with apical basal polarity, whist displaying little or no proliferation, no migration, low inflammatory marker expression, controlled permeability and lower levels of glycolysis. This endothelial quiescence requires active signalling pathways such as Angiopoietin signalling, Wnt signalling and BMP signalling (Ricard et al., 2021). Activity in pathways considered to be pro-angiogenic are also required to play an active role in maintaining this quiescence, such as autocrine VEGF signalling (Lee et al., 2007). It is therefore clear that a complex network of signalling pathways is required for endothelial quiescence and hence, vascular homeostasis.

Although the vast majority of ECs exist in this quiescent state, they retain the ability to undergo phenotypic switching in order to become angiogenic. However, it is critical that this angiogenic switch is tightly governed, with a loss of endothelial homeostasis being associated to endothelial dysfunction (Gimbrone & García-Cardeña, 2016; Ricard et al., 2021). The dysregulation of the angiogenic-quiescence switch can is therefore observed angiogenic disease such as age-related macular degeneration, diabetic retinopathy and peripheral artery disease, or contribute to tumour growth within solid cancers (Carmeliet, 2003). Owing to this, the processes which govern endothelial cell quiescence and overall vascular homeostasis have become a focal point within the research of vascular disease.

As master regulators of gene expression, transcription factors have a significant impact on endothelial cell activity and phenotype, hence receiving a lot of attention within the field. This resulted in the identification of multiple transcription factors involved key endothelial processes such as SOX18 and the ETS family of transcription factors in development, (De Val & Black, 2009), ERG as a regulator of homeostasus (Shah et al., 2016) and FOX01 during quiescence (Andrade et al., 2021; Wilhelm et al., 2016).

A rapidly expanding area of vascular research focuses on endothelial to mesenchymal transition (EndoMT), which involves endothelial cells undergoing phenotypic switching into a mesenchymal phenotype that can occur in a partial or complete manner (Fang et al., 2021; Piera-Velazquez & Jimenez, 2019). The knockout of transcription factors with known roles in EMT has proven to impact angiogenesis and EC signalling pathways. For example, the transcription factor Snail has been demonstrated to regulate capillary branching during developmental angiogenesis via regulation of VEGFR3 expression (Park et al., 2015). Similarly, endothelial Slug was identified to be crucial in regulating the Dll4-Notch-VEGFR2 signalling axis in tumour angiogenesis and transiently during development (Hultgren et al., 2020). This therefore raises the question of whether other transcription factors with known roles in EMT are influencing this quiescent to angiogenic switch.

The initial aim of this chapter was to establish whether growing ECs represent an EndoMT like phenotype. From this original data, along with reports within the literature, ZEB1 was identified as a transcription factor of interest. This then resulted in the secondary aim of this chapter, which was to identify the role of endothelial ZEB1, using transcriptomic analysis and *in vitro* cell culture methods.

A number of experiments within this chapter were performed during a laboratory visited to Dr Joanna Kalucka's lab at Aarhus University, funded by the British Microvascular and Vascular Biology Society. During this time, HUVECs were cultured using the same protocol and reagents, but were isolated from single donors by laboratory manager Bettina Hansen. In this instance, a biological replicate was from a different donor, which induced variability within the data. Whenever this was the case, it is clearly mentioned within the presentation of the data.

3.2 Results

3.2.1 RNA-Seq analysis of confluent and subconfluent HUVECs

HUVECs were seeded to be confluent and subconfluent and 24 hours later RNA extracted and sequenced. Differentially expressed genes were determined by DeSeq2 by Joseph Horder. Genes with an adjusted p value smaller than 0.05 were considered significant. This revealed 4,773 genes differentially expressed between subconfluent and confluent

HUVECs, which can be visualised in the volcano plot in Figure 3.1 A. Out of all the differentially expressed genes, 2,399 (50.26%) were down regulated in confluent HUVECs, and therefore upregulated in subconfluent HUVECs. 2,374 genes (49.75%) were up regulated within confluent HUVECs, and therefore down regulated in subconfluent HUVECs (Figure 3.1 B). This large number of differentially expressed genes is expected of two conditions which vary significantly within their phenotype and their surroundings. To therefore narrow the focus of the data set by only looking at genes that have changed expression beyond a certain threshold, another list of differentially expressed genes was generated which only contained those with a log2 fold change of 1.5. This resulted in 1,628 differentially expressed genes, 696 (42.75%) down regulated and 932 (57.25%) up regulated (Figure 3.1 C).

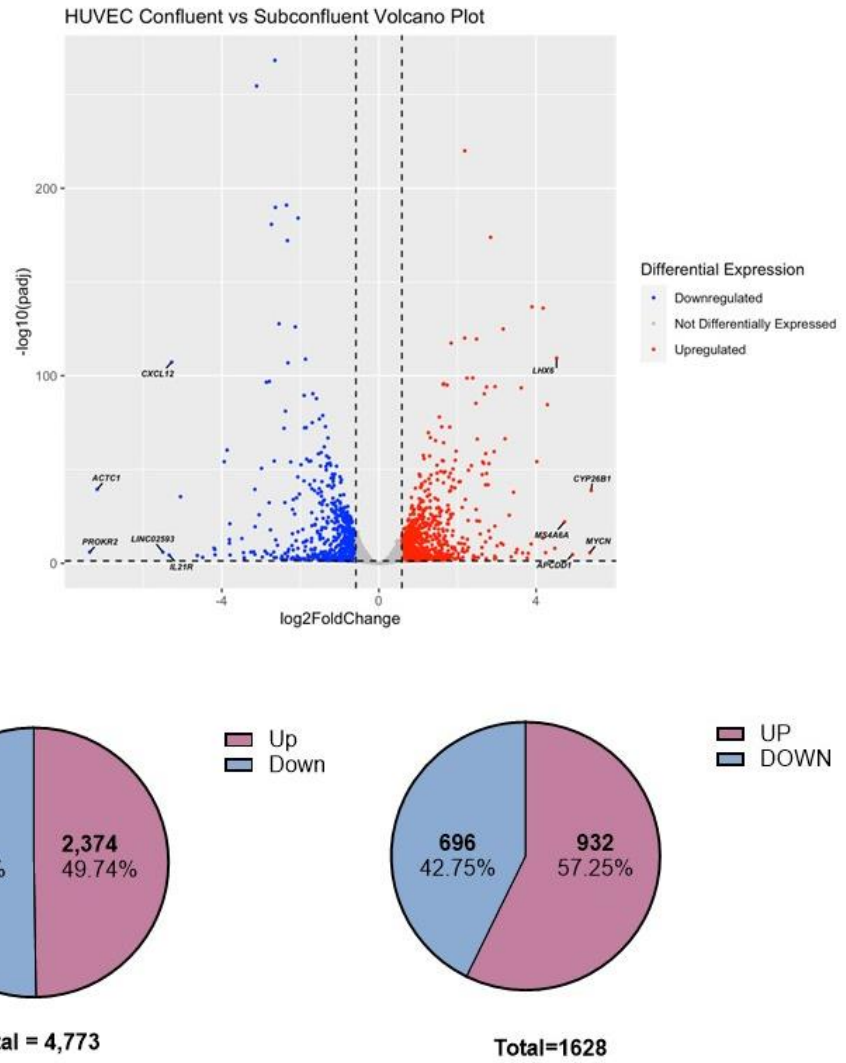

Figure 3.1 RNASeq analysis of subconfluent and confluent HUVECs revealed 4,773 differentially expressed genes. *RNA from confluent and subconfluent HUVECS was sequenced and differentially expressed genes determined by DeSeq2 by Joseph Horder. Genes with an adjusted p value smaller than 0.05 were considered significant.* ***(A)*** *A volcano plot of all differentially expressed genes.* ***(B)*** *A pie chart of all differentially expressed genes.* ***(C)*** *A pie chat of all differentially expressed genes with a 1.5 log2 fold change.*

3.2.1.1 Over representation analysis of differentially expressed genes identified significant GO terms within confluent HUVECSs

To assess how changing confluency affects HUVECs, the list of differentially expressed genes was analysed by ORA to identify significant GO terms. Due to the large number of differentially expressed genes, this analysis was completed using only differentially expressed genes with an adjusted p value lower than 0.05, and a fold change of at least 1.5. GO terms for biological processes, molecular function and cellular component were identified and the top 10 most significant displayed in Figure 3.2. This identified biological processes involved in cell migration, motility, differentiation and adhesion. Molecular functions were centred around signalling receptors, growth factor receptors and adhesion receptors. This was also supported by the majority of cellular components involving the extra cellular matrix, cell surface and cell junctions.

In order to identify GO terms specific to either confluent or subconfluent HUVECs, the differentially expressed genes were split into those that are upregulated and those that are down regulated within the confluent HUVECs. Those genes upregulated within the confluent condition are described as being enriched within confluent HUVECs, whereas genes that are downregulated in the confluent condition are described as being enriched in subconfluent HUVECs. Firstly, ORA was performed on the genes enriched within the confluent condition to identify significant GO terms, and the top 10 presented in Figure 3.3. This revealed biological processes involved in cell migration, adhesion and motility. The molecular functions identified as being significant included signalling receptor binding, metalloprotease binding and receptor tyrosine kinase activity. Whereas the cellular components identified primarily focused around the cell surface, plasma membrane and cell junctions.

Secondly, ORA was performed on the genes downregulated within the confluent condition and therefore enriched within the subconfluent condition. This identified significant GO terms and the top 10 are presented in Figure 3.4. This analysis revealed biological processes involved in development, differentiation and morphogenesis. The molecular functions that are significantly enriched within the data set include signalling receptor activity, constituent of extracellular matrix and glycosaminoglycan binding. Whilst the

cellular components within the data set include cell surface, cell junctions and compartments such as the endoplasmic reticulum and Golgi apparatus, and hence vesicle trafficking. This data provides a greater understanding of genes involved in specific biological processes, that are enriched within confluent or subconfluent HUVECs.

Figure 3.2 The top 10 significant go terms identified from all differentially expressed genes within confluent HUVECs. *RNA from confluent and subconfluent HUVECS was sequenced and differentially expressed genes determined by DeSeq2 by Joseph Horder. Genes with an adjusted p value smaller than 0.05 were considered significant. All differentially expressed genes with a log2 fold change of 1.5 were analysed by over representation analysis to determine significant biological processes, molecular function and cellular component GO terms. The top 10 significant GO terms are presented.*

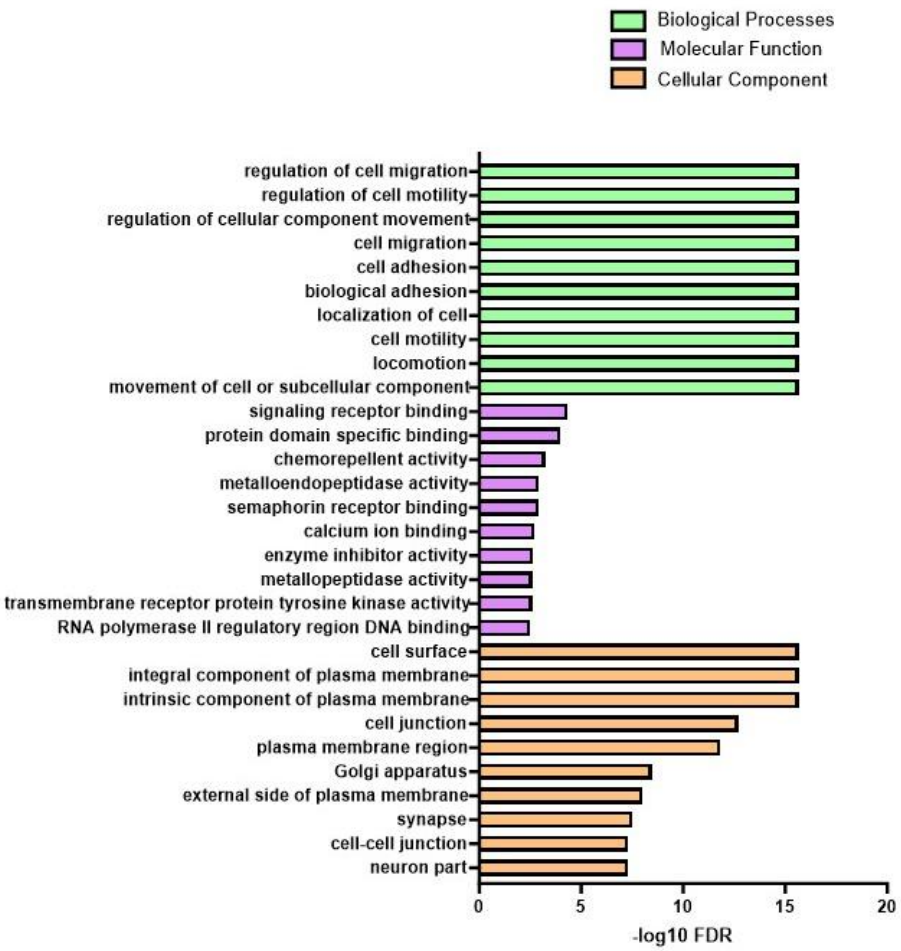

Figure 3.3 The top 10 significant go terms identified from differentially expressed genes that are up-regulated within confluent HUVECs. *RNA from confluent and subconfluent HUVECS was sequenced and differentially expressed genes determined by DeSeq2 by Joseph Horder. Genes with an adjusted p value smaller than 0.05 were considered significant. Up-regulated differentially expressed genes with a log2 fold change of 1.5 were analysed by over representation analysis to determine significant biological processes, molecular function and cellular component GO terms. The top 10 significant GO terms are presented.*

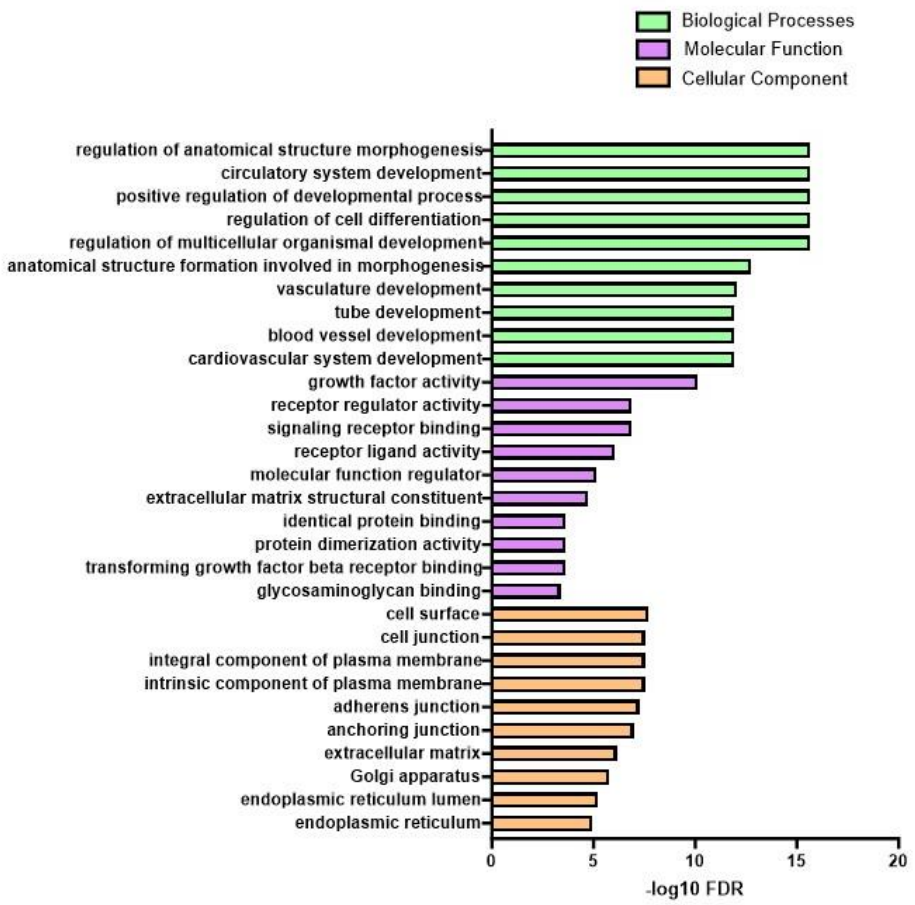

Figure 3.4 The top 10 significant go terms identified from differentially expressed genes that are down-regulated within confluent HUVECs. *RNA from confluent and subconfluent HUVECS was sequenced and differentially expressed genes determined by DeSeq2 by Joseph Horder. Genes with an adjusted p value smaller than 0.05 were considered significant. Down-regulated differentially expressed genes with a log2 fold change of 1.5 were analysed by over representation analysis to determine significant biological processes, molecular function and cellular component GO terms. The top 10 significant GO terms are presented.*

3.2.1.2 Over representation analysis of differentially expressed genes identified significant KEGG pathways within confluent HUVECSs

In order to determine how changing confluency affects the expression of genes within specific signalling pathways HUVECs, the list of differentially expressed genes was analysed by ORA to identify significant KEGG pathways (Figure 3.5). This was also completed using only differentially expressed genes with an adjusted p value lower than 0.05, as well as with a log2 fold change of at least 1.5, due to the large data set. Using all differentially expressed genes, the top 10 significant pathways were identified, which included cell adhesion molecules, extracellular matrix interactions and the TGFβ signaling pathway. The analysis was also repeated using only the genes downregulated in confluent HUVECs and therefore upregulated within subconfluent condition. This identified pathways including TGFβ signaling pathway, various biosynthesis pathways, as well as the PI3K-Akt and MAPK signaling pathways. Finally, the analysis was also completed using only the genes upregulated in the confluent condition. This identified only 4 significant pathways: extracellular matrix interaction, ABC transporters, cell adhesion molecules, and complement and coagulation cascades. This data provides a greater understanding of genes involved in specific signaling pathways, that are enriched within confluent or subconfluent HUVECs.

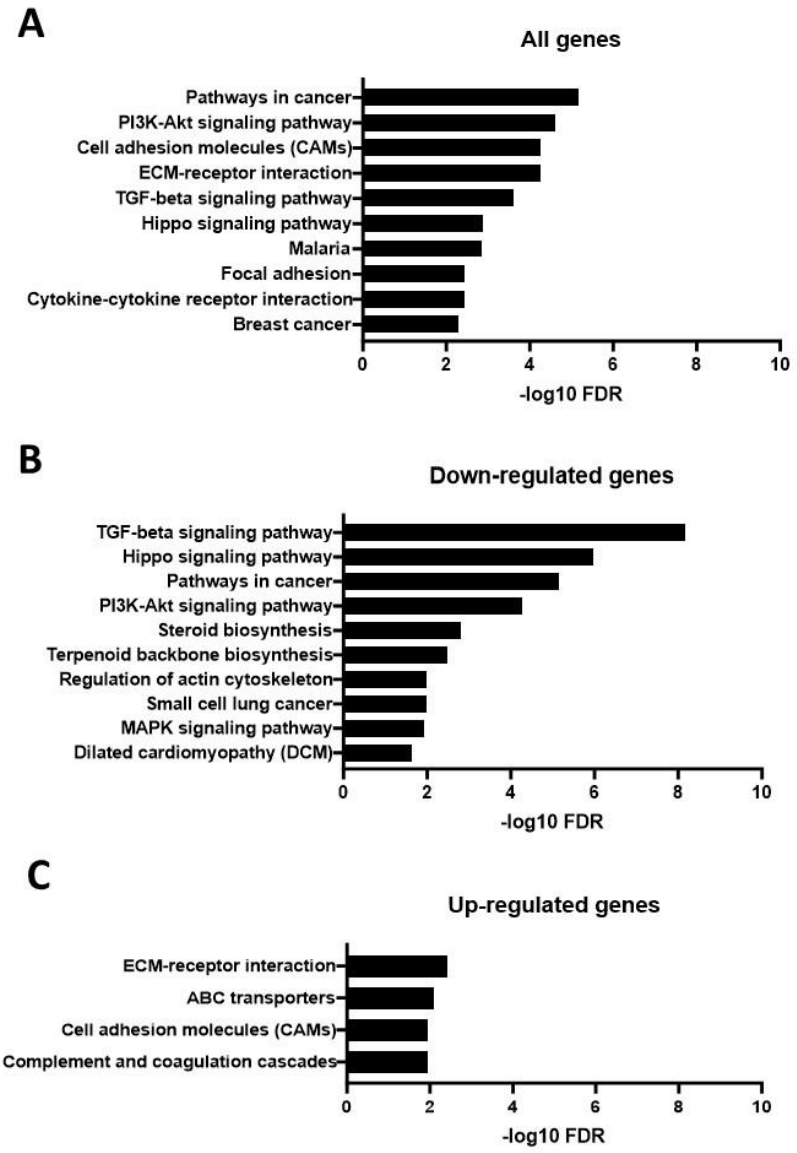

Figure 3.5 The top 10 significant KEGG pathways identified from differentially expressed genes within confluent HUVECs. *RNA from confluent and subconfluent HUVECS was sequenced and differentially expressed genes determined by DeSeq2 by Joseph Horder. Genes with an adjusted p value smaller than 0.05 were considered significant. All differentially expressed genes with a log2 fold change of 1.5 were analysed by over representation analysis to determine significant KEGG pathways.* ***(A)*** *The top 10 significant KEGG pathways are presented for all differentially expressed genes.* ***(B)*** *The top 10 significant KEGG pathways are presented genes down regulated in confluent HUVECs.* ***(C)*** *All significant KEGG pathways are presented for genes up regulated in confluent HUVECs.*

3.2.1.3 Confluent HUVECs express endothelial markers to a greater extent and reduced mesenchymal markers, but have varying levels of EndoMT transcription factor expression

The HUVECs within subconfluent cultures undergo a form of phenotypic switching when they become confluent, which may mimic what is explained in the literature as EndoMT. Therefore, to explore whether there is any indication of EndoMT occurring between confluent and subconfluent HUVECs, the normalised counts of endothelial and mesenchymal genes listed in the literature (Kim, 2018; Platel et al., 2019) were compared between the confluent and subconfluent conditions. This revealed common endothelial genes were increased within the confluent condition, compared to the subconfluent (Figure 3.6 A). These genes included CDH5 (VECAD), PECAM1 (CD31), VWF, TEK (TIE2), TIE1 and ERG and were all significantly upregulated within the confluent condition. The expression of mesenchymal markers was compared between the confluent and subconfluent condition was then compared and presented using a log scale, due to their large variation in normalised counts. This revealed the subconfluent condition had significantly higher expression of mesenchymal markers, compared to the confluent (Figure 3.6 B). These significant markers included SNAI1 (Snail), SNAI2 (Slug), CDH2 (N-Cadherin), TAGLN (SM22α), FN1 and CNN1. However, no significant change was observed in the expression of VIM and ACTA2 (αSMA), indicating this was not a blanket increase in mesenchymal marker expression within subconfluent HUVECs.

To explore if there is any differential expression of transcription factors associated with EndoMT/EMT, normalised counts of a list of transcription factors derived from the literature (Zeisberg & Neilson, 2009) were compared between the confluent and subconfluent conditions. This provided varying results (Figure 3.6 C). Some transcription factors showed no or little expression in either confluent or subconfluent condition, such as TWIST1, GSC and LEF1. Some transcription factors displayed no significant difference in expression, such as TWIST2 and ETS1. For the case of ZEB2, SNAI1 (Snail), SNAI2 (Slug) and FOXC2, the expression of these transcription factors was significantly higher within the subconfluent condition. However, there was only one transcription factor that displayed higher expression within the confluent condition, which was ZEB1. This data indicates that

ZEB1 expression is associated with a confluent monolayer of HUVECs with increased endothelial gene expression and reduced mesenchymal gene expression.

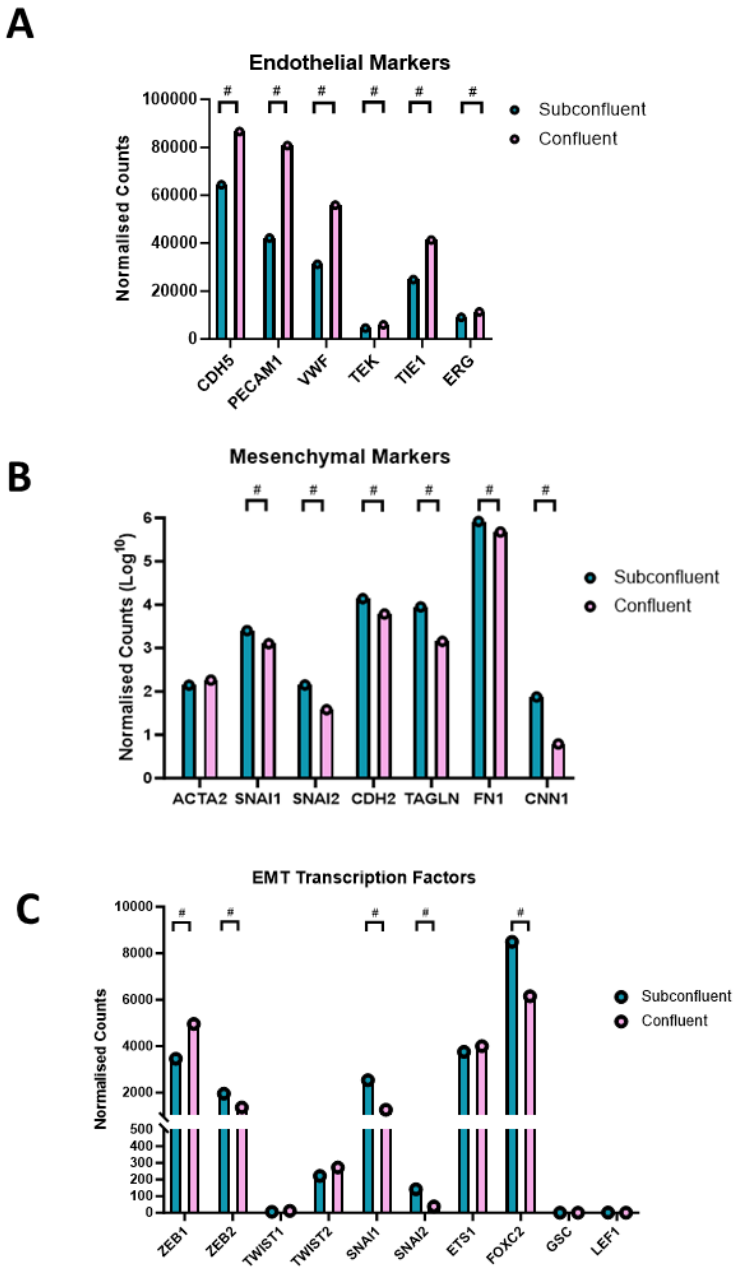

Figure 3.6 Confluent HUVECs have upregulated expression of endothelial genes and decreased expression of mesenchymal genes. *RNA from confluent and subconfluent HUVECS was sequenced and differentially expressed genes determined by DeSeq2 by Joseph Horder.* ***(A)*** *The normalised counts of endothelial genes are compared between subconfluent and confluent HUVECs.* ***(B)*** *The* Log^{10} *of normalised counts of mesenchymal genes are compared between subconfluent and confluent HUVECs.* ***(C)*** *The normalised counts of transcription factors linked to EMT/EndoMT are compared between subconfluent and confluent HUVECs. All data presented as mean of normalised counts, N = 3. Genes with an adjusted p value smaller than 0.05 were considered significant (#).*

3.2.2 mRNA and protein expression of confluent and subconfluent HUVECs identifies ZEB1 as significantly upregulated in the confluent condition

Because of its known roles in EMT, yet little understanding of its role within ECs, ZEB1 has emerged as transcription factor of interest. To confirm that the levels of ZEB1 expression are upregulated within the confluent condition, mRNA was extracted and reverse transcribed to cDNA before ddPCR analysis performed to determine the level of ZEB1 mRNA within both conditions. This also confirmed upregulation of ZEB1 at the mRNA level within confluent HUVECs (1.8 ± 0.1 fold change of subconfluent, Figure 3.7).

Next was to understand how confluency affects HUVECs at a protein level, and to determine whether some of the changes observed with the RNA-Seq are also observed a protein level. Protein was extracted from confluent and subconfluent cells and the levels of proteins determined via western blot (Figure 3.8). Firstly, the protein expression of VECAD (gene name: CDH5) was determined which revealed its protein expression was significantly increased within confluent endothelial cells (1.38 ± 0.08 fold change of subconfluent), which replicates what is observed at the RNA level, as determined by RNA-Seq (Log2 fold change of 0.39, Figure 3.8 B). To also determine whether the functionality of VECAD varies from confluent and subconfluent HUVECs, the phosphorylation levels of tyrosine 731 (pY731) was determined via western blot and normalised to total VECAD. The dephosphorylation of this residue specifically is associated with leukocyte extravasation and therefore under normal condition its constitutively phosphorylated (Arif et al., 2021; Wessel et al., 2014). This revealed a significant increase in pY731 of VECAD within confluent HUVECs (1.56 ± 0.15 fold change of subconfluent, Figure 3.8 C). This suggests that a confluent monolayer of HUVECs holds similar properties of a quiescent vasculature with appropriate barrier properties.

Secondly, the level of ZEB1 and Slug, two EndoMT/EMT transcription factors, was determined at a protein level within confluent and subconfluent HUVECs. This revealed that the levels of ZEB1 protein were significantly upregulated within the confluent condition (3.1 ± 0.34 fold change of subconfluent, Figure 3.8 E), which mirrors what was observed at the mRNA level within the RNA-Seq data. However, the level of Slug did not

appear to significantly change at the protein level ($p > 0.05$, Figure 3.8 F), unlike the RNA-Seq where the level of Slug (SNAI2) decreased in the confluent condition.

Finally, the level of two other proteins of interest were determined. The first being the transcription factor FOXO1, a known regulator of endothelial quiescence (Andrade et al., 2021; Wilhelm et al., 2016). Analysis of its expression at the protein level via western blot revealed FOXO1 was upregulated and close to being stastically significant within the confluent condition (Figure 3.8 G). This provides further evidence that this confluent condition could be considered quiescent. The second marker of interest was PFKFB3, a critical regulator of glycolysis and known to play a role in metabolic adaptations required in angiogenesis (De Bock et al., 2013; Schoors et al., 2014). An increase in PFKFB3 within the confluent condition was observed at the protein level (2.70 ± 0.25 fold change of subconfluent, Figure 3.8 I).

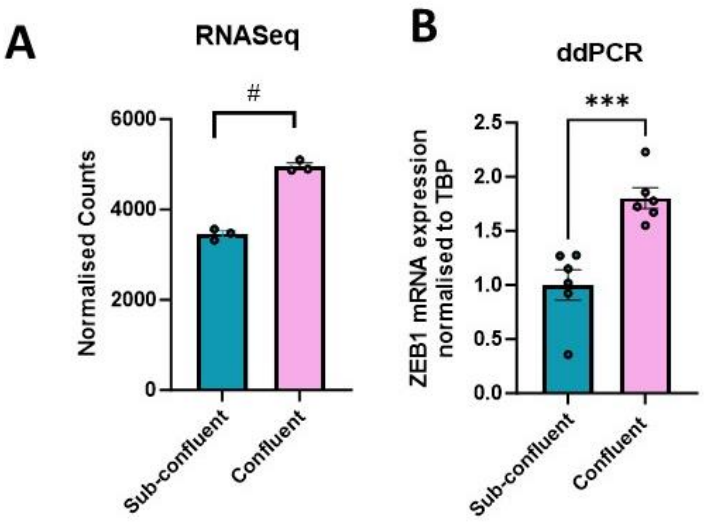

Figure 3.7 ZEB1 is upregulated in confluent HUVECs. *HUVECs were seeded to be either confluent or subconfluent before RNA and protein extracted.* ***(A)*** *RNA from confluent and subconfluent HUVECS was sequenced and differentially expressed genes determined by DeSeq2. Genes with an adjusted p value smaller than 0.05 were considered significant (#). ZEB1 was determined to be significantly upregulated, and the normalised counts are shown, n=3* ***(B)*** *RNA from confluent and subconfluent HUVECS was reverse transcribed to cDNA before performing ddPCR analysis which revealed ZEB1 mRNA is significant upregulated in confluent HUVECs. Presented as mean + SEM and was stastically analysed used an unpaired t-test. *** $p < 0.0005$*

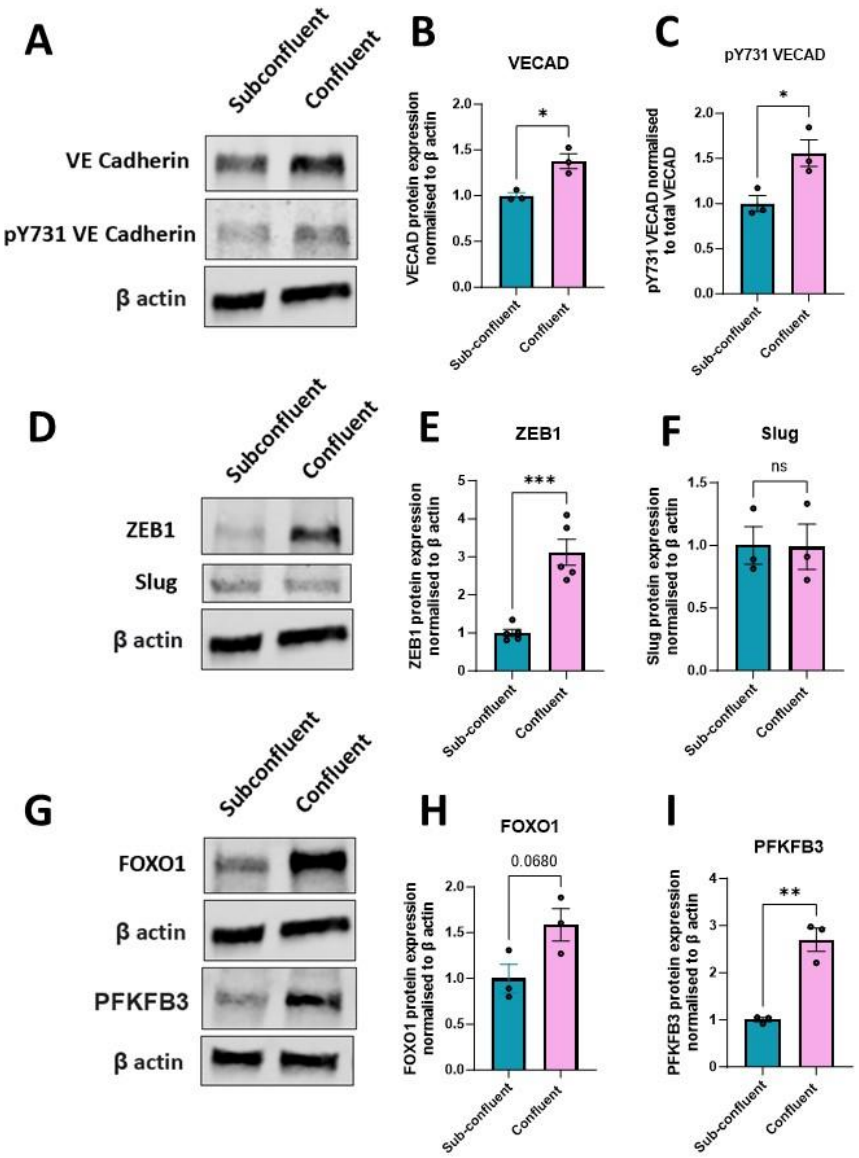

Figure 3.8 Confluent and subconfluent HUVECs protein expression. *HUVECs were seeded to be either confluent or subconfluent before protein was extracted and ran on western blots to observe changes in protein expression.* ***(A)*** *VECAD and pY731 VECAD protein expression was determined via western blot.* ***(B)*** *VECAD expression normalised to β actin.* ***(C)*** *pY731 VECAD expression normalised to total VECAD.* ***(D)*** *ZEB1 and Slug protein expression was determined via western blot.* ***(E)*** *ZEB1 expression normalised to β actin.* ***(F)*** *Slug expression normalised to β actin.* ***(G)*** *FOXO1 and PFKFB3 protein expression was determined via western blot.* ***(H)*** *ZEB1 expression normalised to β actin.* ***(I)*** *Slug expression normalised to β actin. All data are presented as mean + SEM and was statistically analysed used an unpaired t-test. * $p < 0.05$, *** $p < 0.0005$*

3.2.3 siRNA to target ZEB1 resulted in a significant decrease in ZEB1 expression but had no impact on FOXO1 or PFKFB3

To understand the role ZEB1 is playing within ECs, confluent HUVECs were transfected with either siRNA to knockout ZEB1 or non-silencing control (NSC) siRNA. 72 hours post transfection, protein was extracted and the expression of ZEB1 analysed by western blot. This revealed that the siRNA against ZEB1 resulted in a significant decrease in ZEB1 expression (0.49 ± 0.03 fold change compared to NSC, Figure 3.9 B), which is a 51% decrease in ZEB1 expression, and hence will be referred to as ZEB1 KD condition. To determine whether ZEB1 KD affected the expression of FOXO1 or PFKFB3, two protiens idetnfied via the literture as having opposing roles on ECs, their levels of protein expression within ZEB1 KD and NSC cells were determined via western blot. This revealed no significant difference in FOXO1 or PFKFB3 expression ($p > 0.05$, Figure 3.9 C and D). This data therefore indicates that ZEB1 does not influence the expression of FOX01 or PFKFB3.

3.2.4 ZEB1 KD in HUVECs by siRNA results in 296 differentially expressed genes

To explore how loss of ZEB1 expression affects ECs, confluent HUVECs were transfected with either siRNA to KD ZEB1 or NSC siRNA. RNA was then extracted, sequenced and differentially expressed genes identified by DeSeq2 analysis performed by Joseph Horder. Genes with an adjusted p value smaller than 0.05 were considered significant. This identified 296 differentially expressed genes, with 194 genes (65.54%) significantly upregulated and 102 genes (34.46%) significantly down regulated (Figure 3.10 A). This indicates that ZEB1 may have an increased role as a transcriptional repressor, in comparison to a transcriptional activator. These differentially expressed genes are displayed in the volcano plot in Figure 3.10 B. The top 15 up-regulated and down-regulated genes are displayed in Table 4 and Table 5 respectively.

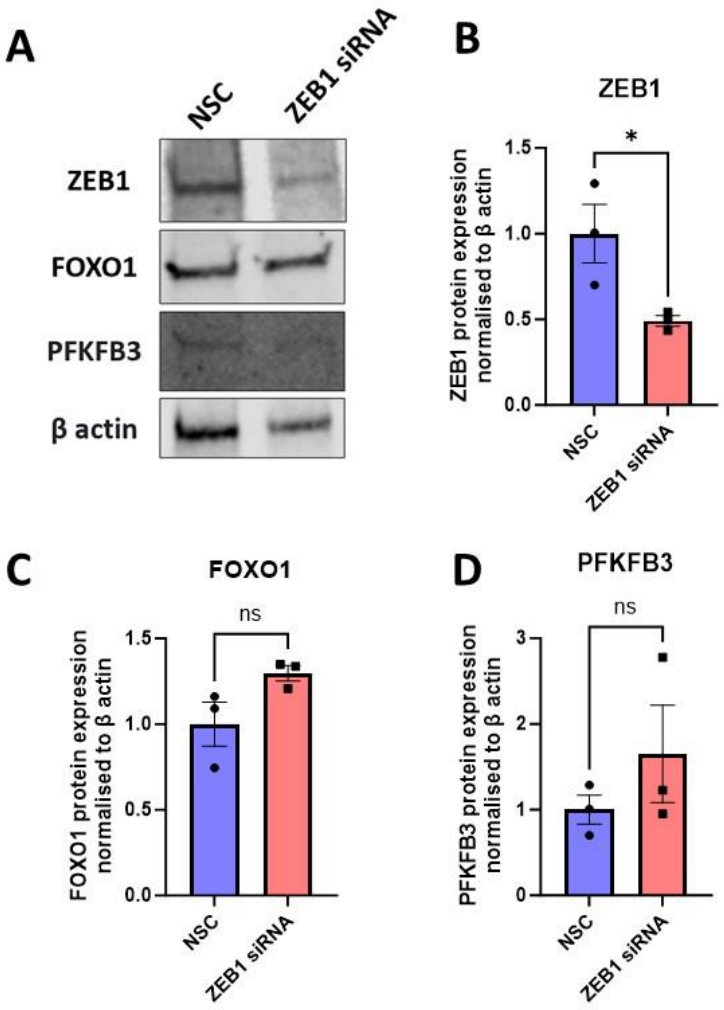

Figure 3.9 ZEB1 siRNA significantly reduced ZEB1 expression but loss of ZEB1 did not affect FOXO1 and PFKFB3. *Confluent HUVECs were treated with control siRNA or siRNA to knock down ZEB1 expression.* ***(A)*** *After 72h protein was extracted and expression of ZEB1, as well as FOXO1 and PFKFB3 was determined via western blot. Densitometry analysis was performed and protein expression for* ***(B)*** *ZEB1,* ***(C)*** *FOXO1,* ***(D)*** *PFKFB3 was determined and normalised to β actin. All data are presented as mean + SEM and was stastically analysed used an unpaired t-test. * $p < 0.05$*

Gene Symbol	Adjusted P Value	Log2 Fold Change
IFI44L	1.62E-05	-1.72043
IFI6	7.52E-06	-1.67968
OAS2	4.39E-07	-1.67308
IFIT1	0.000771	-1.61264
EPSTI1	8.06E-05	-1.3103
CX3CL1	3.84E-09	-1.22312
IFI27	2.76E-07	-1.20725
CMPK2	0.021132	-1.19929
CCL20	0.000298	-1.18945
GNG2	0.005703	-1.13823
NEURL3	0.003479	-1.09058
CXCL10	0.03396	-1.08486
MC5R	0.02095	-1.06812
SELE	1.64E-24	-0.99854
TNFRSF9	0.00181	-0.99482

Table 1 The top 15 down-regulated differentially expressed genes within the ZEB1 KD condition. *Determined via DESeq2 by Joseph Horder. Genes with an adjusted P value smaller than 0.05 were considered significant.*

Gene Symbol	Adjusted P Value	Log2 Fold Change
TMEM92	4.96E-06	4.512057
CBLC	4.46E-05	4.022369
KLC3	8.84E-10	3.543978
PRKCZ	8.14E-36	3.378851
GRB7	2.88E-08	3.153616
TC2N	6.00E-06	3.127319
EPPK1	4.82E-06	3.035372
SPINT2	3.72E-46	2.917085
FAM83H	3.05E-14	2.875946
SLC12A8	2.43E-10	2.72541
SPINT1	4.65E-115	2.596867
BAIAP2L1	7.44E-41	2.371526
CSC42BPG	4.18E-28	2.288792
EPS8L2	1.65E-46	2.257529
SMPDL3B	1.30E-07	2.196325

Table 2 The top 15 up-regulated differentially expressed genes within the ZEB1 KD condition. *Determined via DESeq2 by Joseph Horder. Genes with an adjusted P value smaller than 0.05 were considered significant.*

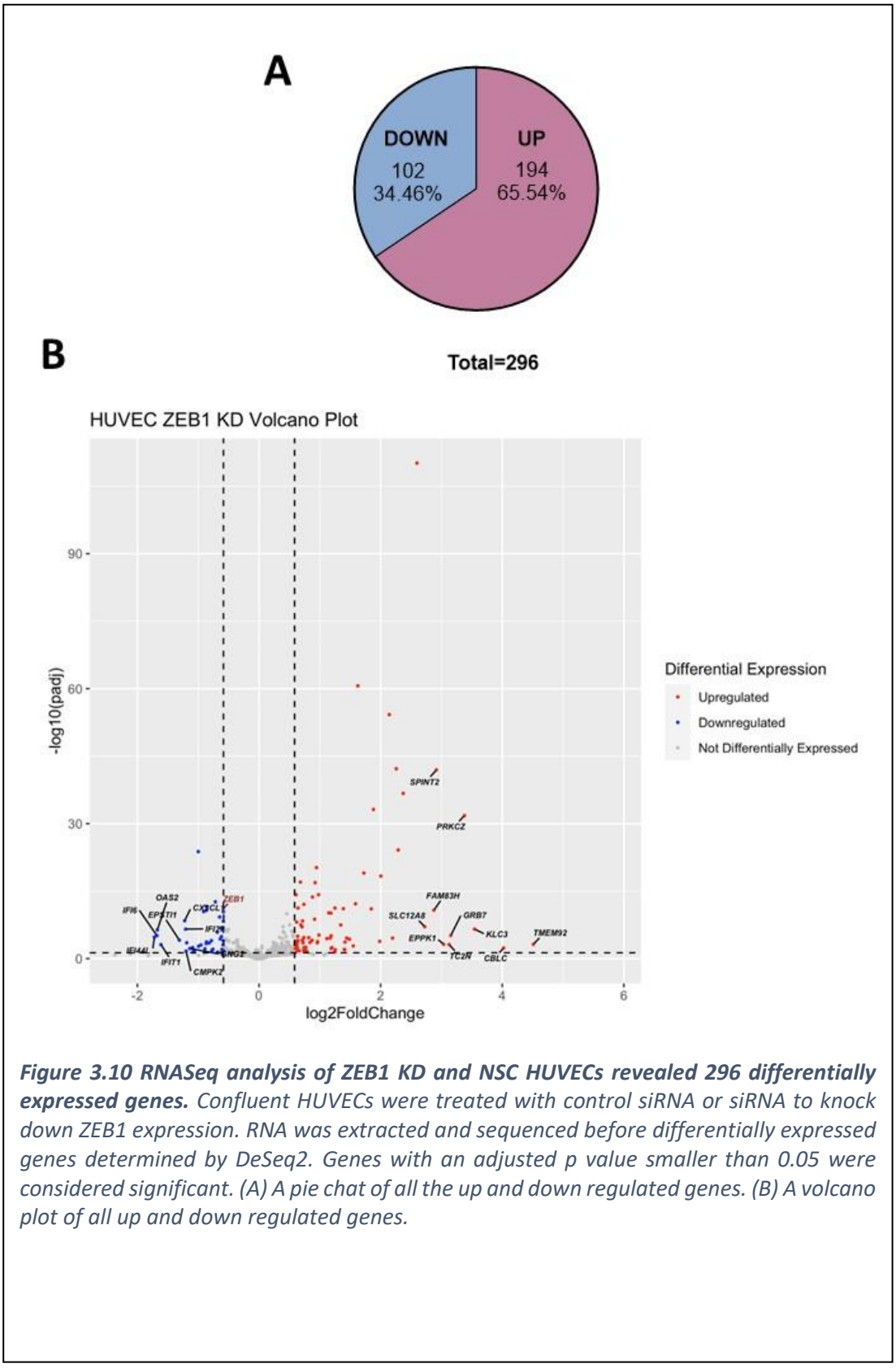

Figure 3.10 RNASeq analysis of ZEB1 KD and NSC HUVECs revealed 296 differentially expressed genes. *Confluent HUVECs were treated with control siRNA or siRNA to knock down ZEB1 expression. RNA was extracted and sequenced before differentially expressed genes determined by DeSeq2. Genes with an adjusted p value smaller than 0.05 were considered significant. (A) A pie chat of all the up and down regulated genes. (B) A volcano plot of all up and down regulated genes.*

3.2.4.1 Over representation analysis of differentially expressed genes identified significant GO terms within ZEB1 KD HUVECSs

The list of differentially expressed genes was analysed by ORA to identify significant GO terms. This analysis was firstly completed using all differentially expressed genes with an adjusted p value lower than 0.05. GO terms for biological processes, molecular function and cellular component were identified and the top 10 most significant displayed in Figure 3.11. This identified biological processes involved in cytokine stimulation, immune response and adhesion. Molecular functions were centred around chemokine activity and adhesion binding. Whereas the cellular components involved cell junctions, focal adhesions and the cell surface.

Although this information provided an insight, it does not specify which processes are upregulated or downregulated, only that they are influenced by the KD of ZEB1. Therefore, the differentially expressed genes as a result of ZEB1 KD were separated into upregulated and downregulated. The analysis was then repeated, firstly on the downregulated genes only, to identify biological processes that contain downregulated genes and hence, may be reduced or at least affected by the reduction of ZEB1. The top 10 biological processes identified are display in Figure 3.12. These GO terms had a significant focus on inflammatory pathways, such as type 1 interferon, chemokine signalling and response to inflammatory stimuli. This association with inflammation is also observed within the significant molecular functions which include chemokine activity and cytokine activity. Finally, the significant cellular components were identified, but only 4 appeared to be significant: external side of plasma membrane, cell surface, side of membrane and endolysosome lumen. These results indicate that inflammatory and immune associated genes are enriched within the down regulated genes within the ZEB1 KD data set, suggesting loss of ZEB1 may affect the inflammatory response.

The analysis was then repeated with only the upregulated genes, to identify biological processes that contain upregulated genes and hence, may be increased or affected by the reduction of ZEB1. The top 10 biological processes identified are display in Figure 3.13. This identified biological processes involved in adhesion and extracellular matrix. This pattern was also observed within the molecular function, which included adhesion

binding, extracellular matrix components, laminin binding and actin binding. The cellular components focused on cell junctions, cell surface and extracellular matrix. Taken together this data indicates that adhesion associated genes are enriched within the upregulated ZEB1 KD data set, suggesting loss of ZEB1 may affect cellular adhesion.

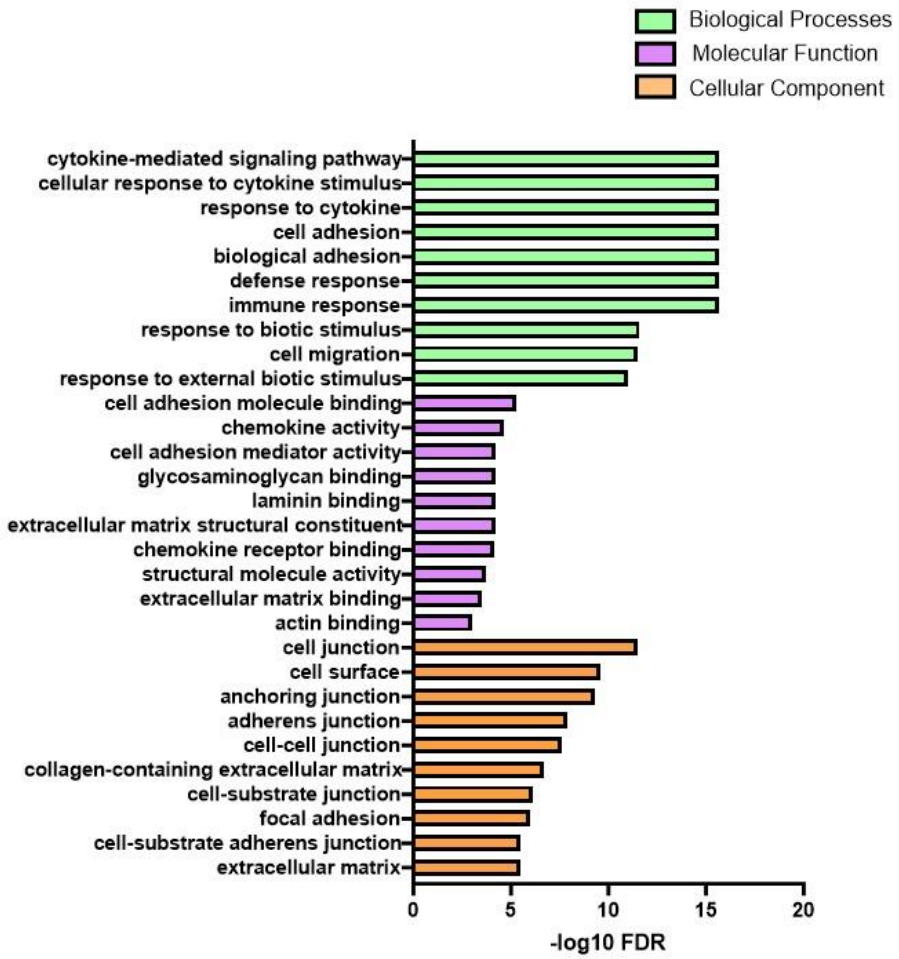

Figure 3.11 The top 10 significant go terms identified from all differentially expressed genes within ZEB1 KD HUVECS. *RNA from ZEB1 siRNA and NSC treated HUVECS was sequenced and differentially expressed genes determined by DeSeq2. Genes with an adjusted p value smaller than 0.05 were considered significant. All differentially expressed genes were analysed by over representation analysis to determine significant biological processes, molecular function and cellular component GO terms. The top 10 significant GO terms are presented.*

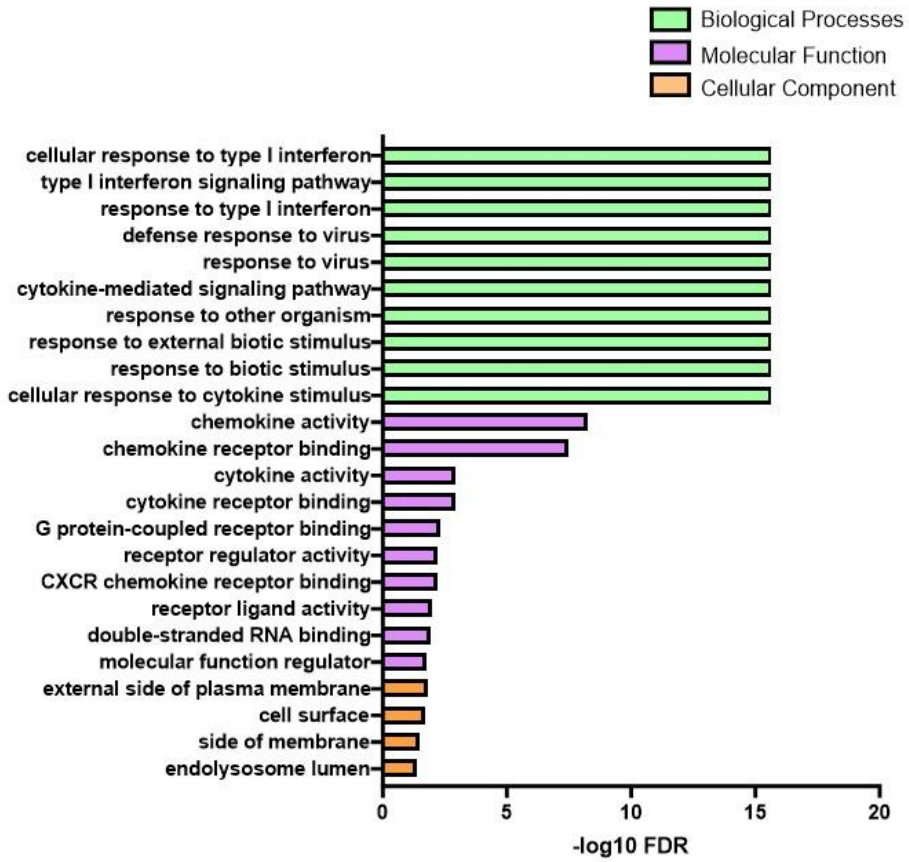

Figure 3.12 The top 10 significant go terms identified from differentially expressed genes that are down-regulated within ZEB1 KD HUVECs. *RNA from ZEB1 siRNA and NSC treated HUVECS was sequenced and differentially expressed genes determined by DeSeq2. Genes with an adjusted p value smaller than 0.05 were considered significant. Down-regulated differentially expressed genes were analysed by over representation analysis to determine significant biological processes, molecular function and cellular component GO terms. The top 10 significant GO terms are presented.*

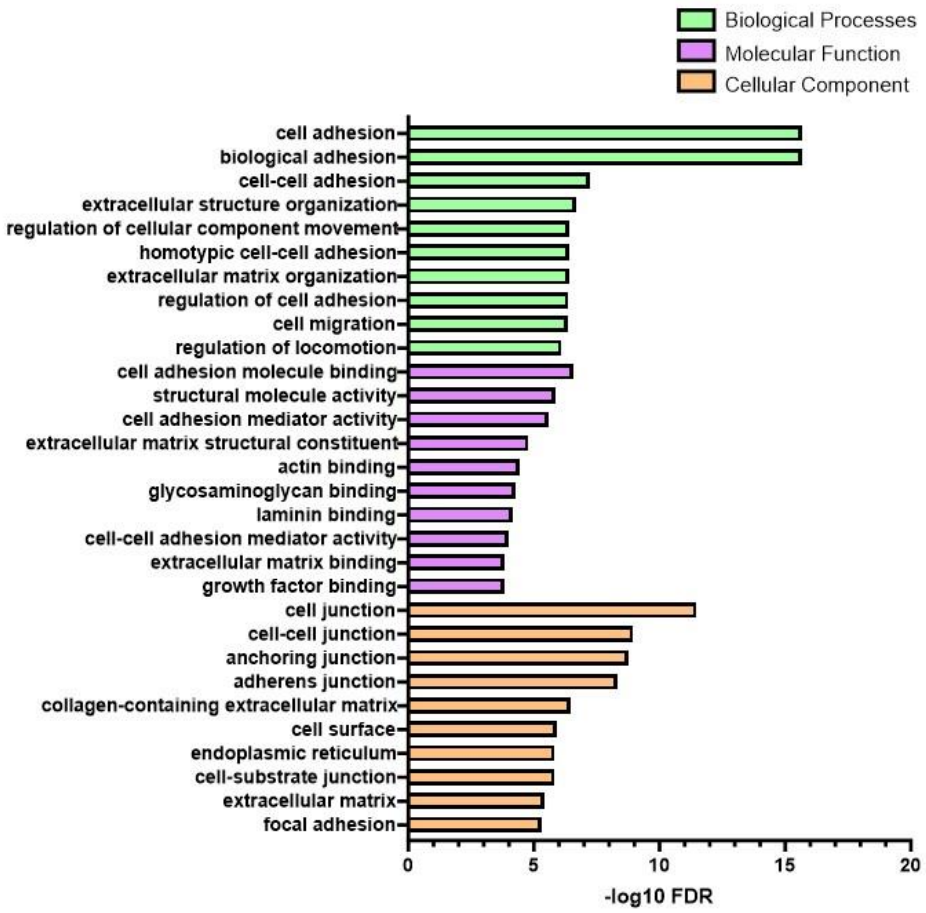

Figure 3.13 The top 10 significant go terms identified from differentially expressed genes that are up-regulated within ZEB1 KD HUVECs. *RNA from ZEB1 siRNA and NSC treated HUVECS was sequenced and differentially expressed genes determined by DeSeq2. Genes with an adjusted p value smaller than 0.05 were considered significant. Up-regulated differentially expressed genes were analysed by over representation analysis to determine significant biological processes, molecular function and cellular component GO terms. The top 10 significant GO terms are presented.*

3.2.4.2 Over representation analysis of differentially expressed genes identified significant KEGG pathways within confluent HUVECs

To determine how reduction of ZEB1 influenced the expression of genes within specific signalling pathways HUVECs, the list of differentially expressed genes was analysed by ORA to identify significant KEGG pathways. This was also completed using only differentially expressed genes with an adjusted p value lower than 0.05. Using all differentially expressed genes, all the identified significant pathways were plotted in Figure 3.14. These include inflammation associated signalling pathways such as TNF signalling pathway, cytokine-cytokine receptor and chemokine signalling pathway. It also included adhesion and cytoskeletal signaling pathways, such as focal adhesion and extracellular matrix receptor interaction.

To uncover how ZEB1 KD affects pathways more specifically, the gene set was again separated into upregulated and downregulated genes. The analysis was then repeated using only the genes downregulated in ZEB1 KD HUVECs. This isolated the majority of the pathways involved in inflammation signaling, such as TNF signaling, chemokine signaling and IL-17 signaling. This indicates that genes involved in these pathways are downregulated as a result of ZEB1 KD. Finally, the analysis was also repeated using only the genes upregulated within ZEB1 KD HUVECs. This identified pathways primarily associated with adhesion, tight junction and extracellular matrix interaction, indicating that the upregulated genes are involved in these adhesion pathways. However, it also identified leukocyte migration and human papillomavirus infection, indicating that the up regulated genes are involved in some inflammatory pathways also.

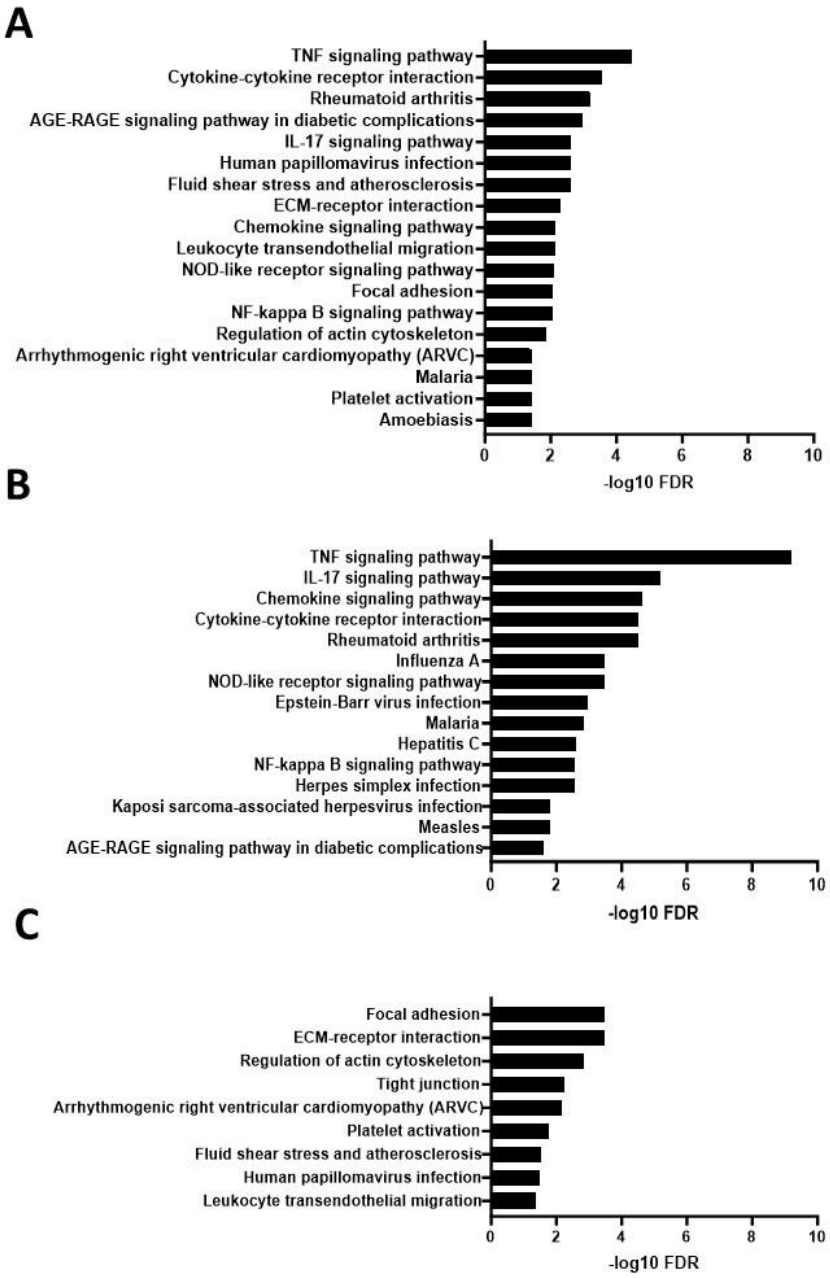

Figure 3.14 The top 10 significant KEGG pathways identified from differentially expressed genes within ZEB1 KD HUVECs. *RNA from ZEB1 siRNA and NSC treated HUVECS was sequenced and differentially expressed genes determined by DeSeq2. Genes with an adjusted p value smaller than 0.05 were considered significant. All differentially expressed genes were analysed by over representation analysis to determine significant KEGG pathways.* ***(A)*** *All significant KEGG pathways are presented for all differentially expressed genes.* ***(B)*** *All significant KEGG pathways are presented genes down regulated in ZEB1 KD HUVECs.* ***(C)*** *All significant KEGG pathways are presented for genes up regulated in ZEB1 KD HUVECs*

3.2.4.3 Confluent HUVECs express more endothelial markers and less mesenchymal markers, but have varying levels of EndoMT transcription factor expression

To explore whether ZEB1 KD influences the expression of EndoMT markers or EndoMT/EMT transcription factors, the expression level of the genes (listed previously in Figure 3.6) was determined and their normalised counts plotted. Firstly, the endothelial genes were plotted (CDH5, PECAM1, VWF, TEK, TIE1 and ERG) and none of these genes were found to be significantly differentially expressed (Figure 3.15 A). The expression of mesenchymal markers was also compared between the ZEB1 KD and NSC condition and presented using a log scale (Figure 3.15 B), due to their large variation in normalised counts. Only TAGLN (SM22α) was found to be differentially expressed, with it being upregulated in the ZEB1 KD condition. The rest of the genes (VIM, ACTA2, SNAI1, SNAI2, CDH2, FN1 and CNN1) were not differentially expressed. Finally, the list of transcription factors derived from the literature as being involved in EMT/EndoMT were compared between ZEB1 KD and NSC (Figure 3.15 C). Only the ETS1 transcription factor was found to be differentially expressed, with it being down regulated within the ZEB1 KD condition. As before TWIST1, GSC and LEF1 showed no or little expression in either the NSC or ZEB1 KD cells. The rest (ZEB2, TWIST2, SNAI1, SNAI2, ETS1, FOXC2) were not differentially expressed. Although TAGLN and EST1 are differentially expressed, there are no major trends within the expression of these markers, suggesting that ZEB1 KD is not influencing a change of gene expression associated with an EndoMT phenotypic switch.

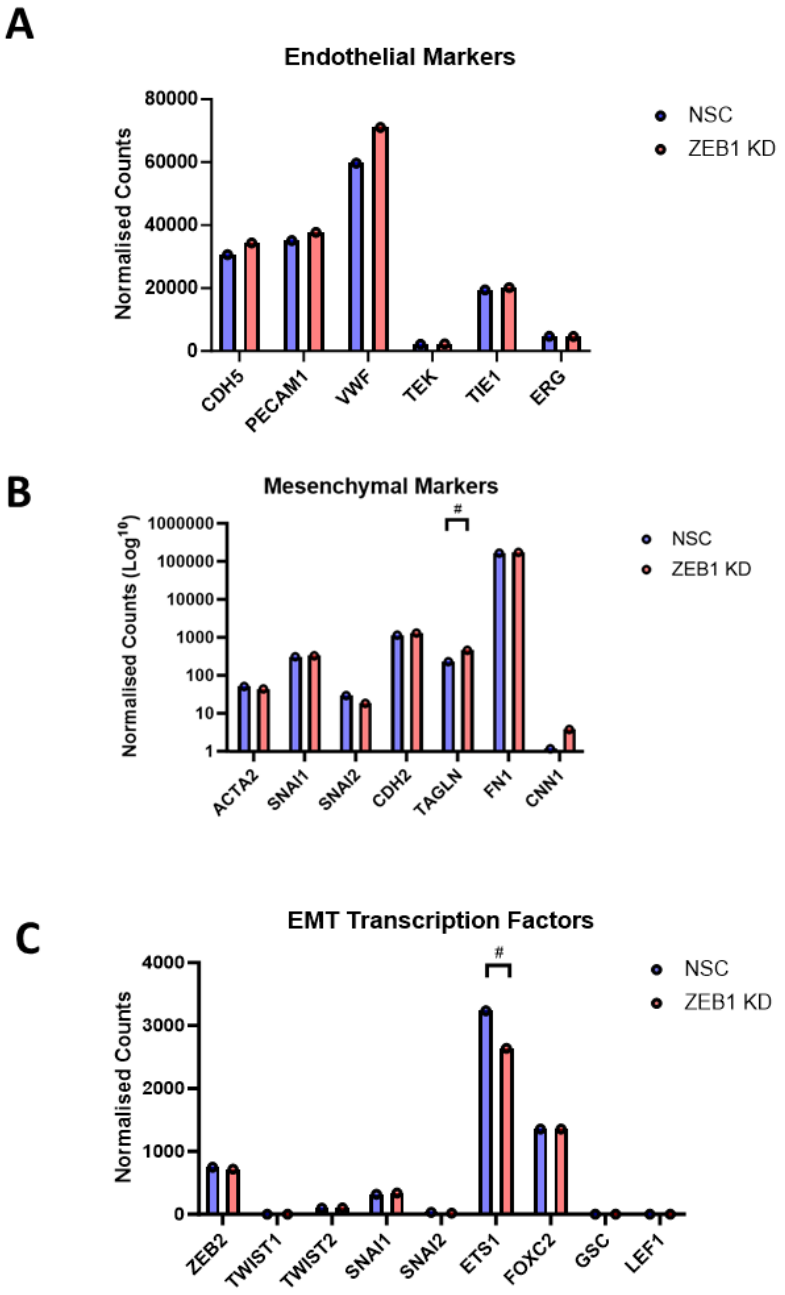

Figure 3.15 ZEB1 KD has limited impact on EndoMT genes. *RNA from confluent and subconfluent HUVECS was sequenced and differentially expressed genes determined by DeSeq2.* ***(A)*** *The normalised counts of endothelial genes are compared between ZEB1 KD and NSC HUVECs* ***(B)*** *The Log^{10} of normalised counts of mesenchymal genes are compared between ZEB1 KD and NSC HUVECs.* ***(C)*** *The normalised counts of transcription factors linked to EMT/EndoMT are compared between ZEB1 KD and NSC HUVECs. All data presented as mean of normalised counts, N = 3. Genes with an adjusted p value smaller than 0.05 were considered significant (#).*

3.2.5 Comparison with a publicly available ZEB1$^{+/-}$ corneal ECs data set exhibited overlapping differentially expressed genes

To compare the HUVEC ZEB1 siRNA KD dataset generated in this study with publicly available data, the Gene Expression Omnibus (GEO) was queried to identify relevant datasets. This search identified an RNA-Seq dataset from human corneal ECs, in which ZEB1 expression was reduced through CRISPR-Cas9-mediated monoallelic gene knockout, generating ZEB1$^{+/-}$ cells (GSE121690)(Frausto et al., 2019). The comparison of the HUVEC ZEB1 siRNA KD dataset with the dataset from Frausto et al. was considered more appropriate than comparing to a total ZEB1 knockout dataset, given the partial reduction of ZEB1 expression achieved by siRNA.

Differentially expressed genes between ZEB1$^{+/-}$ and ZEB1$^{+/+}$ conditions were identified by pre-filtering the data with an adjusted p-value threshold of > 0.05. Log2 fold changes were retained for analysis (DEG data extraction from the raw data files was performed by Dr. Michaela Griffin). This analysis revealed 250 statistically significant DEGs, with 130 upregulated and 120 downregulated in the ZEB1$^{+/-}$ condition compared to the ZEB1$^{+/+}$ control (Figure 3.16 A and B). The top 15 up- and down-regulated genes are shown in Table 6 and Table 7. The corneal EC ZEB1$^{+/-}$ CRISPR-Cas9 dataset from Frausto et al was compared with the HUVEC ZEB1 siRNA KD dataset to identify overlapping genes. This comparison revealed 13 common genes: 8 were upregulated, 1 was downregulated, and 4 exhibited divergent expression changes between the two datasets (Figure 3.16 A and B, with a full list in table Table 8).

Global pathway analysis was subsequently performed using CytoScape to compare the two datasets. This analysis facilitated the identification of similar biological pathways and molecular networks that were impacted in both the HUVEC ZEB1 siRNA KD and corneal EC ZEB1$^{+/-}$ CRISPR-Cas9 datasets (Figure 3.17 and Figure 3.18).

Gene Symbol	Adjusted P Value	Log2 Fold Change
MAGEH1	2.94E-29	-10.1724648
B3GALNT1	2.59E-23	-9.311423657
CUX2	2.56E-06	-3.078636685
RAET1E	0.000693484	-2.849780409
LOC105374117	0.005252171	-2.823558655
SLC12A8	0.00610038	-2.664730854
LOC105377806	0.007965087	-2.644238326
TNRC6C-AS1	0.004992262	-2.465518497
NOS3	0.000164646	-2.17498986
ZNF780B	9.53E-18	-2.147793689
ECM1	0.00011867	-2.102978884
FBXL16	0.001237482	-2.002967765
CHD5	0.00497329	-1.894903922
C13orf46	0.01003376	-1.845109035
FSCN1	5.56E-05	-1.659156987

Table 4 The top 15 downregulated differentially expressed genes within the ZEB1$^{+/-}$ corneal EC condition. *(GSE121690, Frausto et al., 2019). DEGs were identified between ZEB1$^{+/-}$ and ZEB1$^{+/+}$ conditions using a p-value threshold of > 0.05, revealing 250 significant DEGs.*

Gene Symbol	Adjusted P Value	Log2 Fold Change
KCNT2	9.54E-24	9.191238
GIPC3	6.19E-63	7.679895
DDIT4L	4.46E-11	7.033916
CTHRC1	3.57E-09	5.821496
ALDH1L1	2.35E-10	5.433403
UGT3A2	1.12E-13	4.534634
VAMP8	4.81E-26	4.432066
SCIN	0.003369	4.143297
EPCAM	2.29E-15	4.086383
VAMP5	5.99E-09	3.932042
CLDN6	4.12E-10	3.852925
SCUBE2	7.47E-10	3.841911
TMEM52B	0.009754	3.699689
ZNF836	3.19E-06	3.367404
OLR1	0.007301	3.19877

Table 3 The top 15 upregulated differentially expressed genes within the ZEB1$^{+/-}$ corneal EC condition. *(GSE121690, Frausto et al., 2019). DEGs were identified between ZEB1$^{+/-}$ and ZEB1$^{+/+}$ conditions using a p-value threshold of > 0.05, revealing 250 significant DEGs.*

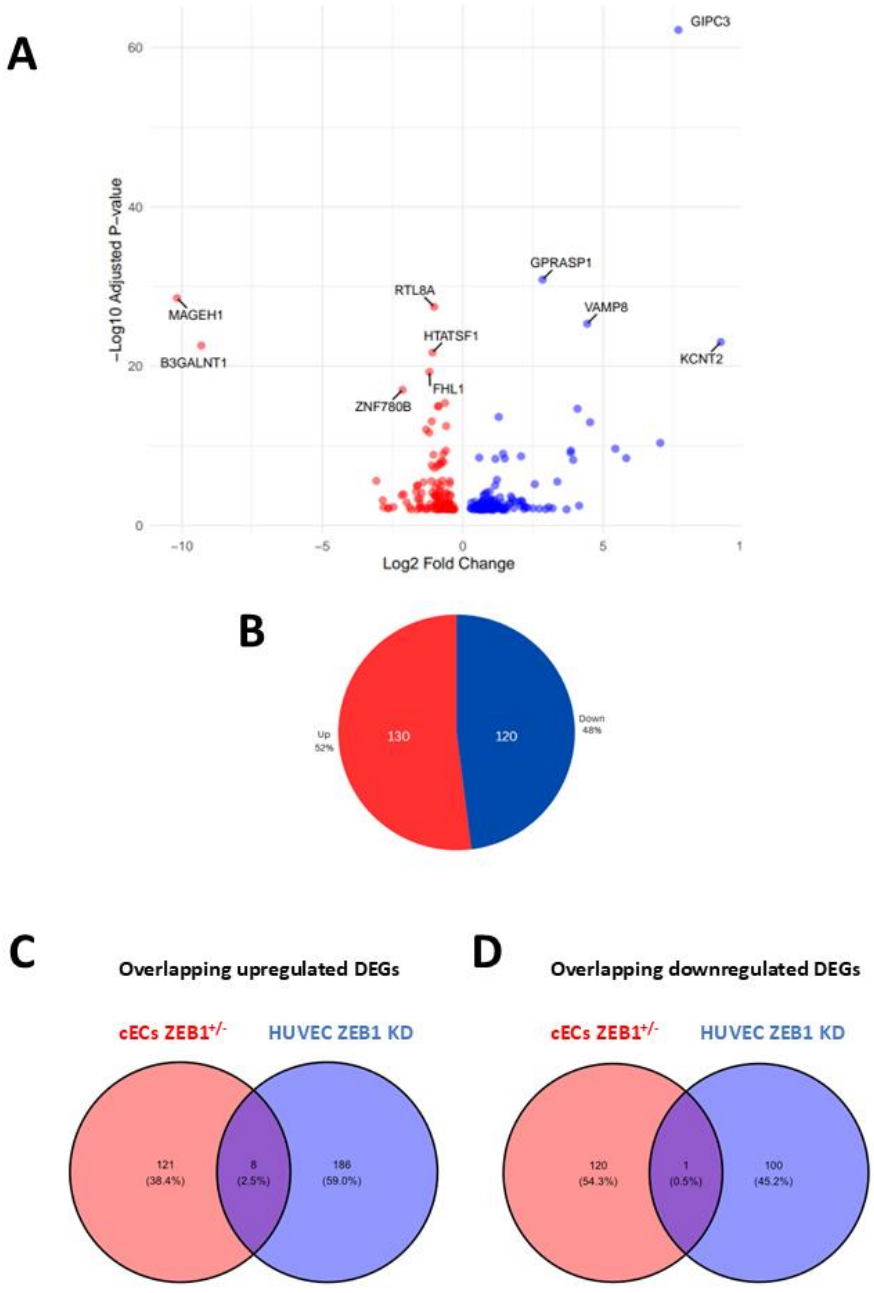

Figure 3.16 Differentially expressed genes in the ZEB1$^{+/-}$ corneal ECs compared with ZEB1$^{+/+}$ controls determined by RNASeq analysis. *Comparison of the HUVEC ZEB1 siRNA KD dataset with a publicly available RNA-Seq dataset from human corneal ECs with CRISPR-Cas9-mediated ZEB1 knockout (GSE121690, Frausto et al., 2019). DEGs were identified between ZEB1$^{+/-}$ and ZEB1$^{+/+}$ conditions using a p-value threshold of > 0.05, revealing 250 significant DEGs.* ***(A)*** *A volcano plot of the DEGs within the ZEB$^{+/-}$ corneal EC data set.* ***(B)*** *A pie chart displaying DEGs as up or down regulated. Overlapping DEGs within the HUVEC ZEB1 KD and ZEB$^{+/-}$ corneal EC data set are shown within the Venn diagrams* ***(C)*** *upregulated and* ***(D)*** *downregulated.*

Gene Symbol	HUVEC siRNA DEGs Log2 Fold Change	Corneal ECs DEGs Log2 Fold Change
Up-regulated in both data sets		
EFEMP1	2.308058671	0.234800451
MYL9	1.161581022	0.357390453
LIMS2	0.658225524	0.400565014
MFSD3	1.135044699	0.556732665
EPCAM	4.0863833	1.252728404
SH2D3A	2.092871937	1.587185612
FAM83H	1.252132688	2.875945697
GRB7	2.564821986	3.153615685
Down-regulated in both data sets		
ETS1	-0.922628727	-0.246098804
Overlapping genes		
IFIT1	1.328085	-1.61264
NOS3	-2.17499	0.298524
EPHA2	-1.18102	0.183157
SLC12A8	-2.66473	2.72541

Table 5 The overlapping DEGs in both the HUVEC ZEB1 siRNA KD data set and the corneal EC ZEB1$^{+/-}$ data set. *Comparison of the HUVEC ZEB1 siRNA KD dataset with a publicly available RNA-Seq dataset from human corneal ECs with CRISPR-Cas9-mediated ZEB1 knockout (GSE121690, Frausto et al., 2019). DEGs were identified between ZEB1$^{+/-}$ and ZEB1$^{+/+}$ conditions using a p-value threshold of > 0.05, revealing 250 significant DEGs.*

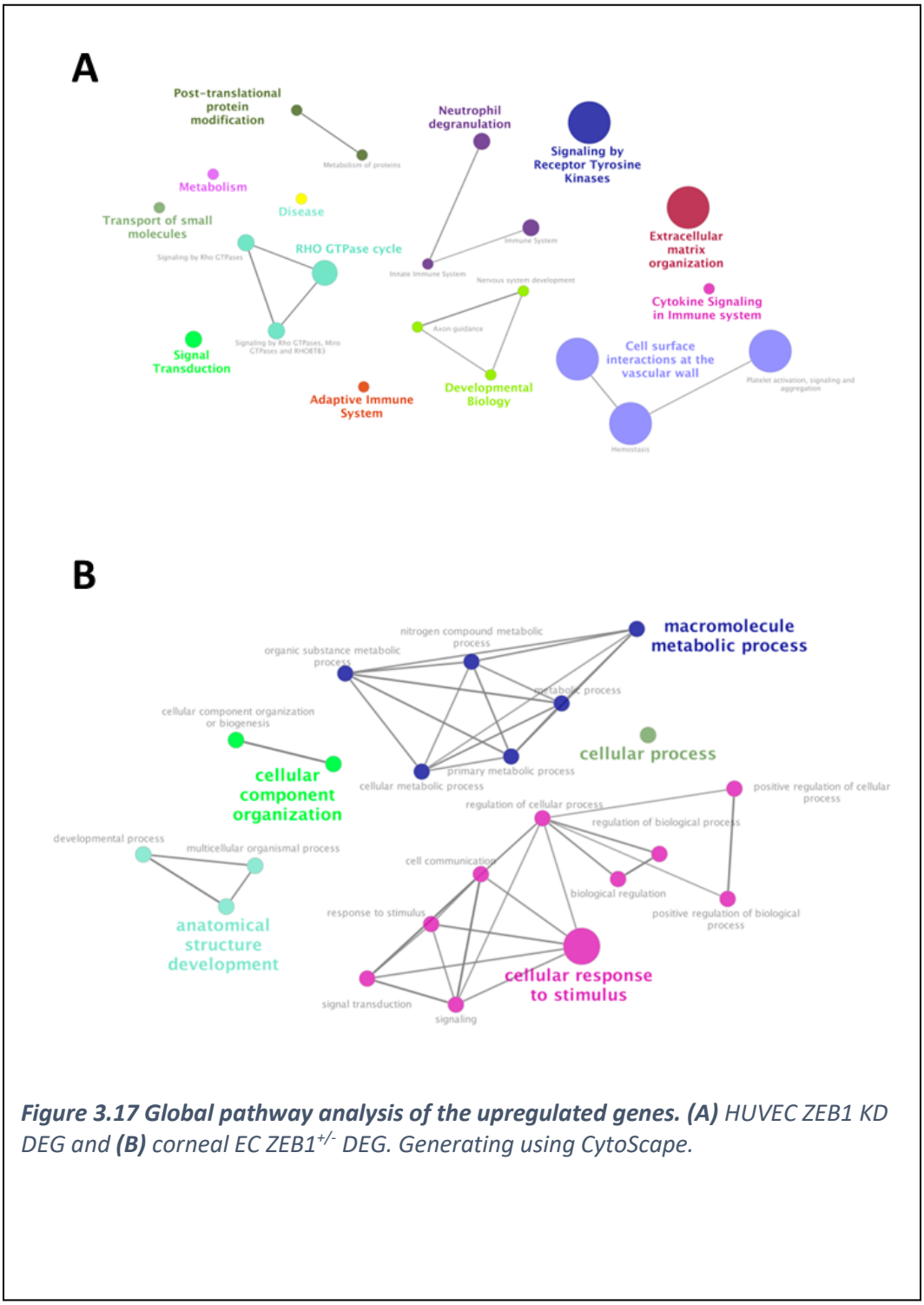

Figure 3.17 Global pathway analysis of the upregulated genes. (A) *HUVEC ZEB1 KD DEG and* ***(B)*** *corneal EC ZEB1$^{+/-}$ DEG. Generating using CytoScape.*

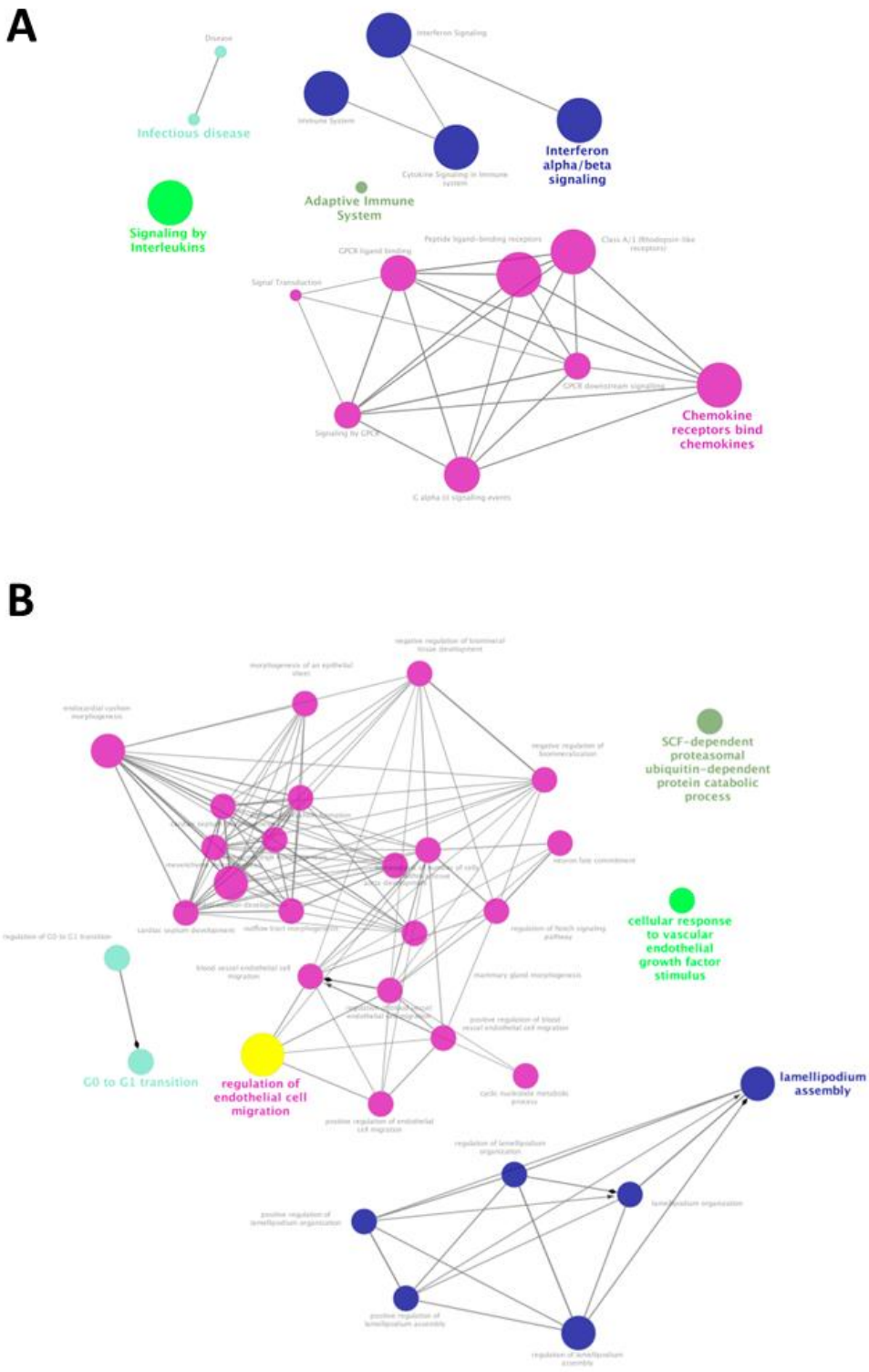

Figure 3.18 Global pathway analysis of the downregulatedngenes. (A) *HUVEC ZEB1 KD DEG and* ***(B)*** *corneal EC ZEB1$^{+/-}$ DEG. Generated using CytoScape,*

3.2.6 ChIP-Seq of ZEB1 within confluent HUVECs

To determine direct binding sites of ZEB1 within the genome, a ChIP experiment was set up. Chromatin from confluent HUVECs was isolated and sheared via sonication before ZEB1 was immunoprecipitated to isolate sheared chromatin bound to ZEB1. The set up was repeated using IgG as a pulldown control. The DNA isolated from the immunoprecipitation was isolated and purified before being sequenced. Quality control assessments were also performed using ChIPQC which indicated a high-quality ChIP-Seq experiment due to a couple of factors (Table 9). Firstly, there is a similar fragment length and read length within all 3 repeats, indicating the repeats are similar in their properties. And secondly, the Read in the Peaks% (RiP%) is particularly good, suggesting a high signal to noise ratio and anything above 5% indicates a successful transcription factor enrichment. A heat map was generated using ChIPQC which represents the signal enrichment of ZEB1 ChIP-Seq and of IgG reads in 2000bp regions that are centered on the peak summit Figure 3.19 A. This clearly shows that the reads are enriched within the peaks of the ZEB1 ChIP-Seq compared to the IgG control. All quality control analysis and figures were made by Joseph Horder.

ID	Tissue	Factor	Condition	Replicate	Reads	Dup%	ReadL	FragL	RelCC	SSD	RiP%
A1		ZEB1		1	3736565	0	138	278	2.1	2.3	20
A2		ZEB2		2	3988022	0	139	279	1.5	2.4	21
A3		ZEB3		3	3241030	0	141	283	1.5	1.8	13
Control	NA	NA	NA	NA	9640501	0	142	285	1.1	1.6	NA

Table 6 ChIPQC analysis results. Results from ChIPQC R program ran by Joseph Horder indicates high quality ChIP-Seq.

3.2.6.1 77.74% of the peaks were within promotor regions of the genome

The analysis of all the raw data was performed by Jospeh Horder to identify and annotate peaks to specific genes. ZEB1 ChIP-Seq identified 12,631 distinct ZEB1 binding regions within the genome. Moreover, gene annotation of the binding peaks revealed 9,206 individual genes. The distribution of ZEB1 peaks within the genome is plotted within the pie chart in Figure 3.19 B to identify the percentage of different genomic features. A promoter was defined as 1000bp upstream and downstream the transcription start site. This identified that majority of peaks (77.74%) were within a promotor region of the genome. The rest of the peaks were with distil intergenic (7.59%), 1st Intron (4.25%) or other Intron regions of the genome (5.2%). Fewer values were observed in other genomic regions, such as 1st Exon (1.42%) or other Exon (1.75%).

3.2.6.2 Known motif analysis identified the ZEB1 motif, along with Fli1, ETV4 and AP-1 binding motifs within the peaks

HOMER known motif analysis was performed to identify known binding motifs within the ZEB1 ChIP-Seq peaks was performed by Jospeh Horder. This software uses publicly available data sets to identify known transcription factor binding motifs. These motifs were identified within 200bp of the center of the peak summit and are assigned to a p value which was adjusted with Benjamini-Hochberg correction Figure 3.19 C). This identified that the ZEB1 peak was the 4th most significantly enriched motif with 27.18% of the binding sites containing the known ZEB1 motif. However, this also identified other transcription factor binding motifs, such as AP-1, ETV4 and Fli1, which may identify them as possible binding partners of ZEB1.

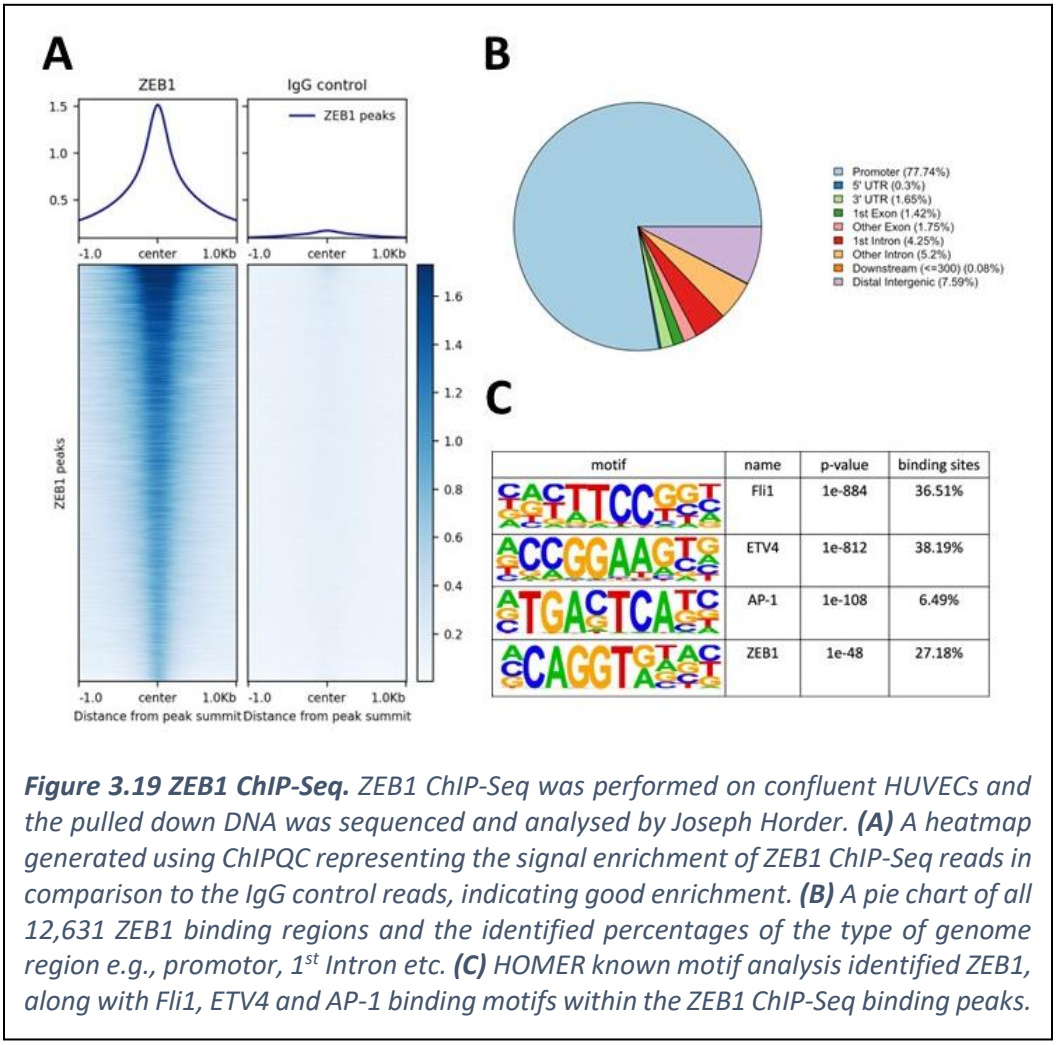

Figure 3.19 ZEB1 ChIP-Seq. *ZEB1 ChIP-Seq was performed on confluent HUVECs and the pulled down DNA was sequenced and analysed by Joseph Horder.* ***(A)*** *A heatmap generated using ChIPQC representing the signal enrichment of ZEB1 ChIP-Seq reads in comparison to the IgG control reads, indicating good enrichment.* ***(B)*** *A pie chart of all 12,631 ZEB1 binding regions and the identified percentages of the type of genome region e.g., promotor, 1st Intron etc.* ***(C)*** *HOMER known motif analysis identified ZEB1, along with Fli1, ETV4 and AP-1 binding motifs within the ZEB1 ChIP-Seq binding peaks.*

3.2.6.3 KEGG pathway analysis of genes identified as binding to ZEB1 within their genome sequence by ChIP-Seq

To explore specifically enriched pathways which contain genes with ZEB1 bound genomic regions, over representation KEGG pathway analysis was performed using the total number of genes identified from ZEB1 ChIP-Seq. This identified 46 significant KEGG pathways (Figure 3.20). Many of these pathways contained similar signaling events, such as MAPK and phosphatidylinositol signaling, which have similar pathways to the various cancer pathways. However, there were also more specific pathways such as endocytosis, as well as fluid shear stress and atherosclerosis. The top 3 significantly overrepresented

KEGG signaling pathways within the data set are presented in Figure 3.21, Figure 3.22 and Figure 3.23. This data provides an indication of how ZEB1 may be influencing EC behavior and activity, via DNA binding of specific pathway genes.

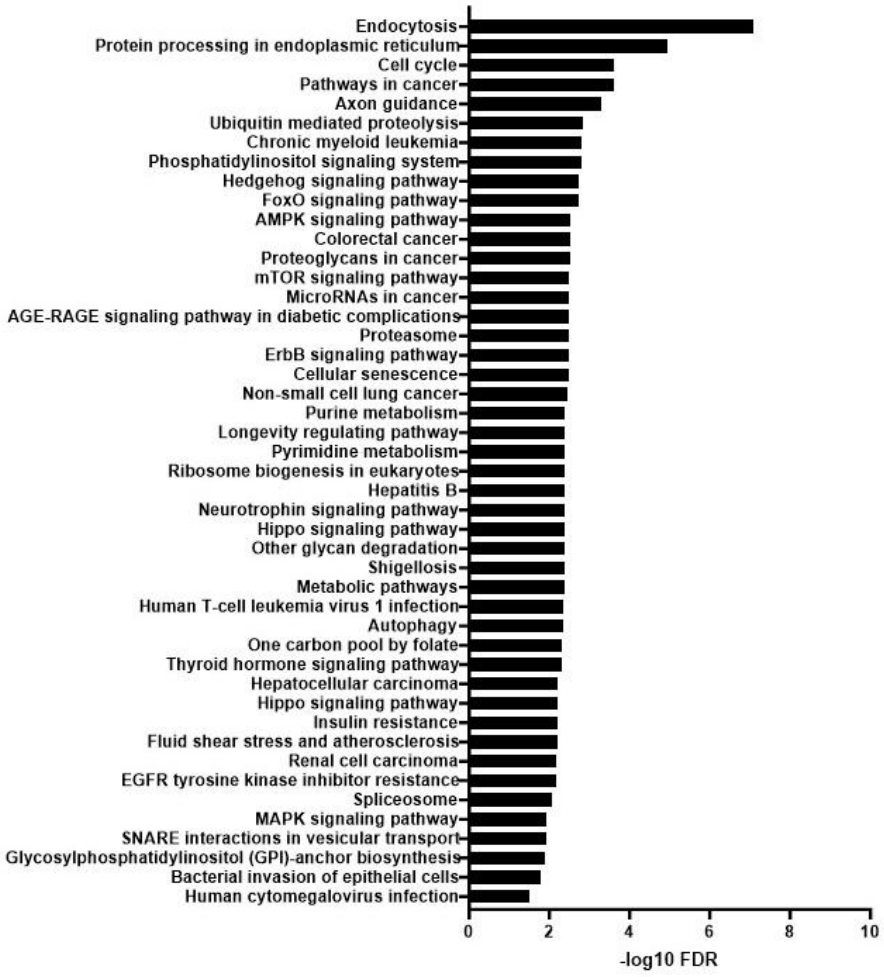

Figure 3.20 Significant KEGG pathways identified from the gene list produced from ZEB1 ChIP. *ZEB1 ChIP was performed on confluent HUVECs. The pulled down DNA was sequenced and assigned to genomic regions for individual genes. The gene list was analysed by over representation analysis to determine significant KEGG pathways. All significant KEGG pathways are presented for genes identified by ZEB1 ChIP in confluent HUVECs.*

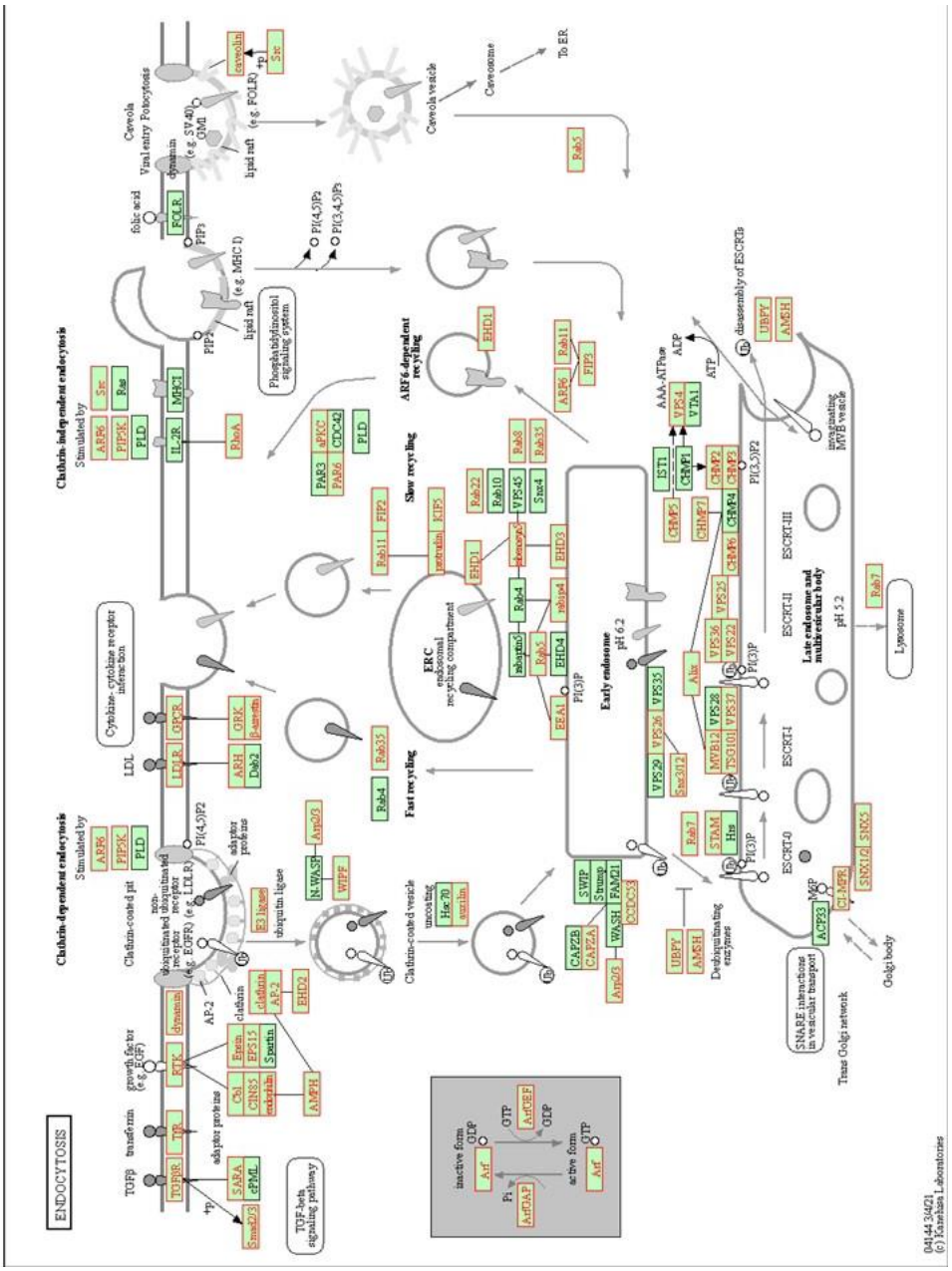

Figure 3.21 Endocytosis KEGG pathway was identified as being significantly overrepresented within gene list produced from ZEB1 ChIP. *ZEB1 ChIP was performed on confluent HUVECs. The pulled down DNA was sequenced and assigned to genomic regions for individual genes. The gene list was analysed by over representation analysis to determine significant KEGG pathways. The Endocytosis KEGG pathway was identified as being the most significantly overrepresented. Genes within the ZEB1 ChIP data set have a red border. Taken from WebGestalt.*

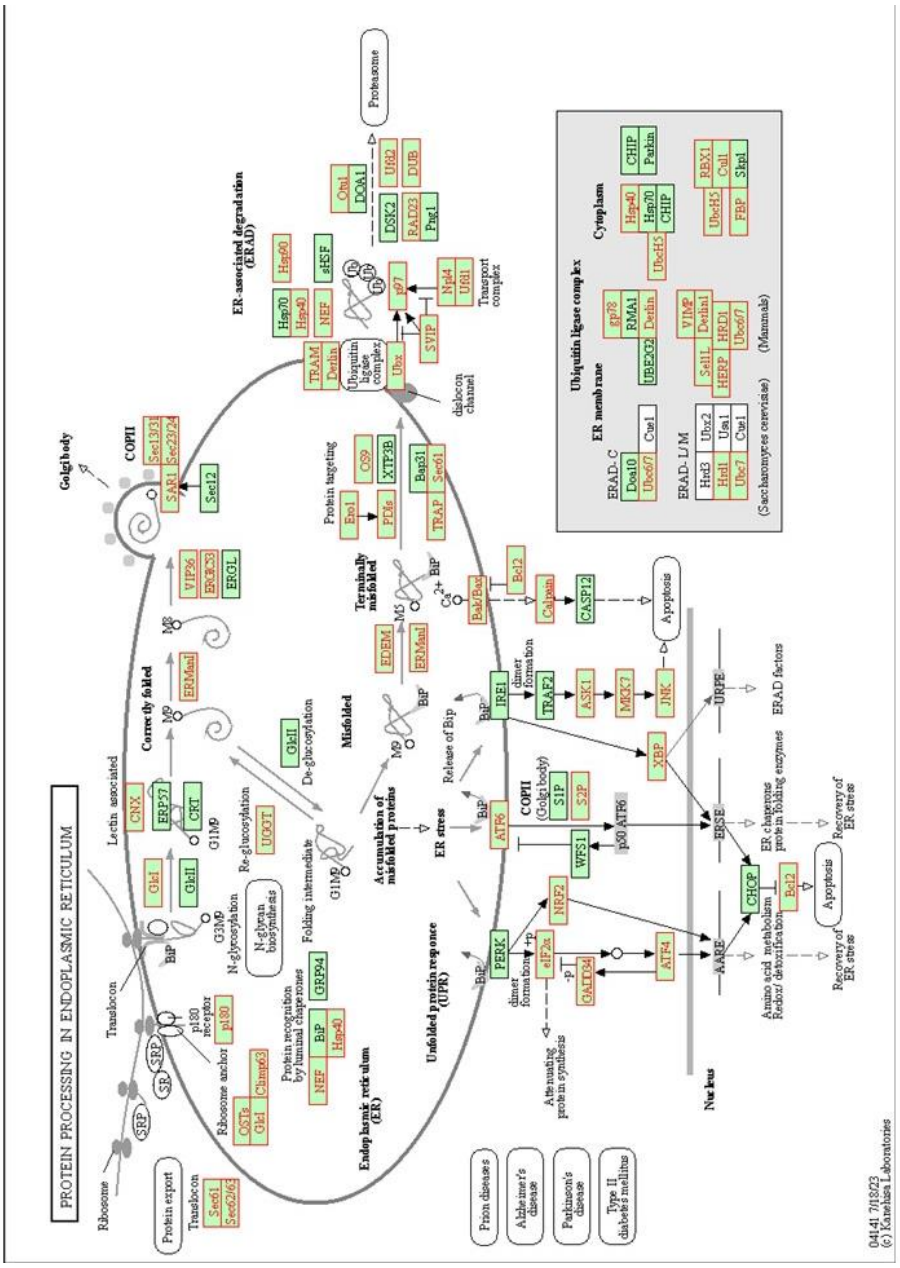

Figure 3.22 Protein processing in endoplasmic reticulum KEGG pathway was identified as being significantly overrepresented within gene list produced from ZEB1 ChIP. *ZEB1 ChIP was performed on confluent HUVECs. The pulled down DNA was sequenced and assigned to genomic regions for individual genes. The gene list was analysed by over representation analysis to determine significant KEGG pathways. The protein processing in endoplasmic reticulum KEGG pathway was identified as being the most significantly overrepresented. Genes within the ZEB1 ChIP data set have a red border. Taken from WebGestalt.*

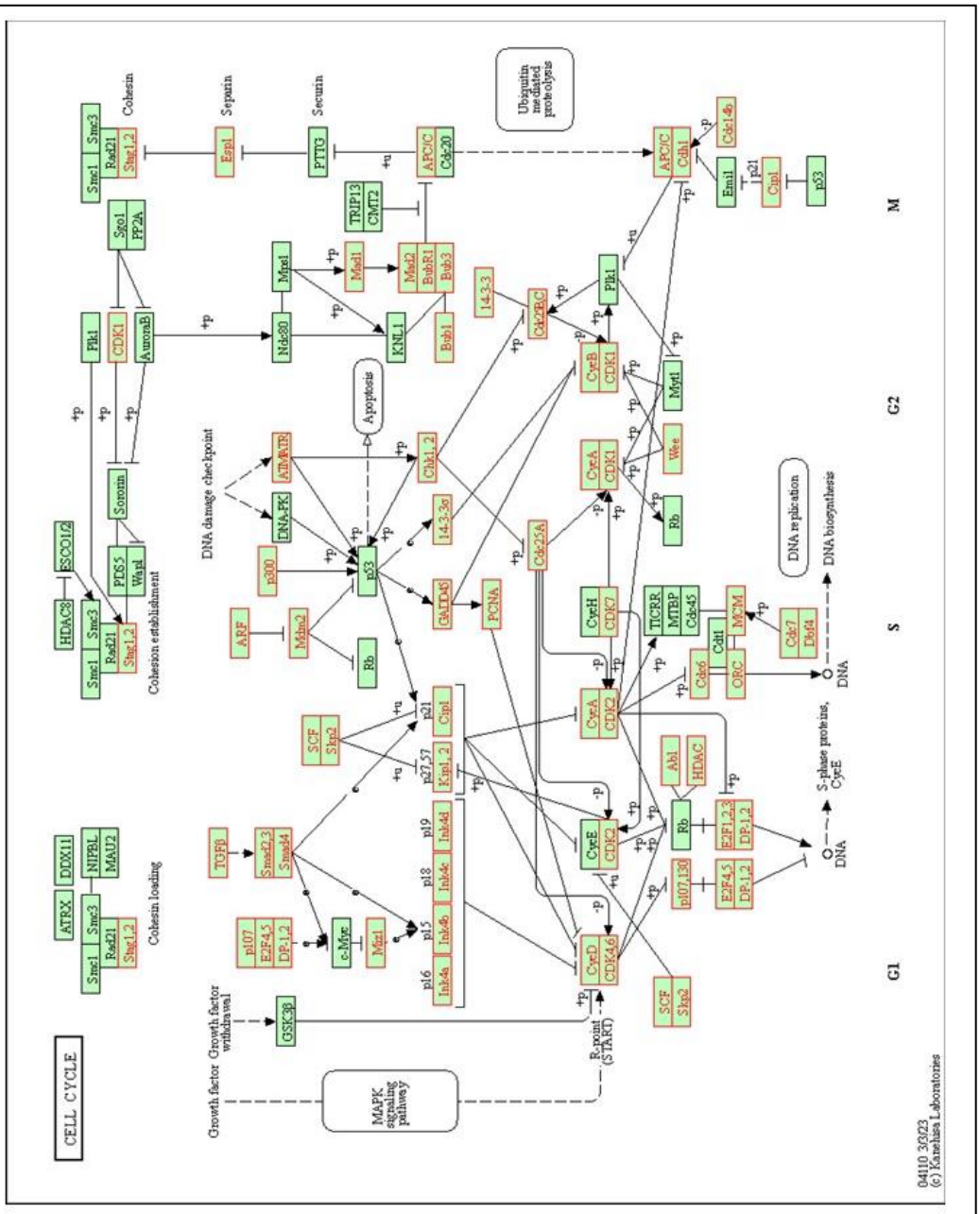

Figure 3.23 Cell cycle KEGG pathway was identified as being significantly overrepresented within gene list produced from ZEB1 ChIP. *ZEB1 ChIP was performed on confluent HUVECs. The pulled down DNA was sequenced and assigned to genomic regions for individual genes. The gene list was analysed by over representation analysis to determine significant KEGG pathways. The cell cycle KEGG pathway was identified as being the most significantly overrepresented. Genes within the ZEB1 ChIP data set have a red border. Taken from WebGestalt.*

3.2.7 RNA-Seq and ChIPSeq identified 163 differentially expressed in ZEB1 KD HUVECs and bound by ZEB1 within their genomic sequence.

RNA-Seq provided an overview of how ZEB1 KD influenced the transcriptome of ECs. However, on its own it cannot identify genes that are directly regulated by ZEB1, as some of the differentially expressed genes might have a change in expression due to downstream effects. ChIP-Seq on the other hand provides evidence of DNA binding but does not give any indication about the consequence of that binding. By combining the RNA-Seq and ChIP-Seq data, this will provide a list of genes that expression changes when ZEB1 expression is knocked down and has been identified as a being bound by ZEB1 within its genomic sequence Figure 3.24. A Venn diagram was generated to observe the overlap of the individual 9,206 genes identified from ChIP-Seq and the 295 significant differentially expressed genes identified from ZEB1 KD RNA-Seq. This revealed that 153 of the genes within the RNA-Seq data set were also observed in the ChIP-Seq data set, which is just over half. This information suggests that ZEB1 may be directly regulating the expression of 163 of these genes. Many of these genes, 122 (74.39%), were upregulated as a result of ZEB1 KD, indicating that ZEB1 has a higher level of transcriptional repression in comparison to transcriptional activation. Only 42 (25.61%) of these genes were down regulated as a result of ZEB1 KD, therefore indicating ZEB1 is positively driving the expression of these genes.

To validate this data set, a literature search was performed to identify if any of these 153 genes have been previously identified as being regulated by ZEB1. These genes are listed in Table 10. A list of the top 15 downregulated and upregulated genes are listed in Table 11 and Table 12 respectively, along with information regarding the positions of ZEB1 peak or peaks, within the ChIP-Seq data.

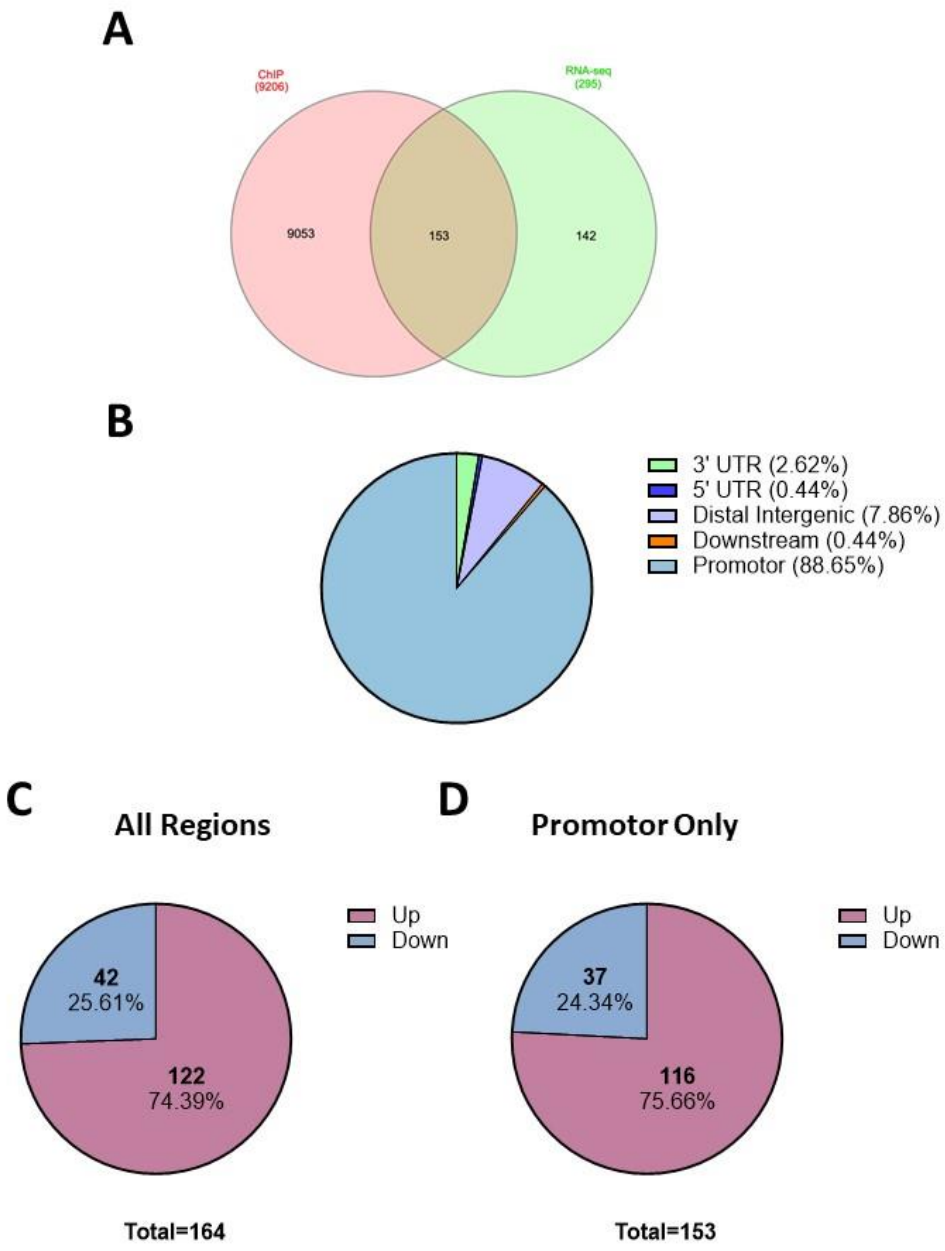

Figure 3.24 Analysis of genes pulled down by ZEB1 ChIP and differentially expressed within ZEB1 KD HUVECs. (A) *A Ven diagram displaying the cross over between the ZEB1 ChIP (promotor bound genes only) and ZEB1 RNA-Seq differentially expressed genes identified 153 genes.* ***(B)*** *164 genes identified in total as being in both data sets, with 88.65% (153) being bound at the promotor and the remaining genes 11.35% (11) being bound elsewhere within the gene DNA sequence.* ***(C)*** *A pie chat for all crossover genes.* ***(D)*** *A pie chart from cross over genes that are bound to the promotor only.*

Gene	Log2FC	Bound region	Reference
ID2	-0.774179	Promoter	Lee et al, 2023
CD274	0.25905554	Promoter	Wirbel et al, 2025
EPCAM	1.2527284	Promoter	Vannier et al, 2013
CXCR4	-0.5708069	Promoter	Beji et al, 2017
BMP4	0.25479536	Promoter	Zhou et al, 2021
ICAM	-0.5043994	Promoter	Abou-Jaoude et al, 2018
HDAC9	-0.6805216	Promoter	Zhong et al, 2021

Table 7 Identified genes within the ZEB1 KD RNA-Seq and identified within the ZEB1 ChIP-Seq that have been previously identified within the literature as being regulated by ZEB1.

Gene Symbol	Gene Region	Distance to Transcription Start Site	Adjusted P Value	Log2 Fold Change
CMPK2	Promoter	0	0.021132	-1.19929
XAF1	Distal Intergenic	-1516	0.0002	-0.86437
OAS3	Promoter	0	1.84E-11	-0.8632
C2CD4A	Promoter	0	0.000335	-0.81924
ID2	Downstream (<=300bp)	1810	0.01427	-0.77418
CHST1	Promoter and Distal Intergenic	0 and 2717	2.45E-13	-0.71868
HDAC9	Promoter	0	0.036492	-0.68052
NID2	Promoter	0	5.65E-10	-0.64806
POU2F2	3' UTR	2590	1.94E-07	-0.62456
UNC5B	Promoter	0	1.28E-05	-0.61812
CXCR4	Promoter	0	5.65E-10	-0.57081
TRAF1	Promoter	0	0.003225	-0.55543
KLF4	Promoter and Distal Intergenic	0 and -146630	0.016591	-0.54737
SOD2	Promoter	0	4.01E-05	-0.54636
ISG20	Promoter	0	0.004917	-0.54131

Table 8 The top 15 down-regulated genes within the ZEB1 KD RNA-Seq and identified within the ZEB1 ChIP-Seq. *A list of the top 15 down-regulated genes within both the RNA-Seq and ChIP-seq data sets, along with information regarding distance to transcription start site and gene region in which ZEB1 is bound.*

Gene Symbol	Gene Region	Distance to Transcription Start Site	Adjusted P Value	Log2 Fold Change
KLC3	Promoter	0	2.77E-07	3.543978
PRKCZ	3' UTR	3042	1.59E-32	3.378851
GRB7	Distal Intergenic	10296	7.28E-06	3.153616
SLC12A8	Promoter	0	8.27E-08	2.72541
BAIAP2L1	Promoter and Promoter	0 and 271	1.94E-37	2.371526
CDC42BPG	Promoter	0	7.28E-25	2.288792
EPS8L2	Promoter	0	6.47E-43	2.257529
LAMC2	Promoter	0	5.93E-55	2.142115
ESRP2	Promoter	0	4.58E-19	2.004425
LLGL2	Promoter	0	7.29E-34	1.882792
CAMSAP3	Promoter	0	8.85E-12	1.84566
FBX02	Promoter and Promoter	0 and 0	4.92E-05	1.48702
PPL	Promoter	0	2.71E-05	1.440083
DENND2D	Promoter	0	0.00021	1.413889
MT1F	Promoter	0	0.01051	1.408614

Table 9 The top 15 up-regulated genes within the ZEB1 KD RNA-Seq and identified within the ZEB1 ChIP-Seq. *A list of the top 15 down-regulated genes within both the RNA-Seq and ChIP-seq data sets, along with information regarding distance to transcription start site and gene region in which ZEB1 is bound.*

3.2.7.1 Significant GO terms were identified within the list of differentially expressed genes in ZEB1 KD HUVECs and bound by ZEB1 within their genomic sequence.

The list of differentially expressed genes within the ZEB1 KD HUVEC condition and bound by ZEB1 within their genomic sequence was analysed by ORA to identify significant GO terms. This analysis was firstly completed using all genes and GO terms for biological processes, molecular function and cellular component were identified and the top 10 most significant displayed in Figure 3.25. This identified biological processes involved in adhesion, circulatory system and proliferation. There was an increase in diversity of the biological processes identified, resulting in no overarching theme. Molecular functions were primarily centred around actin binding, extracellular matrix binding and adhesion binding. Whereas the cellular components involved cell junctions, focal adhesions and the cell surface.

To specify which processes contain upregulated or downregulated genes, the differentially expressed genes as a result of ZEB1 KD were separated into upregulated and downregulated. The analysis was then repeated, firstly on the downregulated genes only, to identify biological processes that contain downregulated genes and hence, may be reduced or affected by the reduction of ZEB1. The top 10 biological processes identified are displayed in Figure 3.26. These GO terms had a significant focus on inflammatory pathways, such as response to cytokine, response to virus and defence response. However, when performing ORA for molecular functions or cellular component, this revealed no significant results.

The analysis was then repeated with only the upregulated genes, to identify biological processes that contain upregulated genes and hence, may be increased or affected by the reduction of ZEB1. The top 10 biological processes identified are display in Figure 3.27. This identified biological processes involved in adhesion, junction organisation and cytoskeletal organisation. The molecular function identified continued this theme, which included actin binding, extracellular matrix components, laminin binding and cadherin binding. The cellular components focused on cell junctions, cell surface and anchoring junctions Taken together this data indicates that adhesion associated genes are enriched within the upregulated ZEB1 KD data set and bound to by ZEB1 at their genomic sequence,

suggesting loss of ZEB1 may directly affect cellular adhesion. ORA to identify significant KEGG pathways was also performed with all genes, as well as up and down regulated genes. Each analysis identified no significant KEGG pathways.

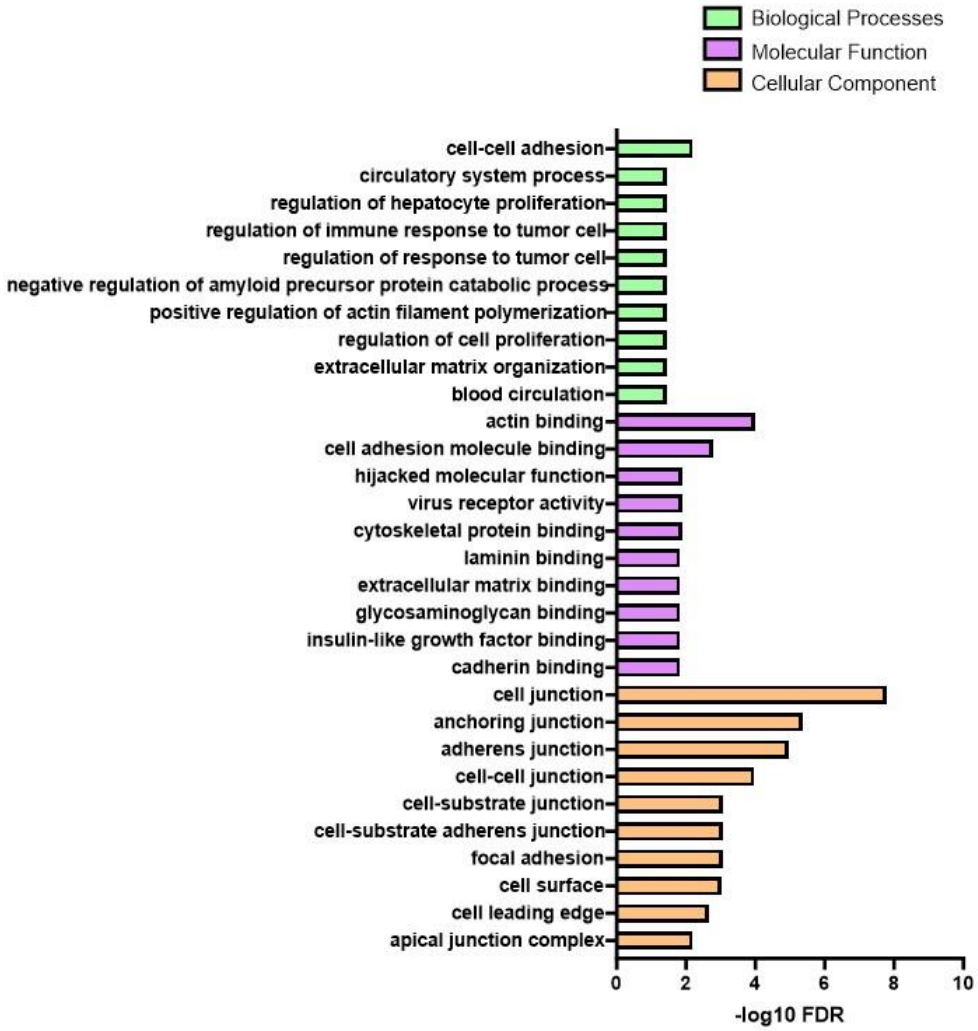

Figure 3.25 The top 10 significant go terms identified from all differentially expressed genes within both ZEB1 KD HUVECS and ZEB1 ChIP. *All 164 differentially expressed genes identified from both ZEB1 KD RNA-Seq and ZEB1 ChIP were analysed by over representation analysis to determine significant biological processes, molecular function and cellular component GO terms. The top 10 significant GO terms are presented.*

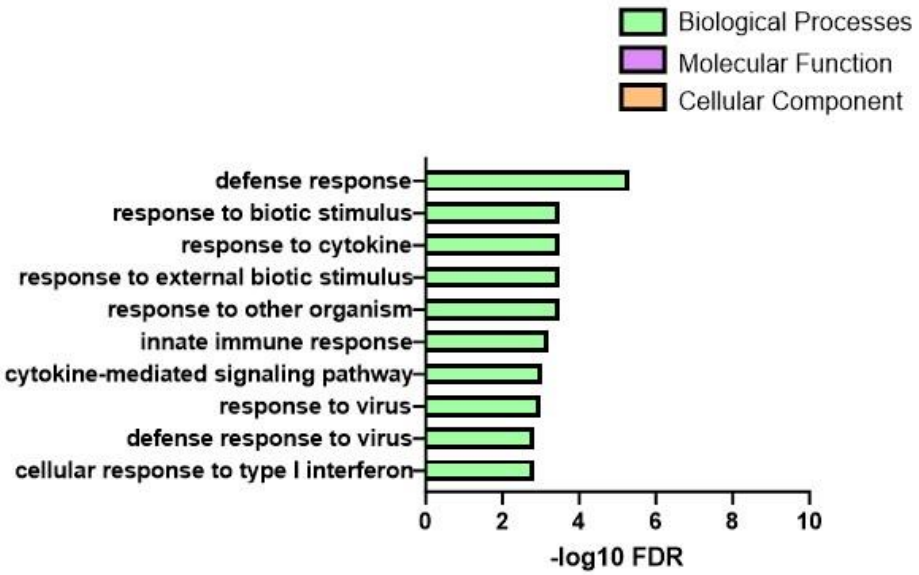

Figure 3.26 The top 10 significant go terms identified from differentially expressed genes that are down-regulated within both ZEB1 KD HUVECS and ZEB1 ChIP. *The 122 significantly down regulated genes identified from both ZEB1 KD RNA-Seq and ZEB1 ChIP were analysed by over representation analysis to determine significant biological processes, molecular function and cellular component GO terms. The top 10 significant GO terms are presented.*

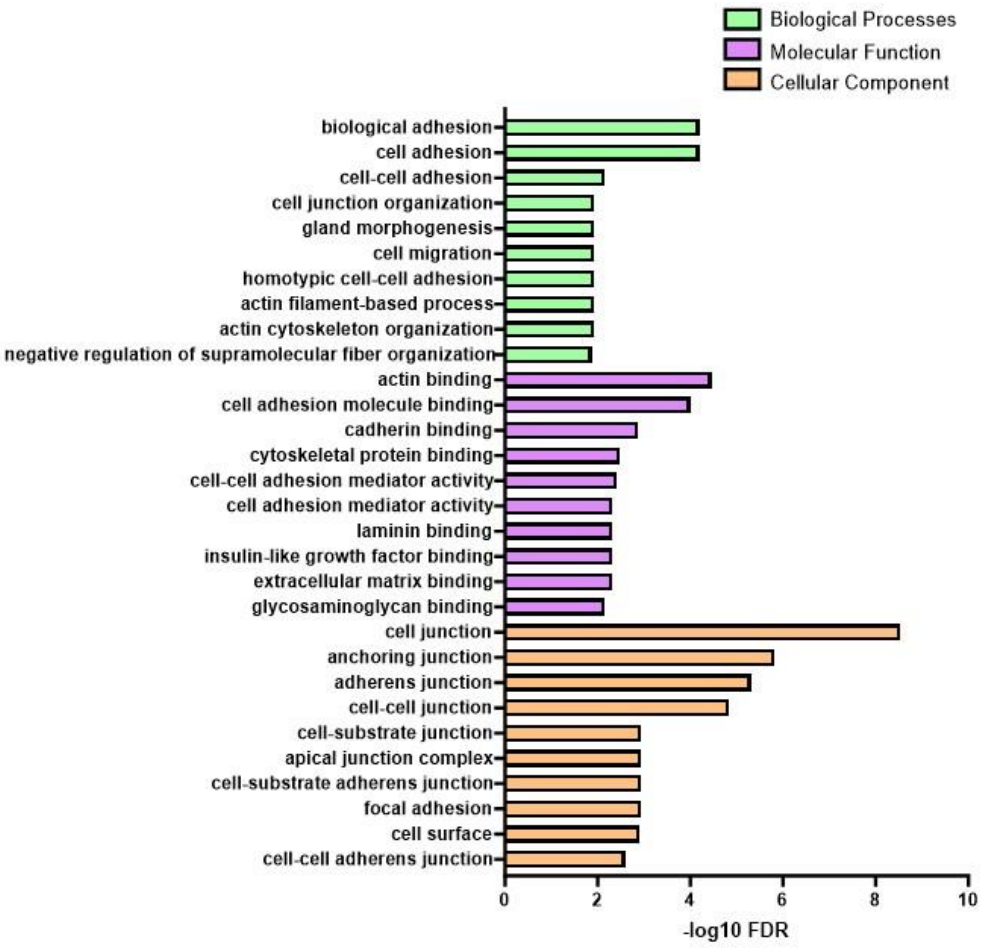

Figure 3.27 The top 10 significant go terms identified from differentially expressed genes that are up-regulated within both ZEB1 KD HUVECS and ZEB1 ChIP/ *The 42 significantly upregulated genes identified from both ZEB1 KD RNA-Seq and ZEB1 ChIP were analysed by over representation analysis to determine significant biological processes, molecular function and cellular component GO terms. The top 10 significant GO terms are presented.*

3.2.8 Specific genes of interest identified as being differentially expressed in ZEB1 KD HUVECs and bound by ZEB1 within their genomic sequence

Out of the 163 genes identified within the ChIP-Seq as being bound by ZEB1 within their genomic promotor sequence and being differentially expressed as a result of ZEB1 KD, a number of genes were of particular interest due to their previously reported roles within the literature and roles within endothelial cells. The first of these genes include EPCAM, which is significantly upregulated in the ZEB1 KD condition, with a Log2 fold change of 1.25 (Figure 3.28 A). EPCAM became a gene of interest due to the fact ZEB1 has previously been identified as a direct regulator of EPCAM during Zebrafish development, as well as within human pancreatic and breast cancer (Vannier et al., 2013). ZEB1 was also found to be bound to the EPCAM promotor within MDA-MB-231 cells via ChIP-Seq (Feldker et al., 2020). EPCAM is also primarily an epithelial gene and a loss of EPCAM expression is highly associated with EMT which is often driven by ZEB1 activity within cancer and metastasis (Sánchez-Tilló et al., 2012).

LAMC2 was also noted as a gene of interest due to its role within the extracellular matrix, which appears in multiple GO analysis. LAMC2 has also been previously identified within the literature as being regulated by ZEB1 in lung adenocarcinoma metastasis driven by EMT (Moon et al., 2015). Not only this but within ECs, LAMC2 has been identified as playing a role in vascular permeability by inducing cytoskeletal changes and EC shrinkage (Sato et al., 2014). The expression of LAMC2 was determined to be significantly upregulated in response to ZEB1 KD, with a Log2 FC of 2.14 of NSC (Figure 3.28 C).

NOS3 was identified due to its major role within vascular homeostasis and vasodilation. Although constitutively expressed in ECs, the expression level of NOS3, as well as its activity at the protein level, can be well manipulated during cellular stress events such as hypoxia and ischemia, as well as during endothelial dysfunction (Kalinowski et al., 2016). In the case of ZEB1 KD in HUVECs, NOS3 was determined to be upregulated in response to ZEB1 KD, with a Log2 fold change of 0.298, which although is not a major change, was still observed to be significant (Figure 3.28 E).

In the ZEB1 KD condition, ICAM1 was determined to be significantly downregulated (Log2 fold change of -0.50, Figure 3.28 G), along with ZEB1 determined as being bound to the

ICAM1 promotor. ICAM1 has for some time known to have an important influence on the inflammatory response and leukocyte recruitment to sites of infection (Bui et al., 2020). Like NOS3 it is also constitutively expressed on ECs, but its expression levels are known to be modulated by pro-inflammatory cytokines (Lawson & Wolf, 2009). ZEB1 KD resulted in a general trend of decreased response to inflammation and hence the reduction of ICAM1 contributes to this trend.

KLF4 was also identified as having ZEB1 bound at its promoter sequence, along with it being differentially expressed within the ZEB1 KD RNA-Seq (Log2 fold change of -0.55, Figure 3.28 I). KLF4 was initially identified as a transcription factor that's expression is upregulated under flow and sheer stress (Mccormick et al., 2001), however since then reports have also identified roles for KLF4 within the regulation of the inflammatory response (Hamik et al., 2007).

Finally, CXCR4 was identified as a gene of interest. Previously published microarray analysis identified CXCR4 as being significantly enriched in angiogenic tip ECs within the neonatal mouse retina (Strasser et al., 2010). Not only this, CXCR4 was noted to play an important function in vascular development, as changes to CXCR4 expression, or activation via its ligand CXCL12, resulted in a failure of hierarchical vascular branching (W. Li et al., 2021). In the case of ZEB1 KD, CXCR4 is significantly down regulated, with a Log2 fold change of -0.57 (Figure 3.28 K).

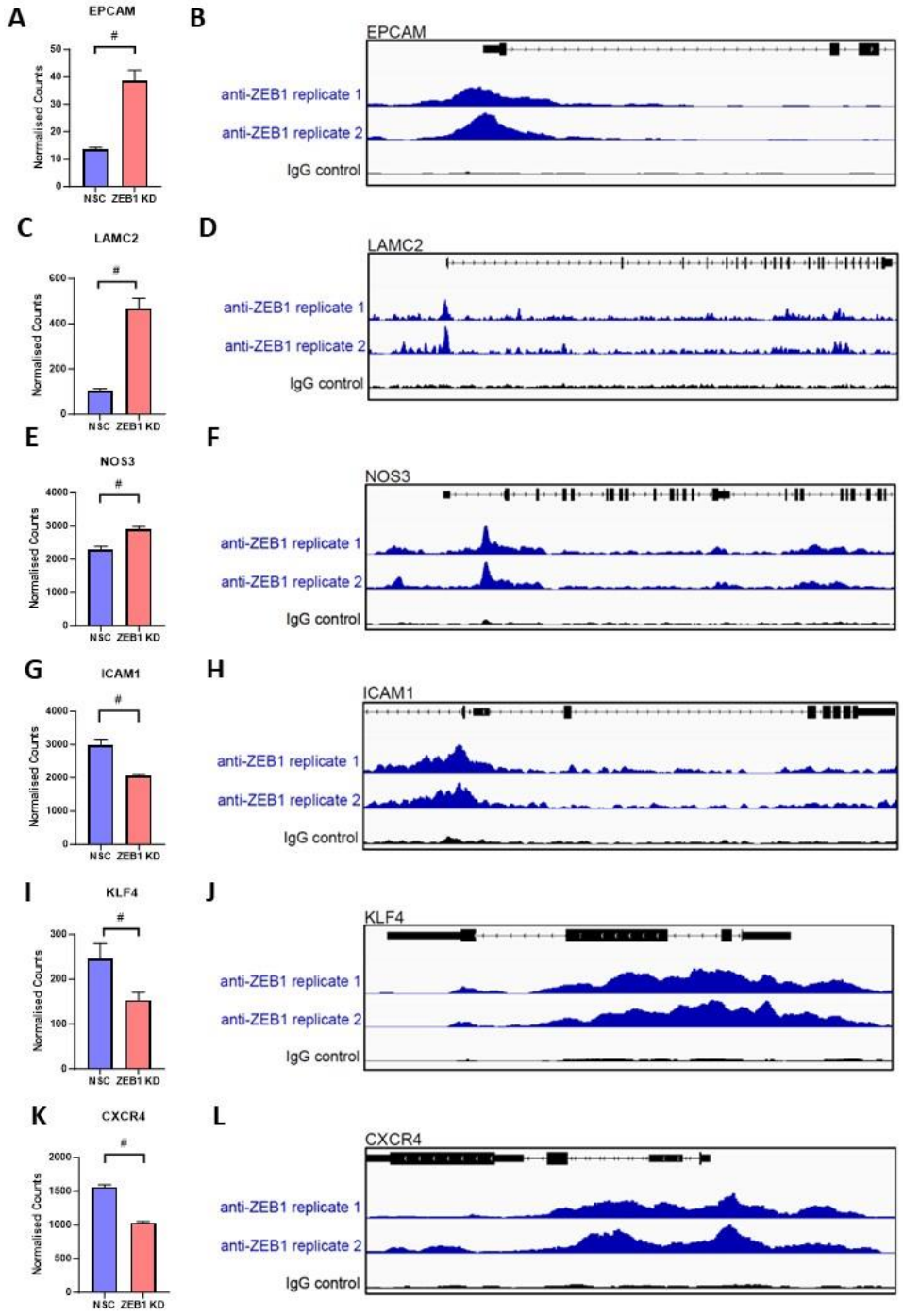

Figure 3.28 Specific genes of interest identified within both ZEB1 KD HUVECS and ZEB1 ChIP at the gene's promotor. (A) *EPCAM normalised counts and* ***(B)*** *EPCAM signal track.* ***(C)*** *LAMC2 normalised counts and* ***(D)*** *LAMC2 signal track.* ***(E)*** *NOS3 normalised counts and* ***(F)*** *NOS3 signal track* ***(G)*** *ICAM1 normalised counts and* ***(H)*** *ICAM1 signal track* ***(I)*** *KLF4 normalised counts and* ***(J)*** *KLF4 signal track* ***(K)*** *CXCR4 normalised counts and* ***(L)*** *CXCR4 signal track. All data presented as mean of normalised counts, N = 3. Genes with an adjusted p value smaller than 0.05 were considered significant (#). Signal track plots generated by Joseph Horder.*

3.2.9 Overlapping hits within HUVEC confluency, HUVEC ZEB1 KD, ZEB1$^{+/-}$ corneal ECs and HUVEC ZEB1 ChIP

All four data sets used within this chapter were analysed to identified overlapping hits. This included DEGs from the RNA-Seq data sets, and those genes identified within the ZEB1 ChIP analysis where ZEB1 was found to be bound at the promotor. This identified three genes which were overlapping in all three data sets: LIMS2, NOS3 and EFEMP1 (Figure 3.29 and Table 12).

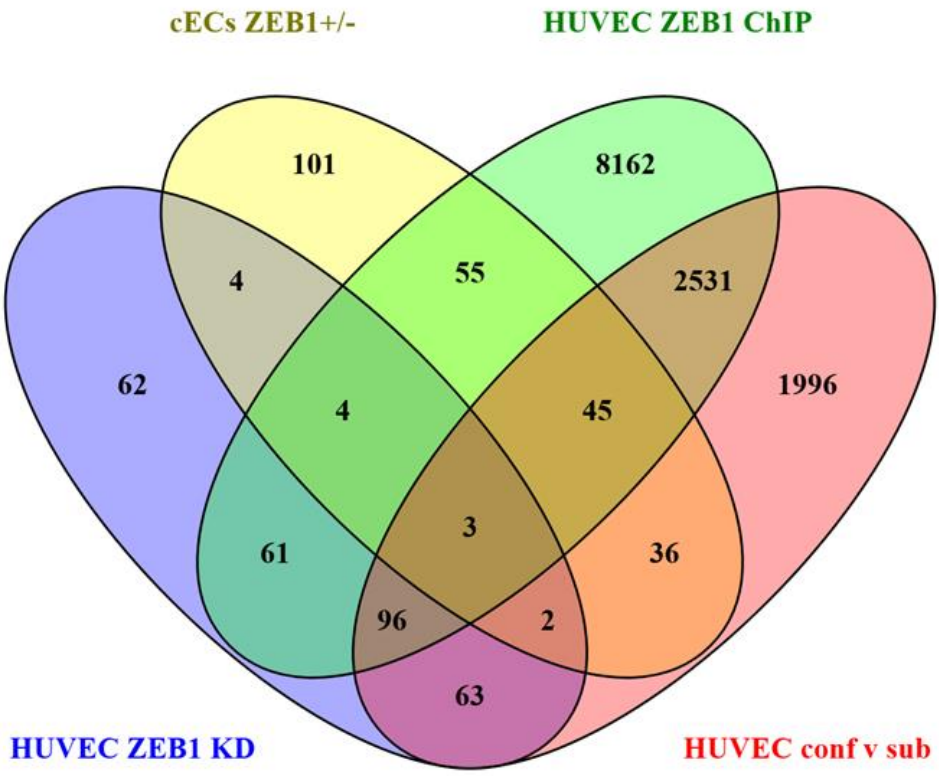

Figure 3.29 Overlapping hits within HUVEC confluency, HUVEC ZEB1 KD, ZEB1+/- corneal ECs and HUVEC ZEB1 ChIP.

Gene Symbol	HUVEC Sub vs Conf Log2FC	HUVEC ZEB1 siRNA Log2FC	cECs ZEB1$^{+/-}$ Log2FC	HUVEC ZEB1 ChIP location
EFEMP1	0.306066	0.2348	2.30806	Promotor
NOS3	0.651447	0.298524	-2.17499	Promotor
LIMS2	-0.620117	0.40057	0.65823	Promotor

Table 10 Overlapping hits within HUVEC confluency, HUVEC ZEB1 KD, ZEB1$^{+/-}$ corneal ECs and HUVEC ZEB1 ChIP.

3.2.10 Generating ZEB1 KO HUVECs using a CRISPR Cas9 method

Using siRNA to KD ZEB1 expression only resulted in a reduction of ZEB1 expression by around 50% at both the protein level determined by western blot, and at the RNA level determined by RNA-Seq. In an attempt to increase the level of knockdown of ZEB1 expression, I visited Dr Joanna Kaluckas lab in Aarhus University to utilise a CRISPR Cas9 method of reducing gene expression. These methods utilised HUVECs from single donors and therefore had slightly different methods of routine culture, which are mentioned within the methods chapter in this thesis. As well as this, wherever possible paired analysis was performed to allow for variation between the donors. In the case of single donors, one individual donor counted as 1 biological replicate, and this is continued throughout this section of this chapter. The data presented in sections 3.2.10–13 were all completed during this laboratory visit.

HUVECs from single donors were electroporated with recombinant Cas9 and either guide RNAs targeting ZEB1 or control guides RNAs. The cells were then seeded, allowed to reach full confluency before protein extracted and ZEB1 expression analysed via western blot (Figure 3.30). This revealed a significant reduction in ZEB1 protein expression (0.25 ± 0.06 fold change of control). This was around a 75% reduction in ZEB1 protein expression, which was higher than siRNA.

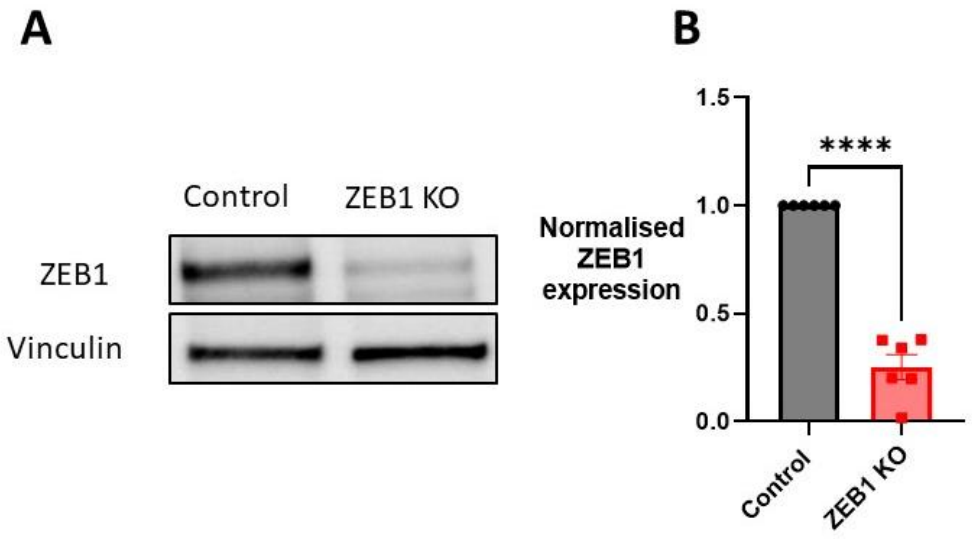

Figure 3.30 ZEB1 KO via a CRISPR method of nucleofecting recombinant Cas9 and guide RNA against ZEB1. *HUVECs were nucelofected with recombinant Cas9 and either control guide RNAs or guide RNAs against ZEB1 in order to KO ZEB1 and reduce ZEB1 expression.* ***(A)*** *Nucleofected cells were grown until they reached confluency plus 72 hours. Protein was then extracted and expression of ZEB1 was determined via western blot.* ***(B)*** *Densitometry analysis was performed and protein expression for ZEB1 was determined and normalised to Vinculin. All data are presented as mean + SEM and was statistically analysed used a paired t-test. **** $p < 0.0001$*

3.2.11 ZEB1 KO in HUVECs did not affect the viability determined by MTT assay

To assess if knocking out ZEB1 influenced the viability of HUVECs, ZEB1 KO cells and their donor control cells were seeded in a 96 well plate and left to incubate in complete media for 24, 48, 72 and 96 hours at 37°C. Following incubation, MTT was added, incubated for 4 hours before solubilisation and absorbance determined at 570nm. The raw absorbance values were plotted for each time point (Figure 3.31 A). A two-way ANOVA was performed, and main effects analysis revealed that time significantly impacted the viability of both control and ZEB1 KO HUVECs. This is to be as expected as the cells become confluent, they increase in number and therefore have a higher MTT assay output. The drop off at 96 hours can be explained by the reduction in serum and growth factors in the media by this

time point, possibly leading to starvation and death. Main effects analysis determined that cell type did not have a significant affect on cell viability, suggesting that KO of ZEB1 is not affecting cell viability. Multiple comparisons analysis was also performed using Sidaks multiple comparison test, which revealed no significant difference between the control and ZEB1 KO cells at any time point ($P > 0.05$).

To adjust for variation within between the specific donors, the MTT readings of the ZEB1 KO cells were normalised to their paired control from the same donor (Figure 3.31 B). Two-way ANOVA analysis was performed again and main effects analysis which revealed that cell type did not significantly impact the absorbance value and hence viability. Sidaks multiple comparison test was also performed, which revealed no significant difference between the control and ZEB1 KO cells at any individual time point ($P > 0.05$). This data therefore indicates that ZEB1 KO does not impact cell viability.

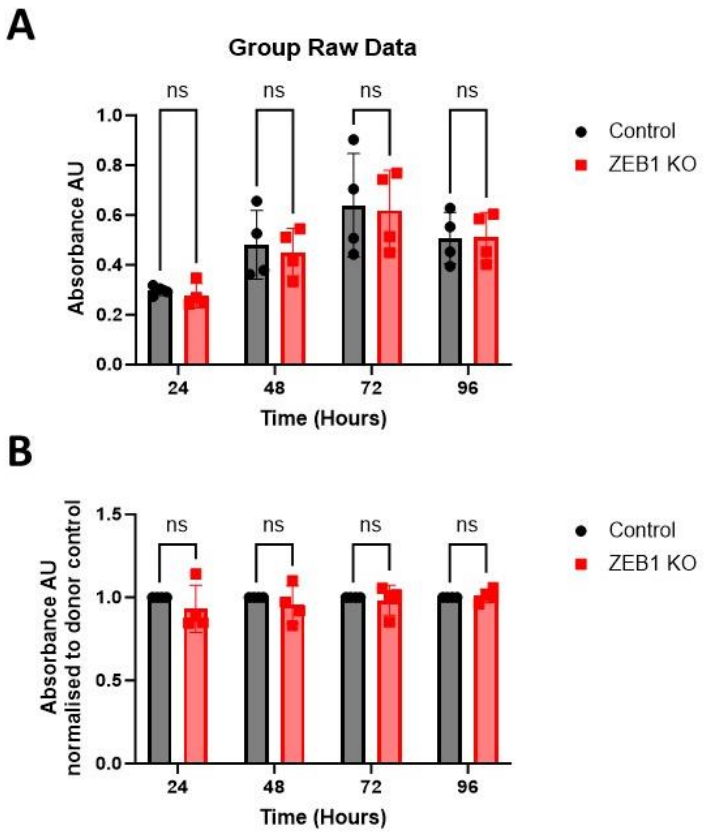

Figure 3.31 ZEB1 KO has no affect on cell viability or proliferation as determined by MTT assay. *ZEB1 KO and paired donor control cells were plated for 24, 48, 72 and 96 hours before an MTT assay was performed and absorbance measured at 570nm.* ***(A)*** *Raw data are displayed.* ***(B)*** *Data are normalised to donor control at each time point. All data are presented as mean + SEM and was stastically analysed used a two-way ANOVA with Sidaks multiple comparisons (ns, P > 0.05).*

3.2.12 ZEB1 KO in HUVECs did not have a significant impact on migration

To assess if ZEB1 KO affects the functionality of ECs, a scratch assay was performed which measures migration and proliferation of endothelial cells, both of which are essential processes in angiogenesis. The assay was also performed with and without the presence of Mitomycin C, a cell cycle inhibitor, which will determine if any of the affects observed are due to migration alone and not proliferation. Confluent ZEB1 KO and control HUVECs were seeded and reached full confluency before a scratch applied to the centre of the well. The closure of the scratch was measured over 2 days, with time points a 4h, 6h, 18h, 24h, 32h and 48h. The relative migration was calculated and plotted in Figure 3.32 for each condition. A two-way ANOVA was performed and main effects analysis revealed that time significantly impacted the migration of HUVECs, which is to be expected. Main effects analysis determined that the condition (KO or control, Mitomycin C or control) did not have a significant effect on migration. Multiple comparisons were also performed using Sidaks multiple comparison test, which revealed no significant difference between the either of the conditions at any time point ($P > 0.05$). Although the raw data viewed in Figure 3.32 displays that the ZEB1 KO cells have reduced migration compared to control, and that mitomycin C further reduced that migration, this difference is not observed to be statistically significant. Therefore, this data suggests that ZEB1 KO does not significantly impact HUVEC migration.

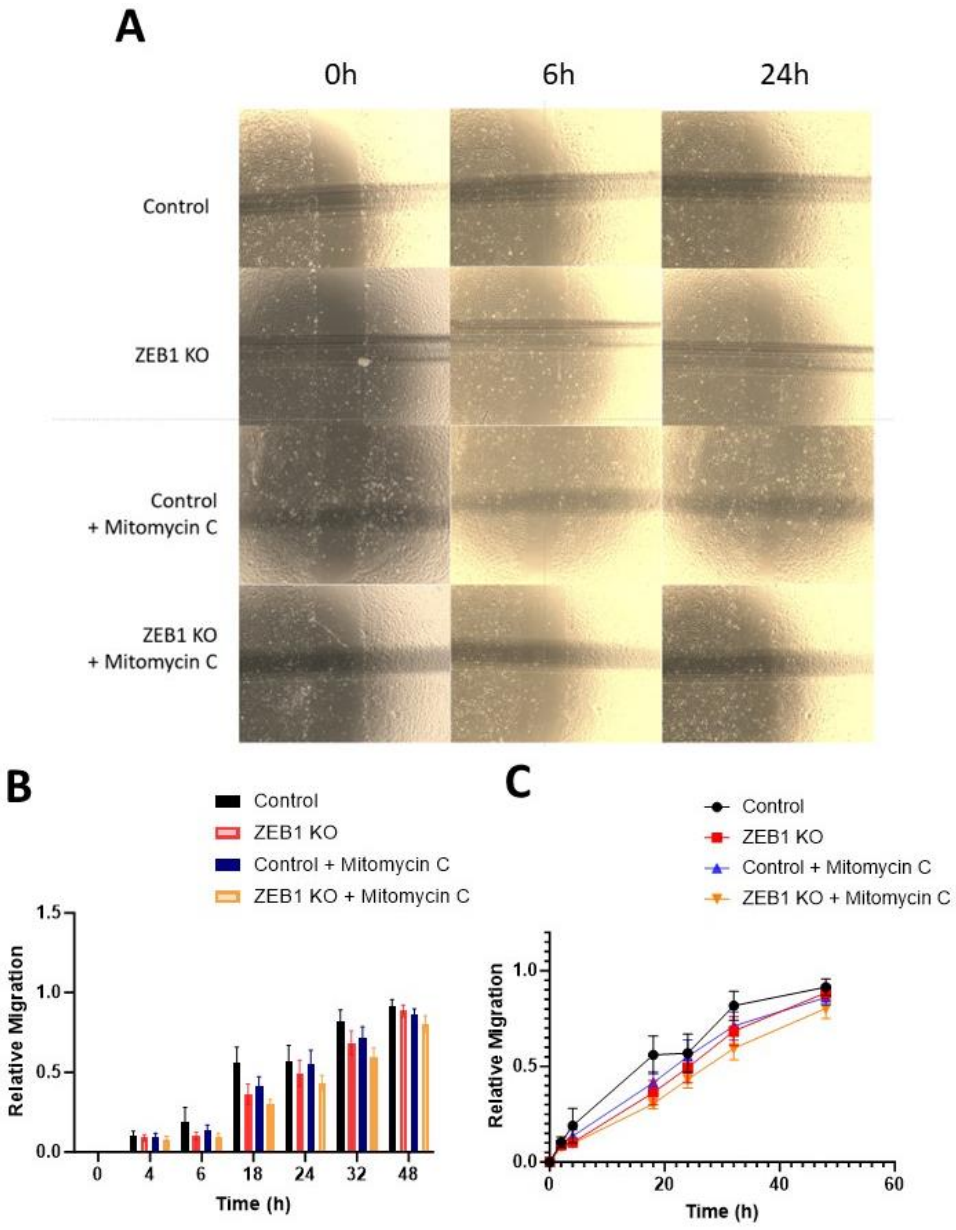

Figure 3.32 ZEB1 KO had a no significant effect on migration in both untreated and mitomycin C treated cells. *ZEB1 KO and paired donor control cells were plated until fully confluent before a scratch assay was performed. Images of the scratch were taken at 0h, 4h, 6h, 18h, 24h, 32h and 48h to monitor wound closure. Images were analysed on Image J.* ***(A)*** *Representative images are shown for 0h, 6h and 24h time points.* ***(B)*** *Relative migration for each condition is displayed.* ***(C)*** *An XY graph to display relative migration over time. Data are normalised to donor control at each time point. All data are presented as mean + SEM and was stastically analysed used a two-way ANOVA with Sidaks multiple comparisons (ns, P > 0.05).*

3.2.13 ZEB1 KO in HUVECs resulted in significantly reduced sprouting

A further functional assay was utilised in assessing how ZEB1 KO influences HUVECs. In this instance, a sprouting assay was set up to determine if ZEB1 KO is affecting HUVECs ability undergo sprouting. This was achieved by generating ZEB1 KO and donor control spheroids using the hanging drop method, followed by seeding into a fibrinogen 3D matrix with complete medium supplemented. The sprouts from these spheroids were analysed 24h and 48h post seeding (Figure 3.33). This revealed a reduction in sprout number per spheroid within the ZEB1 KO cells at both 24 (16.1 ± 0.6 per spheroid compared to 18.6 ± 0.2 control) and 48 (13.3 ± 0.7 per spheroid compared to 18.0 ± 0.7 control) hours, which was confirmed to be significant via a paired t-test. The sprout length was also determined at 24 and 48 hours, which revealed no significant difference via a paired t-test ($P > 0.05$). Despite this, at 48 hours there was a small reduction in sprout length which was almost significant ($P = 0.056$). Finally, the average branch point per spheroid was determined, which revealed no significant difference at the 24-hour time point, but by 48 hours there was a significant reduction in the number of branch points per spheroid within the ZEB1 KO group (0.96 ± 0.17 per spheroid) in comparison to the control group (0.36 ± 0.09 per spheroid). This data therefore indicates that loss of ZEB1 in HUVECs significantly impacts sprouting within the angiogenic process.

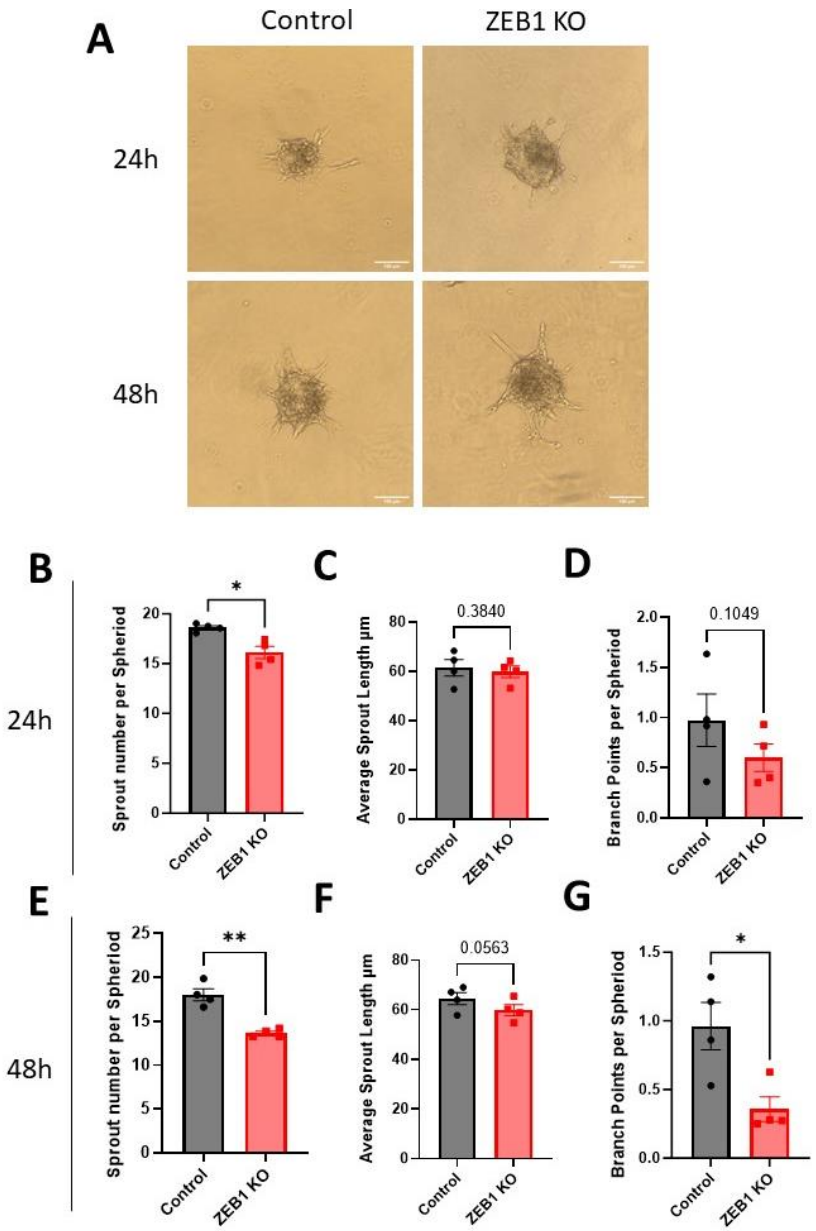

Figure 3.33 ZEB1 KO resulted in a significant reduction in sprout number per spheroid. *Spheroids were generated using ZEB1 KO and paired donor control cells that were then seeded into a 3D fibrinogen gel and incubated with complete media. 24 and 48 hours post seeding the spheroids were imaged to determine sprout number, sprout length and branch number using Image J.* ***(A)*** *Representative images of ZEB1 KO and control spheroids at 24h and 48h. Sprout number per spheroid was displayed in 24h* ***(B)*** *and 48h* ***(E)****. Sprout length was displayed in 24h* ***(C)*** *and 48h* ***(F)****. Branch point number per spheroid was displayed in 24h* ***(D)*** *and 48h* ***(G)****. All data are presented as mean + SEM and was stastically analysed used a paired t-test (* p < 0.05, ** p < 0.005*

3.3 Discussion

3.3.1 Transcriptomic comparison of confluent and subconfluent HUVECs

3.3.1.1 Subconfluent and confluent HUVECs exhibited distinct transcriptomes

The confluency of any EC culture has long been known to be important to the EC phenotype and hence their transcriptome. The literature sometimes uses variation in terminology when describing these EC cultures, e.g. dense vs sparse, proliferating vs quiescent, confluent vs subconfluent; however, the premise of the experiment remains similar (Reine et al., 2015). The large variation in confluent compared to subconfluent ECs is very evident within the data presented in this chapter. The RNA-Seq data from confluent and subconfluent HUVECs determined 4,773 significantly differentially expressed genes. This large amount of differentially expressed genes is expected due to the large differences in the conditions. It was for this reason that a Log2 fold change cut off of 1.5 was applied, to focus on those genes above this threshold.

The confluent condition is model that aims to represent the endothelium within the vasculature owing to its appearance as a complete monolayer. The GO terms identified to be enriched within the confluent condition provide evidence of this, as they focus on biological adhesion and cell shape. This is reminiscent of a condition where a monolayer is established or in the process of establishing itself as being quiescent. The KEGG pathways identified within this condition also provide evidence of this, with extracellular matrix-receptor interaction being the most significant, which can be explained by the apical basal polarity and basal lamina binding that is observed within the quiescent endothelium. Whereas the subconfluent condition does not model the quiescent monolayer observed within the endothelium. Instead, this condition contains HUVECs which are actively proliferating, migrating and have less cell-cell connections. This is also observed within the GO terms and KEGG pathways determined by ORA, with many processes associated with development and differentiation, which are indicative of an immature and unestablished phenotype that does not resemble a confluent monolayer.

An important consideration regarding the quiescent endothelium is that, by definition, ECs in this state are not proliferating (Galley & Webster, 2004; Ricard et al., 2021a; Schlereth et al., 2018). However, upon analysis to identify GO terms and KEGG pathways

that are over-represented in the DEGs between confluent and subconfluent HUVECs, no terms or pathways related to cell cycle or cell proliferation were identified. This indicates that there were no significant differences in cell cycle progression or proliferation between the confluent and subconfluent conditions. Consequently, although the confluent condition effectively models the physical structure of the endothelium, the cells were not in a quiescent state.

The expression level of FOXO1 and PFKFB3 were determined due to their roles in ECs. Both observed to be upregulated within the confluent condition according to RNA-Seq, and this is also confirmed at the protein level for both genes; however, the meaning of this upregulation within the confluent monolayer has a more plausible explanation for FOXO1 in comparison to PFKFB3. FOXO1 is a known regulator of endothelial quiescence (Andrade et al., 2021), and hence its upregulation within a confluent condition as this confluent monolayer structurally resembles the quiescent endothelium. PFKFB3 expression is on the other hand associated with increased metabolism required for angiogenesis via the direct modulation of glycolysis which is necessary for vessel sprouting (De Bock et al., 2013). Alongside the lack of DEGs involved in proliferation and cell cycle, this provides another layer of evidence that suggests the condition is still has a high glycolytic metabolism and proliferating.

3.3.1.2 Phenotypic differences between confluent and subconfluent HUVECs could be explained by EndoMT

An interesting point to emerge for the RNA-Seq data analysis was the differential expression of EndoMT associated genes. Although less understood in comparison to EMT, EndoMT has become an emerging field of interest within vascular health and disease and does draw some parallels to EMT in its function. In a recent review, Peng et al defined that in vitro EndoMT involves the loss of endothelial properties along with the co-expression of endothelial and mesenchymal markers (Peng et al., 2022). To determine this, a list of endothelial and mesenchymal associated genes was derived from the literature (Reviewed and listed in Platel et al., 2019), and the expression of these markers compared between the confluent and subconfluent condition. Interestingly, this revealed that the subconfluent condition had significantly lower expression of endothelial marker genes

CDH5, PECAM1, VWF, TEK, TIE1 and ERG. This was coupled with an increase in mesenchymal marker genes within the subconfluent condition, including CDH2 (N-Cadherin) and TAGLN (SM22α). This data therefore does suggest that there is an EndoMT profile within the subconfluent HUVEC condition.

EndoMT has received a lot of attention in the context of endothelial dysfunction and vascular disease; however, physiological roles of EndoMT have been identified within developmental processes such as cardiac valve development (Armstrong & Bischoff, 2004; Von Gise & Pu, 2012). There is also an indication that mural supporting cells such as pericytes and smooth muscle cells are able to be derived from ECs in vivo, as determined by lineage tracing (Coll-Bonfill et al., 2015; Lee et al., 2023). These reported processes align similarly to the GO terms identified as being overrepresented within the subconfluent condition, such as cardiovascular development, blood vessel development and vascular development.

It could be assumed that the subconfluent condition more accurately represents physiological angiogenesis as the cells are proliferating and migrating. But there are additional factors that are not present within a subconfluent cell culture, such as hypoxia and a chemokine gradient. Angiogenesis itself has also been described as an EndoMT-like or partial EndoMT process within the literature (Platel et al., 2019; Weinstein et al., 2020). This was initially proposed and displayed by Welch-Reardon et al in work which identified Slug (SNAI2) having a role in angiogenic sprouting. During this work, the team similarities between angiogenesis and EndoMT, such as migration, morphological changes and breakdown of extracellular matrix (Welch-Reardon et al., 2014). Continued research to assess whether this is the entire picture, or whether EndoMT is a distinct process is currently a focus within the field, and the application and availability of single cell RNA-Seq data are allowing for that exploration of this.

To explore whether there is any variation in transcription factor expression between the confluent and subconfluent conditions which may account for this change in endothelial and mesenchymal genes, a panel of transcription factors was derived from a literature search and their expression levels plotted. Due to there being less research attention on EndoMT in comparison to EMT, there are fewer publications or reviews that outline a

direct link between a transcription factor and its role within EndoMT. For that reason, the transcription factors within the panel have been identified primarily as direct regulators of EMT (Zeisberg & Neilson, 2009), but with limited direct evidence supporting their involvement in EndoMT. This analysis yielded varied results, with some transcription factors not being present at all within the normalised counts (TWIST1, GSC and LEF1). This absence was not entirely unexpected as it may indicate that these factors are either not expressed in HUVECs or are not generally expressed in ECs. Among the EMT transcription factors that were significantly differentially expressed, all but one showed a decrease in expression in the confluent condition, with higher expression levels in the subconfluent condition. This pattern correlates with the increased expression of mesenchymal genes observed in the subconfluent condition, supporting the hypothesis that these mesenchymal-driving transcription factors are contributing to the upregulation of mesenchymal genes in this state due to their elevated expression. However, one transcription factor, ZEB1, exhibited the opposite pattern, with increased expression in the confluent condition and a corresponding decrease in expression in the subconfluent condition. This change in expression goes against the assumed link between increase in EMT associated transcription factors and the increase in mesenchymal markers, within the subconfluent condition. Instead, the expression of ZEB1, a transcription factor with very well reported roles in EMT (Sánchez-Tilló et al., 2014; Zhang et al., 2015), is increasing within the confluent condition alongside an increase in endothelial markers and a decrease in mesenchymal markers.

3.3.1.3 Translation to protein expression

This increase in ZEB1 expression was confirmed by ddPCR and western blot, proving that this expression increase is translated to the protein level. Interestingly, the difference between the normalized ZEB1 expression in the two conditions was greater at the protein level when compared with the RNA level. This suggests an increase in protein stability and post-transcriptional regulation of ZEB1 protein levels within the confluent condition.

Other markers identified as being significantly differentially expressed by RNA-Seq were also compared at the protein level by western blot, as done for FOXO1 and PFKFB3. VE-Cadherin (CDH5) was also upregulated at the protein level within the confluent condition,

mirroring what is observed within the RNA-Seq data, which further provides evidence of an increase in endothelial genes within the confluent condition. To further understand monolayer integrity within the context of confluent HUVECs, the phosphorylation status of VE-Cadherin was also determined via tyrosine 731 (pY731) as the dephosphorylation of this residue is under normal barrier conditions constitutively phosphorylated (Arif et al., 2021; Wessel et al., 2014). This identified an increase in the level of phosphorylation at this residue, providing evidence to support that this confluent condition holds similarities to the endothelium monolayer.

3.3.2 siRNA knockdown of ZEB1 protein by approximately 50% had an impact on gene transcription within HUVECs

With the aim of exploring the role of ZEB1 within ECs, an siRNA method was deployed to knockdown the expression of ZEB1 within HUVECs. This method was able to reduce ZEB1 expression by around 50% in comparison to the NSC condition. RNA-Seq analysis of ZEB1 KD and NSC HUVECs identified 296 differentially expressed genes as a result of ZEB1 KD, with 65.54% of these genes being upregulated. This indicated that ZEB1 is having an increased role in transcriptional repression, in comparison to activation, as loss of ZEB1 results in a larger number of genes that increase in expression. This is very similar to observed roles of ZEB1 within other cell types, as ZEB1s role as a transcriptional repressor within these contexts has been well reported (Spaderna et al., 2008; Vandewalle et al., 2009).

The identified biological processes GO terms within these upregulate genes had a general theme of adhesion, which was also observed within the KEGG pathways identified from the downregulated genes. These analyses indicate that loss of ZEB1 is influencing cell adhesion by upregulating genes involved in adhesion pathways and processes. Within the ZEB1 KD data set, an upregulation in expression is observed both within extracellular matrix components, such as LAMC2, as well as extracellular matrix binding integrin subunits such as Itgα10, Itgα3, Itgβ4 and Itgβ3 (Reglero-Real et al., 2016). This along with GO terms identified that involve the extracellular matrix, suggest ZEB1 KD is having an impact on cell-extracellular matrix adhesion via the upregulation of these genes. Not only this, cell-cell adhesion proteins are upregulated within the ZEB1 KD data set, such as

desmoplakin, an essential component of desmosomal junctions (Valiron et al., 1996). Together, this identifies a role for ZEB1 in HUVECs in repressing genes involved in adhesion.

Whereas within the downregulated genes, the biological processes GO terms and KEGG pathways display themes within inflammation and cytokine response as a result of ZEB1 KD. This includes chemokine ligands such as CXCL1, CXCL2, CXCL5, CXCL6, CXCL8 and CXCL10 but also receptors involved in leukocyte extravasation such as ICAM1 (C. Lawson & Wolf, 2009). This therefore identifies a possible role for ZEB1 in the preparation and response to inflammation and that loss of ZEB1 reduces the expression of genes involved in these inflammatory signalling pathways. These inflammatory genes have also been identified as playing a direct role in the modulation of tip cell morphology and branching, such as the chemokine receptor CXCR4 (Strasser et al., 2010), which is also down regulated as a result of ZEB1 KD. Therefore, the alteration of inflammatory gene expression by ZEB1 may also influence angiogenic sprouting and branching.

3.3.2.1 ZEB1 KD had a minimal impact on the expression of EndoMT markers

ZEB1 has been well described as an activator of EMT (Sánchez-Tilló et al., 2014; Zhang et al., 2015), however its role within endothelial cells is not well understood. Although reviews and publications focusing on EndoMT often label ZEB1 as an activator of EndoMT, the references used to support this are usually from papers exploring ZEB1 within the context of EMT. These papers provide direct evidence to show ZEB1 as a driver of a mesenchymal phenotype, and this has been observed in many different contexts such as types of cancer (Craene & Berx, 2013; Sánchez-Tilló et al., 2014). But what is important to note is that they only focus on the mesenchymal transition of epithelial lineage cells. Therefore, reviews and publications (such as Fang et al., 2021 and Weinstein et al., 2020) that list ZEB1 as an EndoMT driver are assuming that expression and activation of ZEB1 within epithelial cells is the same within endothelial cells.

In the RNA-Seq analysis of confluent and subconfluent HUVECs, an increase in endothelial genes was observed within the confluent condition and an increase in mesenchymal genes was observed within the subconfluent condition. It was also where ZEB1 was identified as the only transcription factor that increases in expression with confluency. To understand

whether KD of ZEB1 within confluent HUVECs affects the expression of these markers, the normalised counts of the same markers were plotted again, which includes endothelial markers, mesenchymal markers and known EMT/EndoMT driving transcription factors. If ZEB1 is a major driver of the gene expression profile observed in confluent endothelial cells, one would assume a loss of ZEB1 would influence the expression of these markers. This revealed ZEB1 KD had no impact on any of the endothelial markers and therefore can be assumed to have no role in the regulation of these markers. The mesenchymal markers also show no difference, apart from TAGLN (SM22α) which significantly increased in expression. The transcription factors also showed little difference, apart from EST1 which decreased in expression. This was particularly interesting as ETS1 was not identified to be differentially expressed with confluency. Taken together, these data show that loss of ZEB1 within HUVECs does not affect the expression of EndoMT markers.

The biological processes identified from the GO term ORA however do suggest that ZEB1 KD is affecting EndoMT associated processes. One of the major phenotypic outputs of EndoMT is a decrease in adhesion and an increase in migration (Weinstein et al., 2020). Within the upregulated genes, biological processes identified included adhesion and migration, therefore suggesting losing ZEB1 is preventing phenotypes associated with EndoMT. However, cell adhesion changes are also associate with endothelial activation, therefore the changes in biological processes cannot completely be attributed to EndoMT.

3.3.2.2 Comparison to published ZEB1$^{+/-}$ corneal ECs RNA-Seq data exhibited overlapping hits

The DEGs identified via siRNA KD of ZEB1 and subsequent RNA-Seq were compared to a previously published RNA-Seq dataset, which investigated DEGs between ZEB1$^{+/-}$ and ZEB1$^{+/+}$ corneal endothelial cells (Frausto et al., 2019). This dataset was selected for comparison with the total KO model, as it more accurately reflects the level of ZEB1 expression achieved by the siRNA knockdown method used in this thesis. In the Frausto et al. study, corneal ECs with reduced ZEB1 expression were generated through CRISPR-Cas9-mediated ZEB1 knockout, resulting in a ZEB1$^{+/-}$ condition. The dataset displayed a comparable number of DEGs to the HUVEC dataset, indicating a degree of similarity between the two studies. Whilst this is comparing transient KD with monoallelic KO

studied, due to the limited datasets available in appropriate models, this dataset is believed to be appropriate for first line validation of cohort and highlights biological similarities between the two datasets.

The comparison identified several overlapping genes, including ETS1 which is downregulated in both data sets. ETS1, a transcription factor within the ETS family, has been previously implemented in EC differentiation and survival via regulating VEGF and Tie2 expression, along with extracellular proteases, such as Mmp9, involved in cell migration during angiogenesis (Hashiya et al., 2004; Iwasaka et al., 1996; Wei et al., 2009). In contrast, the transcription factor LIMS2, was identified as being up regulated in both data sets and has a role in the inflammatory response to fluid shear stress (Wang & Zhang, 2020). These overlapping genes within both data sets provide further evidence for ZEB1s role within endothelial cells.

The global pathway analysis performed on both the HUVEC siRNA and the corneal ECs ZEB1$^{+/-}$ data sets revealed varying significant pathways within each of the conditions. As both data sets yielded less than 300 DEGs, this may explain the limited overlap, in comparison to gene sets with a far greater number of DEGs, which could be possible if with a total knockout of ZEB1 expression was achieved. Likewise, although there is some overlap between the DEGs identified in the two RNA-Seq datasets, the degree of overlap is relatively low. This may be owing to the variation in EC types. Corneal ECs are situated on the posterior surface of the cornea, forming an endothelial that consists of a semi-permeable monolayer of cells. A key function of the corneal endothelium is to maintain the corneal stroma in a relatively dehydrated state, a process critical for preserving the precise ultrastructural arrangement of collagen fibers which is essential for maintaining corneal transparency (Frausto et al., 2020). Whereas HUVECs line the inner surface of the umbilical vein, where they play a crucial role in maintaining vascular homeostasis and regulating nutrient and oxygen exchange between the mother and fetus (Medina-Leyte et al., 2020). The varying physiological nature of these cells, as well as the varying conditions in which they are cultured *in-vitro* and differences in bioinformatics processing of the raw data may explain the limited overlapping genes within these data sets.

3.3.3 ZEB1 ChIP in HUVECs

3.3.3.1 ZEB1 ChIP-Seq indicative of a transcription factor with binding partners that is also has a level of redundancy

Although ZEB1 ChIP-Seq has been performed in other cell types such as MDA-MB-231 breast cancer cells (Feldker et al., 2020), and glioblastoma multiform cancer stem-like cells (Rosmaninho et al., 2018), this has never been explored within ECs. Initially, what appeared to be interesting within the ChIP-Seq data was that known motif analysis identified not only the ZEB1 motif but also showed high levels of other motifs such as AP1, ETV4 and Fli1. Motif analysis identifies possible transcription factor binding sequences by using known information about canonical motifs (Bailey et al., 2013). It is therefore expected that the ZEB1 binding motif would be identified, because it was ZEB1 that was pulled down, but the reason why other motifs have also been pulled down needs to be explored and discussed.

It is possible that these motifs have been identified because they appear in similar regions of the genome as the ZEB1 motif. Enhancers are regions of the genome that contain a cocktail of regulatory elements and transcription factor binding motifs that are able define and regulate patterns in gene expression (Agrawal et al., 2019). It may therefore be that specific enhancer regions are being pulled down, with the ZEB1 binding regions, and therefore this is why other transcription factor regions have been identified. Additionally, transcription factors often work in conjunction alongside other binding partners and transcription factors, forming larger transcription complexes. It is therefore possible that in the ChIP of ZEB1, other proteins are being pulled down as part of a larger complex, including ZEB1. Feldker et al demonstrated that this is the case with ZEB1 in MD1-MB-231 cancer cells; ZEB1 could work in complexes with YAP, TEAD, and AP-1 factors during transcriptional activation. In this instance, the complex directly bound to the DNA via TEAD and AP-1 motifs, which explained why these were identified within the ChIP-Seq data set. It was also determined that interactions with other proteins, such as CtBP, induced the transcriptional repression (Feldker et al., 2020). To confirm whether this is the case within HUVECs, further experiments could be performed, such as cross-analyses with ChIP data from other transcription factors, as well as CoIP experiments and proximity ligation assays.

Functional analysis was utilised to determine any pathways which had significant representation of genes with ZEB1 within their bound genomic regions. This identified several significant pathways but interestingly the top pathways involved endocytosis and protein trafficking. These were not pathways that were identified within RNA-Seq, therefore the knockdown of ZEB1 did not influence the expression of these genes. There is also a large amount of functional redundancy between transcription factors, whereby the translational of a particular gene can be initiated by several transcription factor and transcription factor complexes (Wu & Lai, 2015). This helps explain why for the ZEB1 ChIP-Seq 9,206 individual genes were identified as have ZEB1 bound at their promotor, however there was only 295 differentially expressed genes. This phenomenon is not uncommon, and was first identified by Hu et al, in which they identified differentially expressed genes from 263 transcription factor knockout yeast strains and found on average only 3% of the binding targets were differentially expressed within these strains (Hu et al., 2007). Functional redundancy is a common process in cellular biology, whereby one or more transcription factors will overcompensate for the loss of another (Gitter et al., 2009; Wu & Lai, 2015). This functional redundancy within many transcription factors could therefore explain why these pathways and genes are being identified within the ZEB1 ChIP, but not via RNA-Seq of ZEB1 KD HUVECs.

3.3.3.2 ChIP-Seq and RNA-Seq overlap genes confirmed ZEB1's role as a transcriptional repressor and supported its involvement in adhesion and inflammation

A total of 153 genes were identified as both differentially expressed upon ZEB1 knockdown and bound by ZEB1 at their promoter regions, suggesting they may represent direct transcriptional targets of ZEB1. Literature review revealed that 7 of these genes have previously been reported as ZEB1-regulated, providing validation for the dataset. However, the relatively small overlap with known targets may reflect the context-specific nature of ZEB1-mediated transcriptional regulation. Notably, this study represents the first application of ZEB1 ChIP-seq in HUVECs, which may account for the identification of novel, endothelial cell-specific targets not previously reported.

The overlap between RNA-Seq and ChIP-Seq data identifies genes likely to be directly regulated by ZEB1. This analysis categorizes genes in the ZEB1 KD RNA-Seq dataset into

two groups: the first includes genes that are differentially expressed and show direct binding by ZEB1 to their genomic sequences, suggesting direct regulation. The second group consists of genes that are differentially expressed upon ZEB1 knockdown but do not show ZEB1 binding at their genomic sequences, indicating that their expression changes are likely due to downstream effects of ZEB1 rather than direct regulation. Notably, 75.66% of genes identified with ZEB1 binding at their promoters were upregulated, further emphasizing ZEB1's role in transcriptional repression within HUVECs.

The GO ORA of these upregulated genes identified the same theme of adhesion and cell junctions; however, actin cytoskeleton organisation was additionally identified, which could be indicative of cell shape and structure. The cytoskeleton in endothelial cells, and other cell types, has been proven to play a significant role within the maintenance of the endothelial barrier, with Rho activation being a method of disrupting the cytoskeleton and therefore cell junctions and permeability (Kása et al., 2015). The cytoskeleton becomes even more relevant with the identification of the most significant molecular function being actin binding, which could encompass both cell adhesion proteins but also proteins that modulate actin structure and function. This data therefore suggests that ZEB1 is directly repressing genes with roles in adhesion and cytoskeleton organisation. It is however important to note that genes within these GO terms are simply identified as having a role in a biological process (e.g. adhesion) and therefore some genes could be increasing that biological process, whereas others may be decreasing it. The downregulated genes and their associated GO terms consistently highlight a theme of response to inflammatory stimuli, suggesting that ZEB1 plays a role in modulating the detection and response to such stimuli. As these biological processes are downregulated in ZEB1 KD HUVECs, it can be hypothesised that inflammatory responses in these cells may be altered or diminished.

3.3.4 Differentially expressed genes associated with angiogenesis and quiescence

Although a lot of the differentially expressed genes have been described in biological processes such as adhesion or inflammation, there are also several genes with known roles within angiogenesis or endothelial cell behaviour. This includes CXCR4 which is downregulated within ZEB1 KD cells and was found to be a gene where ZEB1 binds to its

promotor within the ChIP-Seq data. CXCR4 has been previously identified via microarray analysis of retinal endothelial tip cells as a key regulator of tip cell morphology, as well as vascular branching (Strasser et al., 2010). Not only this, CXCR4 has been found to play an essential role in arterial development, with loss of function studies resulting in failure to develop functional arteries (Ivins et al., 2015) and gain of function experiments resulting in a failure of hierarchical branching (Li et al., 2021). The balance of CXCR4 therefore must be strictly and spatially regulated during vasculature development, and this data indicates that ZEB1 is influencing this tight regulation.

Another gene with known roles in regulating vascular morphology and angiogenesis in BMP4 which is upregulated in ZEB1 KD HUVECs, and ZEB1 was also found to bind its promotor and at a distal intergenic site within its genomic sequence. There are conflicting reports surrounding the role of BMP4 within endothelial cells, with different effects observed in different models and systems. In tumour angiogenesis BMP4 has been identified as being involved in the activation of endothelial cells and promote tumour angiogenesis in malignant melanoma (Rothhammer et al., 2007). The pro-angiogenic activity of BMP4 was later determined to be downstream of VEGFR2 activation via c-Src (Rezzola et al., 2019). Whereas on the other hand BMP4 has been shown to inhibit choroidal neovascularisations by controlling the expression of VEGF (Xu et al., 2012). These reports are indicative of the heterogeneity within the vasculature, within health and disease, and is a good example of how within two different diseases, one gene can have contrasting effects.

FOXO1 was initially identified from the literature as being a regulator of endothelial quiescence via the modulating of endothelial metabolism (Andrade et al., 2021; Wilhelm et al., 2016). Within the differentially expressed genes in the confluent HUVECs compared to the subconfluent, FOXO1 was identified as being upregulated within the confluent HUVECs, both at the RNA and at the protein level. It was therefore interesting to see whether ZEB1 influences FOXO1 expression, but both via both RNA-Seq and western blot the level of FOXO1 expression was determined to be not affected by the loss of ZEB1.

3.3.5 ZEB1 directly inhibits epithelial gene expression in HUVECs

Although ZEB1 KD had no major impact on the expression of endothelial or mesenchymal gene expression, it interestingly resulted in the increase of epithelial gene expression such as EPCAM and ESRP2. Both genes were found to be upregulated in the ZEB1 KD condition and were found to be bound by ZEB1 at their promotor regions within the genome, with EPCAM also identified as being upregulated in the ZEB1$^{+/-}$ corneal EC data set (Frausto et al., 2019). This matches what has been previously observed in the literature, as both EPCAM and ESPR2 are observed to be directly inhibited by ZEB1 (Horiguchi et al., 2012; Vannier et al., 2013). Within epithelial cells, ZEB1 induces EMT not only by the expression of mesenchymal genes, but also via the repression of epithelial genes, including EPCAM and ESPR2 (Sánchez-Tilló et al., 2010). This therefore indicates that ZEB1s role in inhibiting epithelial genes is also present within endothelial cells, and loss of ZEB1 results in an increase in epithelial gene expression. Another major epithelial gene known to be directly repressed by ZEB1 is E-Cadherin (CDH1) (Sánchez-Tilló et al., 2010), but interestingly was not identified within the HUVEC ZEB1 ChIP-Seq, nor was it differentially expressed as a result of ZEB1 KD. This suggests that the repression of epithelial genes remains different between HUVECs, and the cancer models used by Sánchez-Tilló et al. Collectively, these data, in conjunction with the existing literature, suggest that ZEB1 acts as a transcriptional repressor of epithelial genes in ECs.

3.3.6 Overlapping genes were identified in all four data sets

3.3.6.1 NOS3

Endothelial nitric oxide synthase (NOS3) is responsible for most endothelial-derived nitric oxide (NO) production. NO has long been established in the regulation of vessel tone, leukocyte adhesion, platelet aggregation and EC proliferation (Oliveira-Paula et al., 2016). NOS3 KO mice exhibit hypertension and have an increased risk of stroke and other cardiovascular abnormalities (Li et al., 2002). ZEB1 was identified as being bound at the promotor region of NOS3; however, its expression varied between the RNA-Seq sets. In the ZEB1$^{+/-}$ corneal ECs its expression is downregulated, suggesting that ZEB1 could be directly regulating the expression of NOS3, and loss of ZEB1 results in a loss of NOS3. This aligns with the confluency data set, where NOS3 expression was upregulated in the

confluent condition, in which ZEB1 expression is high. However, within the HUVEC siRNA KD data set, the expression of NOS3 is upregulated with ZEB1 KD. This suggests that the regulation of NOS3 by ZEB1 may not be straightforward and could involve epigenetic regulation.

3.3.6.2 EFEMP1

Epidermal growth factor-containing fibulin-like extracellular matrix protein 1 (EFEMP1), is a member of the multifunctional fibulin family of extracellular matrix proteins. It plays a critical role in maintaining basement membrane integrity and maintaining the stability of the extracellular matrix (De Vega et al., 2009). Overexpression of EFEMP1 enhances HUVEC proliferation and tube formation. Additionally, EFEMP1 is upregulated at both transcriptional and protein levels in retinal-choroidal tissues from donor patients with AMD (Cheng et al., 2021). Alongside ZEB1 being bound to its promotor, EFEMP1 was identified as being upregulated in both the HUVEC siRNA ZEB1 KD data set and the ZEB1$^{+/-}$ corneal ECs, suggesting that ZEB1 may be negatively regulating its expression. The loss of ZEB1 may consequently influence the progression of neovascular eye diseases, such as AMD, by removing the inhibitory regulation on EFEMP1 expression.

3.3.6.3 LIMS2

LIM Zinc Finger Domain Containing 2 (LIMS2) a mechanosensitive transcription factor that is regulated by shear stress in ECs and capable of inhibiting inflammation by regulating VCAM-1 and ICAM-1 expression (Wang & Zhang, 2020). Alongside ZEB1 being bound to its promotor, LIMS2 was identified as being up regulated in both the HUVEC siRNA ZEB1 KD data set and the ZEB1$^{+/-}$ corneal ECs. This provides evidence for ZEB1 being a transcriptional repressor for LIMS2. Additionally, LIMS2 was observed to be downregulated in the confluent condition, in which ZEB1 expression is high, which aligns with this hypothesis.

3.3.7 Comparison of ZEB1 protein expression reduction: CRISPR-based system versus siRNA treatment

Since siRNA only reduced ZEB1 expression by approximately 50%, this may limit the ability to identify genes and processes fully regulated by ZEB1. Ideally, a complete loss or genetic knockout of ZEB1 would be required to study ZEB1-null ECs and explore their

transcriptome and behavior more comprehensively. To address this, a collaboration was initiated with Dr. Joanna Kalucka from Aarhus University, who had already developed a CRISPR-Cas9-based method for knocking out genes of interest, achieving complete gene knockout and, in many cases, reducing expression to zero (Wagman et al., 2022). Instead of silencing the expression of ZEB1 using small interfering RNA, this method utilised recombinant Cas9 protein along with guide RNAs to target the ZEB1 gene and its excision. Within this context, HUVECs were no longer used from pooled donors, but instead from individual donors, which meant variation between biological repeats was higher. This method did result in a robust reduction of ZEB1 protein, however the level of knockout varied between HUVEC donors. On average, ZEB1 protein expression was reduced to approximately 25%, representing an improvement over the siRNA treatment, although the reduction was still suboptimal.

3.3.7.1 Knockout of ZEB1 reduced HUVEC sprouting

Angiogenesis is a multi-action process which involves many signalling pathways, as well as interaction with other cell types within the tissue. Because of this, it is very hard to replicate within an *in vitro* setting. Many angiogenic in vitro assays have been developed which mimic certain aspects of angiogenesis, but do not accurately represent physiological angiogenesis completely (Nowak-Sliwinska et al., 2018). A couple of these assays were utilised during the laboratory visit to Aarhus University, which included a scratch migration assay and a spheroid sprouting assay.

The scratch assay is a commonly deployed tool in angiogenic research and although there are variations, the principle remains similar in that it monitors ECs ability to migrate to close a gap within the culture (Nowak-Sliwinska et al., 2018). To note, the assay used in this thesis may also be labelled in the literature as a wound healing assay, due to the fact the gap in the culture is generated by a simple scratch that removes ECs. This induces cell death within these cells and therefore can be considered to be a form of wound healing, in comparison to a migration assay whereby a physical barrier is removed, and the gap closure occurs this way. This assay also does not measure migration alone, as proliferation may be affecting the closing of the scratch, therefore Mitomycin C was also added as a condition within these experiments as it inhibits the cell cycle. ZEB1 KO had an impact on

cell migration both with and without mitomycin C as both conditions saw a decrease in scratch closure. However, this was not significant indicating that loss of ZEB1 is not having a major impact on migration. It may be plausible that ZEB1 is impacting proliferation of HUVECs, and hence the slight reduction in migration observed is due to this only.

Despite this, ZEB1 KO did have a significant impact on the spheroid assay. This assay includes a fair few of the processes that make up angiogenesis, including tip cell sprouting, migration, extracellular matrix breakdown and proliferation (Nowak-Sliwinska et al., 2018); all of which add to the assay's representability. The ZEB1 KO HUVECs had reduced sprouts at both 24h and 48h compared to control cells, indicating that a reduction of ZEB1 was reducing the sprouting ability of these cells. ZEB1 may therefore under normal conditions play an important role in the regulation of genes required for these angiogenic processes. Within the GO ORA from the ZEB1 KD RNA-Seq data set, adhesion was significantly represented within the upregulated genes. It is well understood that both cell-cell adhesion and cell-matrix adhesion is heavily modulating during angiogenic sprouting. The reduction of cell-cell adhesion and cell-matrix adhesion is required for ECs to break out of the endothelial monolayer and begin sprouting (Ramjaun & Hodivala-Dilke, 2009). It could therefore be possible that the upregulation of genes involved in adhesion within HUVECs deficient in ZEB1 may be a cause of the reduced ability to sprout.

3.4 Chapter Summary

This chapter aimed explore the transcriptome of both confluent and subconfluent endothelial cells and to determine whether EndoMT associated gene expression could be observed within these conditions. This identified that subconfluent endothelial cells display a mesenchymal like phenotype indicative of partial EndoMT. Moreover, these analyses identified ZEB1 as a transcription factor that went against the trend of other EMT transcription factors, by increasing in expression within the confluent condition. Although loss of ZEB1 did not influence EndoMT gene expression, various biological processes were identified as being affected by ZEB1 KD, including inflammation and adhesion. These processes likely explain why a reduction in sprouting is observed is ZEB1 KO cells within an angiogenic sprouting assay.

Chapter 4:

Elucidating the impact of endothelial ZEB1 loss on developmental angiogenesis

4 Analyzing the impact of endothelial ZEB1 loss on developmental angiogenesis

4.1 Introduction

The developing mouse retina is a well-used model of physiological angiogenesis (Hultgren et al., 2020; Tisch et al., 2019; Walker et al., 2021, to name a few). During development, hypoxia-induced paracrine release of VEGF from retinal neuroglial cells induces angiogenesis and the growth of the vascular plexus via angiogenesis (Stone et al., 1995). In mice, this process occurs postnatally; unlike humans, where this occurs in utero. This provides an ideal model to study developmental angiogenesis, as the vasculature can be observed via whole mount staining and confocal imaging at different post-natal time points (Figure 4.1) (Fruttiger, 2007).

Initially the primary plexus develops between postnatal days 1 and 10, as the network expands from the optic nerve head towards the edge of the retinal periphery. Tip cells, which are specialised ECs, appear at the leading edge of the angiogenic front are guided by the concentration gradient of pro-angiogenic factors and begin to migrate and form the primary plexus (Gerhardt et al., 2003; Ruhrberg et al., 2002). At around postnatal day 10 the deeper plexus begins to form via sprouting angiogenesis from regions across the primary plexus. These angiogenic sprouts instead dive downwards to create a further vascular network layer and have been identified as having different transcriptional signatures that focuses on TGF-β signaling (Zarkada et al., 2021). Shortly after this, the intermediate plexus is generated, resulting in three vascular layers (Milde et al., 2013; Rust et al., 2019; Stahl et al., 2010). During all stages, network remodeling occurs via vessel pruning, in which coordinated signaling balanced by pro- and anti-angiogenic factors result in the elimination of vessels (Adams & Alitalo, 2007). The process of vessel pruning can occur via re-localisation of ECs, or via selective apoptosis, with leukocytes being identified as playing possible roles in both of these processes (Hughes & Chan-Ling, 2000; Ishida et al., 2003). These phases of remodeling occur up until around post-natal day 30, after which the vasculature begins to enter a state of homeostasis (Fruttiger, 2007). This comprehensive understanding of mouse retinal development at different developmental

time points, along with the availability of transgenic mice stains, allows for the stages of vascular plexus development to be readily observed and compared in response to genetic manipulation.

In chapter 3, I identified that ZEB1 has a transcriptional influence on ECs, and that loss of ZEB1 resulted in reduced angiogenic sprouting *in vitro*. Therefore, exploring how ZEB1 impacts physiological angiogenesis *in vivo* will further elucidate its role within the endothelium. The aim of this research chapter is to explore if loss of endothelial ZEB1 affects physiological developmental angiogenesis by observing the retinal vasculature in a neonatal transgenic mouse model.

4.1.1 The ZEB1^{iECKO} model

To explore the role of endothelial cell ZEB1 in vivo, an inducible endothelial cell specific knockout of ZEB1 was generated by utilising the Cre-ERT2 inducible system: a Cre recombinase is fused to a mutated estrogen receptor. Upon administration of tamoxifen the Cre-ERT2 fusion protein is able to translocate to the nucleus to induce Cre mediated genetic recombination of LoxP sites (Vallier et al., 2001). To ensure the endothelial cell specific knockout of ZEB1, the expression of the Cre-ERT2 system was placed under the transcriptional control of the endothelial cell specific cdh5 (VE-Cadherin) promoter (Alva et al., 2006). Cdh5 CreERT2$^{+/-}$ mice (Sörensen et al., 2009)were crossed with ZEB1$^{fl/fl}$ mice (S. Brabletz et al., 2017), resulting in ZEB1$^{fl/fl}$ cdh5 CreERT2$^{+/-}$ progeny that can undergo EC specific ZEB1 KO upon tamoxifen administration. To ensure littermate mice with WT expression of ZEB1 were available as controls, ZEB1$^{fl/fl}$ cdh5 Cre-ERT2$^{+/-}$ mice were crossed with ZEB1$^{fl/fl}$ cdh5 Cre-ERT2$^{-/-}$ mice. These mating pairs produced a mixed litter of Cre-ERT2$^{+/-}$ and Cre-ERT2$^{-/-}$ mice, which are all ZEB1$^{fl/fl}$. Although both Cre-ERT2$^{+/-}$ and Cre-ERT2$^{-/-}$ were dosed with tamoxifen, only the Cre-ERT2$^{+/-}$ mice are capable of undergoing recombination to induce genetic knout out of ZEB1. Therefore, tamoxifen dosed ZEB1$^{fl/fl}$ cdh5 Cre-ERT2$^{-/-}$ mice will be referred to as controls, whereas tamoxifen dosed ZEB1$^{fl/fl}$ cdh5 Cre-ERT2$^{-/+}$ mice will be referred to as ZEB1 inducible endothelial cell KO (ZEB1^{iECKO}) within this chapter, and throughout this thesis.

4.2 Results

4.2.1 ZEB1^{iECKO} did not affect the developing weight of neonatal mice

Litters from *ZEB1$^{fl/fl}$ cdh5CRE-ERT2$^{+/-}$* and *ZEB1$^{fl/fl}$ cdh5CRE-ERT2$^{-/-}$* mice were treated with tamoxifen on post-natal days 1, 2 and 3 to generate EC specific KO of ZEB1. Neonates were culled at post-natal day 5 to analyse vascular plexus development. Throughout the study, the weight of the neonates was measured daily which determined no significant difference between ZEB1^{iECKO} and controls over the course of the dosing schedule (Figure 4.1 A) and up to the final day (Figure 4.1 B).

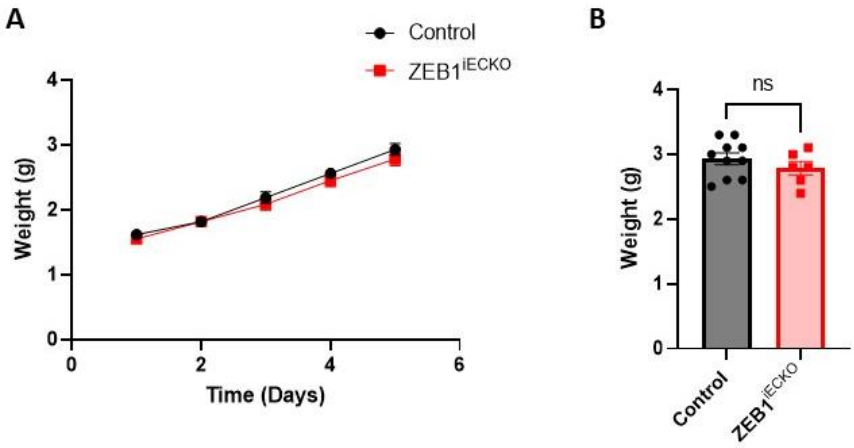

Figure 4.1 No significant difference in weights between ZEB1^{iECKO} neonates and controls. (A) *Neonates weight in grams plotted over time showed no significant difference between ZEB1^{iECKO} neonates and controls (**B**) On post-natal day 5 the mice were weighed prior to sacrifice and no significant difference was observed within their weights. Data are presented as mean + SEM and was stastically analysed used an unpaired t-test. Non-significant = ns, p > 0.05. Control n=10 and ZEB1^{iECKO} n=6.*

4.2.2 ZEB1^{iECKO} mice displayed reduced vascular extension at post-natal day 5

To determine whether loss of endothelial ZEB1 impacts developmental angiogenesis, on post-natal day 5 mice were sacrificed and their eyes fixed, dissected, stained for CD31 and ERG to visualise retinal vascular plexus formation. Firstly, vascular extension was determined as the percentage of which the angiogenic front had progressed along the total length of the retina. ZEB1^{iECKO} mice showed a significant reduction in vascular

extension (64.83% ± 2.64%) compared to control mice (74.42% ± 3.47%, p=0.0011, Figure 4.2). This indicates that loss of EC ZEB1 results in decreased vascular extension in the neonatal mouse retina.

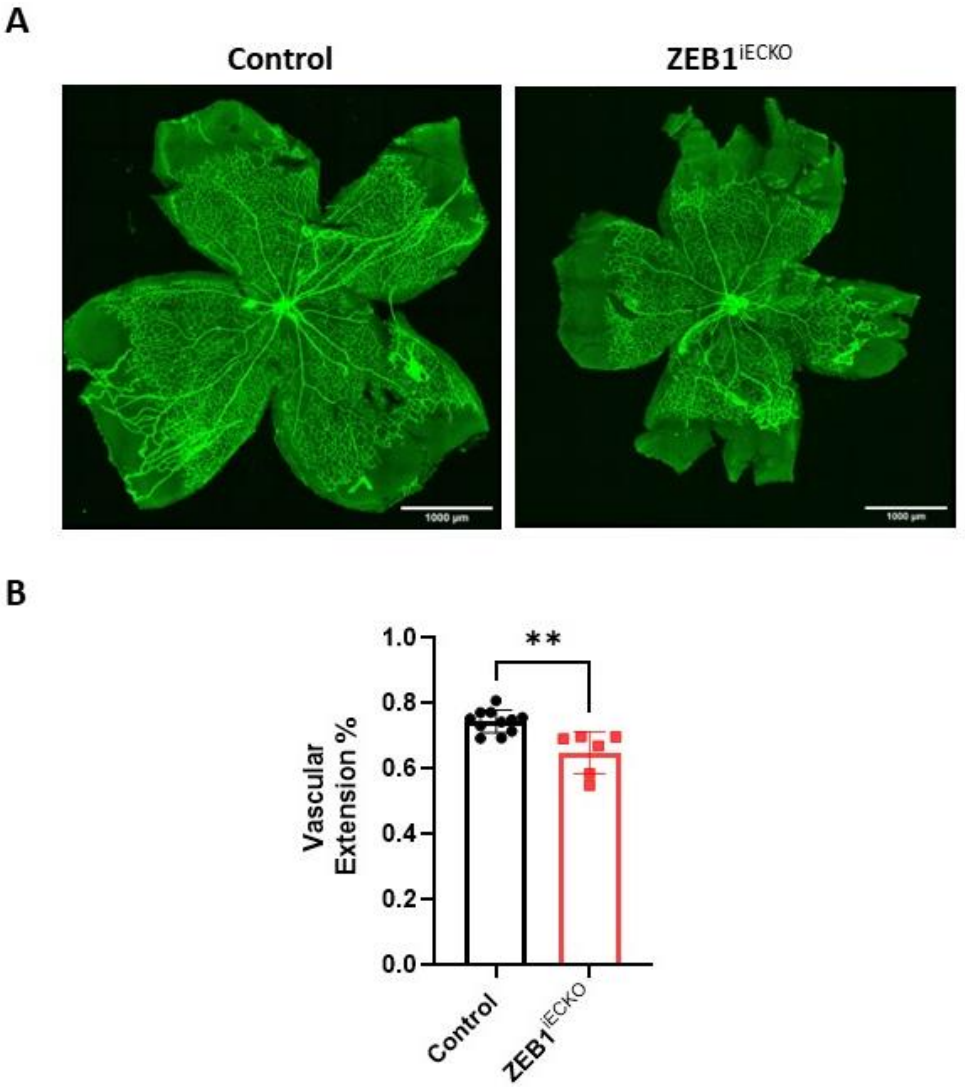

Figure 4.2 ZEB1^{iECKO} mice displayed reduced vascular extension compared to controls. (A) *Representative images of ZEB1^{iECKO} and control P5 retina which were flat mount stained for CD31. Images were acquired on a confocal microscope at 10x magnification and analysed using ImageJ. Scale bar = 1000µm.* ***(B)*** *The calculated percentage extension of the vascular front it presented. Data are presented as mean + SEM and was statistically analysed used an unpaired t-test. ** p < 0.005 control n=11 and ZEB1^{iECKO} n=6.*

4.2.3 ZEB1^{iECKO} mice exhibited altered vascular network structure at the angiogenic front of the post-natal day 5 retina

To further understand the implications of endothelial ZEB1 KO in developmental angiogenesis, structural analysis of the angiogenic front was performed. This was achieved by analysing 20x magnification confocal images of CD31 and ERG-stained post-natal day 5 retinas at the angiogenic front (Figure 4.3 A). The area of CD31 staining was measured to calculate the vessel area which confirmed no significant difference between the control and ZEB1^{iECKO} mice ($p>0.05$, Figure 4.3 B). The images were subsequently skeletonised to assess differences in network patterning and structure. The vascular density was calculated as the number of individual vessel segments per retina area. ZEB1^{iECKO} mice displayed a significantly reduced vascular density (180 ± 14.21 per mm^2) compared to controls (221 ± 10.43/mm^2, $p=0.0341$, Figure 4.3 C). In addition to this, ZEB1^{iECKO} mice had increased vessel segment length (25.54 ± 0.97µm) when compared with control mice (23.03 ± 0.53µm, $p=0.0226$, Figure 4.3 D). The distribution of vessel segment lengths was quantified and compared between control and ZEB1^{iECKO} mice. This was achieved using frequency histogram that displayed the data in 10µm bins (Figure 4.3 E and F). These results indicate that the vessels formed at the angiogenic front in ZEB1^{iECKO} result in an altered structure whereby the vessel segments are longer but are fewer in number.

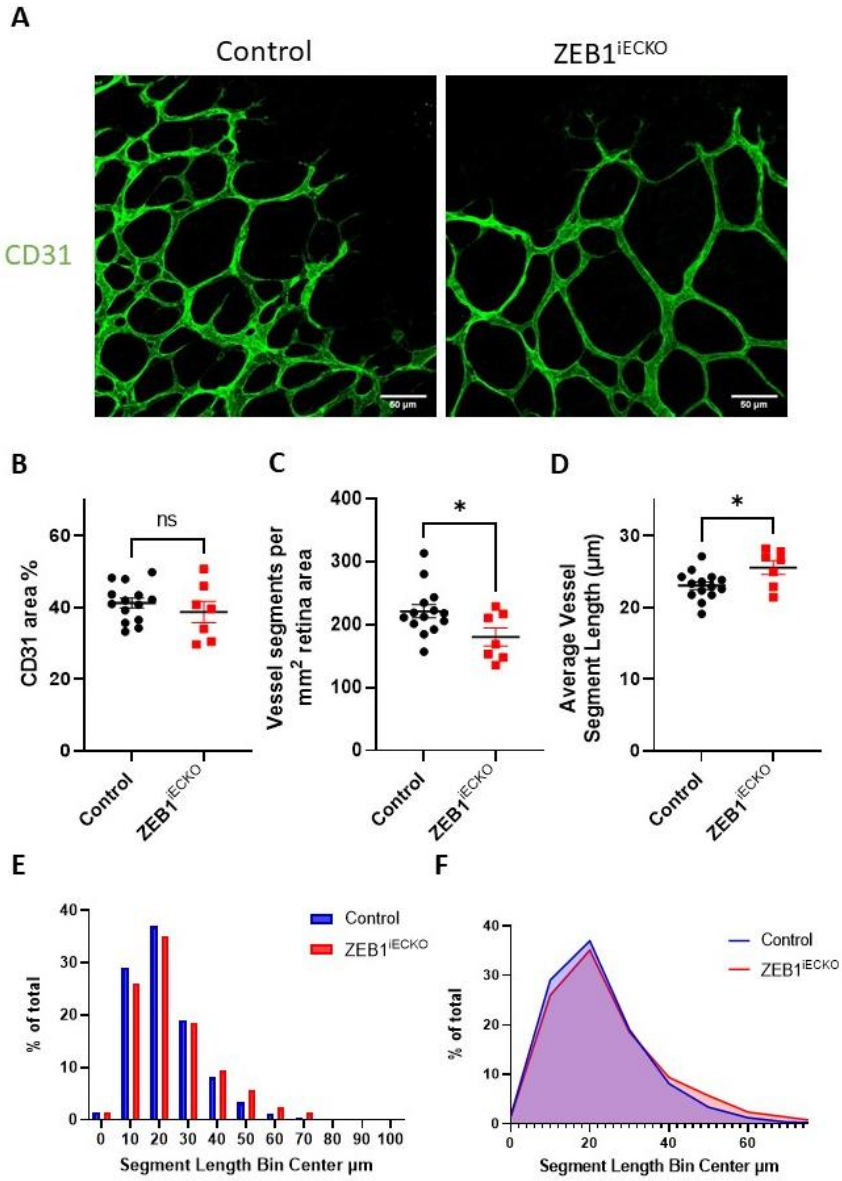

Figure 4.3 ZEB1^{iECKO} mice had decreased vessel density and increased vessel length compared to controls at the angiogenic front. ***(A)*** *Representative images of ZEB1^{iECKO} and control P5 retina which were flat mount stained for CD31. Images were acquired on a confocal microscope at 20x magnification and analysed using ImageJ. Scale bar = 50µm.* ***(B)*** *The calculated percentage of CD31% area showed no significant difference between of ZEB1^{iECKO} and control.* ***(C)*** *Vascular density measured by vessel segments per mm^2 is significantly decreased in ZEB1^{iECKO}* ***(D)*** *Average segment length is significantly increased in ZEB1^{iECKO}. Panels B, C and D are average measurements presented as mean + SEM.* ***(E)*** *and* ***(F)*** *is representative of every measurement from each mouse, then showed as a percentage of the total measurements. Control n=14 and ZEB1^{iECKO} n=7. Statistically analysed by an unpaired t-test. ** p < 0.005*

4.2.4 ZEB1^{iECKO} mice displayed reduced branch points within the angiogenic front of the post-natal day 5 retina

To determine whether the reduction in vessel segment number per mm^2 was due to a change in vessel branching, the branch points per mm^2 retina area were calculated from the skeletonised network (Figure 4.4). This revealed that ZEB1^{iECKO} mice had a significantly decreased number of branch points (112.1 ± 6.7 per mm^2) when compared to controls (153.7 ± 5.9 per mm^2, p=0.0004, Figure 4.4 B). This indicates that at the angiogenic front of developing plexus ZEB1^{iECKO} mice have fewer branch points in the same area of vascularised retina, when compared to control animals, suggesting reduced vessel branching at the angiogenic front.

The vessel node was calculated for each vessel segment. This is defined as the number of connections each vessel segment forms with another. No significant difference in the average vessel node was observed between ZEB1^{iECKO} mice and controls (p>0.05, Figure 4.4 C). A frequency histogram was generated to visualise the distribution of values across each node, rather than looking at the total mean (Figure 4.4 D). Together, there was no difference in Node number between Control and ZEB1^{iECKO}.

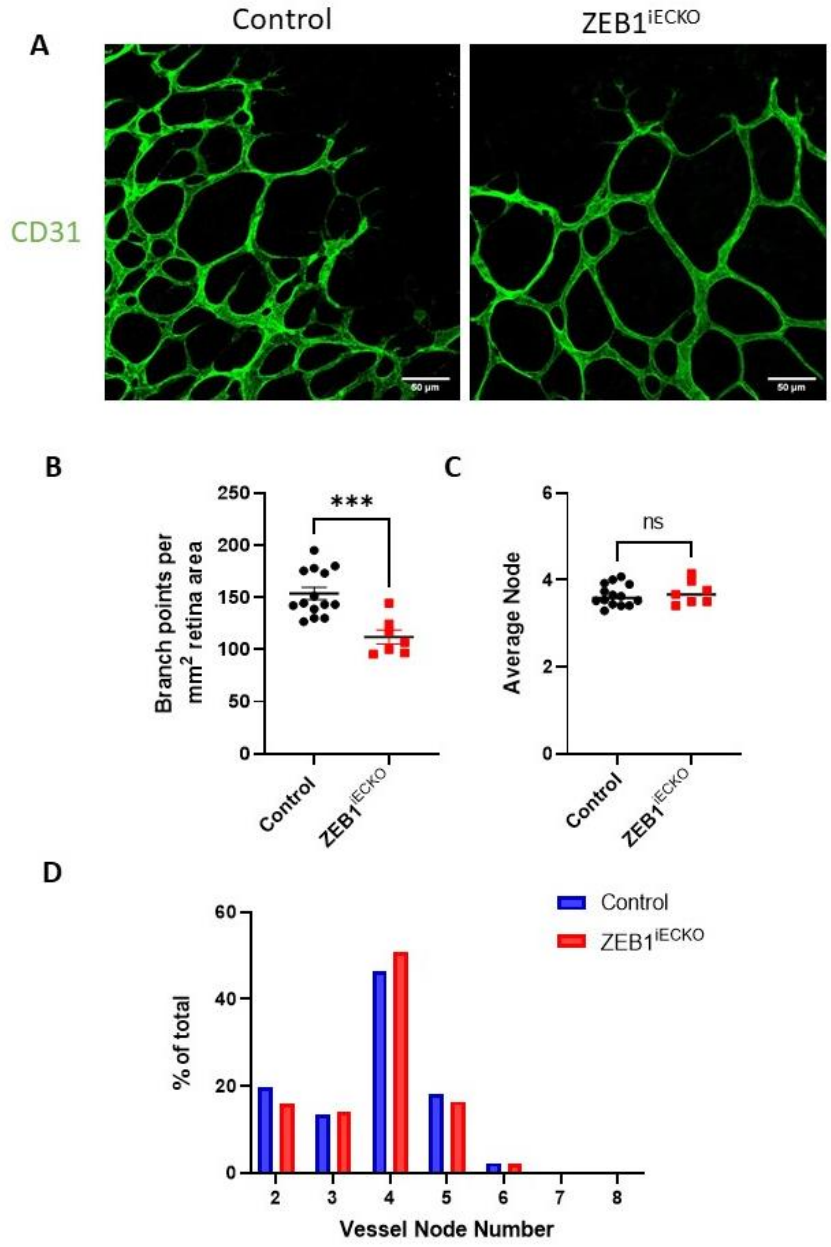

Figure 4.4 ZEB1^{iECKO} mice displayed a decreased number of branch points at the angiogenic front. (A) *Representative images of ZEB1^{iECKO} and control P5 retina which were flat mount stained for CD31. Images were acquired on a confocal microscope at 20x magnification and analysed using ImageJ. Scale bar = 50µm.* ***(B)*** *Branch points per mm^2 is significantly decreased in ZEB1^{iECKO} compared to controls* ***(C)*** *No difference in average vessel node between ZEB1^{iECKO} and controls. B and C are average measurements presented as mean + SEM.* ***(D)*** *is representative of every node measurement from each mouse showed as a percentage of the total node measurements. Stastically analysed by an unpaired t-test. *** $p < 0.0005$. Control n=14 and ZEB1^{iECKO} n=7.*

4.2.5 ZEB1^{iECKO} mice have a reduction in the number of endothelial cells at the angiogenic front of the post-natal day 5 retina

To understand if the reduced vascularity also affects the number of endothelial cells within the angiogenic front as a result of endothelial ZEB1 KO, retinas from neonates dosed with tamoxifen as described previously were stained for ERG, an endothelial specific nuclei marker. 20x magnification images were then analysed and ERG+ nuclei were counted to determine EC number (Figure 4.5 A). This revealed that ZEB1^{iECKO} mice had significantly fewer ECs within the angiogenic front (111.9 ± 4.1 per mm^2) compared to controls (131.4 ± 4.9 per mm^2, p=0.0301, Figure 4.5 B).

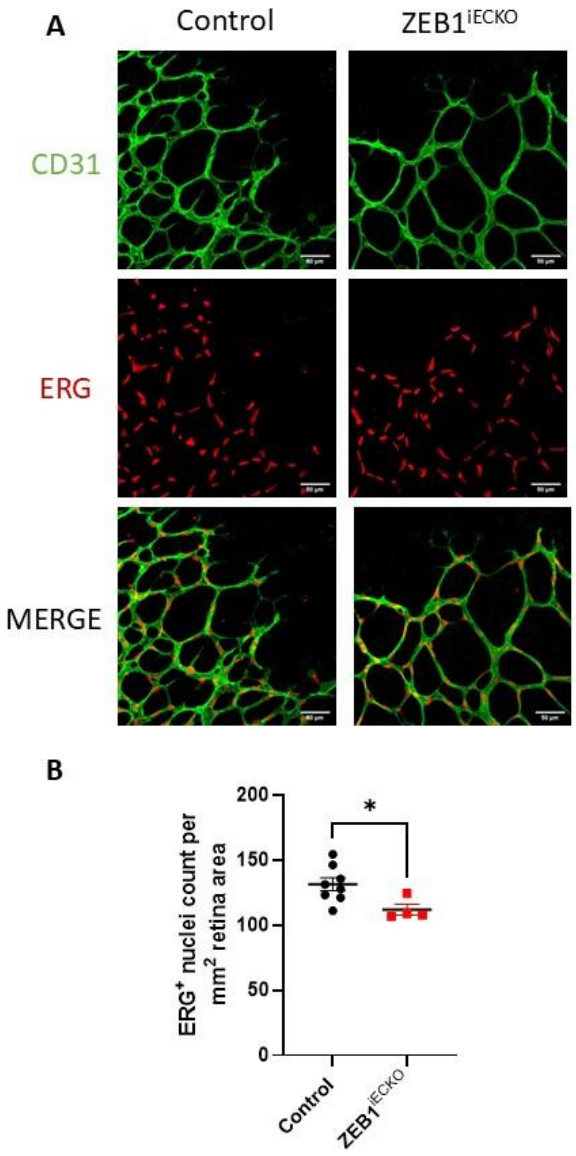

Figure 4.5 ZEB1^{iECKO} mice exhibited fewer endothelial cells at the angiogenic front. ***(A)*** *Representative images of ZEB1^{iECKO} and control P5 retina which were flat mount stained for CD31 and ERG. Images were acquired on a confocal microscope at 20x magnification and analysed using ImageJ. Scale bar = 50µm.* ***(B)*** *ERG^{+} nuclei count is significantly decreased in ZEB1^{iECKO} compared to controls. Data are presented as mean + SEM and was statistically analysed used an unpaired t-test. * $p < 0.05$. Control n=8 and ZEB1^{iECKO} n=4.*

4.2.6 No significant difference observed in the number of tip cells at post-natal day 5 between ZEB1^{iECKO} and Control mice

To determine whether EC ZEB1 KO affected the number of tip cells at the edge of the angiogenic front, the tip cells at the leading edge of the angiogenic front were counted and quantified. This revealed no significant difference in the number of tip cells between ZEB1^{iECKO} and control mice (p = > 0.05, Figure 4.6).

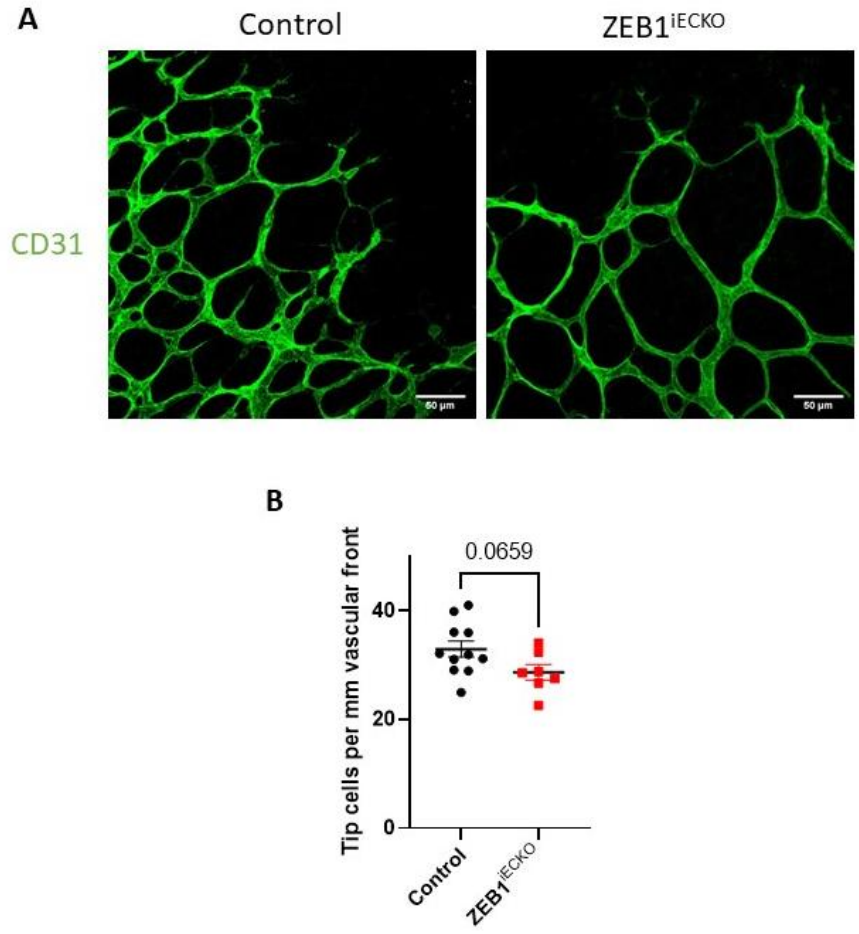

Figure 4.6 No significant difference in the number of tip cells at post-natal day 5 between ZEB1iECKO and Control mice. (A) *Representative images of ZEB1^{iECKO} and control P5 retina which were flat mount stained for CD31. Images were acquired on a confocal microscope at 20x magnification and analysed using ImageJ. Scale bar = 50 µm.* ***(B)*** *Number of tip cells per mm angiogenic front displaced as mean + SEM and was statistically analysed used an unpaired t-test. p = 0.0659 therefore is not significant. Control n=11 and ZEB1^{iECKO} n=7.*

4.2.7 ZEB1^{iECKO} mice also exhibited altered vascular network structure within the central vascular plexus of the developing retina

Within the developing mouse retina, the region behind the angiogenic front is undergoing phases of vessel pruning and network remodeling, whereby there is controlled regression of the vasculature to generate a hierarchical network (Fruttiger, 2007). Therefore, to assess how loss of EC ZEB1 influences the vascular network structure within these regions, the same method of area measurement and skeletonisation was applied to regions further back in the vascular plexus, termed the central plexus (Walker et al., 2021). Regions were selected that were between the angiogenic front and optic nerve, as well as equidistant to major vessels nearby, as described in Figure 2.4.

To quantify the area of the vascular network, the area CD31 staining was measured which revealed there was no significant difference between the control and ZEB1^{iECKO} mice ($p>0.05$, Figure 4.7 B). From the skeletonised information, the vascular density was again determined by the number of vessel segments per retina area. It was observed that within these regions of the plexus, ZEB1^{iECKO} mice had a significantly reduced vessel density (164.9 ± 9.44 per mm^2) in comparison to control mice (215.8 ± 7.68 per mm^2, Figure 4.7 C). When assessing the average length of these vessel segments ZEB1^{iECKO} mice also exhibited increased average vessel length (27.86 ± 0.88µm) compared to control mice (24.29 ± 0.43 µm, Figure 4.7 D). As done previously, the distribution of the vessel segment lengths changes between control and ZEB1^{iECKO} mice was assessed by a frequency histogram that displayed the data in 10µm bins (Figure 4.7 E and F). These results indicate that loss of endothelial ZEB1 also influenced the structure of the central plexus which is away from the angiogenic front. ZEB1^{iECKO} mice displayed a central vascular plexus that has a reduced vessel segment density, alongside an increased vessel segment length.

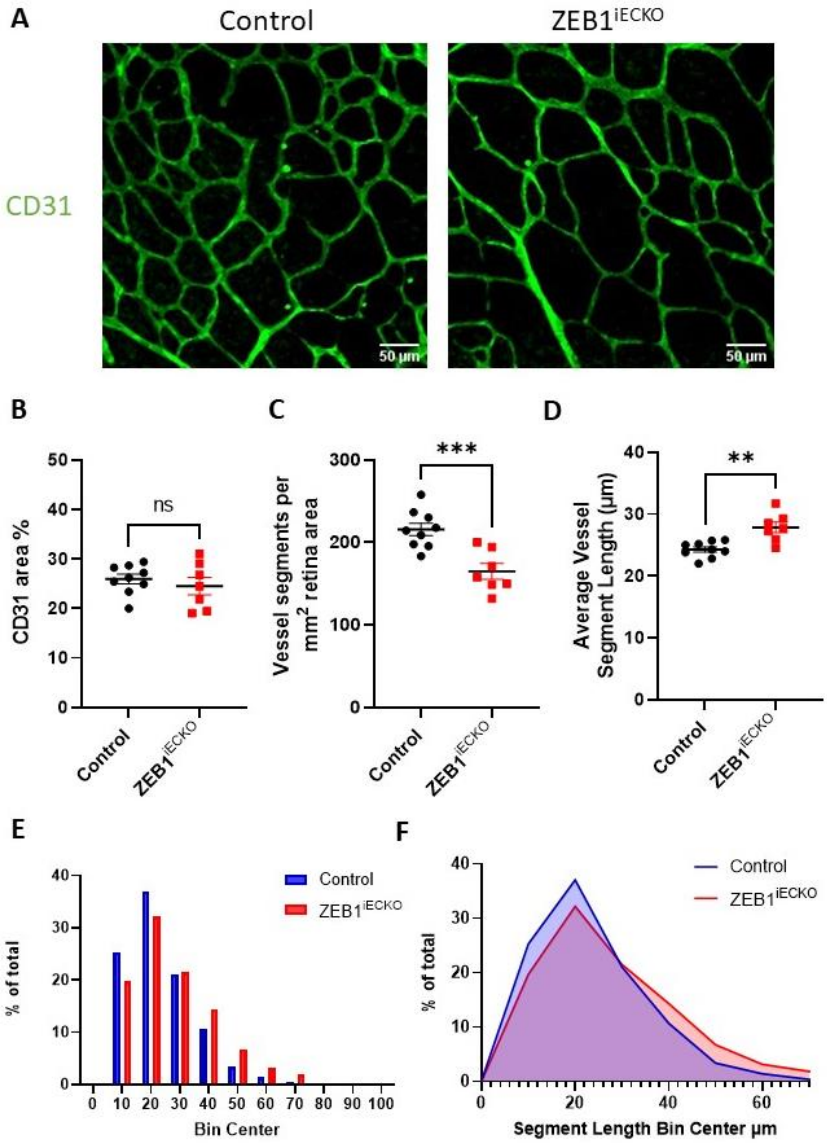

Figure 4.7 ZEB1^{iECKO} mice displayed decreased vessel density and increased vessel length compared to controls within the central plexus. (A) *Representative images of ZEB1^{iECKO} and control P5 retina which were flat mount stained for CD31. Images were acquired on a confocal microscope at 10x magnification and analysed using ImageJ. Scale bar = 50 µm.* ***(B)*** *The calculated percentage of CD31% area showed no significant difference between of ZEB1^{iECKO} and control.* ***(C)*** *Vascular density measured by vessel segments per mm^2 is significantly decreased in ZEB1^{iECKO}* ***(D)*** *Average segment length is significantly increased in ZEB1^{iECKO}. Panels B, C and D are average measurements presented as mean + SEM.* ***(E)*** *and* ***(F)*** *is representative of every measurement from each mouse, then showed as a percentage of the total measurements. Control n=11 and ZEB1^{iECKO} n=7. Statistically analysed by an unpaired t-test. * $p < 0.05$, *** $p < 0.0005$*

4.2.8 ZEB1^{iECKO} mice displayed reduced vascular branching within the central vascular plexus of the developing retina

To elucidate more information about the structure of the central vascular plexus after loss of endothelial ZEB1, the vessel branching per mm^2 was quantified. This revealed that ZEB1^{iECKO} mice had reduced vascular branching (88.3 ± 6.54 per mm^2) when compared to control mice (119.1 ± 4.22 per mm^2, Figure 4.8 B). This showed that within the central plexus, ZEB1^{iECKO} mice had reduced branch points per retina area.

The vessel node was calculated for each vessel segment. This is defined as the number of connections each vessel segment forms with another. No significant difference in the average vessel node was observed between ZEB1^{iECKO} mice and controls ($p > 0.05$, Figure 4.8 C). A frequency histogram was generated to visualise the distribution of values across each node, rather than looking at the total mean (Figure 4.8 D). Together there was no difference in Node number between Control and ZEB1^{iECKO} within the central plexus.

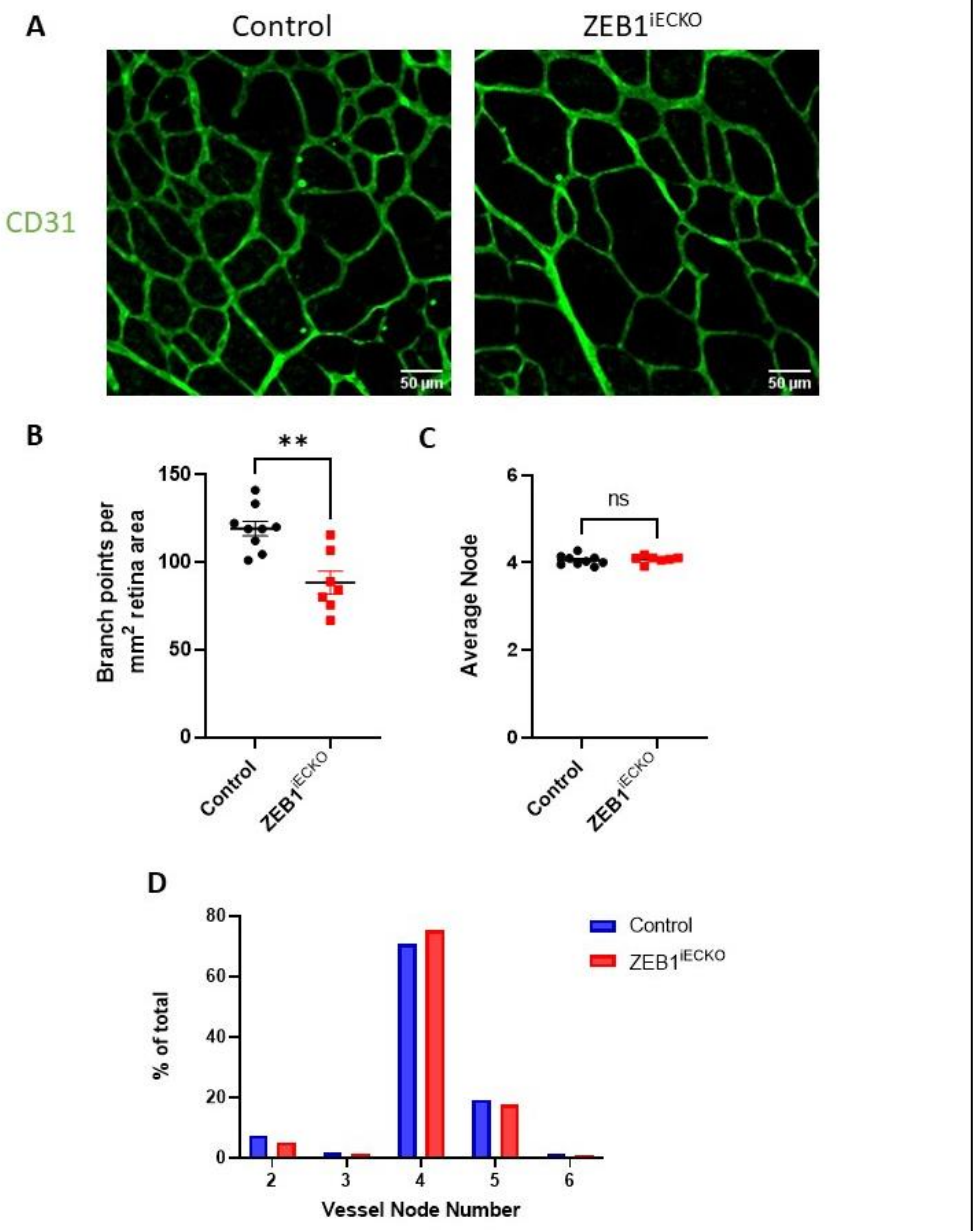

Figure 4.8 ZEB1^{iECKO} mice have a decreased number of branch within the central plexus. (A) *Representative images of ZEB1^{iECKO} and control P5 retina which were flat mount stained for CD31. Images were acquired on a confocal microscope at 20x magnification and analysed using ImageJ. Scale bar = 50 µm.* ***(B)*** *Branch points per mm^2 is significantly decreased in ZEB1^{iECKO} compared to controls* ***(C)*** *No difference in average vessel node between ZEB1^{iECKO} and controls. Data are presented as mean + SEM and was statistically analysed used an unpaired t-test.* ***(D)*** *is representative of every node measurement from each mouse showed as a percentage of the total node measurements. Stastically analysed by an unpaired t-test. ** p < 0.005. Control n=11 and ZEB1^{iECKO} n=7.*

4.3 Discussion

4.3.1 ZEB1^{iECKO} resulted in reduced vessel branching

Measuring angiogenesis by quantifying the percentage of vascular front progression is a widely accepted method and is present in the majority of publications which utilise the neonatal retina. In this study we have determined that loss of EC ZEB1 resulted in reduced vascular extension. These findings suggest that ZEB1 plays a role in the early stages of vascular development. Consequently, the absence of ZEB1 leads to a delay and inefficiency in vascular growth.

Qualitatively, images of the vascular network revealed no significant defects in angiogenesis were observed that led to a completely malformed or deformed network. Examples of such cases include EC KO of the transcription factor FOXO1, whereby deletion leads to over proliferation, uncoordinated branching and blunting of the angiogenic front (Wilhelm et al., 2016). The loss of Notch ligands has a significant phenotype with opposing roles identified; loss of EC Jag1 results in a sparse network, whereas loss of EC Dll4 results in over proliferative dense network (Benedito et al., 2009; Corada et al., 2013).

Since no striking qualitative difference was observed in the ZEB1^{iECKO} mice, morphological analysis of the angiogenic front and tip cell quantification was performed to provide a greater depth of information as to why loss of EC ZEB1 resulted in this inefficiency and reduced outgrowth. From the analysis surrounding network structure, it was identified that in ZEB1^{iECKO} mice had increased individual vessel segment lengths compared with controls. Reduced vascular density was also observed in ZEB1^{iECKO} mice compared with controls. ERG analysis also revealed that there were fewer EC at the angiogenic front. Thus, while segment lengths were greater, there were fewer segment lengths overall, leading to a sparser and elongated network at the leading edge, with fewer ECs.

This raised the question of what mechanism caused these elongated segments. As the overall area of CD31 staining did not change, it suggests that the elongation and reduced number of segments could be arising due to changes in branching, as a reduction in branch points would lead to a sparser network. Quantification of branch points confirmed that ZEB1^{iECKO} had significantly fewer branch points; no changes in the vessel node were

observed. This finding helps explain the reduction in vascular extension, as fewer branch points would limit the formation of new vessels, thereby reducing vascular outgrowth and angiogenesis.

Alternatively, the observation that ZEB1^{iECKO} mice exhibit fewer ECs at the angiogenic front suggests that individual ECs may compensate by covering larger segments of nascent vessels. This implies a potential alteration in EC behavior or morphology, such as increased cell spreading or elongation, which could affect vessel patterning and stability. This finding is mechanistically significant, as it indicates that ZEB1 may regulate EC spatial organisation and coverage within developing vascular structures. Integrating this into the broader context of ZEB1's role in endothelial function could offer new insight into how transcriptional control influences angiogenic remodeling.

4.3.2 The altered network structure in ZEB1^{iECKO} was also present in the central plexus

It was evident from the reduced vascular extension that the loss of EC ZEB1 resulted in altered angiogenesis progression, hence why the angiogenic front was explored; however, the central plexus is also going through phases of remodeling, vessel stabilisation and vessel pruning (Korn & Augustin, 2015). This area is also preparing for later stages of retinal development, by which tip cells drive downwards to complete the 3 layers of the vascular network (Milde et al., 2013; Zarkada et al., 2021). Exploring how loss of EC ZEB1 affects this region of the developing vasculature is therefore key to further understanding ZEB1s role within retinal development angiogenesis.

Structural assessments of the central plexus, like those performed for the angiogenic front, revealed that the changes observed in the vascular front were consistent throughout the plexus. This included a decrease in vessel segment density and an increase in vessel length. Branch point analysis further confirmed this reduction across the central plexus, mirroring the angiogenic front. The altered network initially formed at the angiogenic front in the case of EC ZEB1 KO therefore generates a lasting impact that also affects the structure of the central plexus. Unfortunately, for the central plexus, insufficient retinae were stained and imaged for ERG and hence there is no ERG analysis. However, if I was to speculate what could be observed from this analysis, I would imagine

that the differences in EC count observed at the angiogenic front would also be observed in the central plexus too, as all other parameters showed the same effect in the two regions.

4.3.3 Comparing the endothelial role of other EMT transcription factors

Other transcription factors that have known roles in driving EMT, have been explored within ECs and within the context of angiogenesis. Two of these are Snail (SNAI1) and Slug (SNAI2). ZEB1 plays a similar role to Snail and Slug within the context of EMT (Sánchez-Tilló et al., 2012), and hence it may be assumed that these proteins display similar roles in ECs. Loss of EC Slug reduces the vascular extension; however, the resulting phenotype differs from that observed in ZEB1^{iECKO} mice in this thesis. EC Slug KO produces a dense angiogenic front with increased branching and tip cell number; this is contrasting to what is observed with ZEB1 in this thesis (Hultgren et al., 2020). Therefore, the inefficiency observed within ZEB1^{iECKO} model is likely to be due to an alternative mechanism.

Knockout of Slug using siRNA in neonatal mice specifically affects vessel sprouting and deep plexus formation within the later stages of retinal vasculature formation (Park et al., 2015). This finding does hold similarities to what is observed ZEB1^{iECKO} mice; however, this is at a later developmental stage which involves alternative sprouting angiogenic mechanisms as tip cells dive down to form the deep plexus (Fruttiger, 2007; Zarkada et al., 2021). This research alongside the findings presented in this thesis demonstrates the variation between the roles of these EMT promoting transcription factors within endothelial cells and developmental angiogenesis..

4.3.4 Limitations and potential Cre toxicity

Developmental angiogenesis studies using transgenic neonatal mice, particularly with the Cre-ERT2 system, are well-established in the literature; however, certain limitations merit consideration. Recent research has begun to reveal potential adverse effects associated with the activation of the Cre-ERT2 system. Brash et al highlighted how various endothelial specific Cre-ERT2 systems leads to impaired retinal angiogenesis without the presence of a floxed gene (Brash et al., 2020). This included the Cdh5 (VECAD), a commonly published endothelial specific system (Payne et al., 2018), and what is used throughout this thesis, as well as Pdgfb and Tie2 driven systems. Specifically, their study demonstrated that

tamoxifen-induced activation of the Cre-ERT2 system in neonates resulted in reduced vascular extension and fewer branch points, despite the absence of a floxed gene. This outcome was observed even when compared to tamoxifen-treated wild-type controls, thereby ruling out any effects solely attributed to tamoxifen toxicity (Brash et al., 2020).

To demonstrate this, the team used three different concentrations of tamoxifen (50 µg, 100 µg and 150 µg) which evealed a dose-dependent response (Brash et al., 2020). Many research groups opt for higher concentrations of tamoxifen, to maximise recombination and, consequently, knockout efficiency. The data presented in this chapter were obtained using a 50 µg of tamoxifen dose, which is the lowest dose recommended. Brash et al found no significant difference in vascular extension in the cdh5-CreERT2 mice dosed with only 50 µg doses of tamoxifen, suggesting that Cre-ERT2-specific toxicity is only apparent at higher tamoxifen doses. Nevertheless, the inclusion of Tamoxifen dosed $Cre^{+/-}$ controls, that have no floxed genes, should be considered.

Interestingly, while this toxicity was observed in Cdh5 and Pdgfb-driven Cre-ERT2 systems, it was not present in Tie2-driven systems, suggesting that the observed effects may be driver-specific. Despite all these systems being described as endothelial specific, there are subtle differences which could account for this (Payne et al., 2018). There have been several proposed reasons for this toxicity, such as off-target DNA damage, despite there being no LoxP sites within the mouse genome. It is possible that Cre-ERT2 activation influences endothelial cell proliferation, which could explain the observed changes (Rashbrook et al., 2022).

This important study underscores the necessity of including Tamoxifen-treated $Cre^{+/-}$ controls, which lack floxed genes, in research using the Cre-ERT2 system. Much of the work presented in this chapter, including colony setup and mouse breeding protocols, was carried out prior to the publication of this study, and therefore these controls were not incorporated. Consequently, the potential impact of Cre toxicity on the results presented in this chapter must be considered before drawing definitive conclusions from the data.

Another limitation of the developmental angiogenesis work in this chapter is that the exact level of ZEB1 expression has not been confirmed owing to difficulties in extracting

sufficient ECs and subsequent mRNA from neonate mouse lungs via MACS. The genomic PCRs from Transnetyx confirm whether each neonate is CreERT$^{+/-}$ or CreERT2$^{-/-}$, but do not provide information on the extent of ZEB1 expression reduction or the proportion of ECs that have undergone ZEB1 knockdown. This information is important, as the level of knockout may influence the observed phenotype. Varying tamoxifen dosages can alter the knockout efficiency, potentially leading to a mosaic knockout. A similar effect was observed in a study on the transcription factor FOXO1, where a single small dose of tamoxifen resulted in a mosaic vasculature(Wilhelm et al., 2016). The level of ZEB1 expression within ZEB1^{iECKO} neonates could be achieved by replicating the KO confirmation experiments at the beginning of chapter 5. This, however, would require optimisation owing to the reduced size of lung tissue impacting the cellular and therefore RNA yield.

4.4 Chapter Summary

The work in this chapter aimed to explore the role of endothelial ZEB1 in physiological angiogenesis using a developmental neonatal transgenic mouse model with an inducible endothelial-specific ZEB1 KO. Through image analysis of the developing vascular plexus, it was determined that loss of endothelial ZEB1 led to inefficient angiogenesis, evidenced by reduced vascular front progression. Additionally, significant alterations were observed in the vascular network structure, both at the angiogenic front and within the central plexus. The reduced branching and changes in network organization contributed to the impaired vascular front progression. These findings have elucidated a role for ZEB1 in regulating developmental angiogenesis, specifically in endothelial cell function and vascular network branching.

Chapter 5:

Identifying the effect of endothelial ZEB1 knockout in a model of wet age-related macular degeneration

5 Identifying the effect of endothelial ZEB1 knockout in a model of wet age-related macular degeneration

5.1 Introduction

Within a developed organism, the vascular network is within a state of homeostasis, by which the surrounding tissues are supported by the capillary beds that sustain them. The ECs remain in a quiescent state, with minimal proliferation, migration, and reduced metabolism, yet continuously sensing environmental cues and blood contents (Eelen et al., 2020). The quiescent endothelium still has the capability of undergoing phenotypic changes which can result in EC activation, angiogenesis initiation and vascular remodeling. Having this ability is essential to ensure the vascular network can respond effectively to changes, such as damage, inflammation and growth (Hellste Ylva, 2014). The regulation of this homeostatic balance is highly important and involves a finely tuned balance of signaling pathways such as VEGF/VEGFR (Eremina et al., 2003; Kasahara et al., 2000), and ANG/TIE (Augustin et al., 2009), which activate transcription factors such as FOXO1 (Dharaneeswaran et al., 2014),and ERG (Shah et al., 2016), in a way that promotes survival and vascular stability, without initiating EC activation and an unrequired angiogenic response. Any loss to this regulation of endothelial quiescence and vascular homeostasis is a hallmark of many diseases (Eelen et al., 2020). An example of such disease is wet age-related macular degeneration (wAMD, sometimes termed neovascular AMD or nAMD but will be referred to as wAMD throughout this thesis).

AMD is the leading cause of vision loss in developed countries in those aged 60 or over and is predicted to affect 288 million people worldwide by 2040 (Wong et al., 2014). In wAMD, unwanted angiogenesis occurs within the choroidal vessels at the back of the eye in a process called choroidal neovascularisation (CNV). The exact triggering of angiogenesis and loss of quiescence is yet to be fully elucidated and may be down to several factors. One of these factors is due to hypoxia occurring within the RPE as a result of extracellular deposits called drusen which limit oxygen diffusion (Mammadzada et al., 2020). The subsequent release of pro-angiogenic factors triggers the endothelial cells of the choriocapillaris undergo proliferation and migration which leads to rupture of the

Bruchs membrane, followed by invasion of the retinal pigment epithelial cells, as well as neuronal layers of the retina (see Figure 5.1). The vision loss comes about due to the aberrant neovascularisation causing structural damage to the neuronal cells of the retina (Mcleod et al., 2009; Wang & Hartnett, 2016). Along with this, the highly fenestrated choriocapillaris result in vascular leakage and as well immune cell infiltration, activation and cytokine release, which further increases inflammation and fluid build-up that exacerbates the disease (Ambati et al., 2013).

Although there are multiple forms of AMD, including dry AMD where there is no neovascularisation but RPE drusen deposits result in vision loss, wet AMD is more severe and has a profound impact on patients due to its acute loss of central vision (Ferris et al., 2013). Dry AMD can also develop into wAMD as the disease progresses; therefore, a significant proportion of research has been focused on therapeutics to target wAMD (Wolf et al., 2022). Importantly, much of this therapeutic focus stems from the fact that wAMD involves a functional and accessible pathological mechanism, choroidal neovascularisation, which can be directly targeted to preserve or restore vision. In contrast, the mechanisms behind dry AMD are more degenerative and less amenable to current therapeutic intervention. As VEGF-A is a prominent pro-angiogenic factor, and wAMD patients have higher levels of VEGF-A within their aqueous humour (Zhou et al., 2020), therapeutic strategies were aimed at targeting VEGF-A. Because of this, the most common therapeutic agents used to treat wAMD are anti-VEGF-A antibodies such as Bevacizumab, Ranibizumab and Aflibercept, which are delivered via ocular injection (recently reviewed in Chen et al., 2023). However, limitations of current therapies such as reduced efficacy with time, as well as discomfort and anxiety surrounding ocular injections (Wolf et al., 2022), has mean that research into alternative mechanisms is still on going. Much of the reduced efficacy experienced with anti-VEGF therapy is due to the VEGF independent mechanisms which lead to the progression of wAMD. This includes interactions between semaphorins and their receptors, termed neuropilins (NRP), which are known co-receptors for VEGFRs. Knockout of NRP-1 was observed to reduced choroidal neovascularisation (Fernández-Robredo et al., 2017), and it was identified that NRP-1 was capable of inducing vascular permeability independently of VEGF (Roth et al., 2016). Other factors such as TGFβ have been identified as being higher in the aqueous

humour of patients with wAMD in comparison to healthy subjects (Tosi et al., 2017). As well as this, PDGF signaling has also been identified as possible treatment target, as anti-PDGF treatment reduced AMD pathophysiology in rabbit models (Ding et al., 2017).

Modelling AMD using laser photocoagulation to rupture the Bruchs membrane was first developed by S J Ryan in non-human primates in the late 1970s (Ryan, 1979). The resulting inflammatory and angiogenic response was subsequently found to replicate some aspects of what is observed in patients with wAMD (Miller et al., 1990), leading to the model being widely accepted. Since then, the method has been adapted to use mice and rats, with the laser induction of CNV within mice first being published as a model for wAMD in the 1990s by the Campochairo group, in their research showing targeting fibroblast growth factor 2 does not alter disease progression (Tobe et al., 1998). The laser-CNV model has therefore continued to be used throughout the literature and within drug development for wAMD. The assay is widely reported as well-tolerated and is able to replicate the angiogenic and inflammatory processes that occur during wAMD (Lambert et al., 2013).

The protocol for laser-CNV involves the burning of lesions using an Argon laser focused on the RPE layers at the back of the eye. This is achieved under general anaesthesia and with the aid of eye drops that dilate the pupils to make the retina accessible (Lambert et al., 2013). The lesion generated disrupts the Bruchs membrane and RPE layer, resulting in inflammation and hypoxia which leads to neovascularisation. The protocol can be modified using transgenic mice, or administration of compounds either via intravenous, intraperitoneally or intravitreal injections. In the days following lasering, the mice can be imaged using fundus fluorescein angiography (FFA) to quantify lesion leakage, again using pupil dilating drugs and under general anaesthesia. Once the study timeline is complete and mice sacrificed, the lasered eyes can be dissected and stained to observe the neovascular lesion and any surrounding inflammation (Green et al., 2022).

In chapter 4 I demonstrated that loss of endothelial ZEB1 impacted developmental angiogenesis by reducing vascular front progression and branching. But until now this has not been explored in the context of angiogenic disease in the form of wAMD. The work in this chapter will focus on exploring how loss of endothelial ZEB1 affects wAMD by utilising the murine laser-CNV model.

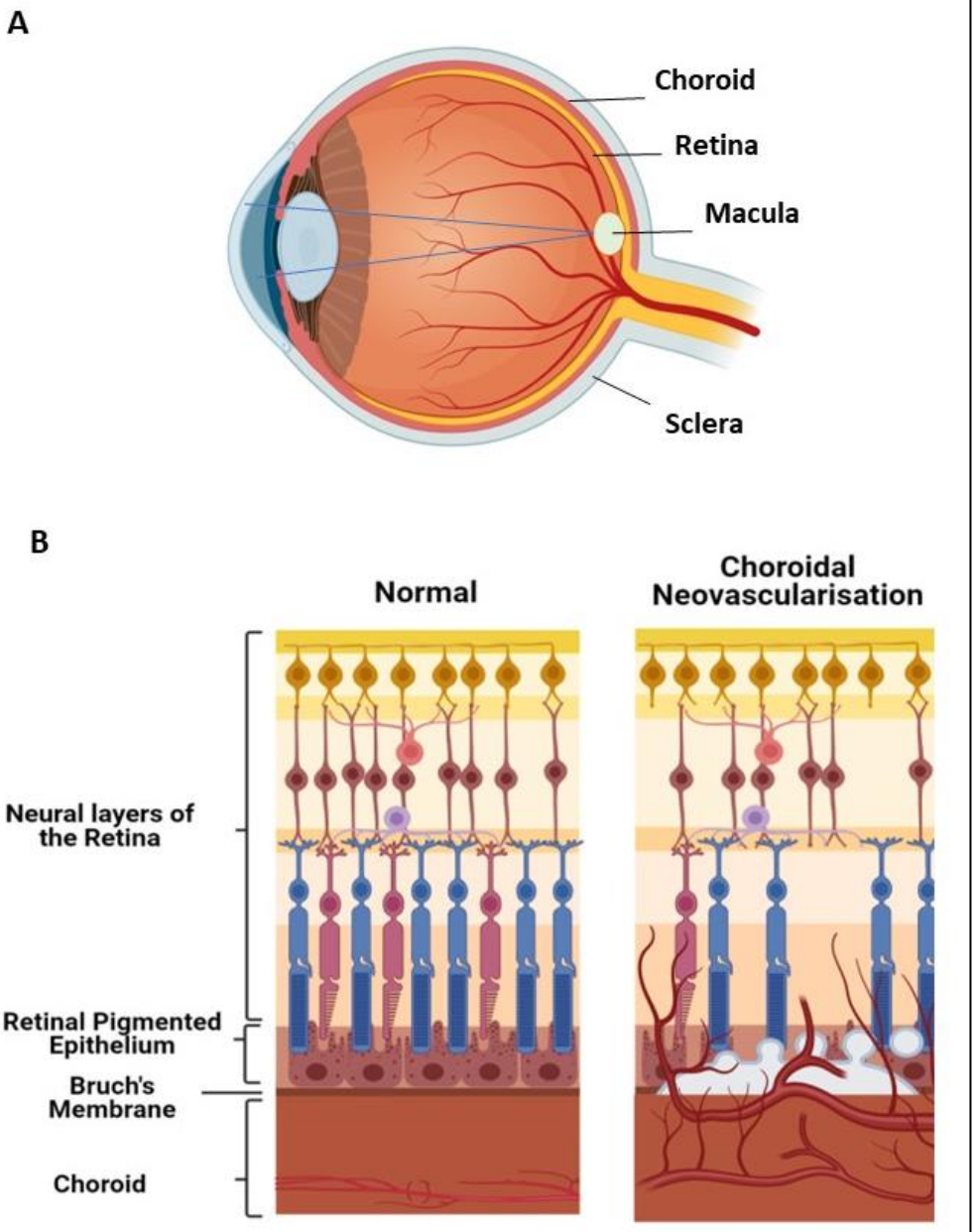

Figure 5.1 Choroidal Neovascularisation within wet Age-Related Macular Degeneration. (A) *A cross section of a human eye to display the location of the macula, as well as labelling the layers of the back of the eye.* ***(B)*** *A schematic comparing the structural layers of the retina and the back of the eye in the case of a normal patient, and one with wAMD. In the AMD case, CNV has occurred which has resulted in structural damage to the retinal pigmented epithelium and neural layers, as well as fluid leakage into the retina. Created with biorender.*

5.2 Results

5.2.1 ZEB1^{iECKO} mice have reduced ZEB1 mRNA expression following tamoxifen administration

ZEB1$^{fl/fl}$cdh5CRE-ERT2$^{+/-}$ and *ZEB1$^{fl/fl}$cdh5CRE-ERT$^{-/-}$* were ear notched at between 4-5 weeks old and tissue sent to Transnetyx for genomic DNA PCR genotyping. Lungs from dosed adult *ZEB1$^{fl/fl}$cdh5CRE-ERT2$^{+/-}$* and *ZEB1$^{fl/fl}$cdh5CRE-ERT2$^{-/-}$* mice underwent digestion and magnetic cell sorting to isolate CD31^{+} endothelial cells. mRNA was extracted from both the input, CD31^{-} and CD31^{+}, converted to cDNA and taken for digital droplet PCR analysis.

To first assess the accuracy of the CD31 pull down, the expression levels of PECAM-1 (CD31) within all cell fractions were determined via ddPCR and normalised to GAPDH. This revealed that magnetic cell sorting achieved a high level of CD31^{+} cell enrichment in both the control and ZEB1^{iECKO} mice. Only low levels of CD31 are observed within the CD31^{-} or 'flow-through' fractions, indicating the pull down of CD31^{+} cells in an attempt to enrich for CD31^{+} endothelial cells was successful (Figure 5.2 A).

Following this, the level of ZEB1 mRNA expression in all fractions was determined and normalised to GAPDH in the control mice. This revealed that ZEB1 mRNA expression is enriched in the CD31^{+} fraction (1.566 ± 0.144) in comparison to the CD31^{-} fraction (0.209 ± 0.023), indicating expression of ZEB1 within the lung is associated within the CD31^{+} cell population (Figure 5.2 B). The level of ZEB1 mRNA expression was then determined within the CD31^{+} cell fractions of both control and ZEB1^{iECKO} mice. This identified that the ZEB1^{iECKO} mice had significantly reduced ZEB1 mRNA expression (0.436 ± 0.044), in comparison to control mice (1.000 ± 0.092, Figure 5.2 D, $P < 0.05$). This confirmed that the inducible transgenic KO of ZEB1 was leading to a reduction in ZEB1 expression in CD31^{+} cells. The level of ZEB1 mRNA was also assessed within the CD31^{-} or 'flow-through' fraction to assess whether there had been any change in CD31^{-} cell types. This revealed that there was no significant difference in ZEB1 mRNA expression in the CD31^{-} cell fraction between the control and ZEB1^{iECKO} mice ($P > 0.05$, Figure 5.2 C). Taken together these results indicate that ZEB1^{iECKO} mice display a reduction of ZEB1 mRNA expression that is CD31^{+} specific and does not alter ZEB1 expression in any CD31^{-} cell types.

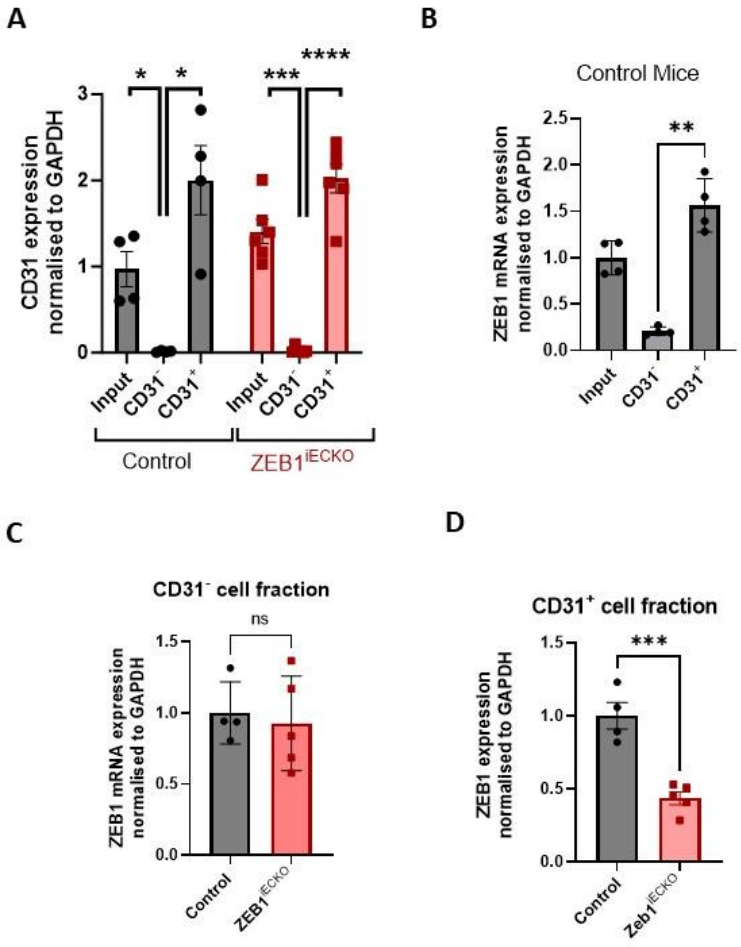

Figure 5.2 ZEB1 mRNA expression was determined to be significantly reduced in ZEB1^{iECKO} CD31^{+} cells isolated by magnetic cell sorting, compared to controls. *ZEB1^{iECKO} and control mice received daily doses of tamoxifen via IP injection over 5 days to induced Endothelial specific Cre-ERT mediated KO of ZEB1. 3 weeks after dosing, mice were culled, lungs dissected and dissociated, followed by magnetic cell sorting for CD31. mRNA was extracted from input, CD31^{-} and CD31^{+} cells, reverse transcribed to cDNA, followed by ddPCR analysis to assess changes in RNA expression.* ***(A)*** *CD31 expression normalised to GAPDH is displayed across all fractions and revealed a strong enrichment of CD31 expressing cells in the CD31^{+} cell fraction. Input vs CD31^{-} and CD31^{-} vs CD31^{+} were compared using a paired t-test which revealed statistical significance between all groups* ***(B)*** *ZEB1 expression normalised to GAPDH across all cell fractions in control animals only. Data expressed relative to input.* ***(C)*** *ZEB1 mRNA expression in CD31^{-} cell compared between control and ZEB1^{iECKO} groups. Data expressed relative to control* ***(D)*** *ZEB1 mRNA expression in CD31^{+} cell compared between control and ZEB1^{iECKO} groups. Equal amounts of cDNA were used in the ddPCR and expression was normalised to GAPDH. Data expressed relative to control. All data are presented as mean + SEM and al but* ***(A)*** *and* ***(B)*** *were stastically analysed used a paired t-test. ** p < 0.005, *** p < 0.0005, **** p < 0.0001*

5.2.2 ZEB1^{iECKO} display increased leakage area over time despite being not significant at individual time points

Once dosed to induced knockout and lasered to induced CNV, control and ZEB1^{iECKO} mice underwent FFA imaging on days 3, 7 and 14 post-lasering. FFA images were analysed by measuring the size of the leakage area on image J. The mean leakage area was then plotted against time to observe any differences between the ZEB1^{iECKO} group and the control group (Figure 5.3). A two-way ANOVA was performed to analyse the effect of varying genotype (control or ZEB1^{iECKO}) and time (days) on lesion leakage. Simple main effects analysis revealed that genotype had a statistically significant impact on lesion leakage (*, $P < 0.05$), suggesting that knockout of endothelial ZEB1 is generating changes in lesion leakage. Ontop of the two-way ANOVA, Sidaks multiple comparisons test was performed to determine differences between control and or ZEB1^{iECKO} at individual time points. Although a reduction is observed, the difference was determined not to be statistically significant ($P > 0.05$). Therefore, although the effect of genotypes had a statistically significant effect on leakage area, this effect was not great enough at individual time points for it to be significant.

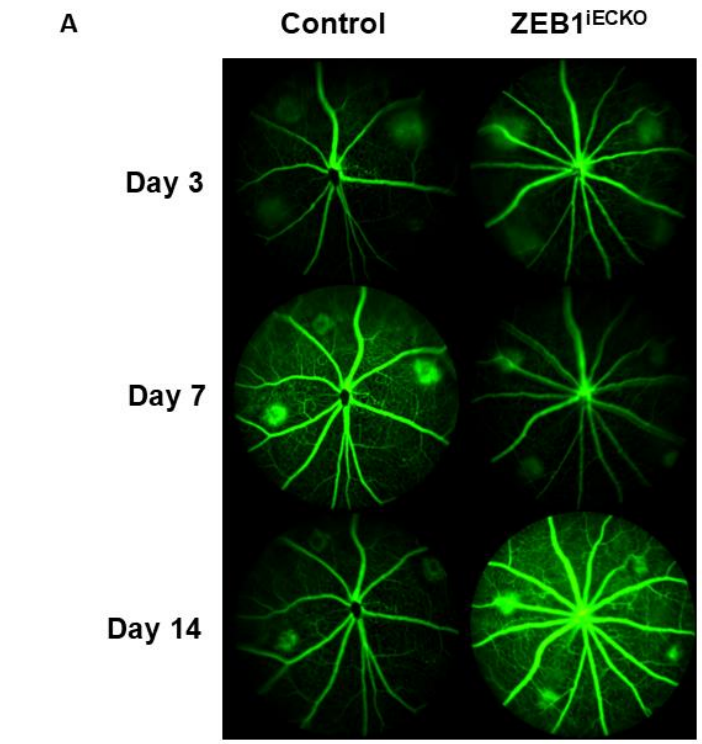

Figure 5.3 Main effects analysis revealed ZEB1^{iECKO} mice had significantly increased lesion leakage area throughout the study but there was significant difference at individual time points. *ZEB1^{iECKO} and control mice received daily doses of tamoxifen via IP injection over 5 days before undergoing laser CNV. Fundus fluoresceine angiography (FFA) was performed on days 3, 7 and 14 post-lasering.* ***(A)*** *Representative FFA images are shown.* ***(B)*** *The area of lesion leakage was measured using Image J and plotted against time (days).* ***(C)*** *Leakage size was analysed by a Two-way ANOVA with Sidaks multiple comparisons test. Simple main effects analysis showed that genotype (control or ZEB1^{iECKO}) had a stastically significant effect on leakage area (*) P < 0.05. Sidaks multiple comparisons test revealed the difference in leakage area between control and ZEB1^{iECKO} was not statistically significant at any time point P > 0.05. Data presented as mean + SEM. Control day 3, day 7 and day 14 N= 10, 13, 12 respectively. ZEB1^{iECKO} day 3, day 7 and day 14 N= 19, 19, 19 respectively.*

5.2.3 Male ZEB1^{iECKO} mice have a significantly increased lesion leakage area at day 3 and day 7 post-lasering

It was noted that within the FFA leakage area data for the ZEB1^{iECKO} group there was a large amount of variation. Because sex differences have been reported in multiple animal studies, especially in laser induced CNV (Gong et al., 2015), the data was split between male and female mice. Analysis from FFA images from male control and male ZEB1^{iECKO} mice were then plotted against time to observe any differences in these two groups (Figure 5.4). Two-way ANOVA analysis again revealed by simple main effects analysis that genotype had a statistically significant impact on lesion leakage, but with increased significance (****, $P < 0.0001$). As done previously, Sidaks multiple comparisons was performed to analyse any differences between male control and male ZEB1^{iECKO} groups at individual time points during the study. This revealed that at 3 days post-lasering male ZEB1^{iECKO} mice have an increase in leakage area compared to control male mice (47,484 ± 5716 AU compared to 24,114 ± 5801 AU control, $P < 0.05$). This was also the case at 7 days post-lasering where male ZEB1^{iECKO} mice have an increase in leakage area compared to control male mice (42,973 ± 7669 AU compared to 17,470 ± 3383 AU control, $P < 0.05$). Although a difference is still observed on day 14, it is not calculated as significant at $P = 0.105$. Together this data indicates knockout of endothelial ZEB1 has a profound effect on fluorescein leakage from CNV lesions in male mice. This is seen as a significant increase the area of fluorescein on days 3 and 7, whereas the effect observed decreases over time as the lesion size reduces, hence by day 14 this difference is not observed to be statistically significant.

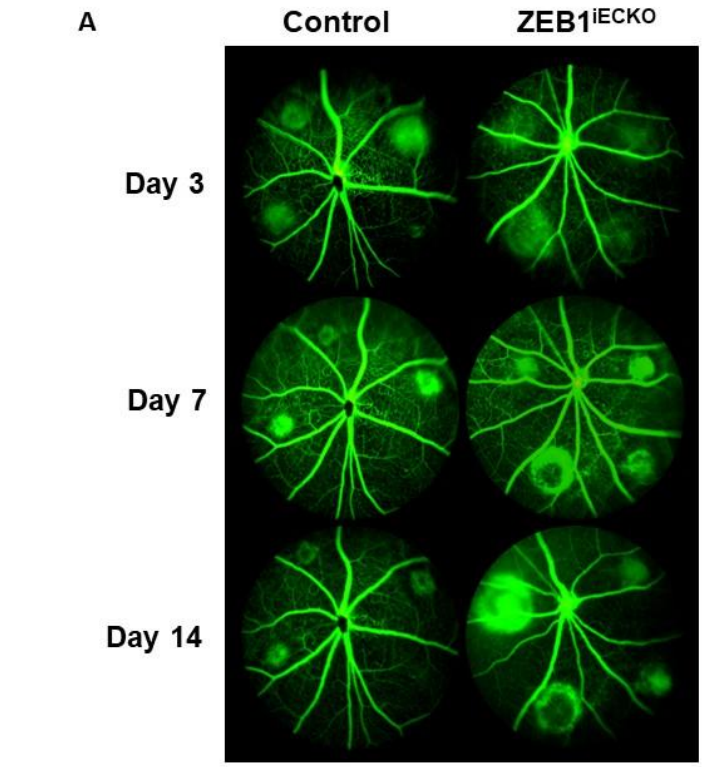

Figure 5.4 Male ZEB1^{iECKO} mice have increased leakage areas compared to control male mice. *ZEB1^{iECKO} male and control male mice received daily doses of tamoxifen via IP injection over 5 days before undergoing laser CNV. Fundus fluoresceine angiography (FFA) was performed on days 3, 7 and 14 post-lasering.* ***(A)*** *Male data weres replotted and representative male FFA images are shown.* ***(B)*** *Data was replotted to separate out sex. The area of lesion leakage was measured using Image J and plotted against time (days).* ***(C)*** *Leakage size was analysed by a Two-way ANOVA with Sidaks multiple comparisons test. Simple main effects analysis showed that genotype (control or ZEB1^{iECKO}) had a statistically significant effect on leakage area (****) P < 0.0001. Sidaks multiple comparisons test indicated statically significant differences at days 3 and 7. * P < 0.05, ** P < 0.005. Data presented as mean + SEM. Control day 3, day 7 and day 14 N= 5, 7, 7 respectively. ZEB1^{iECKO} day 3, day 7 and day 14 N= 9, 9, 7 respectively.*

5.2.4 Female ZEB1^{iECKO} mice show no increase in lesion leakage area

Next was to determine how the female mice responded to laser-CNV by the means of lesion leakage area. Analysis from FFA images from female control and female ZEB1^{iECKO} mice were plotted against time to observe any differences in these two groups. However, with the female mice no major differences were observed (Figure 5.5). A two-way ANOVA was performed to determine whether genotype affected lesion leakage across the 3 days. Simple main effects analysis determine that genotype did not have a statistically significant effect on lesion leakage ($P > 0.05$). Sidaks multiple comparisons test was performed to analyse any differences between female control and female ZEB1^{iECKO} groups at individual time points during the study, which also revealed no significant differences at any time point ($P > 0.05$). This indicates that knockout of endothelial ZEB1 has no impact on lesion leakage after laser induced CNV in female mice.

To compare how male and female, ZEB1^{iECKO} and control mice respond to laser CNV in the form of lesion leakage over the 3 time points, all four groups were plotted together (Figure 5.6). This highlighted that ZEB1^{iECKO} male mice had much larger areas of lesion leakage, compared to the other 3 groups, with both female control and female ZEB1^{iECKO} mice responding similarly to male controls. A two-way ANOVA with Sidaks multiple comparisons test was performed to identify any differences between these groups at individual time points. As previously explained, male ZEB1^{iECKO} mice had significantly larger areas of lesion leakage at days 3 and 7, compared to control males. However, this identified a statistically significant difference in the lesion leakage area between male ZEB1^{iECKO} mice and female ZEB1^{iECKO} mice, also on day 3 and day 7. Taken together, this data indicates that endothelial ZEB1 knockout influences lesion leakage area differently in males compared to females, in response to laser CNV. ZEB1^{iECKO} male mice have larger areas of lesion leakage, whilst ZEB1^{iECKO} female mice do not vary from that of control female mice.

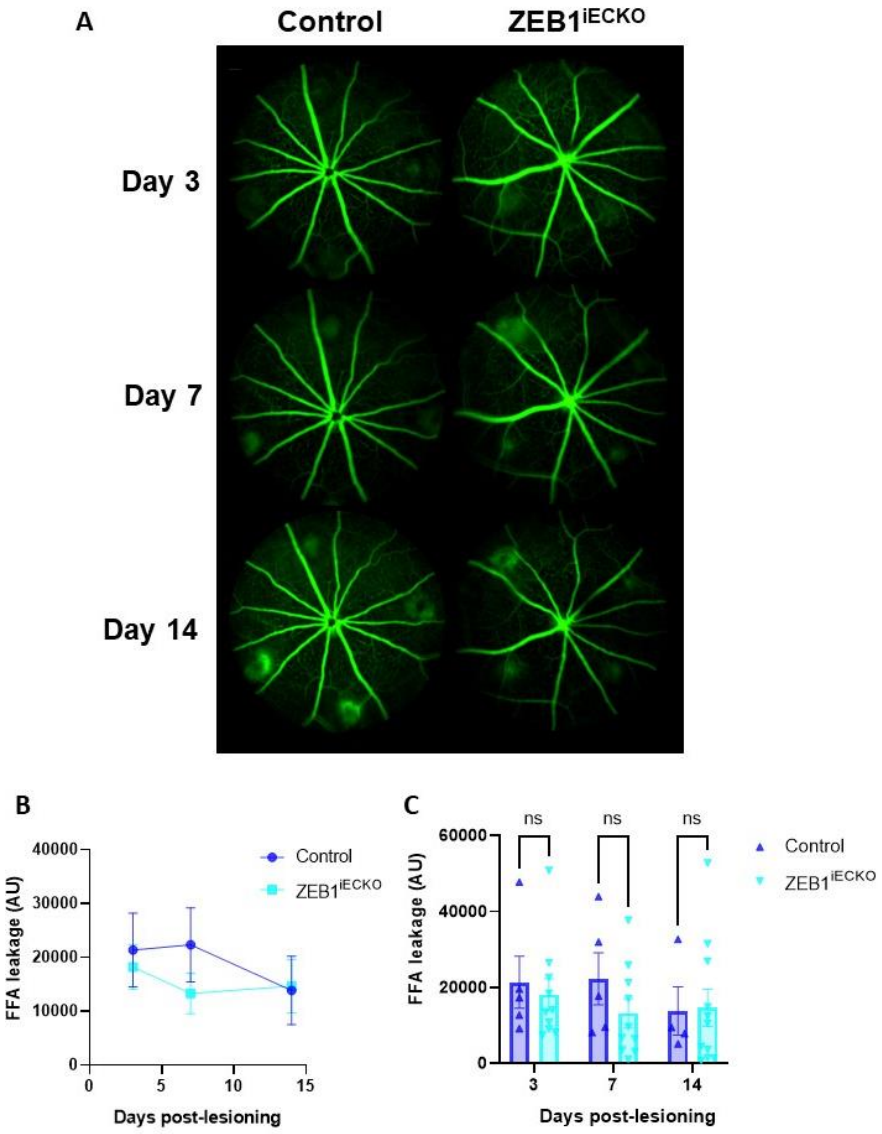

Figure 5.5 Female ZEB1^{iECKO} mice display no change in lesion leakage area compared to control female mice. *Rehearsal of data from Figure 5.4: ZEB1^{iECKO} female and control^{female} mice received daily doses of tamoxifen via IP injection over 5 days before undergoing laser CNV. Fundus fluoresceine angiography (FFA) was performed on days 3, 7 and 14 post-lasering.* ***(A)*** *Representative female FFA images are shown.* ***(B)*** *Data was replotted to separate out sex. The area of lesion leakage was measured using Image J and plotted against time (days).* ***(C)*** *Leakage size was analysed by a Two-way ANOVA with Sidaks multiple comparisons test. Simple main effects analysis revealed that genotype (control or ZEB1^{iECKO}) had no effect on leakage area P > 0.05. Sidaks multiple comparisons test also revealed no difference in leakage area between control and ZEB1^{iECKO} at any time point P > 0.05. Data presented as mean + SEM. Control day 3, day 7 and day 14 N= 5, 5, 4 respectively. ZEB1^{iECKO} day 3, day 7 and day 14 N= 10, 10, 11 respectively.*

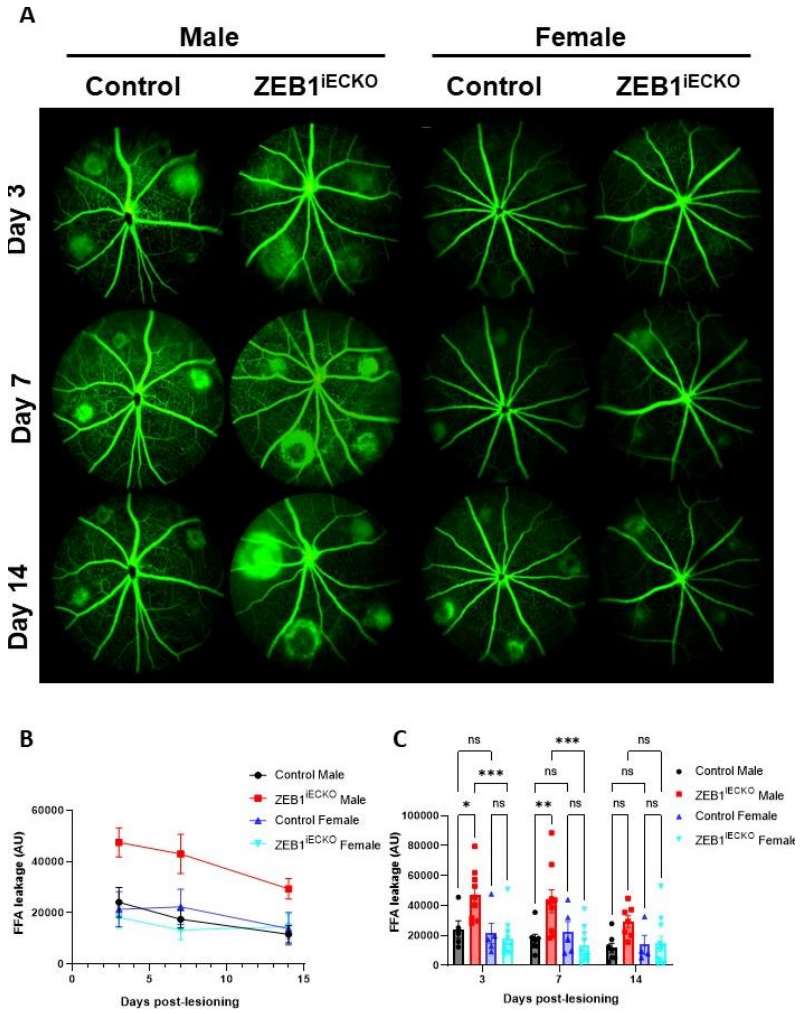

Figure 5.6 Male ZEB1^{iECKO} mice and female ZEB1^{iECKO} have different FFA leakage areas and do not respond in the same way to laser CNV. *Rehearsal of data from Figure 5.4: ZEB1^{iECKO} and control male and female mice received daily doses of tamoxifen via IP injection over 5 days before undergoing laser CNV. Fundus fluoresceine angiography (FFA) was performed on days 3, 7 and 14 post-lasering.* ***(A)*** *Representative male and female FFA images are shown.* ***(B)*** *The area of lesion leakage was measured using Image J and plotted against time (days).* ***(C)*** *Data was replotted to separate out sex. Leakage size was analysed by a Two-way ANOVA with Sidaks multiple comparisons test. Simple main effects analysis showed that genotype (control or ZEB1^{iECKO}) had a statistically significant effect on leakage area (****) P <0.0001. Sidaks multiple comparisons test revealed that in female mice there was no significant difference in lesion leakage between control and ZEB1^{iECKO} at any time point. Sidaks multiple comparisons also revealed that the leakage area was significantly increased in to ZEB1^{iECKO} male mice compared to to ZEB1^{iECKO} female mice on day 3 and 7. * P < 0.05, ** P < 0.005, *** P < 0.0005, Data presented as mean + SEM. Male control day 3, day 7 and day 14 N= 5, 7, 7 respectively. Male ZEB1^{iECKO} day 3, day 7 and day 14 N= 9, 9, 7 respectively. Female control day 3, day 7 and day 14 N= 5, 5, 4 respectively. Female ZEB1^{iECKO} day 3, day 7 and day 14 N= 10, 10, 11 respectively.*

5.2.5 ZEB1^{iECKO} results in increased CD31 neovascular lesion in both male and female mice laser CNV

On day 14 post lasering, the mice were sacrificed and eyes fixed. The choroids were then dissected, whole mount stained for CD31 and image using a confocal microscope. The area of the neovascularised region was calculated by image J. Because a sex difference was observed in fluorescein leakage area size, and there have been numerous reports identifying sex difference in the murine laser-CNV model, primarily highlighting that female mice display larger and greater variation in lesion sizes (Gong et al., 2015), the data was split into male and female groups (Figure 5.7). This was then plotted separately in order to determine whether a sex difference is also seen when observing the neovascular lesion size (Figure 5.7 B). In this case, individual lesions were plotted, and outliers were identified and removed using ROUT (where Q = 1%) before being analysed by 2-way ANOVA with Sidaks multiple comparisons test. This revealed that both male and female ZEB1^{iECKO} mice had significantly larger neovascular lesion sizes when compared to their sex control mice (for male ZEB1^{iECKO} 105,800 ± 13703 μm^2 compared to 49,284 ± 9013 μm^2 control males; for female ZEB1^{iECKO} 66,585 ± 8243 μm^2 compared to 27,000 ± 3278 μm^2 control females).

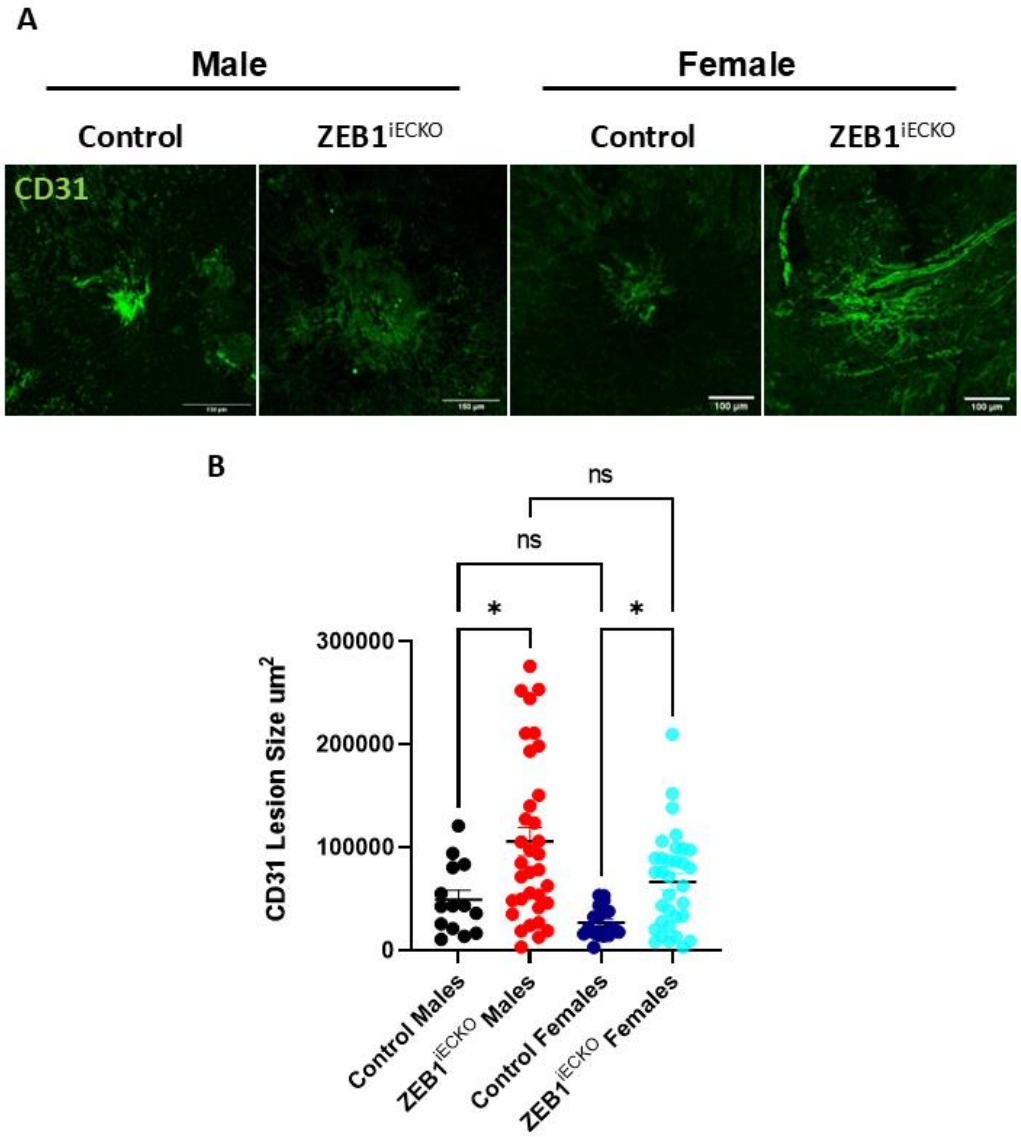

Figure 5.7 Both male and female ZEB1^{iECKO} mice have larger CD31 stained neovascularised lesions compared to control mice after laser-CNV. *ZEB1^{iECKO} and control male and female mice underwent laser-CNV. On day 14 mice were sacrificed, choroid dissected and fixed before being stained for CD31 and imaged using confocal microscopy and analysed using Image J.* ***(A)*** *Representative images are shown* ***(B)*** *CD31 Lesion size is plotted per lesion and is significantly increased in ZEB1^{iECKO} male and females, compared to male and female controls. Data plotted as individual lesions. Outliers were identified and removed using ROUT identify outliers test where Q = 1%. Data presented as mean + SEM. Control N = 12, ZEB1^{iECKO} N = 18. Statistically analysed by 2-way ANOVA with Sidaks multiple comparisons test.* P < 0.05*

5.2.6 Female ZEB1^{iECKO} mice have a significantly decreased CD45 integrated density compared to male ZEB1^{iECKO} mice

To assess the immune cell infiltration occurring within the neovascular lesions, CD45 staining was also performed and imaged. The CD45 staining was quantified by determining the integrated density of the lesion area, identified by CD31. To determine whether there is a sex difference in the integrated density of the inflammation marker, CD45, the data was split into male and female groups (Figure 5.8). This was achieved by plotting individual lesions and removing outliers by ROUT (where Q = 1%), before being analysed by 2-way ANOVA with Sidaks multiple comparisons test. This revealed that both male and female ZEB1^{iECKO} mice display no significant difference in CD45 integrated density when compared to the same sex controls ($P > 0.05$). However, what was noteworthy is that female ZEB1^{iECKO} mice displayed a significantly reduced CD45 integrated density in comparison to male ZEB1^{iECKO} mice ($1.276x10^6 \pm 0.198x10^6$ AU compared to male ZEB1^{iECKO} at $3.332x10^6 \pm 0.450x10^6$ AU). This data suggests that both male and female ZEB1^{iECKO} mice show no change in inflammation as measured by CD45 integrated density when compared to same sex controls. However, this has identified that female ZEB1^{iECKO} mice display a significantly decrease level of inflammation and immune cell infiltration when compared to male ZEB1^{iECKO} mice.

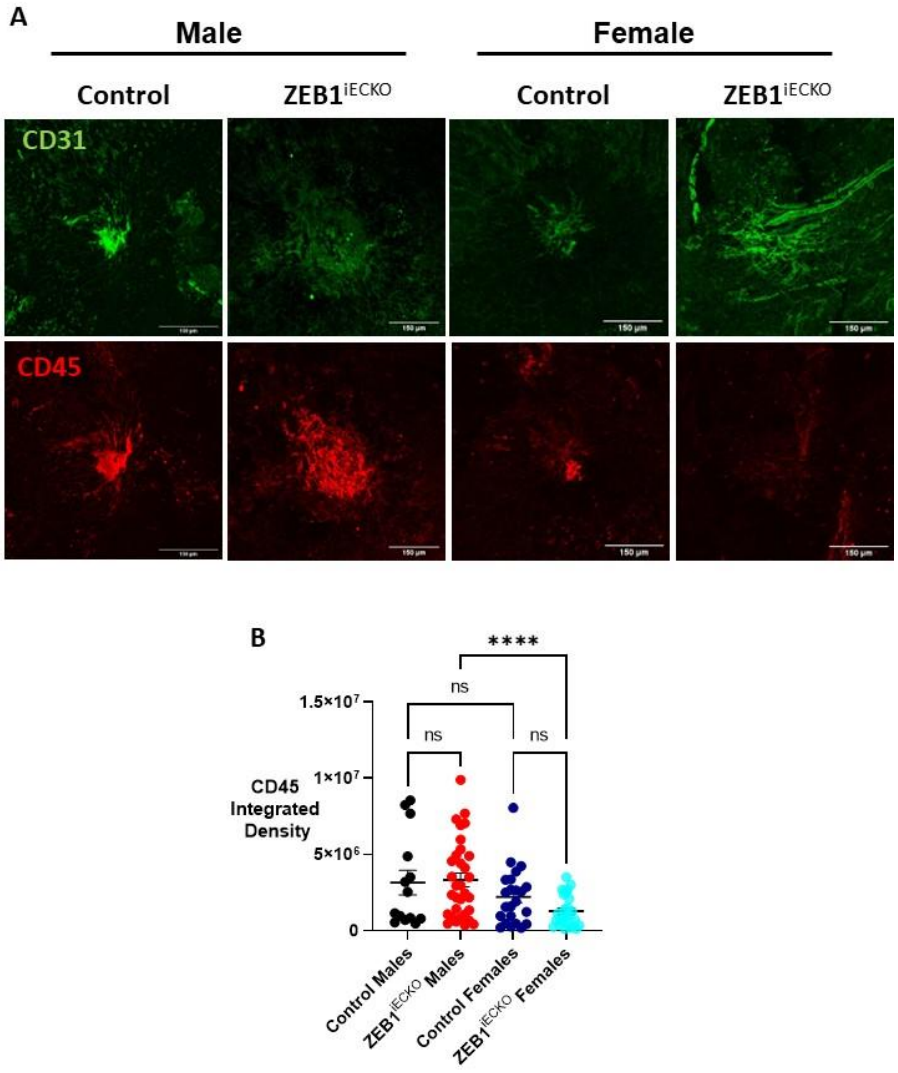

Figure 5.8 Female ZEB1^{iECKO} mice exhibited reduced CD45-associated inflammation compared to male ZEB1^{iECKO} mice after laser-CNV. *ZEB1^{iECKO} and control male and female mice underwent laser-CNV. On day 14 mice were sacrificed, choroid dissected and fixed before being stained for CD31 and CD45 and imaged using confocal microscopy and analysed using Image J.* ***(A)*** *Representative images are shown* ***(B)*** *CD45 integrated density was determined in the CD31 lesion area. CD45 integrated density is plotted per lesion shows no change between ZEB1^{iECKO} male and females, and their controls. However, ZEB1^{iECKO} male mice do have a significantly increased CD45 integrated density when compared to ZEB1^{iECKO} female mice. Data plotted as individual lesions. Outliers were identified and removed using ROUT identify outliers test where Q = 1%. Data presented as mean + SEM. Control N = 12, ZEB1^{iECKO} N = 18. Statistically analysed by 2-way ANOVA with Sidaks multiple comparisons test.**** P < 0.0001*

5.3 Discussion

5.3.1 Determining the level of ZEB1 expression

In this chapter I was able to determine via reverse transcription and digital droplet PCR, the level at which ZEB1 mRNA was reduced after tamoxifen dosing of *ZEB1$^{fl/fl}$ cdh5 Cre-ERT2^{+}* mice. The isolation and enrichment of endothelial cells by CD31^{+} pull down via magnetic cell sorting, yielded a high level of endothelial cells. The lungs were chosen as an ideal tissue to isolate ECs due to the fact they are highly vascularized, therefore having a high EC density compared to other tissues. From the CD31^{+} isolated cell fraction from both control and ZEB1^{iECKO} mice, the level of ZEB1 mRNA was determined which proved a robust reduction in ZEB1 expression within the iECKO group, averaging around 55%. This level of reduction was evidently enough to create a phenotype within the context of the laser-CNV model. Nonetheless, this does bring into question whether a greater reduction may have increased effects or even give rise to alternative effects.

5.3.2 Quantification of the reduction in endothelial ZEB1 expression within the iECKO model is comparable other reports within literature

To discover whether it is possible to further decrease the level of ZEB1 expression, the literature was searched to determine if greater levels of KO are achieved; however, groups who utilise the iECKO model confirm their reduction in their chosen KO gene expression in a variety of ways. Crist et al applied a similar method to that used within this thesis when determining the level of Smad4 within lung ECs isolated from Smad4^{iECKO} mice; revealing around 50% reduction on Smad4 expression (Crist et al., 2018). This is similar to what is seen with ZEB1^{iECKO} mice, indicating that the reduction in expression level that is observed is not dissimilar to what has been achieved previously. The approach displayed in this thesis was adapted from a previously published method in determining the level of VEGFR2 expression in a Tie2 Cre driven VEFR2^{iECKO} model (Beazley-Long et al., 2018). This publication also reported a similarity in the level of reduction of the transgene, further confirming that the reduction in ZEB1 expression seen here, are comparable and consistent with the field.

There have been publications whereby a greater level of reduction of transgene expression was achieved, such as the research using BMPR1A^{iECKO} by Lee et al. This work

determined a very large reduction in BMPR1A expression via western blot, however the samples ran on this western were not directly from tamoxifen induced BMPR1A^{iECKO} mice. Instead, it appears that they isolated ECs from un-dosed mice before treating them in culture with a Cre expressed adenovirus to induce recombination and BMPR1A KO (Lee et al., 2022). Although this method shows that the recombination site is correct and recombination is possible, it does not determine the level of protein expression in dosed mice. Therefore, publications like these should be observed with caution when comparing expression levels.

Another publication which reports the reduction of multiple transgenes, describes the effects of knocking out VEGFRs on the developing vasculature by Karaman et al. Although an influential publication, they did not isolate endothelial cells to test for the level of transgene expression; instead performing qPCR analysis on whole lungs, which gave them a robust level of KO (Karaman et al., 2022). This was likely achievable in this way because the VEGFRs are primarily expressed on endothelial cells, and less frequently on other cell types (Shibuya, 2006). However, this method is unlikely to be suitable for determining the level of ZEB1 within the iECKO model used in this thesis, due to the known expression of ZEB1 in other cell types.

5.3.3 ZEB1^{iECKO} results in increased lesion leakage in male mice

When knocking out endothelial ZEB1 in male mice, the lesions created by the laser-CNV method produce larger fluoresceine leakage in comparison to control male mice. This suggests that the neovascular lesions are larger and more permeable. The increased permeability seen in wAMD/CNV, is as a result pathological neovessels that form within the disease (Wolf et al., 2022). Loss of ZEB1 is therefore observed to be exacerbating the pathology within this model.

Whole mount staining of choroids from male ZEB1^{iECKO} mice proved that there is an increase in neovascular lesion size in comparison to control. This alone may have been enough to directly cause the increase in lesion leakage seen by FFA; however, there are multiple other factors which can increase the permeability of the vasculature and therefore impact the permeability of the neovascular lesions seen in laser induced CNV. As previously stated, the levels of VEGF within the aqueous humour are raised within

wAMD patients (Zhou et al., 2020). VEGF is known to be key driver of vascular permeability in a variety of physiological and disease states, including wAMD (Bates, 2010). The role VEGF plays in CNV lesion leakage is evident due to the success in anti-VEGF therapies in clinical trials (recently reviewed in Chen et al., 2023). Not only this, VEGF is also capable of promoting recruitment of inflammatory cells (Barleon et al., 1996). The recruitment of inflammatory cells, as well as release of pro-inflammatory cytokines, further increases the permeability of these angiogenic choriocapillaris, and hence generate greater leakage from CNV lesions. It would therefore be interesting to determine the levels of these pro-permeability cytokines, including VEGF, in response to laser-CNV when EC ZEB1 has been knocked out. Confirming this by ELISA at a local level within the eye, as well as a systemic level may provide a link between EC KO of ZEB1, and the increase in leakage observed.

5.3.4 The increase in fluorescein leakage in ZEB1^{iECKO} is sex dependent, but CNV lesion area is not

It is evident from the FFA data that the increase in fluoresceine leakage in ZEB1^{iECKO} mice is a male-only phenomenon. When assessing fluoresceine leakage from these lesions, female ZEB1^{iECKO} mice do not respond at all in the same way that male ZEB1^{iECKO} mice do, with the difference between the two being statistically significant. From the confirmation of ZEB1 knockout and reduction in ZEB1 mRNA expression, there is little reason to suggest the level of knockout varies between male and female mice. Therefore, this brings about the possibility that the reduction of EC ZEB1 expression has alternative effects in male and female mice, in response to laser induced CNV.

It has been actively reported in the literature that there is a difference in which male and female mice respond to the laser-CNV model. Gong et al reported that both male and female mice had increased lesion size with age. However, this increase in lesion size with age was much more profound in female mice, compared to male mice. They reported 12–16-week-old female mice having significantly larger lesion sizes compared to 12-16-week-old males (Gong et al., 2015). This had been described previously and the cause of such increase suggested as being due to the heightened estrogen levels in older female mice, as estrogenic supplementation also increased lesion size (Espinosa-Heidmann et al., 2005). It is because of these reported sex differences, many research groups utilising the

laser-CNV method chose to only use male mice to reduce variability; however, in line with increased expectations to use both sexes in animal research (Child et al., 2022), both sexes were used in this thesis. As prior knowledge of a laser-CNV sex dependent affect was known, the data was therefore subsequently presented as both sexes, as well as male and female separately, to ensure any sex differences were reported. The data presented in this chapter demonstrate a sex difference, as evidenced by the absence of fluorescein leakage in female ZEB1^{iECKO} mice, despite a marked increase in leakage observed in male ZEB1^{iECKO} mice. The presence of this increase in male ZEB1^{iECKO} mice, when compared to same sex controls, suggests that the observed sex difference is specific to the ZEB1 knockout.

Gong et al published an extensive study into the optimisation of laser-induced CNV in 2015, which highlighted variables that can affect CNV lesion size. The age and sex of mice was observed as being highly influential in the size of lesion produced. Both male and female mice produced on average larger lesions, with an increase in lesion size variation, if lasered between the 12-16 weeks of age, compared to those lasered at 8-6 weeks of age (Gong et al., 2015). This agreed with previously reported aged differences in response to murine laser induced CNV already within the literature (Espinosa-Heidmann et al., 2002). However, this previous study used 2-month-old and 16-month-old mice, whereas Gong et al noted these differences in much smaller age gaps in ages of mice more commonly used in research. As previously mentioned, this increase in lesion size with age was even more profound in female mice (Gong et al., 2015), likely due to the increase in estragon levels (Espinosa-Heidmann et al., 2005). The age of mice within thesis chapter was kept to a minimum owing to this. What must be noted is that the sex difference reported by Gong et al was identified within flat mount staining of choroid lesions. No FFA imaging published within this study to confirm whether this sex difference was also observed within fluorescein leakage from lesions. Therefore, it is not currently known whether this general sex difference extends onto fluoresceine leakage.

Although female ZEB1^{iECKO} mice do not display the same increase in lesion leakage as male ZEB1^{iECKO} mice, this sex difference is not observed when determining lesion size by CD31 flat mount staining of the neovascular lesion. From the data displayed in this chapter, both

male and female mice show an increase in CD31 neovascular lesion size compared to their same sex controls. This indicates that the sex difference in CNV lesions observed in this study is only within the fluorescein leakage of the lesion, and not the neovascular lesion size itself. One possible explanation is that estrogen in female mice may confer vasoprotective effects by enhancing endothelial barrier integrity, thereby limiting leakage despite similar levels of neovascularisation. Alternatively, sex-dependent inflammatory or permeability responses, possibly involving differential expression of tight junction proteins or cytokine sensitivity, may underlie the observed difference (Xing et al., 2009).

5.3.5 ZEB1^{iECKO} female mice had reduced lesion inflammation when compared with ZEB1^{iECKO} male mice

Angiogenesis in both its physiological and pathological forms is associated with inflammatory processes. Angiogenesis that occurs within disease states, such as wAMD, is especially linked to inflammation. In certain cases of wAMD, it is understood that underlying inflammation from uveitis has directly contributed to the disease presenting (Baxter et al., 2013). But what is common generally for wAMD patients is that the neovascularisation that occurs triggers inflammation which further progresses the disease. This generates a type of feedback loop, whereby inflammation from the RPE cells triggers endothelial activation, which in-turn prompts immune cell infiltration, leading to further cytokine release and greater vascular leakage (Kauppinen et al., 2016; Sprague & Khalil, 2009). Many cytokines have been observed to have been elevated in patients with AMD, either systemically or locally. These include but are not limited to: IL-6, IL-8 (Miao et al., 2012), IL-17 (Ardeljan et al., 2014), and CCL2 (Jonas et al., 2010).

Assessing the level of inflammation within neovascular lesions within the ZEB1^{iECKO} group was therefore an important part of assessing how loss of endothelial ZEB1 affects the neovascular process in laser induced CNV. This was achieved by staining for CD45, a leucocyte common antigen that is expressed on almost all haematopoietic cells (Barford et al., 1994). The type of CD45 staining varied quite significantly throughout all of the groups. Some CD45 staining had undefined edges, which made getting an accurate area measurement difficult; hence the integrated density of the lesion, as measured by the CD31 area was utilised. The inflammation assessed by CD45 integrated density

measurement of the neovascular lesion area revealed there was no significant difference between the ZEB1^{iECKO} males and control males. This therefore implied that knocking out endothelial ZEB1 resulted in an increase in neovascularization but did not significantly impact inflammation. While this analysis revealed no significant difference in inflammation between ZEB1^{iECKO} and control males, the diffuse nature of CD45 staining in some ZEB1^{iECKO} lesions suggests a possible alteration in vascular barrier properties. This could indicate that loss of endothelial ZEB1 may impair endothelial junction integrity, allowing immune cells to infiltrate more diffusely rather than accumulating at defined sites.

It was noted that female ZEB1^{iECKO} mice had significantly reduced CD45 integrated density, compared to male ZEB1^{iECKO} mice. This provides further evidence that loss of endothelial ZEB1 within male and female mice has alternative effects in response to laser CNV. The reduced inflammation displayed by the ZEB1^{iECKO} mice is likely explained by the reduction in fluorescein leakage resulting in a reduced immune cell infiltrate. The FFA data provides information regarding the leakiness and permeability of the neovascular region. Because this leakage is observed as being reduced in the female ZEB1^{iECKO} group compared to the control, this indicates the endothelial barrier is less permeable. This could therefore significantly impaire the ability of leucocytes and immune cells to extravasate and infiltrate the surrounding tissues within the female ZEB1^{iECKO} group, in comparison to the male ZEB1^{iECKO}, where the leakage is largest and therefore infiltration can occur.

There are a number of other molecular and signalling factors which may result in this reduction in inflammation observed in ZEB1^{iECKO} females compared with ZEB1^{iECKO} males. ECs within the choriocapillaris express cell adhesion molecules such as ICAM-1, which is responsible for leukocyte adhesion, therefore increasing the opportunity for leukocyte transmigration (Mcleod et al., 1995). Circulating immune cells detect the site of inflammation by following a chemokine gradient before migrating out of the bloodstream. This extravasation process is facilitated by endothelial cell responses to cytokine signals from the surrounding environment, leading to the upregulation of adhesion molecules, including JAMs, selectins, ICAM-1, and VCAM-1. These molecules promote the adhesion of circulating leukocytes to the vascular wall (Weber et al., 2007). It is possible that the

loss of endothelial ZEB1 is affecting the endothelium's role in the extravasation and infiltration process.

ECs are the source of some inflammatory cytokines, including IL-1a and IL-1b, which act upon various target cells including NK cells and B cells to initiate inflammatory activation responses (Sprague & Khalil, 2009). The loss of endothelial ZEB1 may impair the ECs' ability to release cytokines, leading to a reduced level of immune cell activation. The observed altered response could stem from changes at any stage of the process, ranging from the initial sensing of stimuli to the activation of signaling pathways, followed by gene expression changes that ultimately activate the endothelium in an inflammatory context.

5.3.6 Limitation in clinical translation of the laser-CNV model

Although the laser-CNV model has been extensively utilised and allowed for the development of anti-VEGF agents now used in the clinic, it does display differences from wAMD. The use of a laser to damage the Bruchs membrane drives a wound-healing reaction which is not strictly true of what occurs in wAMD. It is understood that this wound healing process and triggering of immune cells has a major role in promoting the neovascularisation observed within the laser-CNV model, as studies which depleted macrophages showed that this reduced the size of laser-CNV induced neovascular lesions and lesion leakage (Espinosa-Heidmann et al., 2003). However, the triggering of neovascularisation within wAMD differs from this, and displays other factors that are not present in this model, such as drusden, and increased levels of VEGF released by the RPE. Therefore, the effects observed when endothelial ZEB1 is knocked out in this model cannot be directly linked to wAMD itself but instead can be linked to the effects of laser-CNV, which includes wound healing in response to laser injury. This still provides insights into the role of endothelial ZEB1 in a disease model such as this, but the triggering of that disease model also induces events which are not completely true of wAMD.

5.4 Chapter Summary

The work in this chapter aimed to explore how loss of endothelial ZEB1 affects pathological angiogenesis. This was achieved by using the laser-CNV model of wetAMD, a disease whereby aberrant angiogenesis occurs within choriocapillaris, leading to blindness. KO of endothelial ZEB1 in male mice resulted in an increase in FFA leakage

within the lesion, but this effect was not observed in female mice. Loss of EC ZEB1 increased CD31 neovascular lesion size in both sexes; however, Female ZEB1^{iECKO} mice exhibited reduced inflammation compared to male ZEB1^{iECKO} mice. Taken together this data suggests that loss of EC ZEB1 results in increased pathological angiogenesis; however, there appears to be a sex difference in the lesion leakage and subsequent inflammation within ZEB1^{iECKO} groups.

Chapter 6:

Exploring how loss of endothelial ZEB1 affects revascularization in a model of peripheral artery disease

6 Exploring how loss of endothelial ZEB1 affects revascularization in a model of peripheral artery disease

6.1 Introduction

Peripheral arterial disease (PAD) is a condition characterized by endothelial dysfunction, which contributes to arterial blockage and insufficient collateral vessel formation and revascularisation (Figure 6.1). PAD is a major cardiovascular disease (CVD) that specifically affects the arteries supplying blood to the legs, leading to partial or complete blockage (Kavurma et al., 2022). This arterial occlusion results in reduced blood flow and hypoperfusion, causing tissue ischemia, which in turn leads to pain. Over time, this can progress to ulceration and gangrene, often culminating in limb amputation (Ouriel, 2001). The clinical relevance of PAD is evident, as it is predicted to affect over 200 million people wordwide (Virani et al., 2021).

Tissue homeostasis is maintained through the endothelium's ability to respond to changes in oxygen tension and acidosis. Insufficient blood supply leads to tissue ischemia, reducing the delivery of oxygen and nutrients to the affected area. When the endothelium cannot appropriately respond by initiating vessel dilation and new vessel growth, prolonged ischemia results in tissue damage (Hernández-Reséndiz et al., 2018). The response to ischaemia is primarily regulated by HIF signalling and the production of pro-angiogenic factors such as VEGF (Pugh & Ratcliffe, 2003). In addition, both arteriolargenesis and arteriogenesis are essential processes in response to ischemic injury. In arteriolargenesis, smooth muscle cells are recruited to the expanding capillary network to generate arterioles, which is regulated by eNOS, VEGF and Ang-1 (Benest et al., 2008). Whereas arteriogenesis is the process in which arteries are generated though remodelling of preexisting arterioles, which therefore compensate for occluded arteries (Van Royen et al., 2001). Together, arteriogenesis, arteriolargenesis, and angiogenesis contribute to the revascularization of ischemic tissue.

In the context of PAD, there is an impaired response to hypoxic stimuli, leading to an insufficient angiogenic response (Kavurma et al., 2022). This dysfunction has been

observed in both humans and animal models, with comorbidities such as aging (Hodges et al., 2018), diabetes (Fadini et al., 2019), and high cholesterol (Jang et al., 2000) having a negative impact on the ability of the vasculature to respond to the blockage. Additionally, microvascular dysfunction, characterized by impaired oxygen delivery due to disruptions in blood flow regulation and vessel tone, has been associated with an increased risk of amputation in patients with PAD (Behroozian & Beckman, 2020). As a result, understanding the transcriptional response of ECs during ischemic injury is a critical focus of current PAD research.

In the late 1980s and early 1990s, animal models of PAD were being developed to research disease progression and evaluate novel treatments. These models typically involved inducing ischemia in the selected limb artery occlusion, either by ligation, constriction or electrocoagulation. Initially these experiments were performed in larger animals such as rabbits, dogs and pigs, but advances in expertise have allowed for murine and rat models of PAD to be developed (Aref et al., 2019). The hind limb ischaemia (HLI) model of peripheral artery disease has been published throughout the cardiovascular literature and has led to advances in understanding PAD and collateral vessel formation (Aref et al., 2019; Takeshita et al., 1994).

The first description of the HLI mouse model of PAD was published by Couffinhal et al. This model built upon a previous approach developed by Wolfgang Shaper (Arras et al., 1998), which initially utilised rabbits. In the murine version, hind limb ischemia was induced by ligating the femoral artery at the proximal end, as well as the distal portion of the saphenous artery, followed by excision of the femoral artery. Postoperative blood flow recovery to the ischemic limb was monitored for a total of 5 weeks (Couffinhal et al., 1998). Various adaptations of this procedure have been developed, including ligation at different site (Aref et al., 2019); however, all these methods aim to induce ischaemia within the hind limb before monitoring blood flow recovery using Laser Doppler Perfusion Imaging. Methods have also been developed to assess the level of collateralisation and angiogenic response within the ischaemic tissue via immunohistochemistry staining of vascular markers. The work in this chapter will focus on exploring how loss of endothelial

ZEB1 influences collateral vessel formation and blood flow recovery using a mouse model of PAD.

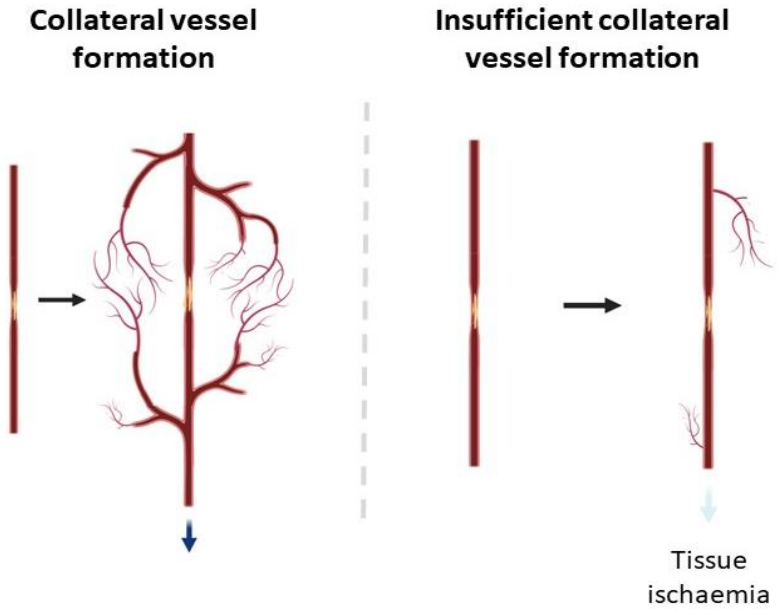

Figure 6.1 Insufficient collateral vessel formation. *A schematic to explain the insufficient collateral vessel formation and subsequent tissue ischaemia observed in PAD. Created with biorender.*

6.2 Results

6.2.1 ZEB1^{iECKO} mice displayed no significant difference in blood flow recovery compared with control mice

After the standard tamoxifen dosing regime, control and ZEB1^{iECKO} underwent left femoral artery ligation surgery to induce HLI. Prior to surgery the blood flow to both paws were determined by laser speckle imaging and the raw speckle intensity data plotted in Figure 6.2 B. This revealed no significant difference between the baseline blood flow between ZEB1^{iECKO} mice and control mice ($P > 0.05$). Immediately after surgery the reduction in blood flow was also determined. This revealed that ZEB1^{iECKO} mice have a higher blood flow in the ischaemic paw (17.33 ± 0.84%) compared to the ischaemic paw of the control mice (14.06 ± 1.00%) and this difference is observed to be statistically significant via an

unpaired t-test ($P < 0.05$). This therefore indicates the response to HLI surgery is not as great in ZEB1^{iECKO} mice.

The blood flow recovery was also determined on days 3, 7, 14 and 21 after surgery and was plotted for both control and ZEB1^{iECKO} mice in Figure 6.2 D. Mixed-effects analysis was performed to analyse the effect of genotype on blood flow recovery. This revealed that there was no significant difference in blood flow recovery between control and ZEB1^{iECKO} mice ($P > 0.05$). Multiple comparison analysis to determine differences at individual time points also revealed no significant difference at any time point within the study. Taken together these results show that ZEB1^{iECKO} mice show no significant difference in blood flow recovery in response to HLI surgery.

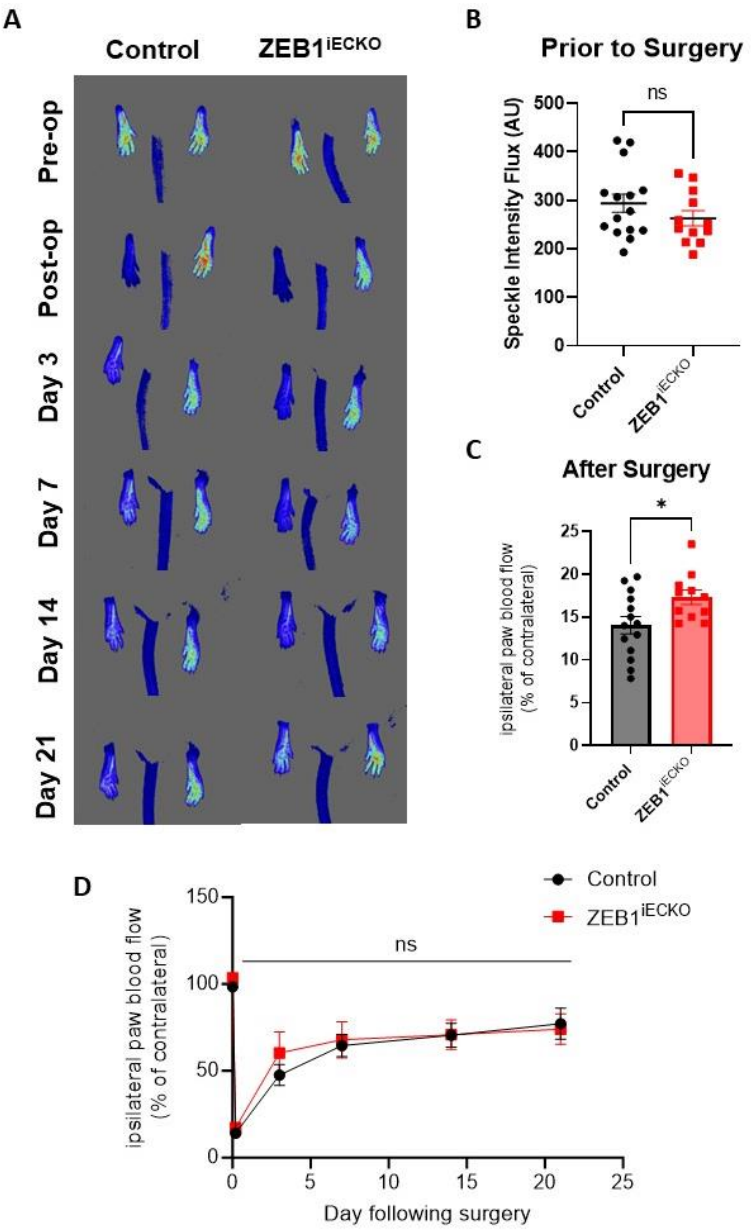

Figure 6.2 ZEB1^{iECKO} had no effect on blood flow recovery after ischaemic injury of the left femoral artery. (A) *Representative blood flow images are shown for all time points.* ***(B)*** *Raw values of speckle intensity flux determined no significant difference between ZEB1^{iECKO} and control mice using an unpaired t-test ($p > 0.05$).* ***(C)*** *% of blood flow normalised to the contralateral paw was determined to be significantly increased in ZEB1^{iECKO} mice compared to controls immediately after surgery (* = $p < 0.05$).* ***(D)*** *Mixed effects analysis of % of blood flow normalised to the contralateral paw over the time course of the study revealed no significant difference in response to left femoral artery ligation over time, ($p = > 0.05$). All data presented as mean + SEM. Control N = 15, ZEB1^{iECKO} N = 12.*

6.2.2 ZEB1^{iECKO} mice display no difference in muscle fibre area when compared to control mice

21 days following surgery the mice were cardiac perfused and gastrocnemius muscle prepared for sectioning and staining to determine capillary and arteriolar density. Alongside vascular remodelling, angiogenesis and astrogenesis, the ischaemia produced by ligation of the femoral artery has various implications on the surrounding tissue. This includes tissue necrosis and fibrosis, which can alter the area and structure of the muscle fibres (reported in Xie et al., 2016). To assess whether there was variation in muscle fibre area, indicating changes in the level of fibrosis, the muscle fibre area was calculated as a percentage of the total imaged area (Figure 6.3). This revealed no significant difference between the control mice contralateral and ipsilateral muscle, as well as the ZEB1^{iECKO} ipsilateral and contralateral, as determined by paired ratio t-test ($P > 0.05$).

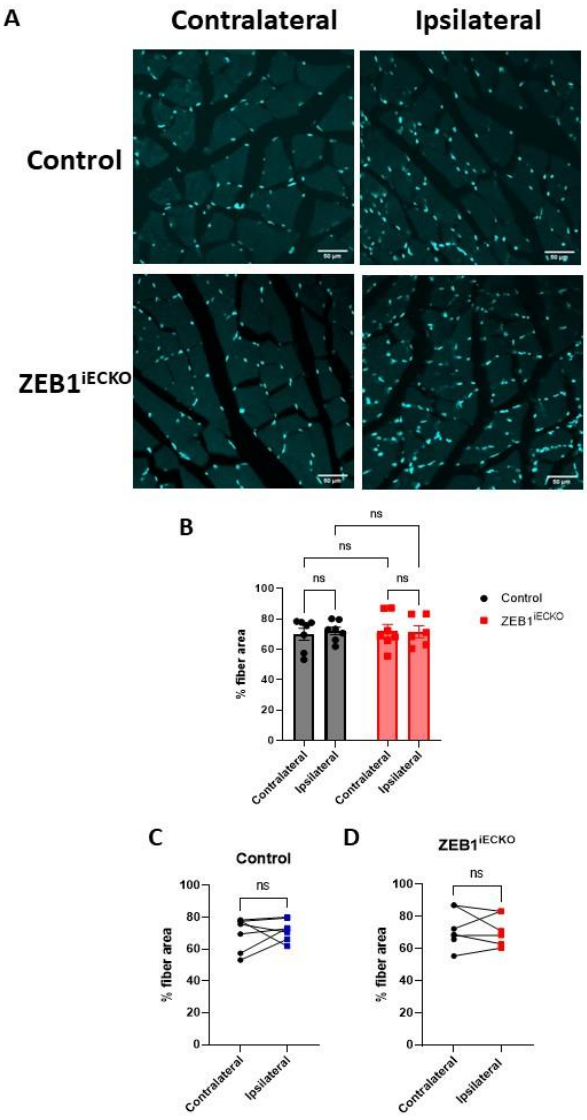

Figure 6.3 There is no difference in gastrocnemius muscle fibre area between contralateral and ipsilateral, ZEB1^{iECKO} and control mice. *21 days after HLI surgery the mice were culled by cardiac perfusion with 4% PFA. Both gastrocnemius muscle was dissected, fixed in 4% PFA, dehydrated in 30% sucrose before being embedded in OCT ready for cryosectioning. 16 µm thick sections were stained for DAPI and imaged using a confocal microscope. (A) Representative DAPI stained images are shown with low contrast to show background staining of muscle fibres. (B) quantification of muscle fibre area was determined as a % for both control and ZEB1^{iECKO} mice. 2-way ANOVA with mixed affects analysis revealed no significant difference in muscle fibre area with genotype or leg type, P > 0.05. (C) Control mice had no significant difference in muscle fibre area % between contralateral and ipsilateral as determined by a paired ratio t-test, P > 0.05. (D) ZEB1^{iECKO} mice had no significant difference in muscle fibre area % between contralateral and ipsilateral as determined by a paired ratio t-test, P > 0.05. All data presented as mean + SEM. Control N = 7, ZEB1^{iECKO} N = 7. Scale bar = 50µm*

6.2.3 The hind limb ischaemia surgery induced an angiogenic response determined by an increase in capillary number and area

To first confirm whether the induction of ischaemia within the hind limb had induced an angiogenic response in the form of an increase in capillary number and area, the contralateral (non-ischaemia) and ipsilateral (ischaemia) gastrocnemius muscle of control mice were sectioned and stained for isolectin-B_4 (IB_4, Figure 6.4). Firstly, the percentage of IB_4 staining was quantified per fibre area, which revealed a stastically significant increase within the ipsilateral muscle (4.14 ± 0.61%, compared to 3.31 ± 0.47% within the contralateral, $P < 0.05$, Figure 6.4 B). Secondly, the capillary density was determined by the number of IB_4 vessels per mm^2 fibre area. This revealed a significant increase in the number of IB_4 vessels within the ipsilateral muscle (891.3 ± 115.8 per mm^2 compared to 605 ± 38.58 per mm^2 contralateral, $P < 0.05$, Figure 6.4 C). These results taken together indicate that hindlimb ischemia surgery induced a sufficient angiogenic response within control mice of this study, as determined by an increase in capillary density, and IB_4 area.

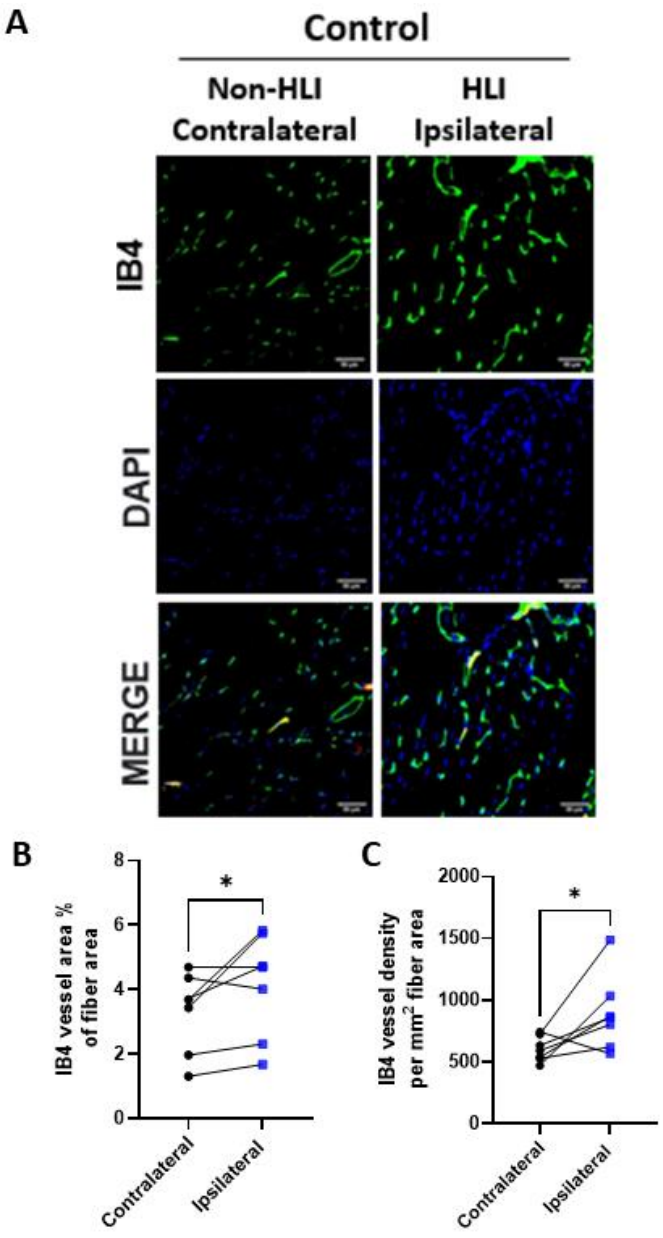

Figure 6.4 Control mice have an increased capillary area and density in response to HLI. *Control mice underwent HLI surgery and after 21 days both contralateral and ipsilateral gastrocnemius muscle was fixed, sectioned and stained with isolectin-B_4 (IB_4) to quantify capillaries.* ***(A)*** *Representative images from contralateral and ipsilateral sections.* ***(B)*** *Quantification of IB_4 capillary area as a percentage of fiber area.* ***(C)*** *Quantification of IB_4 capillary number per mm^2 fiber area. Data analysed by paired ratio t-test, * = p <0.05. All data presented as mean + SEM. Control N = 7. Scale bar 50µm.*

6.2.4 The increase in capillary density in response to hind limb ischaemia is not observed in ZEB1^{iECKO} mice

To then determine whether knocking out endothelial ZEB1 influences this angiogenic response to hind limb ischaemia, the contralateral and ipsilateral gastrocnemius muscle from both control and ZEB1^{iECKO} mice were sectioned and stained for IB_4 (Figure 6.5). Firstly, the number of IB_4 capillaries per fibre area was determined in both control and ZEB1^{iECKO} mice in both the contralateral and ipsilateral limb (Figure 6.5 B). A two-way ANOVA was performed to analyse the effect of genotype and ischaemic surgery on the capillary density. This revealed there was a stastically significant interaction between the two variables on IB_4 capillary density ($P < 0.05$). Also, multiple comparison analysis using Tukeys multiple comparison test revealed no significant difference between contralateral and ipsilateral in both the control and ZEB1^{iECKO} groups, or between ZEB1^{iECKO} and control groups within the same muscle type. To display the data to show the response to ischaemia, the IB_4 per mm^2 value for the individual ipsilateral muscle was divided by the corresponding contralateral value. This displayed the data whereby anything above 0 indicates an increase in IB_4 vessel density, were as anything below 0 indicates a decrease in IB_4 vessel density (Figure 6.5 C). The values for both control and ZEB1^{iECKO} mice were compared and analysed using an unpaired t-test which revealed a significant decrease in ipsilateral-contralateral value (-0.14 ± 0.15) compared to controls (0.50 ± 0.18, $P < 0.05$).

Although IB_4 capillary number per mm^2 is a good read out of vessel density, it does not account for changes in the type of vessels that are present within the tissue, e.g. traversing vessels. As well as this, vessels dilate in response changes in blood flow and ischaemia (Morita et al., 1997), and hence this could also be a factor that is not account for in capillary density measurements alone. To account for this, IB_4 area percentages were calculated. Firstly, the percentage of IB_4 staining within the area of muscle fibres was determined in both control and ZEB1^{iECKO} mice in both the contralateral and ipsilateral limb (Figure 6.5 D). A two-way ANOVA was performed to analyse the effect of genotype and ischaemic surgery on the IB_4 percentage area which revealed no significant interaction between the two variables on IB_4 percentage area ($P > 0.05$). Tukeys multiple comparison test also determined there was no significant differences between the individual variables

within the analysis. As done with previously with the IB_4 capillary density, the data was displayed to show the response to ischaemia whereby the IB_4 percentage value for the individual ipsilateral muscle was divided by the corresponding contralateral value. This displayed the data a value greater than 0 indicates an increase in IB_4 percentage, were as anything less than 0 indicates a decrease in IB_4 percentage (Figure 6.5 E). An unpaired t-test revealed no significant difference between the control and $ZEB1^{iECKO}$ mice in response to ischaemia when monitoring IB_4 area as a percentage of fibre area. Both control and $ZEB1^{iECKO}$ had an average positive value of around 0.25, indicating that both groups ipsilateral muscle displayed a small increase in IB_4 area compared to the contralateral limb.

Taken together these data indicate that the increase in IB_4 vessel density in response to ischaemia observed in the control mice, is not observed in the $ZEB1^{iECKO}$ mice. However, when measuring IB_4 area in response to ischaemia, there appears to be no significant difference in the response within the control group compared to the $ZEB1^{iECKO}$ group. This therefore indicates that both control and $ZEB1^{iECKO}$ are responding similarly to ischaemia in the increase in IB_4 area, but $ZEB1^{iECKO}$ group do not elicit the same increase IB_4 capillary density as the control group in response to ischaemia.

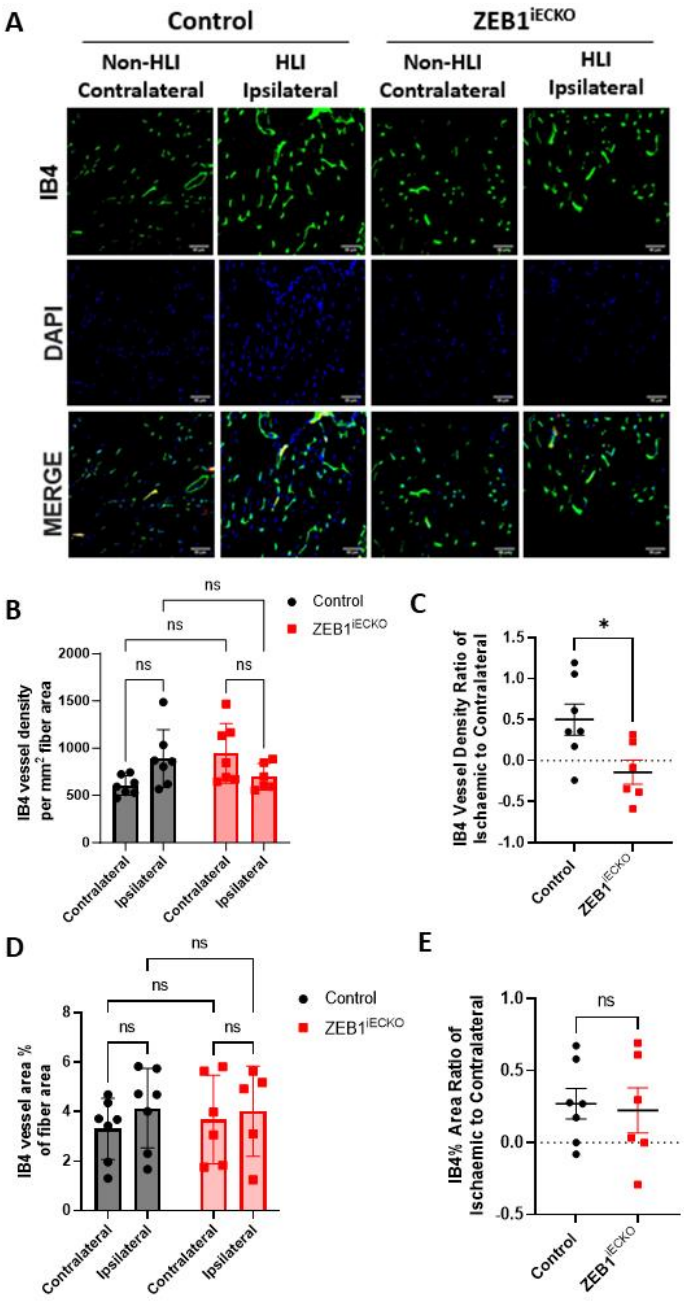

Figure 6.5 ZEB1^{iECKO} mice have significantly reduced ratio of ipsilateral/contralateral IB$_4$ capillary number per mm^2 compared to control mice. *ZEB1^{iECKO} and control mice underwent HLI surgery and after 21 days both contralateral and ipsilateral gastrocnemius muscle was fixed, sectioned and stained with isolectin-B$_4$ (IB$_4$) to quantify capillaries.* ***(A)*** *Representative images from contralateral and ipsilateral sections.* ***(B)*** *Quantification of IB$_4$ capillary number per mm^2 fiber area* ***(C)*** *IB$_4$ capillary number per mm^2 fiber area displayed as ipsilateral/contralateral* ***(D)*** *Quantification of IB$_4$ capillary area % of fiber area* ***(E)*** *IB$_4$ capillary area % of fiber area displayed as ipsilateral/contralateral.* ***(B)*** *and* ***(D)*** *analysed by 2-way ANOVA with multiple comparisons (ns, P > 0.05).* ***(C)*** *and* ***(E)*** *analysed by unpaired t-test, * = p <0.05. All data presented as mean + SEM. Control N = 7, ZEB1^{iECKO} N = 7. Scale bar 50µm.*

6.2.5 ZEB1^{iECKO} mice have increased capillary density within the non-ischaemic limb

From the two-way ANOVA analysis of IB_4 capillary density in Figure 6.5, it was noted that the contralateral values for control group were lower than that of the ZEB1^{iECKO} group, although this difference was not significant according to Tukeys multiple comparisons test ($P = 0.624$). The calculated two-way ANOVA interaction value however was significant, despite neither main effect analyses (genotype or ischaemia) being significant, indicating both variables are together having a significant effect on capillary density. As well as this, it was noted that when normalising the ipsilateral value to the contralateral value, a significant decrease in the value was seen within the ZEB1^{iECKO} group compared to control. This raised the question of whether the knockout of endothelial ZEB1 was influencing the capillary density without a direct ischaemic stimulus and therefore affecting the contralateral leg. To determine whether this was the case, the contralateral IB_4 capillary number per mm^2 compared between the control and ZEB1^{iECKO} groups (Figure 6.6). An unpaired t-test revealed a significant increase in capillary number per mm^2 fibre within the ZEB1^{iECKO} group (945.5 ± 119.0 per mm^2 fibre area) compared to control (605.0 ± 38.58 per mm^2 fibre area, $P < 0.05$, Figure 6.6 B). To determine whether there were any differences in IB_4 area within the contralateral legs, which could account for changes in vessel size due to vascular dilation, or traversing vessels, the IB_4 area was compared between the two groups. Firstly, the IB_4 area was calculated as percentage of fibre area. An unpaired t-test revealed no significant difference between the area of IB_4 staining within the ZEB1^{iECKO} group, compared to the control mice ($P > 0.05$, Figure 6.6 C). This therefore indicates that although knockout out of endothelial ZEB1 appears to induce an increase in capillary density within the contralateral limb, it has no effect on the overall IB_4 area.

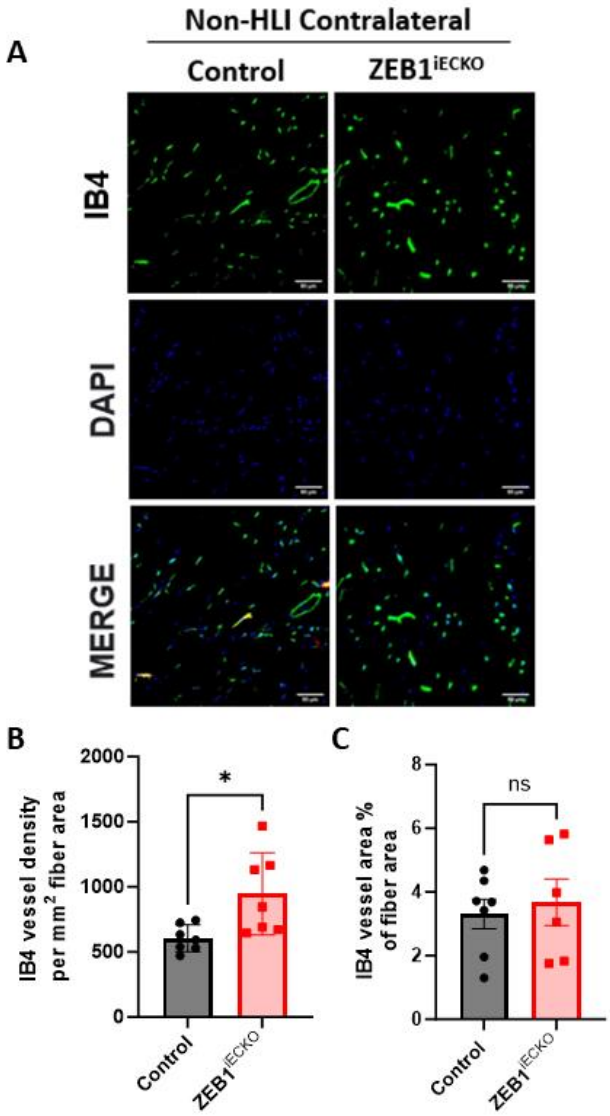

Figure 6.6 ZEB1^{iECKO} mice display increased IB$_4$ capillary number per mm^2 within the contralateral, non-ischaemic muscle, compared to control mice. *ZEB1^{iECKO} and control mice underwent HLI surgery and after 21 days the contralateral, non-ischaemic gastrocnemius muscle was fixed, sectioned and stained with isolectin-B$_4$ (IB$_4$) to quantify capillaries.* ***(A)*** *Representative images from contralateral sections.* ***(B)*** *Quantification of IB$_4$ capillary number per mm^2 fiber area.* ***(C)*** *Quantification of IB$_4$ capillary area % of fiber area. Data analysed by unpaired t-test, * = p <0.05. All data presented as mean + SEM. Control N = 7, ZEB1^{iECKO} N = 7. Scale bar 50µm.*

6.2.6 The hind limb ischaemia surgery induced an increase in arteriolar number and area as determine by α-smooth muscle actin

Another response to artery occlusion and ischaemia is to induce collateral vessel formation in the form of larger vessels such as arterioles via arteriogenesis or arteriolargenesis. To assess whether the hind limb ischaemia surgery induced any changes in arteriolar density and area, contralateral and ipsilateral 16μm sections of gastrocnemius muscle from control animals were stained for α-smooth muscle actin (αSMA) to quantify larger vessels such as arterioles which are supported by smooth muscle cells (Figure 6.7). Firstly, the αSMA area was calculated as a percentage of fibre area, which will account for an increased number of arterioles but also an increase in the size of individual arterioles or any vasodilation in response to ischaemia. A paired ratio t-test between the contralateral and ipsilateral muscle revealed a significant increase in the percentage of αSMA staining (0.637 ± 0.121% compared to contralateral at 0.435 ± 0.106%, $P < 0.05$, Figure 6.7 B). Secondly, the αSMA vessel density was determined by the number of αSMA associated vessels per mm^2 fibre area. This revealed a significant increase in the number of αSMA associated vessels within the ipsilateral muscle (25.42 ± 2.12 per mm^2 compared to 18.90 ± 1.75 per mm^2 contralateral, $P < 0.05$, Figure 6.7 C). These data taken together indicates that in response to HLI surgery, the control mice displayed an increase in αSMA vessel area and number.

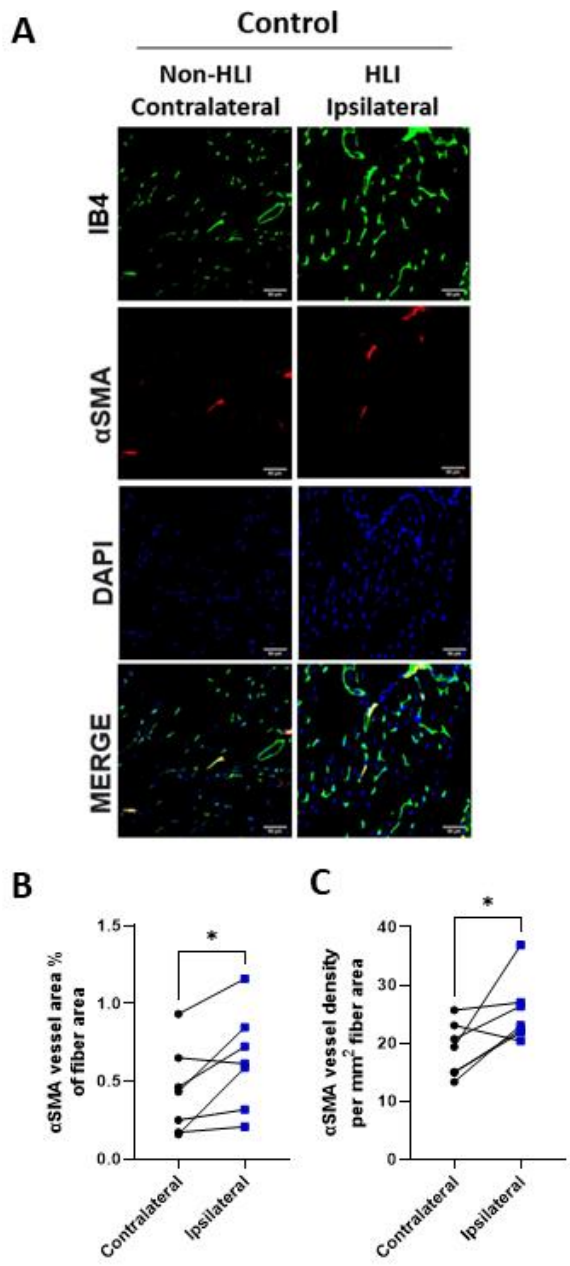

Figure 6.7 Control mice have an increased arteriolar area and density in response to HLI. *Control mice underwent HLI surgery and after 21 days both contralateral and ipsilateral gastrocnemius muscle was fixed, sectioned and stained with α-smooth muscle actin (αSMA) to quantify arterioles.* ***(A)*** *Representative images from contralateral and ipsilateral sections.* ***(B)*** *Quantification of αSMA arteriole area as a percentage of fiber area.* ***(C)*** *Quantification of αSMA arteriole number per mm^2 fiber area. Data analysed by paired ratio t-test, * = p <0.05. All data presented as mean + SEM. Control N = 7. Scale bar 50µm.*

6.2.7 The increase in αSMA associated vessels in response to ischemia is significantly greater in ZEB1^{iECKO} mice compared to controls

To then determine whether knocking out endothelial ZEB1 influences the response to hind limb ischaemia within the context of αSMA associated vessels, the contralateral and ipsilateral gastrocnemius muscle from both control and ZEB1^{iECKO} mice were sectioned and stained for αSMA (Figure 6.8). Firstly, the number of αSMA associated vessels per fibre area was determined in both control and ZEB1^{iECKO} mice in both the contralateral and ipsilateral limb (Figure 6.8 B). A two-way ANOVA was performed to analyse the effect of genotype and ischaemic surgery on the αSMA vessel density, which revealed there was not a significant interaction affect. Simple main effects analysis did however reveal that ischaemia had a stastically significant effect on αSMA vessels per fibre area ($P < 0.05$). Simple main effects analysis of the role in genotype in αSMA vessels per fibre area did not reveal statistical significance. Using Tukey's multiple comparison analysis, it was revealed that there is a significant increase within the αSMA^{+} vessels per fibre area within the ZEB1^{iECKO} ipsilateral muscle (24.05 ± 3.49 per mm^2), compared to the ZEB1^{iECKO} contralateral (11.67 ± 3.49 per mm^2, $P < 0.05$).

To assess this and display the data to show the response to ischaemia, the αSMA per mm^2 fibre value for the individual ipsilateral muscle was divided by the corresponding contralateral value. This displayed the data whereby anything above 0 indicates an increase in IB_4 vessel density, whereas anything below 0 indicates a decrease in IB_4 vessel density. This was performed for both the control group and the ZEB1^{iECKO} group (Figure 6.8 C). An unpaired t-test revealed a significant increase within the ZEB1^{iECKO} group (1.153 ± 0.281) in comparison to the control group (0.397 ± 0.136, $P < 0.05$). Although both numbers are positive within both groups indicating an increase in αSMA vessel density, the mean value for ZEB1^{iECKO} was significantly higher, indicated a greater increase from the contralateral baseline.

Secondly, the αSMA area was also quantified to assess how the control and ZEB1^{iECKO} groups response to ischemia. In the case of αSMA vessels, this may account for larger vessels with a greater diameter but also instances of traversing vessels throughout the section. The αSMA area was calculated as a percentage of fibre area (Figure 6.8 D). A two-

way ANOVA was then performed to analyse the effect of genotype and ischaemic surgery on the αSMA area which revealed no significant interaction between the two variables on αSMA area ($P > 0.05$). Simple main effects analysis however did reveal that the effect of ischaemia on αSMA vessel area was close to significance ($P = 0.053$). Tukeys multiple comparison test also determined there were no significant differences between the individual variables within the analysis. As done with previously with the IB_4 capillary density, the data was displayed to show the response to ischaemia whereby the percentage value for the individual ipsilateral muscle was divided by the corresponding contralateral value. This displayed the data whereby anything above 0 indicates an increase in αSMA area, were as anything below 0 indicates a decrease in αSMA area (Figure 6.8 E). An unpaired t-test revealed no significant difference between the control and $ZEB1^{iECKO}$ mice in response to ischaemia when monitoring αSMA area as a percentage of fibre area. Both control and $ZEB1^{iECKO}$ had an average positive value, indicating that both groups ipsilateral muscle displayed an increase in αSMA area compared to contralateral. Although the $ZEB1^{iECKO}$ group had larger ratio values, indicating a greater response, this was not seen to be significant.

Taken together these data indicate that both $ZEB1^{iECKO}$ and control groups responded to ischaemia via an increase in the αSMA vessel density. For the $ZEB1^{iECKO}$ group, this response appears to have been a greater intensity. The area of αSMA appears to have increased in both control and $ZEB1^{iECKO}$ groups in response to ischemia, and there appears to be no difference in the level of response between the two groups. This therefore indicates that loss of endothelial ZEB1 influences the response in αSMA vessel density to ischemia, but not αSMA area.

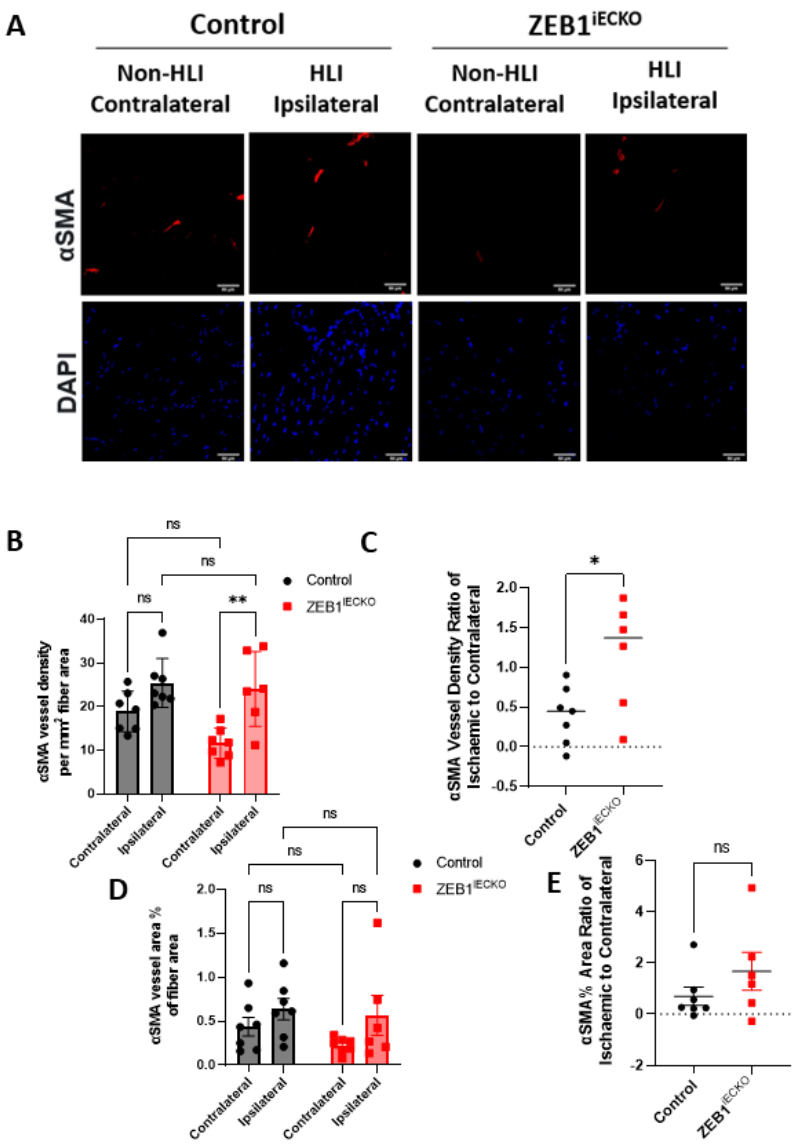

Figure 6.8 ZEB1^{iECKO} mice have a significantly increased ratio of ipsilateral/contralateral αSMA arteriole number per mm^2 compared to control mice. *ZEB1^{iECKO} and control mice underwent HLI surgery and after 21 days both contralateral and ipsilateral gastrocnemius muscle was fixed, sectioned and stained with αSMA to quantify arterioles.* ***(A)*** *Representative images from contralateral and ipsilateral sections.* ***(B)*** *Quantification of αSMA arteriole number per mm^2 fiber area* ***(C)*** *αSMA arteriole number per mm^2 fiber area displayed as ipsilateral/contralateral.* ***(D)*** *Quantification of αSMA arteriole area % of fiber area* ***(E)*** *αSMA arteriole area % of fiber area displayed as ipsilateral/contralateral.* ***(B)*** *and* ***(D)*** *analysed by 2-way ANOVA with multiple comparisons (ns, P > 0.05).* ***(C)*** *and* ***(E)*** *analysed by unpaired t-test, * = p <0.05. All data presented as mean + SEM. Control N = 7, ZEB1^{iECKO} N = 7. Scale bar 50µm.*

6.2.8 ZEB1^{iECKO} mice have decreased αSMA vessel density within the non-ischaemic limb

During the two-way ANOVA analysis, it was noted that ZEB1^{iECKO} mice appear to have an altered response to ischaemia in the context of αSMA vessel density (Figure 6.8 B). This was owing to the ZEB1^{iECKO} exhibiting a larger increase in αSMA vessel number within the ipsilateral limb compared to the contralateral, in comparison to the control group (Figure 6.8 B). This is evident from its statistical significance in Tukeys multiple comparison test, but also in the unpaired t-test observing the rate of change within the ipsilateral compared to the contralateral, compared to the control group. However, the ZEB1^{iECKO} group did not exhibit a higher αSMA vessel density within the ipsilateral limb compared to the ipsilateral limb of the control group. Tukeys multiple comparison analysis showed that this was not statistically different, with the ZEB1^{iECKO} reaching an average of 24.05 ± 3.49 per mm^2 fibre area, and the control an average of 25.42 ± 2.12 per mm^2 fibre area. Therefore, it was not the level at which the αSMA vessel density reached in response to ischemia that appear to be different, but instead it was the baseline of αSMA vessel density within the contralateral limb.

To test this, the αSMA vessel number per mm^2 fibre area for the contralateral muscle for control and ZEB1^{iECKO} mice were plotted against each other and compared using an unpaired t-test (Figure 6.9 B). This revealed that the ZEB1^{iECKO} group had a significantly reduced number of αSMA vessels (11.67 ± 1.30 per mm^2 fibre) compared to the control group (18.99 ± 1.52 per mm^2 fibre, $P < 0.05$). This indicates that loss of endothelial ZEB1 influences the density of αSMA vessel within the muscle, without the presence of ischemia. This provides an alternative baseline compared to the control animals, and therefore this data explains why within the ZEB1^{iECKO} group, when quantifying αSMA vessel density, there is a significant increase in the response to ischaemia, despite the level of αSMA vessel density within the ischemic limb being the same.

To also assess whether there is any difference in the αSMA area within the contralateral limb of control or ZEB1^{iECKO} groups, this was also statistically analysed using an unpaired t-test. Firstly, the αSMA area as a percentage of fibre area was assessed and a non-significant decrease was also observed within the ZEB1^{iECKO} group ($P = 0.0704$, Figure 6.9

C). This therefore indicates that there are changes within the contralateral baseline when knocking out endothelial ZEB1, primarily a decrease in αSMA vessel density, although non-significant changes are also observed within αSMA area also.

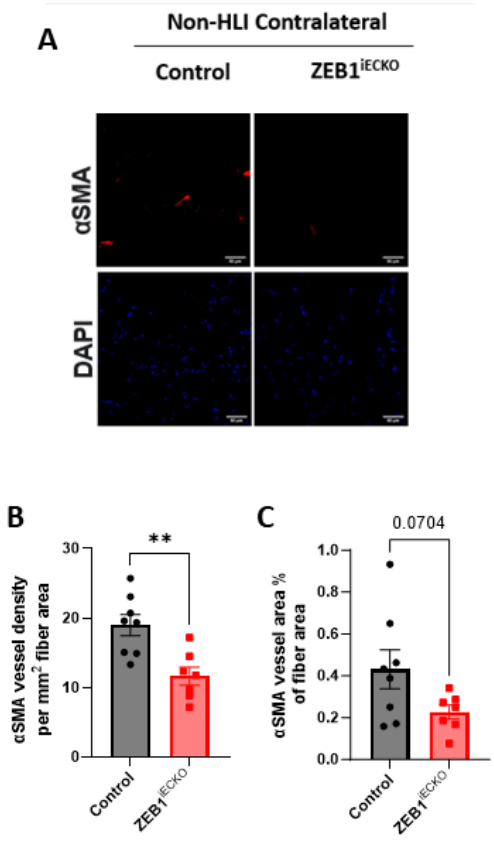

Figure 6.9 ZEB1^{iECKO} mice display decreased αSMA arteriole number per mm^2 within the contralateral, non-ischaemic muscle, compared to control mice. *ZEB1^{iECKO} and control mice underwent HLI surgery and after 21 days the contralateral, non-ischaemic gastrocnemius muscle was fixed, sectioned and stained with αSMA to quantify arterioles.* ***(A)*** *Representative images from contralateral sections.* ***(B)*** *Quantification of αSMA capillary number per mm^2 fiber area.* ***(C)*** *Quantification of αSMA capillary area % of fiber area. Data analysed by unpaired t-test, * = p <0.05. All data presented as mean + SEM. Control N = 7, ZEB1^{iECKO} N = 7. Scale bar 50μm.*

6.2.9 Assessing the level of inflammation by CD45 revealed no significant differences in control or ZEB1iECKO groups in response to ischaemia

The collateral vessel formation and vascular remodelling processes that occur during ischaemia are partly driven by inflammatory stimuli from local and invading leukocytes (Reviewed in Silvestre et al., 2008). From the work achieved in chapter 5 it was clear that ZEB1^{iECKO} affected the level of CD45 associated inflammation within a model of wAMD. This therefore raises the question of how loss of endothelial ZEB1 influences the inflammatory response to HLI surgery. To achieve this, 16µm sections from contralateral and ipsilateral (ischaemic) gastrocnemius muscle were stained for CD45, a leukocyte marker (Barford et al., 1994), to quantify the level of inflammation.

When assessing both capillary density (IB_4) and arteriole density (αSMA), it was revealed that loss of endothelial ZEB1 influenced changes within the non-ischemic contralateral limb. Therefore, the level of CD45 associated inflammation after loss of endothelial ZEB1 was first assessed within the contralateral muscle. Firstly, the number of $CD45^+$ cells per mm^2 fibre was quantified within the contralateral muscle and compared between ZEB1^{iECKO} and control mice (Figure 6.10 B). This determined there was no significant difference between the two groups and was confirmed by an unpaired t-test ($P > 0.05$). Secondly, the CD45 area was quantified as a percentage of the fibre area which also revealed no significant difference between ZEB1^{iECKO} and control muscle ($P > 0.05$, Figure 6.10 C). Together these data indicate that there is no difference in the level of CD45 associated inflammation between the ZEB1^{iECKO} and control groups, within the contralateral, non-ischemic limb.

To then assess whether in the inflammatory response to ischemia varied between the control and the ZEB1^{iECKO} group, both the contralateral and ipsilateral sections from each group were stained for CD45 and quantified. Firstly, the number of $CD45^+$ cells per mm^2 fibre area was quantified (Figure 6.11 B). Two-way ANOVA analysis revealed no significant interaction between genotype and ischemia in the number of $CD45^+$ cells per mm^2. Main effects analysis of genotype or ischemia separately also revealed no significant difference. Tukey's multiple comparison test also revealed no significant changes in any of the variables within the test.

To display the data to show the response to ischaemia, the $CD45^+$ cell per mm^2 value for the individual ipsilateral muscle was divided by the corresponding contralateral value. This displayed the data whereby anything above 0 indicates an increase in $CD45^+$ cell number, whereas anything below 0 indicates a decrease in $CD45^+$ cell number (Figure 6.11 C). This was performed for both the control group and the $ZEB1^{iECKO}$ group and compared. An unpaired t-test revealed no significant difference between the $ZEB1^{iECKO}$ group and the control group.

Finally, the CD45 area was quantified to assess whether there was any variation in response to ischemia varied between the control and the $ZEB1^{iECKO}$ group (Figure 3.16). The CD45 area was initially quantified as a percentage of the fibre area and statistically analysed using a two-way ANOVA (Figure 6.11 D). This revealed no significant interaction between genotype and ischemia. Main effects analysis of genotype or ischemia separately also revealed no significant difference. Tukey's multiple comparison test further revealed no significant changes in any of the variables within the test. The data was displayed as done previously by normalizing the ipsilateral value to the paired contralateral value to display the direction of change in response to surgery (Figure 6.11 E). An unpaired t-test for both the CD45 area % within the fibre and within the field both revealed no significant difference between the control and the $ZEB1^{iECKO}$ group. Taken together this data indicates that loss of endothelial ZEB1 has no significant effect on the inflammatory response to ischaemia when quantifying the number of $CD45^+$ leukocytes as well as the CD45 area within the gastrocnemius muscle.

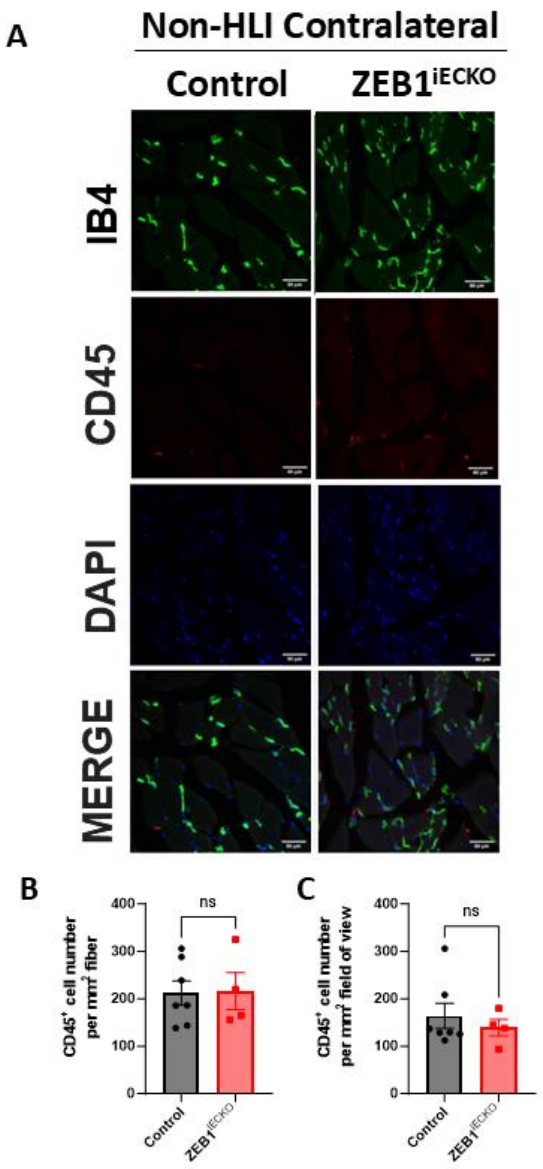

Figure 6.10 ZEB1^{iECKO} mice have no difference in the quantity of CD45 within the contralateral muscle. *ZEB1^{iECKO} and control mice underwent HLI surgery and after 21 days the contralateral, non-ischaemic gastrocnemius muscle was fixed, sectioned and stained with CD45 to quantify leukocytes* ***(A)*** *Representative images from contralateral sections.* ***(B)*** *Quantification of CD45^{+} cell number per mm^{2} fiber area.* ***(C)*** *Quantification of CD45^{+} cell number per mm^{2} field of view. Data analysed by unpaired t-test, (ns, P > 0.05). All data presented as mean + SEM. Control N = 7, ZEB1^{iECKO} N = 4. Scale bar 50µm.*

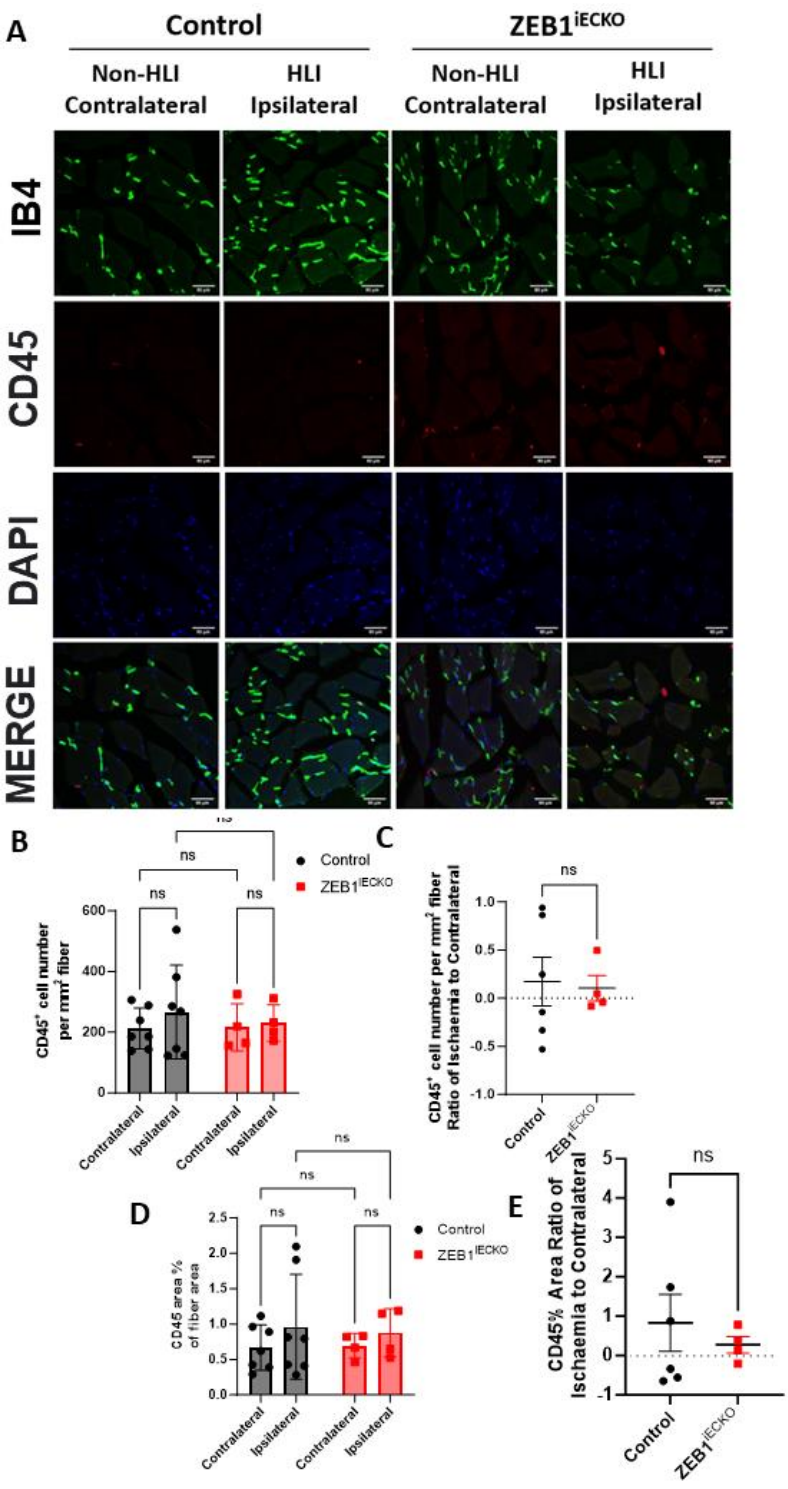

Figure 6.11 No change in CD45⁺ cell number in response to ischaemia was observed in ZEB1^{iECKO} or control mice. *ZEB1^{iECKO} and control mice underwent HLI surgery and after 21 days both contralateral and ipsilateral gastrocnemius muscle was fixed, sectioned and stained with CD45 to quantify leukocytes.* ***(A)*** *Representative images from contralateral and ipsilateral sections.* ***(B)*** *Quantification of CD45⁺ cell number per mm²*

6.3 Discussion

6.3.1 Loss of endothelial ZEB1 did not impact blood flow recovery within this model

Laser speckle imaging data indicate that the loss of endothelial ZEB1 does not affect blood flow recovery following ischemic surgery. The blood flow recovery patterns in both control and ZEB1^{iECKO} mice are similar, with both groups showing a rapid initial recovery, followed by a plateau around day 7. These results suggest that the absence of endothelial ZEB1 does not influence the recovery of blood flow post-HLI.

6.3.2 Loss of endothelial ZEB1 influenced changes to the vasculature within the non-ischaemic contralateral limb

Upon analysing capillary and arteriole density in both the contralateral and ipsilateral limbs of control and ZEB1^{iECKO} mice, it was noted that the contralateral baseline within the ZEB1^{iECKO} group varied form the control. In the IB4 analysis, which identifies capillaries, a significant increase in capillary density was observed in the ZEB1^{iECKO} group compared to controls. This suggests that the loss of endothelial ZEB1 may induce an increase in capillary density in the absence of ischemia. Potential mechanisms for this include endothelial-driven alterations in the local environment, such as the release of pro-angiogenic factors, possibly through modulation of circulating monocytes. Alternatively, the loss of endothelial ZEB1 may disrupt negative feedback mechanisms that prevent endothelial cells from undergoing phenotypic switching without external stimuli. Either scenario indicates that endothelial ZEB1 could play a role in maintaining endothelial quiescence, with its absence leading to angiogenesis in the contralateral limb in the absence of hypoxic stimulation. Furthermore, when assessing arteriolar density by quantifying αSMA-positive vessels in the contralateral limbs, a significant decrease in arteriolar density was noted in the ZEB1^{iECKO} group. These data suggest that the loss of endothelial ZEB1 affects the vascular network structure in the gastrocnemius muscle, with a reduction in αSMA-positive vessels indicating impaired vascular maturity and hierarchy. In support of these histological findings, qualitative Doppler blood flow observation from Figure 6.2 also indicated alterations in perfusion within the contralateral limb of ZEB1^{iECKO} mice. Although

not quantitatively assessed, these changes suggest broader systemic or compensatory vascular effects in response to endothelial ZEB1 deletion.

Arterioles are defined as vessels that distribute blood flow to the capillary plexus within an organ or tissue. The media, or middle layer, of arterioles, comprise of vascular smooth muscle cells (vSMCs) which express αSMA, hence the use of the marker to identify arterioles. Classed as mural cells, vSMCs communicate with ECs within the intima and play an important role in regulating vascular tone, and therefore blood pressure and perfusion (Martinez-Lemus, 2012). Early studies have shown that arteriolar density is reduced in cardiac and skeletal muscle under conditions of hypertension (Kubis et al., 2002; Vitullo et al., 1993). Therefore, the loss of endothelial ZEB1 may influence vasodilation, potentially contributing to the observed reduction in arteriolar density.

Another possible explanation could be that loss of endothelial ZEB1 reduces the abundance of vSMC, which may be a result of altered communication between ECs and vSMCs. This communication between ECs and vSMCs has been extensively studied, and processes vary between direct interactions via adhesion molecules such as N-cadherin, VCAM1 and ICAM1, receptor and soluble ligand interactions, as well as gap junction proteins such as connexins which facilitate the passage of second messengers and electrical signals (Sorokin et al., 2020; Straub et al., 2014). Vascular homeostasis therefore requires appropriate communication between ECs and vSMCs to generate a perfused downstream capillary network, with an appropriate hierarchical vascular tree.

Endothelial cells can recruit and initiate the differentiation of vascular smooth muscle cells via a variety of means. This includes platelet-dervied growth factor, transforming growth factor B and Notch signaling, all of which have been identified as being involved in vSMC recruitment to endothelial cells to generate vessel hierarchy (Gaengel et al., 2009). It has also been demonstrated that recruitment of vSMCs to endothelial cells to generate arterioles can occur because of increased vasodilation, via eNOS, alongside both VEGF-A and Ang-1 (Benest et al., 2008). It may therefore be plausible that loss of endothelial ZEB1 is influencing the generation and stabilisation of vSMCs recruitment.

There has been increasing evidence that ECs have the ability to undergo transdifferntiaton into other cell types, including vSMCs. This process has been heavily linked to endoMT, due to the loss of endothelial phenotype and gain of a more mesenchymal phenotype observed in vSMCs (Coll-Bonfill et al., 2015). Interestingly, very recently Lee *et al* identified the inhibition of endothelial ZEB1 via BMPR1A activation of ID2 as a mechanism to prevent endoMT driven pathogenesis of pulmonary hypertension. The group concluded that without this inhibition of ZEB1 activity within ECs, the expression of endoMT genes, including TGFBR2, promoted the transdifferentiation of ECs to αSMA expressing vSMCs (Lee et al., 2023). This therefore may provide an explanation as to why loss of endothelial ZEB1 is resulting in a loss of αSMA. However, it must be noted that this was within a pathological context of pulmonary hypertension and the vast majority of research into transdifferentiation of ECs to vSMCs via endoMT has been observed within pathological settings such as pulmonary hypertension (Zhu et al., 2006). Therefore, without confirming ZEB1 driven transdifferentation via endoMT as a normal physiological process, it is hard to conclude that this is the reason for a loss of αSMA within the contralateral limb.

6.3.3 Despite no difference in blood flow recovery, ZEB1^{iECKO} and control mice exhibited different vasculature structural responses to ischemia

To quantify the response to ischemia, both capillary and arteriolar densities were assessed in the contralateral and ipsilateral limbs. Initially, control mice were analysed to determine the angiogenic response to ischemia, as indicated by increases in capillary and arteriolar densities. Significant increases in both IB4 (capillary marker) and αSMA (arteriolar marker) were observed in the control group, indicating an angiogenic response.

To investigate the effect of ZEB1 loss on this response, these data were analysed using a two-way ANOVA to identify any differences between the ZEB1^{iECKO} and control groups. Additionally, to evaluate changes in the ipsilateral limb relative to the contralateral limb, data were normalized to the contralateral control leg. A positive value indicated an increase in density in the ipsilateral limb, while a negative value indicated a decrease. These normalized values were then compared between control and ZEB1^{iECKO} mice using an unpaired t-test to assess any significant changes in the angiogenic response.

Blood flow recovery was similar between the control and ZEB1^{iECKO} groups; however, the capillary and arteriolar densities in both the contralateral and ipsilateral limbs exhibited differences in their response to ischemia. Notably, when comparing changes in capillary density in response to ischemia, the ZEB1^{iECKO} group displayed a distinct response compared to the control group. The data showed that while the control group exhibited an increase in capillary density in response to ischemia, the ZEB1^{iECKO} group did not exhibit this response. This was further reflected in the fold change plot (Figure 6.5 C), where the control group showed a mean positive value, indicating an increase, while the ZEB1^{iECKO} group displayed a mean negative value, which was significantly lower than the control group. This indicates that ZEB1^{iECKO} mice did not display the same response to ischaemia as the control mice with regards to capillary density. A key aspect of this finding is that the contralateral limb of the ZEB1^{iECKO} group demonstrated increased capillary density despite the absence of any ischemic stimulus. Consequently, when comparing the ischemic response, either via two-way ANOVA or by normalising to the contralateral limb, an alternative response pattern was observed in the ZEB1^{iECKO} group.

6.3.3.1 ZEB1^{iECKO} mice exhibit increased arteriolar density in response to ischaemia

When comparing changes in arteriolar density in response to ischemia, both the control and ZEB1^{iECKO} groups showed an increase in arteriolar density. Two-way ANOVA analysis revealed a statistically significant main effect of ischemia on arteriolar density, independent of genotype; however, Tukey's multiple comparisons indicated that the increase in arteriolar density within the ipsilateral limb of the ZEB1^{iECKO} group was statistically significant when compared to the contralateral limb. This resulted in a significantly higher fold change in Figure 6.8, suggesting that the ZEB1^{iECKO} group elicited a more pronounced response to ischemia compared to the controls.

It is important to note, however, that these findings may be influenced by changes observed in the contralateral limb of the ZEB1^{iECKO} group. Specifically, the ZEB1^{iECKO} group showed a significant reduction in arteriolar density within the contralateral limb compared to the control group. On the other hand, the arteriolar density within the ipsilateral limbs of both the control and ZEB1^{iECKO} groups were similar (25.4 per mm² fiber for control and 24.0 per mm² fiber for ZEB1^{iECKO}), with no significant differences between them. This

suggests that, despite the reduction in contralateral arteriolar density due to the loss of endothelial ZEB1, the ZEB1^{iECKO} group is still capable of responding to ischemia by achieving a level of arteriolar density comparable to that of the control group. Since the baseline arteriolar density was lower in the ZEB1^{iECKO} group, this increase in arteriolar density represents a significantly greater relative response compared to the control group

Taken together, these data suggest that the loss of endothelial ZEB1 may induce a more plastic state in endothelial cells, thereby disrupting their quiescent state and enabling them to more readily respond to environmental stimuli. This is supported by the observation that ECs in the ZEB1^{iECKO} group exhibit a significant increase in arteriolar density, reaching levels similar to those observed in control animals, despite a lower baseline. The concept of a plastic state may also explain the increased capillary density observed in the contralateral limb of the ZEB1^{iECKO} group, as endothelial cells transition from quiescence to angiogenesis in response to intrinsic changes. Additionally, the loss of vSMCs in the KO model may be attributed to this loss of quiescence, which disrupts mural cell attachment and promotes endothelial cell-driven angiogenesis (Quiescence review in Ricard et al., 2021).

6.3.4 Limitations and considerations for the HLI model of PAD

6.3.4.1 Changes affecting the contralateral limb

The standard within the HLI model of PAD is that the contralateral limb is used as a control or baseline to normalise the findings from the ischemic ipsilateral limb. However, there are some limitations to this and assuming the contralateral limb is normal and unaffected is not completely true. Firstly, although the actual surgery itself is done on the opposite leg, as with all surgeries there will still be a significant increase in systemic inflammation as a result (Bain et al., 2023). This inflammation is essential to allow for wound healing and to prevent post-operative infection. During tissue repair, inflammatory cells such as monocytes and neutrophils induced angiogenesis by the production of pro-angiogenic factors, such as VEGF (Ribatti & Crivellato, 2009). The majority of immune cell infiltration will be occurring at the surgical site; however, it is likely that at least within the initial phases after surgery there is an increase in inflammatory markers within other regions of the mouse, including within the contralateral leg. This systemic inflammation as a result

of surgery may therefore influence the vasculature of the contralateral limb. This could in part provide an explanation as to why alterations within the contralateral limb are observed.

An important consideration is the variation in weight-bearing following the surgery. For a period after the ischemic surgery, the mice were observed to walk on only three legs, likely due to the pain induced by the surgical procedure. This behavior resulted in increased reliance on the contralateral limb, which assumed the weight typically borne by the ischemic limb. It is well-established that physical activity, such as exercise, can stimulate angiogenesis in skeletal muscle to meet the increased oxygen and nutrient demands required for muscle repair following injury. Early studies by August Krogh highlighted the high vascularity of skeletal muscle, attributing it to the tissue's significant oxygen and nutrient requirements (Krogh, 1919). Consequently, the skeletal muscle vasculature is highly adaptable, with angiogenesis and capillary network growth being induced by varying demands, such as exercise (Bloor, 2005; Gorski & De Bock, 2019). This adaptive response may help explain the observed increase in capillary density in the contralateral limb in the current study.

Despite this, the HLI model remains a valuable tool for investigating ischemic responses and collateral vessel formation in PAD and is well-established within the field of vascular biology. In the current chapter, I have identified an increase in capillary density within the contralateral skeletal muscle following the loss of endothelial ZEB1. To confirm that this observation is indeed a result of ZEB1 loss and to exclude potential confounding factors such as inflammation or exercise-induced angiogenesis, a control study would be necessary, wherein endothelial ZEB1 knockout is induced without additional stimuli. Nevertheless, the observed reduction in αSMA-associated vessels presents an intriguing finding that warrants further investigation.

6.3.4.2 Translation to the endothelial dysfunction observed in PAD

A limitation of the HLI model employed in this thesis is its limited translational relevance to PAD as the mice used were young, of normal weight, and non-diabetic. In contrast, PAD patients frequently present with comorbidities such asaging (Hodges et al., 2018), diabetes (Fadini et al., 2019), and hyperlipidemia (Jang et al., 2000), which contribute to

the disease state. The decision to use young, healthy mice was driven by the novel nature of ZEB1 deletion in ECs as it was essential to assess the effects of ZEB1 loss in isolation, without the confounding influence of additional comorbid factors.

As shown in the data presented in this chapter, the blood flow recovery appears to be quick, which is to be expected from mice without these comorbidities (Lotfi et al., 2013). However, this swift recovery may not be fully representative of PAD pathology, where comorbidities typically lead to a reduced rate of blood flow recovery. In these conditions, the response to ischemia may be delayed, and alterations in blood flow recovery can be observed over a prolonged period, unlike the early plateau observed in the wild-type mice used in this study.

Most of these comorbidities with PAD lead to endothelial dysfunction which in-turn results in impaired angiogenesis and collateral vessel formation (Lotfi et al., 2013). Because of this endothelial dysfunction, there is an inefficient response to artery occlusion, leading to a reduction in blood flow and tissue ischaemia. This model provided a good starting point to assess how loss of EC ZEB1 impacts collateral vessel formation in response to ischaemia; however, there is reduced clinical translation to EC dysfunction occurring during clinical PAD.

6.4 Chapter Summary

The work in this chapter aimed to explore how loss of endothelial ZEB1 affected a model of collateral vessel formation after ischaemic injury. This was achieved using the HLI model of PAD. This revealed that loss of endothelial ZEB1 had no impact on blood flow recovery after HLI surgery. However, loss of endothelial ZEB1 did influence alternative vascular remodelling events in both capillaries and arterioles in response to ischaemia. These alternative remodelling events stem from the fact loss of endothelial ZEB1 influenced vascular remodelling in the contralateral limb, without a direct ischaemic stimulus.

Chapter 7:

Discussion, Summary and Supplementary Information

7 Discussion

The endothelium is a heterogeneous tissue that plays a pivotal role in maintaining vascular homeostasis and overall health. The diverse responsibilities for ECs across different organs and tissues are a clear example of the adaptability of the endothelium (Aird, 2007; Becker et al., 2023; Kalucka et al., 2020). During development, it is essential for the endothelium to expand the vascular network through angiogenesis to support tissue growth; however, in adult tissues, the endothelium must remain quiescent and only respond to appropriate homeostatic stimuli, such as during repair or in response to infection. Dysregulation of this quiescent-activated angiogenic switch is a hallmark of several diseases, including wAMD, PAD and cancer (Carmeliet, 2003; Carmeliet & Jain, 2011; Potente et al., 2011). Consequently, understanding the regulation of this phenotypic switch and the disruptions that occur in disease is crucial for advancing our knowledge of vascular health and disease. This thesis aimed to explore how ZEB1, a transcription factor that has well described roles in phenotype regulation and phenotypic transition events in other cell types, yet little is known about its role within ECs, with the limited literature displaying conflicting reports (Fu, et al., 2020; Jin et al., 2020; Lee et al., 2023).

7.1 Loss of endothelial ZEB1 does result in an alternative phenotype but this does not involve EndoMT

There is a growing understanding that angiogenesis is an EndoMT like event, due to the phenotype switching from quiescent phlanax ECs, into a more migratory and active ECs within the angiogenic sprout (Fang et al., 2021; Welch-Reardon et al., 2015). This has been demonstrated with depletion of endothelial Slug, a prominent EMT transcription factor, resulting in reduced angiogenic sprouting (Welch-Reardon et al., 2014). Here I have demonstrated that loss of ZEB1 in developmental angiogenesis resulted in reduced angiogenic front progression and decreased branching, as well as reduced sprouting *in vitro*. This is similar to what is observed by Welch-Reardon et al with EC KO of Slug, which supports the idea that angiogenesis is a partial EndoMT-like event.

Despite this, there is little transcriptomic evidence *in vitro* to suggest loss of ZEB1 is implicating EndoMT. ZEB1 was initially identified when comparing the transcriptomes of

confluent compared to subconfluent HUVECs as a model of quiescent vs proliferating ECs. In this model, endothelial markers went up with confluency, whereas mesenchymal markers were higher in proliferating cells. The analysis of transcription factors known to regulate EMT or EndoMT revealed that, with the exception of ZEB1, all factors with differential expression were reduced under the confluent condition. ZEB1, however, exhibited a significant increase in expression. This prompted the question of how the increase in ZEB1 influences confluent/quiescent ECs and how the loss of ZEB1 affects the transcriptome of HUVECs. ZEB1 KD in HUVECs had no impact on the expression of key EC markers. Only one mesenchymal marker, TAGLN, was differentially expressed, showing an increased expression following ZEB1 KD. This suggests that ZEB1 has no major effect on EndoMT, despite displaying an effect on angiogenesis *in vivo*.

A number of reasons may explain this. Firstly, it may be that loss of ZEB1 can influence EndoMT and the expression of mesenchymal marker genes, but this is not observed within an *in vitro* condition of confluent endothelial cells. It may be that this expression change could only be observed within a model of angiogenesis. Therefore, an ideal follow up experiment would be to determine the transcriptomic differences between control and ZEB1 KO angiogenic ECs. This could be done *in vitro* or *in vivo* by using models of developmental or pathological angiogenesis. Secondly, the idea that angiogenesis is a partial EndoMT-like event is still yet to be fully understood. The angiogenic process itself varies significantly depending on the context of the angiogenic trigger, as well as the tissue the ECs reside within (Becker et al., 2023). Thirdly, it is important to consider that the in vitro culture model used may not accurately replicate the physiological conditions necessary for EndoMT, which typically involves multiple biochemical and mechanical cues present in vivo. Thus, the absence of a mesenchymal gene expression signature in this system does not preclude a role for ZEB1 in EndoMT under more physiologically relevant conditions.

EndoMT is described not only as a potential mechanism in angiogenesis, but also as a process by which endothelial cells transdifferentiate into mesenchymal smooth muscle cells during vascular maturation, a process that is hijacked in pulmonary hypertension (Lee et al., 2023). Interestingly, ZEB1 is identified as a promoter of the EndoMT driven

production of smooth muscle cells within pulmonary hypertension. nhibition of ZEB1 via ID2 prevents this transdifferentiation, thereby reducing the number of smooth muscle cells (Lee et al., 2023). There are similarities in the study by Lee et al to what is observed when EC ZEB1 is knocked out in the HLI study of PAD. ZEB1^{iECKO} mice displayed reduced αSMA within the gastrocnemius of the non-ischemic leg, indicating a loss of smooth muscle cell coated vessels. This could provide an explanation as to why there is a reduction in smooth muscle cell coverage, as lack of ZEB1 results in reduced EndoMT and therefore reduced EC transdifferenation into smooth muscle cells; however, this process is not completely understood, with only limited reports. It could therefore be that this disruption of smooth muscle cell attachment to ECs in ZEB1^{iECKO} mice is actually a result of a disruption of signaling between these individual cell types, and not this transdifferentiation process.

What was noticed within the ChIP-Seq data in chapter 3 was that ZEB1 was bound to the promoters of multiple epithelial marker genes such as EPCAM, and ESRP2 (epithelial splicing regulatory proteins) and that loss of ZEB1 induced the expression of these genes, indicating ZEB1 is inhibiting their expression. This is also observed in the literature on EMT, where ZEB1 is identified as a repressor of epithelial genes and a promoter of mesenchymal genes (Horiguchi et al., 2012b; Vannier et al., 2013)(Krebs et al., 2017). Notably, this is the first time ZEB1 has been shown to regulate these genes within an endothelial cell context. Although the ChIP-Seq identified this phenomenon within this thesis, the direct effects of the expression of these markers have yet to have been explored. What is plausible to suggest is that within an endothelial context, ZEB1 is preventing the expression of epithelial genes, and hence although ZEB1 had no direct impact on endothelial genes expression as seen by the RNA-Seq, it is having an indirect impact on the endothelial phenotype by suppressing other phenotypic genes. There is little information within the literature surrounding how expression of epithelial markers affects the endothelial cell, hence follow up research would be to identify how an increase in epithelial genes directly influences quiescence and angiogenesis.

7.2 Inefficient developmental and sprouting angiogenesis observed with loss of endothelial ZEB1 could be explained by insights gained within the RNA-Seq data

In chapter 4 I demonstrated that loss of ZEB1 impacted developmental angiogenesis by reducing the vascular front extension and by reduced branching. Reduced endothelial sprouting was also observed within the angiogenic sprouting assay in chapter 3. These data therefore implicate ZEB1 in the regulation of angiogenic sprouting. This phenomenon could be explained by the insights gained from the RNA-Seq analysis from ZEB1 KD in HUVECs.

Firstly, the ZEB1 KD condition was enriched for genes regulating cell adhesion and extracellular structure organisation. When analysing the GO terms for biological processes in the list of upregulated genes in response to ZEB1 KD, this further demonstrated the focus on cell-cell adhesion, as well as regulation of cell migration. During sprouting angiogenesis, ECs are required to break away from their quiescent monolayer, break down the extracellular matrix and migrate (Eelen et al., 2020). The generation of a stable vasculature also requires the upregulation of adhesion molecules and extracellular matrix components which activate downstream signaling pathways, along with the downregulation of genes involved in migration in order to regain quiescence (Ramjaun & Hodivala-Dilke, 2009). The fact that ZEB1 KD has been identified as impacting the expression of genes known to play a role in these processes could therefore explain why reduced branching and angiogenic progression is observed. For example, an increase in genes involved in extracellular matrix ogranisaion may prevent the efficient breakdown on the ECM, thereby affecting EC sprouting. Likewise, an increase in the expression of genes known to be involved in ECM binding may prevent ECs from breaking away from the basement membrane and beginning angiogenic sprouting.

Secondly, numerous pathways were identified that impact the interaction of ECs with neighbouring cells, either by cell-cell interactions or local signaling. The interaction between ECs and their local environment is of importance; substantial interactions between growing astrocytes and the developing vascular plexus within retinal development have been identified to be essential (Duan & Fong, 2019; Fruttiger, 2007).

Similarly to murine retinal vascular development, astrocytes emerge from the retinal nerve postnatally; however, in the developmental sequence, astrocytes first appear and begin migrating towards the peripheral retina, with blood vessels subsequently following their path (Tao & Zhang, 2014). These astrocytes, along with their chemoattractant gradient of pro-angiogenic factors, also provide a structural template that the developing vascular network utilises during retinal angiogenesis (Fruttiger, 2007). This is supported by numerous reports, including those that highlight the link between PDGF (Fruttiger & Calver, 1996), and HIF signaling in astrocytes and vascular development (Duan et al., 2014). A complete loss of astrocytes also resulted in failure of the vascular plexus to develop (Tao & Zhang, 2016); this could be due to a lack of pro-angiogenic factors released by the astrocytes, an absence of their physical presence, or a combination of both. The study by Tao and Zhang also highlighted how proteoglycans provide structural guidance for basement membrane assembly during angiogenesis, hence adding to this notion. Finally, a study which disrupted astrocyte guidance is disrupted, resulting in an inability for the astrocyte colonisation of retina, also lead to the disruption of angiogenesis and vessel patterning, further highlighting the importance of endothelial cell and astrocyte interactions in the development of this vascular bed (O'Sullivan et al., 2017).

This phenomenon could also provide a possible explanation as to why disruption in angiogenesis and vascular patterning is observed when endothelial ZEB1 is knocked out. The RNA-Seq GO term analysis identified changes in interactions with the ECM, along with changes in cell-cell adhesion interactions. These processes could encompass physical interactions between ECs and astrocytes, which hence may be altered within ZEB1^{iECKO} mice and might explain the findings observed in development *in vivo*.

The ORA identified an enrichment in genes involved in inflammatory responses and pathways within the downregulated genes. This included type 1 interferon pathway, as well as chemokine and cytokine mediated pathways. It is already well understood that chemokine and cytokine signaling is involved in leukocyte recruitment, but they also have been demonstrated to have roles in angiogenesis (Mehrad et al., 2007). CXCR2 expression and signaling has been identified as being essential for the chemotaxis of ECs towards the pro-angiogenic stimulus (Addison et al., 2000). CXCR4 has also been demonstrated as a

key driver of tip cell morphology required for angiogenic sprouting (Strasser et al., 2010). Whereas CXCR3 has been described as an angiogenic inhibitor due to its promotion of an angiostastic phenotype and its negative regulation of cell cycle progression within ECs (Romagnani et al., 2001). It therefore is plausible that loss of ZEB1 is impacting the expression of genes within these pathways and hence influencing the disruption of developmental angiogenesis observed within the neonatal mouse retina. Not only this, the roles of leukocytes in angiogenesis have been well studied, hence loss of ZEB1 may be impacting the recruitment of leukocytes via these pathways. For example, macrophages are known to play facilitatory roles in anastomosis (Fantin et al., 2010), which could explain why there are reduced branch points within ZEB1^{iECKO} neonatal retina, due to reduced macrophage recruitment leading to reduced anastomosis. In addition, work within chapter 5 identified differences in the leukocyte infiltration in response to loss of ZEB1 in the laser-CNV model, which also supports this idea of reduced leukocyte interactions as a result of loss of EC ZEB1. With leukocytes also identified as being able to aid vascular remodeling and pruning (Hughes & Chan-Ling, 2000; Ishida et al., 2003), this may also demonstrate how reduced expression of genes involved in regulating inflammatory pathways and immune cell recruitment affects the development of a vascular network.

7.3 Developmental and pathological angiogenesis are physiologically different; loss of endothelial ZEB1 affects these processes differently

In chapter 4, I demonstrated that loss of ZEB1 reduced angiogenic front progression within the developing retina, a model of physiological angiogenesis in development. However, in chapter 5, ZEB1^{iECKO} mice undergoing laser induced CNV had larger angiogenic lesions, suggesting that loss of endothelial ZEB1 accelerated pathological angiogenesis. Although this may appear to be contrasting evidence for the role of ZEB1, it needs to be highlighted that developmental and pathological angiogenesis are quite distinct processes and this could therefore explain why loss of ZEB1 impacts them both differently.

Developmental and pathological angiogenesis are two distinct processes involving the formation of neo vessels, but each with unique characteristics and underlying mechanisms. In pathological angiogenesis, aberrant endothelial behavior occurs in which

a loss of vascular homeostasis and quiescence results in chaotic angiogenic sprouting, leading to the generation of abnormal vascular structures and networks, which are often defective and leaky (Dudley & Griffioen, 2023). Dysfunctional activation of signaling pathways and unregulated expression of pro-angiogenic factors such as VEGF and FGF are part of the molecular mechanisms that drive this angiogenesis, along with a loss of stabilisation signaling and quiescence associated signaling (Carmeliet & Jain, 2011; Potente et al., 2011). An interesting study published by Seaman et al compared the transcriptomes ECs within the liver in three separate states: resting state in which ECs are generally quiescent, regenerative state in which ECs are actively performing angiogenesis as the liver regenerates, and the tumour baring liver which was undergoing pathological angiogenesis. This study identified various genes which were enriched within these population groups, such as PTPRN, apelin and CD109, which were enriched in the tumour ECs undergoing pathological angiogenesis and not the ECs undergoing physiological angiogenesis (Seaman et al., 2007). This therefore indicates that ECs have different transcriptomes, depending on the context of their angiogenesis.

There have been reports of context dependent roles of proteins, such as that described for ZEB1 in this thesis. For example, Tie/Ang signaling has been regularly demonstrated as having different roles and impacts on the vasculature, depending on the vascular bed and the context (Eklund & Olsen, 2006). Loss of either Tie2, or its ligand Ang2, results in severe impacts in developmental angiogenesis observed within the retina, including venous specification (Chu et al., 2016; Hackett et al., 2002). However, it has also been demonstrated that the over expression of Ang2 was demonstrated to disrupt developmental angiogenesis *in vivo*, suggesting the balance between these factors are particularly important to their context dependent roles (Maisonpierre et al., 1997). Tie2 has also been described as the master regulator of endothelial quiescence by promoting EC survival and enhancing vascular stability, indicating that it not only has a role in promoting angiogenesis during vascular development, but also a pro-quiescent role (Augustin et al., 2009). This understanding of Tie2 within quiescence has been the premise of research into vascular normalisation within the treatment of cancers, in an attempt to increase chemotherapy delivery once the tumour vasculature has achieved a level of normalisation (Park et al., 2016). However, high levels of Ang2 have also been associated

with vascular leakiness within inflammatory conditions such as sepsis in humans, providing another contextually role for this signaling (Parikh et al., 2006).

The heterogeneity of the vasculature is likely to be the cause of these context depending roles. The significant variation in EC phenotype and behavior, both across and within tissues, occurs due to variations in gene expression, which ultimately can lead to signaling pathway variation and differential modulation of protein behavior (Aird, 2007; Becker et al., 2023; Kalucka et al., 2020). It is therefore quite plausible that ZEB1 is playing context dependent roles within the endothelium. This theory is especially probable if the activation of different ZEB1 binding partners is implemented within specific physiological or pathological contexts, as it is already well known that these binding partners regulate its transcriptional regulation activity (Postigo et al., 2003; Postigo & Dean, 1999). It would therefore be interesting to identify if this is the case within the different contexts observed in this thesis, which could be achieved by experiments which aim to prevent this regulation. Examples of these experiments include specific knockout of ZEB1 binding partners (CtBP, Smads etc), or by mutation of the ZEB1 structure to prevent certain proteins from binding and hence modulating ZEB1s activity specifically. This would be an ideal next step to identify how ZEB1 can have alternative roles in different biological contexts.

In chapter 5, ZEEB1^{iECKO} in male mice resulted in increased lesion leakage suggesting changes in endothelial barrier integrity. Several of the DEGs in ZEB1 KD HUVECs are involved in EC barrier regulation, structure and function. These include ICAM-1, VCAM-1 and SELE (Chistiakov et al., 2015; Claesson-Welsh et al., 2021; C. Lawson & Wolf, 2009), which could explain why this leakage is observed in mice deficient in EC ZEB1. Interestingly, sex differences were observed in chapter 5, where female ZEB1^{iECKO} mice did not have the same increase in vascular leakage as male ZEB1^{iECKO} mice. The list of DEGs in ZEB1 KD HUVECs was assessed for sex specific genes and although none of these genes are exclusively sex-specific, several exhibit sex-biased expression patterns or are influenced by sex hormones, thereby contributing to observed differences in immune responses between males and females. For example, genes such as OAS1, MX1, IFIT1, and IFIT3 (which were found to be differentially expressed in ZEB1 KD HUVECs) are classified

as interferon-stimulated genes and play pivotal roles in the innate immune response, particularly in antiviral defense (Schoggins, 2025). Notably, studies have demonstrated that these genes exhibit sex-biased expression in various species. For instance, in pigs, OAS1 and CXCL10 were found to be significantly upregulated in females compared to males in subcutaneous adipose tissue, suggesting a sex-specific role in inflammation and immune responses (Wang et al., 2022). This could begin to explain the sex difference observed in chapter 5.

7.4 The level of ZEB1 knockout and reduced expression may impact the phenotype of ZEB1 deficient ECs

Within chapter 5 of this thesis, the level of ZEB1 expression within EC of ZEB1^{iECKO} mice was determined to be around 50%. Although this reduction was significant and robust, the expression of ZEB1 was still apparent, which would therefore have an impact on ECs behavior. The transcriptome is sensitive to changes in transcription factor levels, which in turn impacts the phenotype and physiology of an organism. This is observed within human disease, with diseases that arise because of haploinsufficiency, being strongly associated with mutations of transcription factors, suggesting that even a 50% loss is sufficient to result in disease (Seidman & Seidman, 2002). Therefore, a 50% reduction in ECs should be significant enough to observe a phenotypic response, if that gene is playing a role within that cell type; however, it must be noted that there is often significant redundancy between transcription factors, and hence some transcription factor knockout studies display no or little phenotype (Wu & Lai, 2015). It may therefore be plausible that ZEB1 is acting within transcription factor families to induce its biological function, hence why loss of EC ZEB1 is not having a major impact on angiogenic development or the progression of disease.

In a recent study, Naqvi et al were able to demonstrate how varying levels of the SOX9 transcription factor affected craniofacial shape variation in development. In this study, the team showed that specific response elements within the genome are sensitive to the levels of their associated transcription factor, which can in turn affect gene expression and developmental outcome (Naqvi et al., 2023). This work reveals key insights into how changes in transcription factor abundance can impact gene regulation. This phenomenon,

along with the fact that I have demonstrated effects as a result of a 50% reduction in ZEB1 levels *in vivo*, provides evidence that ZEB1 plays a significant role in ECs.

A limitation of the developmental angiogenesis work in this thesis performed *in vivo* on ZEB1^{iECKO} neonates is that the exact level of ZEB1 expression has not been confirmed. Although the reduction in ZEB1 expression within the adult dosed mice was confirmed in chapter 5, the exact level was not determined in neonates owing to difficulties in extracting sufficient ECs and subsequent mRNA from neonate mouse lungs via MACS. Because they undergo a different dosing regime, it may be plausible that the level of ZEB1 expression may vary between neonates and adults. Given what Naqvi et al demonstrates with SOX9, it could therefore be possible that the alternative roles for ZEB1 in development and disease presented within this thesis, could be a result of differing levels of ZEB1 knockout. Therefore, the next step within this research would be to identify if there is any difference in the level of ZEB1 expression in both adult ZEB1^{iECKO} mice and neonate ZEB1^{iECKO} mice. Given the high level of heterogeneity within ECs (Becker et al., 2023; Kalucka et al., 2020), it is therefore even more important to take this into account, as varying levels of ZEB1 may influence different vascular beds in different developmental and pathological processes.

In addition, it would also be interesting to observe whether the expression of ZEB1 varies depending on the context and tissue type. With the advances in single cell RNA-sequencing and the availability of published single cell data, insights could be gained into this without the need for multiple *in vivo* studies to be set up. Taken together, these extra proposed experiments and analysis may therefore be a possible route to follow in order to fully elucidate the role of ZEB1 within EC heterogeneity, as differing levels of ZEB1 expression between vascular beds may be having alternative effects.

7.5 Published research on endothelial ZEB1 may be conflicting

At the outset of this research, there was limited published information on the role of endothelial ZEB1. To our knowledge, no studies focused on ZEB1 as a primary factor influencing endothelial cell-specific behavior; however, in early 2020, Fu et al published work that highlighted endothelial ZEB1's involvement in tumour angiogenesis. Their research demonstrated that inactivation of endothelial ZEB1 via the ZEB1^{iECKO} model led to

reduced tumour angiogenesis and normalization of tumour-associated vasculature, thereby improving the delivery of chemotherapy agents to the tumor (Fu et al., 2020).

In the supplementary data of this research paper by Fu et al, the team described how they determined that developmental angiogenesis was unaffected by ZEB1 EC KO (Fu et al., 2020). Within this study, the same neonatal angiogenesis model was used but with some notable differences in experimental design. First, their neonates received only two doses of tamoxifen, on post-natal days 3 and 6, whereas in this study, tamoxifen was administered on post-natal days 1, 2, and 3. The delay in tamoxifen administration in Fu et al.'s study likely affected the timing of transgene inactivation, as the transgene would remain at normal levels until the first dose (on post-natal day 3). In contrast, in this study, the final tamoxifen dose was given on post-natal day 3, at which point significant vascular outgrowth had already occurred. Inducing ZEB1 KO at this stage may reduce ZEB1 expression in vasculature that has already undergone a certain level of development. Additionally, the multiple doses administered in this study ensured that Cre-mediated recombination was sufficient to achieve significant reduction of ZEB1 expression by post-natal day 3, whereas Fu et al.'s second dose was not given until post-natal day 6, potentially delaying the maximal effect of ZEB1 KO.

Another important difference between the studies is the timing of sacrifice. In this thesis, animals were sacrificed at post-natal day 5, whereas Fu et al. sacrificed their animals at post-natal day 7. This difference has a substantial impact on plexus development, particularly vascular extension, which would be near completion at post-natal day 7. Furthermore, the $ZEB1^{fl/fl}$ mice used within this chapter and this thesis were gifted from Thomas Brabletz (S. Brabletz et al., 2017), whereas Fu et al developed their own $ZEB1^{fl/fl}$ in-house, which may result in some experimental variation.

In addition, assessed only vascular extension as a measure of developmental angiogenesis. Although vascular extension is a common metric, it is not the only relevant parameter. Other key aspects, such as tip cell number, branching, segment length, segment density, and area, were not measured or reported in their study. This limited analysis may have overlooked important information regarding endothelial ZEB1's role. Furthermore, their method of vascular extension also varied from that used in chapter 4. Instead of working

out the percentage of vascular extension by normalising to the entire retina length (Fantin, 2022), Fu et al displayed the raw measurement of vascular front length only. The lack of comprehensive analysis, combined with variation in study timelines, may explain why Fu et al did not observe any changes in developmental angiogenesis, which is conflicting to the results displayed in chapter 4.

7.6 ZEB1 is transcriptionally linked with the inflammatory response *in vitro*, with sex-specific inflammatory differences observed *in vivo*

The emergence of inflammatory themes throughout this thesis was unexpected prior to initiating the research. This link with ZEB1 and inflammation was initially identified via RNA-Seq analysis of the transcriptome of ZEB1 KD HUVECs, which revealed enrichment of genes involved in regulation the inflammatory response. Notably, the enrichment of inflammatory genes was profound within the genes that were downregulated, which could suggest that loss of ZEB1 reduces the response to inflammation by downregulating these genes. Over representation analysis of the RNA-Seq data in ZEB1 KD had a distinct enrichment in genes involved in type 1 interferon signaling, but also response to cytokine stimulation and chemokine stimulation. An altered inflammatory response was also observed *in vivo* within the laser induced CNV study in chapter 5, where male and female $ZEB1^{iECKO}$ mice exhibited different CD45-associated inflammatory responses. This effect observed within the laser-CNV could be at least partially explained by the RNA-Seq results in chapter 3, which do suggest a reduction in genes involved in pro-inflammatory pathways. This ponders the question of exactly how loss of ZEB1 impacts the response to inflammatory stimuli and why this is a sex-specific response.

7.7 Possible future research directions

7.7.1 Overexpression studies

Exploring the effects of ZEB1 overexpression would be an ideal next step in this research, as it would provide valuable insights into the reverse of ZEB1 loss and help clarify its functional role in the regulation of the endothelial transcriptome and behavior, as well as angiogenic processes. Overexpressing ZEB1 in HUVECs could be achieved through the use of plasmid-based expression systems or viral vectors, allowing for controlled

overexpression *in vitro*. Performing RNA-Seq on these ZEB1 over expressing cells would provide an ideal overview of how increased ZEB1 expression impacts ECs an would navigate the direction of further experiments. The exploration of how ZEB1 over-expression influences developmental and pathological models of angiogenesis in vivo could also prove to be insightful. Generating an endothelial specific over expression transgenic mouse model, as done previously (Mould et al., 2005), would therefore be a pivotal next step in this research.

7.7.2 Work to explore if loss of ZEB1 impacts EC proliferation

7.7.2.1 Investigating the role of ZEB1 in subconfluent HUVECs

Since ZEB1 was identified as being upregulated within confluent HUVECs, the work in chapter 3 focused on understanding the role of ZEB1 within this condition. Although its expression was reduced in subconfluent HUVECs, ZEB1 expression is still observed. The subconfluent condition exists within a different state to confluent ECs, with room for proliferation and migration. It would therefore be of interest to understand the different roles of ZEB1 within confluent and subconfluent endothelial cells. This could be performed by knocking down ZEB1 using siRNA in subconfluent endothelial cells and comparing the differentially expressed genes to that of the confluent. It would be particurly interesting to observe the levels of EndoMT markers within the subconfluent HUVECs once ZEB1 has been knocked out. The subconfluent condition expressed higher levels of mesenchymal markers and lower levels of endothelial markers, indicating a certain level of EndoMT, therefore observing how loss of ZEB1 affects this would be interesting. The ChIP-Seq analysis could also be performed on subconfluent endothelial cells, to observe any differences ZEB1 in genomic binding that occur with confluency. The crossover between ChIP-Seq and RNA-Seq data sets could then also be performed to find genes directly regulated within the subconfluent condition, which could then be compared to the confluent to identify any differences.

7.7.2.2 Investigating proliferation and metabolism

Another future experiment which would be important to perform would be an accurate proliferation assay, such as EdU assay. The MTT ((3-(4,5-dimethylthiazol-2-yl)-2,5-diphenyl-2H-tetrazolium bromide) assay performed in chapter 3 gave a good indication of

cell viability; however, it does not provide a completely accurate view of proliferation. MTT assays work by assessing cell viability by measuring the metabolic activity via the level of NADPH-dependant oxidoreductase enzymes. These mitochondrial reductases are able to convert the yellow coloured MTT reagent to a purple-coloured Formazan product with an absorbance that can be measured using a spectrophotometer at 570nm. Higher levels of metabolic activity produce higher levels of absorbance, hence equating to viability (Ghasemi et al., 2021). An Edu assay is an example of an appropriate alternative method as this assay monitors proliferation via the quantification of newly synthesised DNA. The proliferation rate of the conditions is therefore determined by the level of new DNA synthesised, which is required for cells to proliferate (Flomerfelt & Gress, 2015). Seeding sparse levels of ZEB1 KO or KD HUVECs and monitoring the proliferation via EdU incorporation would therefore be an important next step within this research. And to add to this, in order to understand whether there are any metabolic differences between ZEB1 KO/KD cells and control cells, a Seahorse assay could be performed, which provides a more thorough exploration of the metabolic state of the cell (Gu et al., 2021).

7.7.2.3 In vivo to explore proliferation

ERG analysis revealed a reduced EC number at the angiogenic front in ZEB1^{iECKO} mice, suggesting that the observed reduction in branching may be due to decreased EC proliferation resulting from ZEB1 KO. However, the decrease in vascular density, caused by reduced vessel segment lengths, could also explain the lower number of ECs, as there are simply fewer vessels to accommodate them. Further investigation using an in vivo proliferation-based measurement, such as 5-bromo-2'-deoxyuridine (BrdU) incorporation (like that used in the study of FOXO1 by Wilhelm et al), would determine whether proliferation is the cause of the observed structural changes.

Further investigation into the effects of ZEB1^{iECKO} on EC proliferation and cell cycle regulation would represent an important next step in this research. Such studies could elucidate whether ZEB1 modulates EC proliferation and potentially identify the mechanisms responsible for the observed reduction in branching within both the angiogenic and central regions of the developing plexus. It is well established that the differential responses of ECs to pro-mitotic and pro-angiogenic signals, such as VEGF are

mediated by concentration gradients within the vascular plexus; with ECs at the leading edge, exposed to the highest VEGF concentrations undergo tip cell selection, while surrounding cells remain proliferative (Gerhardt et al., 2003). These distinct cellular responses to VEGF are regulated by Notch-DLL4 signaling (Hellström et al., 2007). Notably, Pontes-Quero et al. demonstrated that loss of DLL4/Notch using an EC Rbpj^{iECKO} model results in cell cycle arrest at the angiogenic front, where stalk cells, which are typically proliferative, adopt a tip cell-like phenotype and cease to proliferate. Conversely, in the central plexus, where Notch signaling normally maintains endothelial cell quiescence, DLL4/Notch loss induces cell cycle re-entry and proliferation (Pontes-Quero et al., 2019). Similarly, to ZEB1^{iECKO}, loss of DLL4/Notch signaling leads to a reduction in EC number at the angiogenic front; however, the structure of the plexus in the case of Rbpj^{iECKO} is qualitatively completely different to that of ZEB1^{iECKO}. It is therefore unlikely that changes observed in ZEB1^{iECKO} are simply in response to changes in VEGF stimulation or Notch signaling. Although a reduction in EC number at the angiogenic front was also observed in ZEB1^{iECKO}, the structural alterations in the plexus are qualitatively distinct from those seen in Rbpj^{iECKO}. Furthermore, investigating the impact of ZEB1^{iECKO} on EC cell cycle progression and proliferation in the angiogenic retina would be an important next step in advancing this research.

7.7.3 Studies to explore if ZEB1 impacts EndoMT *in vitro* and *in vivo*

Many research groups have reported being able to stimulate EndoMT within ECs in culture. These often include the addition of TGFβ (sometimes specifically TGFβ1), along with another stimulus such as AngII (Krishnamoorthi et al., 2022) or an inflammatory stimulus such as TNF-α or IFN-γ (Haynes et al., 2019). It would therefore be an interesting next step to see how ZEB1 KD affects this stimulated EndoMT. There is also the argument that observing EndoMT within an *in vitro* cell culture model is a highly manipulated situation and therefore not representative of EndoMT within physiology. EndoMT has been observed and measured *in vivo* using a number of models, such as lineage tracing experiments which demonstrate that mesenchymal cell types, such as fibroblasts and smooth muscle cells, have derived from endothelial cells (Lee et al., 2023; Zeisberg et al., 2007). This is ideal future work to determine whether ZEB1 influences EndoMT.

7.7.4 Further studies to determine if loss of EC ZEB1 impacts vessel normalisation

7.7.4.1 Exploration of vessel pruning and regression

In chapter 4, the structural changes that were observed in the vascular front were determined to be consistent within the central plexus; however, it is important to consider the differences in the physiological processes occurring within these regions at this developmental stage. In the central plexus during retinal vascular development, the vasculature undergoes vessel pruning and remodeling to establish a hierarchical capillary network (Adams & Alitalo, 2007). During this phase, the balance between pro- and anti-angiogenic factors and signaling pathways tightly regulates vessel regression and removal (Korn et al., 2014; Scott et al., 2010). This pruning is also influenced by oxygen-sensing prolyl hydroxylase domain (PHD) proteins, which are expressed by astrocytes in the retina. For example, PHD2 astrocyte-specific knockout mice, using a GFAP-Cre driver, exhibited an abnormally crowded vascular plexus with poor hierarchy and no vessel pruning. This was attributed to the inability of astrocytes to sense oxygen levels, leading to sustained hypoxic signaling and preventing normal pruning and remodeling (Pugh & Ratcliffe, 2003). The angiogenic response of endothelial cells to pro-angiogenic factors drives the expansion of a nascent vascular network capable of meeting tissue demands. Thus, the ability of endothelial cells to adapt and undergo angiogenesis is a critical aspect of their function.

To further explore this in future work, staining for Collagen IV empty sheets, (sometimes called empty basement membrane sleeves) which are left behind once a vessel has regressed (Hashizume et al., 2010; Mcdonald & Choyke, 2003), will help determine whether there is a significant difference in vessel pruning between ZEB1iECKO and controls. This will in turn help determine whether the alterations in network structure and vessel branching are as a result of inefficient branching at the vascular front continuing to impact the central plexus, or from altered vessel remodeling. It could be possible that these open-ended vessel segments with a node of 2 in the central plexus are angiogenic sprouts, which are normally only observed at the angiogenic front (Fruttiger, 2007). This would also need to be confirmed by staining for a tip cell marker, such as ESM1, as without

this information it is hard to understand what process that vessel is currently undergoing (Rocha et al., 2014).

Many inducible transgenic models also have reporter genes within their systems so that the percentage of recombination can be determined via confocal imaging e.g. the expression of EGFP (Kretzschmar & Watt, 2012). This lineage tracing technique is also particularly useful in determining what happens to these ECs deficient in a specific gene overtime. It would be particularly interesting to apply this to the ZEB1iECKO model used in this thesis as this would help identify what happens to these ECs as a direct consequence of loss of ZEB1.

7.7.4.2 Studies to assess the loss of EC ZEB1 during later phases of retinal vascular plexus development

Neonatal angiogenesis studies, such as those presented in this chapter, exhibit significant variability in experimental design, depending on the research question. Key variables include the timing and dosage of tamoxifen administration and the timing of sacrifice. These factors can profoundly affect study outcomes. Notably, the timing of sacrifice is crucial due to the rapid developmental changes occurring in the first few days of life. For instance, vascular outgrowth is time-dependent: at P3, outgrowth is approximately 20%, increasing to 75% by P7 and reaching the retinal periphery by P10 (Rust et al., 2019). Additionally, vascular parameters such as segment length and branch point number also vary with developmental timing. Therefore, the timing of sacrifice and retinal dissection can significantly influence results. The timing of KO induction is another critical factor. Delaying KO induction allows normal vascular development before the intervention, which can alter experimental comparisons. This must be considered when comparing findings from this thesis to existing literature.

To study EC ZEB1 loss in angiogenesis, we adopted a schedule similar to the EC FOXO1 study (Wilhelm et al., 2016). Animals were sacrificed on post-natal day 5 to capture early developmental changes, providing a clear view of the angiogenic front as it progressed across the retina. Tamoxifen administration was administered on P1, P2, and P3 to induce the KO early, ensuring sufficient recombination for potential downstream effects. While this timeline provided valuable insights into early EC ZEB1 function, later stages of

angiogenesis were not addressed. Around P10, vertical angiogenesis occurs, forming the intermediate and deep vascular plexus layers (Fruttiger, 2007; Rust et al., 2019, and demonstrated in Figure 1.1). This phase differs from the earlier stages, especially in terms of tip cells, called D-tip cells, that guide new plexus formation. These cells have a distinct transcriptional signature, including high TGF-β signaling. In fact, loss of Alk5 (TGF- β receptor 1) prevents the formation of these D-tip cells, results in a failure to form the intermediate and deep plexus (Zarkada et al., 2021). Exploring how loss of EC ZEB1 affects this stage of angiogenesis would therefore be an interesting next step. Not only this, ZEB1 has been heavily linked to TGF- β signalling in other cell systems (Joseph et al., 2014), as well as in endothelial cells (Fu et al., 2020).

Conducting a study to assess whether loss of EC ZEB1 affects developmental angiogenesis during later stages would provide valuable insights into whether the effects observed in this thesis extend into later phases of development. Careful attention must be given to factors such as the dosing schedule, tamoxifen quantity, and timing of sacrifice. These variables are critical to ensure sustained ZEB1 knockout through deep plexus formation and to identify any changes in plexus development, as well as the timing of these alterations. While this falls outside the scope of the current thesis, it represents an important next step in this line of research.

7.7.4.3 Determining how ZEB1 EC KO impacts supporting cells within the vascular network

This chapter primarily investigates the impact of EC ZEB1 loss on vascular structure and development, focusing specifically on the endothelial cells; however, the role of supporting cells within the vasculature also warrants consideration, as their involvement may contribute to the observed phenotypic alterations. A more comprehensive understanding of how ZEB1 loss in ECs influences interactions with these supporting cells could provide valuable insights into the underlying mechanisms. One such class of supporting cells are pericytes, which play critical roles in stabilizing the endothelial network. Pericytes are also known to guide angiogenic sprouting, sense pro-angiogenic signals, and participate in vessel pruning (Bergers & Song, 2005). Further underscoring the relevance of investigating pericyte behavior in the context of ZEB1^{iECKO} retinas. Given that loss of EC ZEB1 has resulted in alterations to vascular structure and branching, potentially

through changes in sprouting and/or pruning, it would be valuable to explore whether these effects are mediated by alterations in pericyte recruitment or function. Staining for pericyte markers, such as NG2 (Tual-Chalot et al., 2013), could provide further insights into this potential interaction.

7.7.5 Research directions centered on inflammation

7.7.5.1 Expansion beyond CD45 inflammation

In chapter 3, RNA-Seq analysis identified DEG associated with inflammation and inflammatory signaling. To explore this, analysis of CD45-associated inflammation was performed within the two disease models within this thesis in chapters 5 and 6. CD45 is a good marker of inflammation due to its expression almost all haematopoietic cells (Barford et al., 1994); however, it only provides a blanket description of inflammation. Immune cell activation and inflammation cascades are complex, therefore further information would be needed to determine specifically how the inflammatory processes are varying between the female and male ZEB1^{iECKO} groups.

Several markers can be stained to provide further insights into the inflammatory processes occurring within the CNV lesions in response to ZEB1 knockout. Staining for immune cell adhesion molecules, such as ICAM-1, VCAM-1, P-Selectin, or E-Selectin, would enable comparison of their expression across different groups. Additionally, staining for markers specific to particular immune cell types would help identify the specific cell types involved and the nature of the inflammatory response.

This could also be achieved by completing qPCR for immune cell markers such as Ncf1 for activated neutrophils and CD68 for activated infiltrated macrophages, which have both been previously identified as being upregulated in bulk RNA-Seq of CNV tissue (Brandli et al., 2022). Macrophage polarisation has also been observed within laser induced CNV, with M1 macrophages appearing earlier followed by a sustained M2 macrophage population that developed in later days post lasering (Yang et al., 2016). Peng et al have also shown this by determining the expression of M1 maker CXCL10, and M2 markers CD206 and CCL2, over time and in response to therapeutic agents(Peng et al., 2018). It would therefore be of great interest to determine further information regarding the immune cell profile within the neovascular lesions in the control and ZEB1^{iECKO} groups. This could be

achieved by staining for well-established markers, but to save time optimising, a bulk RNA-Seq approach like that used by Brandi et al would provide a wider variety of information to allow for streamlined analysis.

Given the RNA-Seq results within chapter 3 linking ZEB1 with immune pathway regulation, and the fact in metabolic conditions such as PAD, monocytes have been identified as regulators of cytokine production, including VEGF-A (Lolmède et al., 2011), exploring this further will be an ideal next step in this research. Although this staining provided evidence that the $CD45^{+}$ leukocytes did not vary between the two groups, there are methods in which inflammation could be explored further. The level of pro-inflammatory and pro-angiogenic cytokines between control and $ZEB1^{iECKO}$ could be assessed by qPCR or ELISA; this could be determined systemically using blood, or locally by using tissue extracted from the ischemic limb.

7.7.5.2 Studies to specifically monitor inflammation

I would propose experiments that involve a direct inflammatory stimulus with well described outputs and downstream signaling pathways to explore how loss of ZEB1 affects these. Although some methods within this thesis have a inflammatory associated output ie the laser-CNV with CD45 staining within the lesion and FFA leakage, these are as a consequence of the angiogenesis induced by the laser, which makes it difficult to separate the angiogenic affects from the inflammatory affects. Therefore, a more distinct inflammatory stimulus would provide a greater level of information on inflammation alone, without angiogenesis. An example of this would be induction of systemic inflammation and sepsis via lipopolysaccharide (LPS). This is a commonly used model of inflammation *in vitro* (Zheng et al., 2018), but also *in vivo* (Seemann et al., 2017), and the effect on the endothelium has been well charecterised (Dauphinee & Karsan, 2006). Subjecting $ZEB1^{iECKO}$ and control mice to systemic inflammation via LPS injection would therefore provide information as to how loss of endothelial ZEB1 responds to this type of inflammation. This inflammatory response can be measured by numerous factors, as outlined in Seemann et al, which includes health status measurements such as body temperature, blood pressure and weight, as well as measurements of the inflammation signaling by determining the level of inflammatory cytokines such as TNF-α, IFN-γ, IL-6, IL-

10 and CXCL12, and finally oxidative stress markers as well as Breadykinin and Histamine (Seemann et al., 2017). Recently, a less invasive model of measuring the effect LPS on the vasculature was published. This involves the local application of LPS to the ear of a mouse, followed by photoacoustic microscopy to determine vascular leakage. This may be a more simple and realistic experiment to be performed in future (Li et al., 2022). On top of this, experiments can be performed *in vitro* on HUVECs which could help identify alterations in inflammatory signaling with and without ZEB1. This includes time dependent LPS stimulation assays, as well as immunofluorescence staining experiments to determine EC barrier composition after LPS stimulation (Zheng et al., 2018). It has already been demonstrated that the response to LPS is heterogeneous within the EC population, with differential activated EC phenotypes charectrised depending on their expression of certain inflammatory markers, including E selectin, ICAM-1 and VCAM-1 (Dayang et al., 2019). Both ICAM-1 and VCAM-1 were observed to be downregulated in response to ZEB1 KD in HUVECs via RNA-Seq. Therefore, it would be right to assume that the response to LPS will be different in conditions where ZEB1 is depleted as it may affect the abundance of these different EC subpopulations. Finally, within the context of cancer, ZEB1 has also been demonstrated to regulate gene expression that promotes evasion from the immune system, which provides evidence of ZEB1s regulation of inflammation within another cell context (Lu et al., 2022). But until further experiments which isolate inflammation from other pathological process, ZEB1s role within the inflammation of ECs is not fully elucidated.

7.7.6 Further exploration of how loss of ZEB1 impacts lesion leakage and neovascularisation in laser-CNV

7.7.6.1 Exploring lesion fibrosis

Fibrosis starts to occur within the laser CNV model at later time points within the study; this can be measured by staining for collagens and fibronectins. The level of fibrosis as determined by collagen staining increases with time, with studies reporting the highest level of fibrosis at 35 days post lasering (Peng et al., 2018). There is evidence within the literature that associates macrophage and immune cell activity with fibrosis (Reviewed in Wynn & Vannella, 2016). Therefore, given that female ZEB1^{iECKO} mice exhibit an altered

inflammatory state compared to males, this could potentially influence the extent of fibrosis. This is also pathologically important to study as current anti-VEGF therapies work well at reducing lesion leakage but do not prevent fibrosis. 45.3% of patients on anti-VEGF therapy developed fibrovascular scaring within 2 years (Daniel et al., 2014), highlighting the need for alternative therapeutic agents that target this process. Staining for collagen I and fibronectin will provide information as to how loss of EC ZEB1 impacts the fibrosis process post laser-CNV. This can be done in the study timeline used in this thesis, but could also be extended into later time points, as this is where there are higher levels of fibrosis.

7.7.6.2 Inhibition of VEGF

It would be interesting to determine if the use of anti-VEGF agents were able to prevent this increase in lesion leakage and neovascular lesion size in ZEB1^{iECKO} mice. This would help determine the mechanism of action in which endothelial cells lacking ZEB1 display increased pathological angiogenesis and vascular leakage. If anti-VEGF agents were able to prevent this increase, it would indicate that the mechanism of action observed in ZEB1^{iECKO} mice was via VEGF, or the ECs ability to respond to VEGF. However, if anti-VEGF agents were not able to have an effect on the increased lesion leakage observed in ZEB1^{iECKO} mice, this may suggest that the mechanism in which this group undergoes greater neovascularisation and lesion leakage is via an alternative pathway that does not involve VEGF. This would be interesting because it is known that a subset of patients do not respond well to anti-VEGF therapy for neovascular ocular diseases, as well as anti-VEGF therapy generally having reduced efficacy with time (Chen et al., 2023; Suzuki et al., 2014). Therefore, if loss of EC ZEB1 influences the increase in neovascularisation via alternative pathways, this may identify other therapeutic targets that may benefit those who do not respond to traditional anti-VEGF therapies

7.7.7 Investigation of how loss of ZEB1 influences endothelial dysfunction within the HLI model

To improve the translatability of the findings and explore potential changes in the response to HLI within the ZEB1^{iECKO} group, several studies could be pursued. One such study involves incorporating models of type 1 diabetes, such as the administration of streptozotocin to induce pancreatic β-cell damage. This model has been used alongside

HLI to provide a more clinically relevant representation of PAD (Yan et al., 2009). Further to this, another option for future work is raising the control and ZEB1^{iECKO} on a high fat, high sucrose diet. This was observed to induce both obesity and significantly higher fasting blood glucose, associated with insulin resistant diabetes. These factors together reduced the blood flow recovery with ischaemia (Nguyen et al., 2021). This model is able to illustrate multiple factors which lead to comorbidities and endothelial dysfunction, without the administration of toxic compounds. The increased dietary intake of high fat and high sugar food mimics what is observed within the human population very closely and therefore could be an ideal next step in this research.

7.8 Conclusion and Implications

This thesis aimed to explore the role of endothelial ZEB1 within physiological and pathological angiogenesis. ZEB1 was initially identified as being a transcription factor that was enriched within confluent ECs *in vitro*. The knockdown of ZEB1 proved to influence HUVEC gene expression, with direct gene expression identified using ChIP-Seq and RNA-Seq identifying enrichment of genes involved in inflammation and adhesion. In an *in vitro* sprouting assay, loss of ZEB1 was observed to reduce sprouting, which was also partly observed *in vivo*, with loss of EC ZEB1 resulting in impaired angiogenic front progression and reduced branching. Whereas within the context of angiogenic disease, loss of ZEB1 resulted in increased lesion size and leakage in a laser induced CNV model of wAMD, suggesting loss of ZEB1 within alternative angiogenic contexts has differing roles. Finally, when knocking out ZEB1 in an HLI model of PAD, remodeling is observed within the vasculature is observed even without the presence of an ischemic stimulus, indicating that ZEB1 may be playing a role in vascular maintenance and quiescence.

The impact of this work is that these findings provide evidence to support ZEB1 being involved in multiple processes which govern EC behavior. This work does provide some evidence to suggest that angiogenesis is an EndoMT like event, however it also identified multiple other roles for ZEB1 which have not previously been linked with EndoMT, such as regulation of inflammation and vascular leakage. This therefore highlights that infamous EMT transcription factors, such as ZEB1, could be involved in the transcriptional control of ECs in ways far greater than initially imagined.

7.9 Supplementary information and statements

7.9.1 COVID-19 impact statement

The COVID-19 pandemic impacted the production of this thesis in numerous ways. Firstly, the abrupt closure of the University and the newly built Biodiscovery Institute occurred at the beginning of my final lab rotation, which meant I did not receive training within that placement. This closure lasted for roughly 6 months, during which time I had confirmed my PhD project but had no access to the laboratory or any data to analyse. In an attempt to regain some normality and to contribute what I could to help, I worked within the COVID-19 Light House Laboratory at Alderley Park in Manchester, processing samples from the general public. During which time, I travelled regularly up to Manchester and stayed within a hotel. Once the Biodiscovery Institute opened again, the social distancing rules, reduced working hours, along with the fact the brand-new labs were barely set up prior to their closure, meant that training on equipment and techniques took a larger amount of time. Consequently, my research was unable to progress at rate that was considered satisfactory pre-pandemic. Not only this, but I was also unable to complete the assessments to gain my Home Office Personal License for animal work until late 2020, with my license being granted in March 2021. This resulted in the HLI studies being performed prior to me receiving my license, and often without me being present during the surgery or imaging due to the COVID restrictions with the BSU. The licensed work within these studies was performed by other lab members (Dr Sohini Ria Bhalla, Dr Mussarat Wahid or Dr Nick Beazley-Long) which have been noted throughout chapter 6. Fortunately, I have assisted on HLI surgeries and imaging on separate studies not presented in this thesis, which has given me a good level of understanding which can be applied to the previously done ZEB1^{iECKO} mice. Finally, it must be noted that this delay in receiving my license also impacted my ability to be trained in licensed procedures, due to the contracts of senior licensed lab members ending before receiving my license.

This was also a particularly difficult time for myself and others in regards to mental health, as everyone began to navigate a post-lock down world, in which many felt uncomfortable, leading to an uneasy working environment and a lack of interaction and support particularly within the early career research (ECR) community. This was something I felt

incredibly passionate about and hence worked hard to improve the environment by setting up initiatives and providing training opportunities as well as scientific social events, such as the 'ECR social seminar series' to improve the confidence of ECRs and build our research community. I believe the initial delay and pro-longed impact of both the pandemic and the building move is a prime example of the resilience, persistence and dedication of myself and all PhD students during the last few years.

7.9.2 PhD Professional Internship Placement

As part of my BBSRC DTP funded PhD I had to complete a 3-month internship outside of my PhD research. To satisfy this requirement I completed this internship with Proteintech Group at their European HQ in central Manchester. I worked closely with technical specialists, scientific marketing coordinators and product managers to understand how they impacted the business. In the first weeks of my placement I was tasked with organising a Proteintech sponsored 'Pint of Science' event within the Biodisocvery Institute for postdoc appreciation week. This involved project managing every aspect of the event, from organising and liaising with speakers, booking rooms, ordering refreshments and food, as well as chairing the event. I was also tasked with updating online content for the technical support side of the company's website for specific antibody utilising techniques. This included a complete overhaul of the western blot protocol section and an update of the immunofluorescent staining section of the website. The content I created for the western blot protocols was also placed into printed protocol booklets that are available online. I also organised and generated content for a brand-new landing page for Proteintech products on ThermoFischers's website, which involved creating content which had strict criteria so that it fit into the template of the website. Following this, I was tasked with producing online technical support blogs, which focused on using terms identified using search engine optimisation identified terms to generate website hits. I then proceeded to update and refresh older blogs in order to increase website hits due to the refreshing of content, also with the aim of introducing new search engine optimsied terms. Since this time, I have produced 3 published blogs which are all available online:

1. ‘Detecting low abundance proteins via Western Blot; https://www.ptglab.com/news/blog/detecting-low-abundance-proteins-via-western-blot/
2. ‘Overview of the vascular system and the importance of endothelial cells’ https://www.ptglab.com/news/blog/overview-of-the-vascular-system-and-the-importance-of-endothelial-cells/
3. ‘How to write a PhD thesis: 10 top tips’ https://www.ptglab.com/news/blog/how-to-write-a-phd-thesis-10-top-tips/

Overall, my time at Proteinech allowed me to gain valuable skills in marketing, project management and technical writing. It also provided me with an insight into what jobs and positions are available outside of the laboratory and academia.

References

Abshire, C. F., Carroll, J. L., & Dragoi, A. M. (2016). FLASH protects ZEB1 from degradation and supports cancer cells' epithelial-to-mesenchymal transition. *Oncogenesis*, *5*(8), e254. https://doi.org/10.1038/oncsis.2016.55

Achen, M. G., Jeltsch, M., Kukk, E., Ma¨kinenma¨kinen, T., Vitali, A., Wilks, A. F., Alitalo, K., & Stacker, S. A. (1998). Vascular endothelial growth factor D (VEGF-D) is a ligand for thetyrosine kinases VEGF receptor 2 (Flk1) and VEGFreceptor 3 (Flt4). *Cell Biology*, *95*, 548–553. www.pnas.org.

Adams, R. H., & Alitalo, K. (2007). Molecular regulation of angiogenesis and lymphangiogenesis. In *Nature Reviews Molecular Cell Biology* (Vol. 8, Issue 6, pp. 464–478). https://doi.org/10.1038/nrm2183

Addison, C. L., Daniel, T. O., Burdick, M. D., Liu, H., Ehlert, J. E., Xue, Y. Y., Buechi, L., Walz, A., Richmond, A., & Strieter, R. M. (2000). The CXC Chemokine Receptor 2, CXCR2, Is the Putative Receptor for ELR+ CXC Chemokine-Induced Angiogenic Activity. *The Journal of Immunology*, *165*(9), 5269–5277. https://doi.org/10.4049/jimmunol.165.9.5269

Agrawal, P., Heimbruch, K. E., & Rao, S. (2019). Genome-wide maps of transcription regulatory elements and transcription enhancers in development and disease. *Comprehensive Physiology*, *9*(1), 439–455. https://doi.org/10.1002/cphy.c180028

Aird, W. C. (2007). Phenotypic heterogeneity of the endothelium: I. Structure, function, and mechanisms. In *Circulation Research* (Vol. 100, Issue 2, pp. 158–173). https://doi.org/10.1161/01.RES.0000255691.76142.4a

Aisagbonhi, O., Rai, M., Ryzhov, S., Atria, N., Feoktistov, I., & Hatzopoulos, A. K. (2011). Experimental myocardial infarction triggers canonical Wnt signaling and endothelial-to-mesenchymal transition. *DMM Disease Models and Mechanisms*, *4*(4), 469–483. https://doi.org/10.1242/dmm.006510

Akwii, R. G., & Mikelis, C. M. (2021). Targeting the Angiopoietin/Tie Pathway: Prospects for Treatment of Retinal and Respiratory Disorders. *Drugs*, *81*(15), 1731–1749. https://doi.org/10.1007/s40265-021-01605-y

Alva, J. A., Zovein, A. C., Monvoisin, A., Murphy, T., Salazar, A., Harvey, N. L., Carmeliet, P., & Iruela-Arispe, M. L. (2006). VE-cadherin-cre-recombinase transgenic mouse: A tool for lineage analysis and gene deletion in endothelial cells. *Developmental Dynamics*, *235*(3), 759–767. https://doi.org/10.1002/dvdy.20643

Alvandi, Z., & Bischoff, J. (2021). Endothelial-Mesenchymal Transition in Cardiovascular Disease. *Arteriosclerosis, Thrombosis, and Vascular Biology*, *41*(9), 2357–2369. https://doi.org/10.1161/ATVBAHA.121.313788

Ambati, J., Atkinson, J. P., & Gelfand, B. D. (2013). Immunology of age-related macular degeneration. In *Nature Reviews Immunology* (Vol. 13, Issue 6, pp. 438–451). https://doi.org/10.1038/nri3459

Andrade, J., Shi, C., Costa, A. S. H., Choi, J., Kim, J., Doddaballapur, A., Sugino, T., Ong, Y. T., Castro, M., Zimmermann, B., Kaulich, M., Guenther, S., Wilhelm, K., Kubota, Y., Braun, T., Koh, G. Y., Grosso, A. R., Frezza, C., & Potente, M. (2021). Control of endothelial quiescence by FOXO-regulated metabolites. *Nature Cell Biology*, *23*(4), 413–423. https://doi.org/10.1038/s41556-021-00637-6

Ara, T., Tokoyoda, K., Okamoto, R., Koni, P. A., & Nagasawa, T. (2005). The role of CXCL12 in the organ-specific process of artery formation. *Blood*, *105*(8), 3155–3161. https://doi.org/10.1182/blood

Arciniegas, E., Neves, C. Y., Carrillo, L. M., Zambrano, E. A., & Ramírez, R. (2005). Endothelial-Mesenchymal Transition Occurs during Embryonic Pulmonary Artery Development. *Endothelium*, *12*(4), 193–200.

Ardeljan, D., Wang, Y., Park, S., Shen, D., Chu, X. K., Yu, C. R., Abu-Asab, M., Tuo, J., Eberhart, C. G., Olsen, T. W., Mullins, R. F., White, G., Wadsworth, S., Scaria, A., & Chan, C. C. (2014). Interleukin-17 retinotoxicity is prevented by gene transfer of a soluble interleukin-17 receptor acting as a cytokine blocker: Implications for age-related macular degeneration. *PLoS ONE*, *9*(4). https://doi.org/10.1371/journal.pone.0095900

Aref, Z., de Vries, M. R., & Quax, P. H. A. (2019). Variations in surgical procedures for inducing hind limb ischemia in mice and the impact of these variations on neovascularization assessment. In *International Journal of Molecular Sciences* (Vol. 20, Issue 15). MDPI AG. https://doi.org/10.3390/ijms20153704

Arif, N., Zinnhardt, M., Nyamay'Antu, A., Teber, D., Brückner, R., Schaefer, K., Li, Y., Trappmann, B., Grashoff, C., & Vestweber, D. (2021). PECAM-1 supports leukocyte diapedesis by tension-dependent dephosphorylation of VE-cadherin. *The EMBO Journal*, *40*(9). https://doi.org/10.15252/embj.2020106113

Armstrong, E. J., & Bischoff, J. (2004). Heart valve development: Endothelial cell signaling and differentiation. In *Circulation Research* (Vol. 95, Issue 5, pp. 459–470). https://doi.org/10.1161/01.RES.0000141146.95728.da

Armulik, A., Abramsson, A., & Betsholtz, C. (2005). Endothelial/pericyte interactions. In *Circulation Research* (Vol. 97, Issue 6, pp. 512–523). https://doi.org/10.1161/01.RES.0000182903.16652.d7

Arras, M., Ito, W. D., Scholz, D., Winkler, B., Schaper, J., & Schaper, W. (1998). Monocyte Activation in Angiogenesis and Collateral Growth in the Rabbit Hindlimb. In *J. Clin. Invest* (Vol. 101, Issue 1). http://www.jci.org

Arreola, A., Payne, L. B., Julian, M. H., de Cubas, A. A., Daniels, A. B., Taylor, S., Zhao, H., Darden, J., Bautch, V. L., Rathmell, W. K., & Chappell, J. C. (2018). Von Hippel-Lindau mutations disrupt vascular patterning and maturation via Notch. *JCI Insight*, *3*(4). https://doi.org/10.1172/jci.insight.92193

August Krogh, B. (1919). THE NUMBER AND DISTRIBUTION OF CAPILLARIES IN MUSCLES WITH CALCULATIONS OF THE OXY-GEN PRESSURE HEAD NECESSARY FOR SUPPLYING THE TISSUE. *The Journal of Physiology*, *62*(6), 409–415.

Augustin, H. G., Young Koh, G., Thurston, G., & Alitalo, K. (2009). Control of vascular morphogenesis and homeostasis through the angiopoietin - Tie system. In *Nature Reviews Molecular Cell Biology* (Vol. 10, Issue 3, pp. 165–177). https://doi.org/10.1038/nrm2639

Baeyens, N., Mulligan-Kehoe, M. J., Corti, F., Simon, D. D., Ross, T. D., Rhodes, J. M., Wang, T. Z., Mejean, C. O., Simons, M., Humphrey, J., & Schwartz, M. A. (2014). Syndecan 4 is required for endothelial alignment in flow and atheroprotective signaling. *Proceedings of the National Academy of Sciences of the United States of America*, *111*(48), 17308–17313. https://doi.org/10.1073/pnas.1413725111

Bailey, T., Krajewski, P., Ladunga, I., Lefebvre, C., Li, Q., Liu, T., Madrigal, P., Taslim, C., & Zhang, J. (2013). Practical Guidelines for the Comprehensive Analysis of ChIP-seq Data. *PLoS Computational Biology*, *9*(11). https://doi.org/10.1371/journal.pcbi.1003326

Bain, C. R., Myles, P. S., Corcoran, T., & Dieleman, J. M. (2023). Postoperative systemic inflammatory dysregulation and corticosteroids: a narrative review. In *Anaesthesia* (Vol. 78, Issue 3, pp. 356–370). John Wiley and Sons Inc. https://doi.org/10.1111/anae.15896

Banerjee-Basu, S., & Baxevanis, A. D. (2001). Molecular evolution of the homeodomain family of transcription factors. In *Nucleic Acids Research* (Vol. 29, Issue 15). http://ftp.sunet.se/

Barford, D., Flint, A. J., & Tonks, N. K. (1994). Crystal structure of human protein tyrosine phosphatase 1B. *Science*, *263*(5152), 1397–1404.

Barleon, B., Sozzani, S., Zhou, D., Weich, H. A., Mantovani, A., & Marme, D. (1996). Migration of Human Monocytes in Response to Vascular Endothelial Growth Factor (VEGF) Is Mediated via the VEGF Receptor flt-1. *Blood*, *87*(6), 3336–3343.

Bates, D. O. (2010). Vascular endothelial growth factors and vascular permeability. In *Cardiovascular Research* (Vol. 87, Issue 2, pp. 262–271). Oxford University Press. https://doi.org/10.1093/cvr/cvq105

Bates, D. O., Cui, T.-G., Doughty, J. M., Winkler, M., Sugiono, M., Shields, J. D., Peat, D., Gillatt, D., & Harper, S. J. (2002). VEGF 165 b, an Inhibitory Splice Variant of Vascular Endothelial Growth Factor, Is Down-Regulated in Renal Cell Carcinoma 1. *CANCER RESEARCH*, *62*, 4123–4131. http://aacrjournals.org/cancerres/article-pdf/62/14/4123/2495309/ch1402004123.pdf

Baxter, S. L., Pistilli, M., Pujari, S. S., Liesegang, T. L., Suhler, E. B., Thorne, J. E., Foster, C. S., Jabs, D. A., Levy-Clarke, G. A., Nussenblatt, R. B., Rosenbaum, J. T., & Kempen, J. H. (2013). Risk of choroidal neovascularization among the uveitides. *American Journal of Ophthalmology*, *156*(3). https://doi.org/10.1016/j.ajo.2013.04.040

Beazley-Long, N., Hodge, D., Ashby, W. R., Bestall, S. M., Almahasneh, F., Durrant, A. M., Benest, A. V., Blackley, Z., Ballmer-Hofer, K., Hirashima, M., Hulse, R. P., Bates, D. O., & Donaldson, L. F. (2018). VEGFR2 promotes central endothelial activation and the spread of pain in inflammatory arthritis. *Brain, Behavior, and Immunity*, *74*, 49–67. https://doi.org/10.1016/j.bbi.2018.03.012

Becker, L. M., Chen, S. H., Rodor, J., de Rooij, L. P. M. H., Baker, A. H., & Carmeliet, P. (2023). Deciphering endothelial heterogeneity in health and disease at single-cell resolution: progress and perspectives. In *Cardiovascular Research* (Vol. 119, Issue 1, pp. 6–27). Oxford University Press. https://doi.org/10.1093/cvr/cvac018

Behroozian, A., & Beckman, J. A. (2020). Microvascular Disease Increases Amputation in Patients With Peripheral Artery Disease. *Arteriosclerosis, Thrombosis, and Vascular Biology*, *40*(3), 534–540. https://doi.org/10.1161/ATVBAHA.119.312859

Benedito, R., Roca, C., Sörensen, I., Adams, S., Gossler, A., Fruttiger, M., & Adams, R. H. (2009). The Notch Ligands Dll4 and Jagged1 Have Opposing Effects on Angiogenesis. *Cell*, *137*(6), 1124–1135. https://doi.org/10.1016/j.cell.2009.03.025

Benest, A. V., Stone, O. A., Miller, W. H., Glover, C. P., Uney, J. B., Baker, A. H., Harper, S. J., & Bates, D. O. (2008). Arteriolar genesis and angiogenesis induced by endothelial nitric oxide synthase overexpression results in a mature vasculature. *Arteriosclerosis, Thrombosis, and Vascular Biology*, *28*(8), 1462–1468. https://doi.org/10.1161/ATVBAHA.108.169375

Bentley, K., Franco, C. A., Philippides, A., Blanco, R., Dierkes, M., Gebala, V., Stanchi, F., Jones, M., Aspalter, I. M., Cagna, G., Weström, S., Claesson-Welsh, L., Vestweber, D., & Gerhardt, H. (2014). The role of differential VE-cadherin dynamics in cell rearrangement during angiogenesis. *Nature Cell Biology*, *16*(4), 309–321. https://doi.org/10.1038/ncb2926

Bergers, G., & Song, S. (2005). The role of pericytes in blood-vessel formation and maintenance. In *Neuro-Oncology* (Vol. 7, Issue 4, pp. 452–464). https://doi.org/10.1215/S1152851705000232

Bergmann, O., Zdunek, S., Felker, A., Salehpour, M., Alkass, K., Bernard, S., Sjostrom, S. L., Szewczykowska, M., Jackowska, T., Dos Remedios, C., Malm, T., Andrä, M., Jashari, R., Nyengaard, J. R., Possnert, G., Jovinge, S., Druid, H., & Frisén, J. (2015). Dynamics of Cell Generation and Turnover in the Human Heart. *Cell*, *161*(7), 1566–1575. https://doi.org/10.1016/j.cell.2015.05.026

Bhalla, S. R., Riu, F., Machado, M. J. C., & Bates, D. O. (2022). Measurement of Revascularization in the Hind Limb After Experimental Ischemia in Mice. In A. V. Benest (Ed.), *Angiogenesis. Methods in Molecular Biology,* (Vol. 2441, pp. 105–113).

Birdsey, G. M., Dryden, N. H., Amsellem, V., Gebhardt, F., Sahnan, K., Haskard, D. O., Dejana, E., Mason, J. C., & Randi, A. M. (2008). Transcription factor erg regulates angiogenesis and endothelial apoptosis through VE-cadherin. *Blood*, *111*(7), 3498–3506. https://doi.org/10.1182/blood-2007-08-105346

Birdsey, G. M., Shah, A. V., Dufton, N., Reynolds, L. E., Almagro, L. O., Yang, Y., Aspalter, I. M., Khan, S. T., Mason, J. C., Dejana, E., Göttgens, B., Hodivala-Dilke, K., Gerhardt, H., Adams, R. H., & Randi, A. M. (2015). The endothelial transcription factor erg promotes vascular stability and growth through Wnt/β-catenin signaling. *Developmental Cell*, *32*(1), 82–96. https://doi.org/10.1016/j.devcel.2014.11.016

Bloor, C. M. (2005). Angiogenesis during exercise and training. In *Angiogenesis* (Vol. 8, Issue 3, pp. 263–271). https://doi.org/10.1007/s10456-005-9013-x

Bondareva, O., Rodríguez-Aguilera, J. R., Oliveira, F., Liao, L., Rose, A., Gupta, A., Singh, K., Geier, F., Schuster, J., Boeckel, J. N., Buescher, J. M., Kohli, S., Klöting, N., Isermann, B., Blüher, M., & Sheikh, B. N. (2022). Single-cell profiling of vascular endothelial cells reveals progressive organ-specific vulnerabilities during obesity. *Nature Metabolism*, *4*(11), 1591–1610. https://doi.org/10.1038/s42255-022-00674-x

Bontzos, G., Bagheri, S., Ioanidi, L., Kim, I., Datseris, I., Gragoudas, E., Kabanarou, S., Miller, J., Tsilimbaris, M., & Vavvas, D. G. (2020). Nonresponders to Ranibizumab Anti-VEGF Treatment Are Actually Short-term Responders: A Prospective Spectral-Domain OCT Study. *Ophthalmology Retina*, *4*(12), 1138–1145. https://doi.org/10.1016/j.oret.2019.11.004

Brabletz, S., & Brabletz, T. (2010). The ZEB/miR-200 feedback loop-a motor of cellular plasticity in development and cancer? In *EMBO Reports* (Vol. 11, Issue 9, pp. 670–677). https://doi.org/10.1038/embor.2010.117

Brabletz, S., Lasierra Losada, M., Schmalhofer, O., Mitschke, J., Krebs, A., Brabletz, T., & Stemmler, M. P. (2017). Generation and characterization of mice for conditional inactivation of Zeb1. *Genesis*, *55*(4). https://doi.org/10.1002/dvg.23024

Brabletz, T., Kalluri, R., Nieto, M. A., & Weinberg, R. A. (2018). EMT in cancer. In *Nature Reviews Cancer* (Vol. 18, Issue 2, pp. 128–134). Nature Publishing Group. https://doi.org/10.1038/nrc.2017.118

Brandli, A., Khong, F. L., Kong, R. C. K., Kelly, D. J., & Fletcher, E. L. (2022). Transcriptomic analysis of choroidal neovascularization reveals dysregulation of immune and fibrosis pathways that are attenuated by a novel anti-fibrotic treatment. *Scientific Reports*, *12*(1). https://doi.org/10.1038/s41598-022-04845-4

Brash, J. T., Bolton, R. L., Rashbrook, V. S., Denti, L., Kubota, Y., & Ruhrberg, C. (2020). Tamoxifen-Activated CreERT Impairs Retinal Angiogenesis Independently of Gene Deletion. In *Circulation Research* (Vol. 127, Issue 6, pp. 849–850). Lippincott Williams and Wilkins. https://doi.org/10.1161/CIRCRESAHA.120.317025

Bui, T. M., Wiesolek, H. L., & Sumagin, R. (2020). ICAM-1: A master regulator of cellular responses in inflammation, injury resolution, and tumorigenesis. In *Journal of Leukocyte Biology* (Vol. 108, Issue 3, pp. 787–799). John Wiley and Sons Inc. https://doi.org/10.1002/JLB.2MR0220-549R

Bürglin, T. R., & Affolter, M. (2016). Homeodomain proteins: an update. In *Chromosoma* (Vol. 125, Issue 3, pp. 497–521). Springer Science and Business Media Deutschland GmbH. https://doi.org/10.1007/s00412-015-0543-8

Caduff, J. H., Fischer, L. C., & Burri, P. H. (1986). Scanning electron microscope study of the developing microvasculature in the postnatal rat lung. *The Anatomical Record*, *216*(2), 154–164. https://doi.org/10.1002/ar.1092160207

Caramel, J., Ligier, M., & Puisieux, A. (2018). Pleiotropic roles for ZEB1 in cancer. In *Cancer Research* (Vol. 78, Issue 1, pp. 30–35). American Association for Cancer Research Inc. https://doi.org/10.1158/0008-5472.CAN-17-2476

Carmeliet, P. (2003). Angiogenesis in health and disease. *Nature Medicine*, *9*(6), 653–660. http://www.nature.com/naturemedicine

Carmeliet, P., & Jain, R. K. (2011). Molecular mechanisms and clinical applications of angiogenesis. In *Nature* (Vol. 473, Issue 7347, pp. 298–307). https://doi.org/10.1038/nature10144

Casie Chetty, S., Rost, M. S., Enriquez, J. R., Schumacher, J. A., Baltrunaite, K., Rossi, A., Stainier, D. Y. R., & Sumanas, S. (2017). Vegf signaling promotes vascular endothelial differentiation by modulating etv2 expression. *Developmental Biology*, *424*(2), 147–161. https://doi.org/10.1016/j.ydbio.2017.03.005

Castro-Ferreira, R., Cardoso, R., Leite-Moreira, A., & Mansilha, A. (2018). The Role of Endothelial Dysfunction and Inflammation in Chronic Venous Disease. In *Annals of Vascular Surgery* (Vol. 46, pp. 380–393). Elsevier Inc. https://doi.org/10.1016/j.avsg.2017.06.131

Chang, J. H., Garg, N. K., Lunde, E., Han, K. Y., Jain, S., & Azar, D. T. (2012). Corneal Neovascularization: An Anti-VEGF Therapy Review. In *Survey of Ophthalmology* (Vol. 57, Issue 5, pp. 415–429). https://doi.org/10.1016/j.survophthal.2012.01.007

Chen, A., Wong, C. S. F., Liu, M. C. P., House, C. M., Sceneay, J., Bowtell, D. D., Thompson, E. W., & Möller, A. (2014). The ubiquitin ligase Siah is a novel regulator of Zeb1 in breast cancer. *Oncotarget*, *6*(2). www.impactjournals.com/oncotarget

Chen, P. Y., Qin, L., Baeyens, N., Li, G., Afolabi, T., Budatha, M., Tellides, G., Schwartz, M. A., & Simons, M. (2015). Endothelial-to-mesenchymal transition drives atherosclerosis progression. *Journal of Clinical Investigation*, *125*(12), 4514–4528. https://doi.org/10.1172/JCI82719

Chen, P. Y., Qin, L., Barnes, C., Charisse, K., Yi, T., Zhang, X., Ali, R., Medina, P. P., Yu, J., Slack, F. J., Anderson, D. G., Kotelianski, V., Wang, F., Tellides, G., & Simons, M. (2012). FGF Regulates TGF-β Signaling and Endothelial-to-Mesenchymal Transition via Control of let-7 miRNA Expression. *Cell Reports*, *2*(6), 1684–1696. https://doi.org/10.1016/j.celrep.2012.10.021

Chen, R., Zhu, J., Hu, J., & Li, X. (2023). Antiangiogenic therapy for ocular diseases: Current status and challenges. *MedComm – Future Medicine*, *2*(1). https://doi.org/10.1002/mef2.33

Cheng, C., Haasdijk, R., Tempel, D., Van De Kamp, E. H. M., Herpers, R., Bos, F., Den Dekker, W. K., Lau, ;, Blonden, A. J., De Jong, R., Bürgisser, P. E., Chrifi, I., Biessen, E. A. L., Dimmeler, S., Schulte-Merker, S., Henricus, ;, & Duckers, J. (2012). Molecular Cardiology Endothelial Cell-Specific FGD5 Involvement in Vascular Pruning Defines Neovessel Fate in Mice. *Circulation*, *125*(25), 3142–3159. https://doi.org/10.1161/CIRCULATIONAHA

Cheng, L., Chen, C., Guo, W., Liu, K., Zhao, Q., Lu, P., Yu, F., & Xu, X. (2021). EFEMP1 Overexpression Contributes to Neovascularization in Age-Related Macular Degeneration. *Frontiers in Pharmacology*, *11*. https://doi.org/10.3389/fphar.2020.547436

Child, S., Karp, N., & Wells, S. (2022). MRC/NC3Rs webinar: Using both sexes in animal experiments. In *National Centre for the Replacement Refinement and Reduction of Animals in Research: Vol. Webinar*. National Centre for the Replacement Refinement and Reduction of Animals in Research.

Chistiakov, D. A., Orekhov, A. N., & Bobryshev, Y. V. (2015). Endothelial barrier and its abnormalities in cardiovascular disease. In *Frontiers in Physiology* (Vol. 6, Issue DEC). Frontiers Media S.A. https://doi.org/10.3389/fphys.2015.00365

Chu, M., Li, T., Shen, B., Cao, X., Zhong, H., Zhang, L., Zhou, F., Ma, W., Jiang, H., Xie, P., Liu, Z., Dong, N., Xu, Y., Zhao, Y., Xu, G., Lu, P., Luo, J., Wu, Q., Alitalo, K., … He, Y. (2016). Angiopoietin receptor Tie2 is required for vein specification and maintenance via regulating COUP-TFII. *ELIFE*, *e21032*, 5. https://doi.org/10.7554/eLife.21032.001

Chua, H. L., Bhat-Nakshatri, P., Clare, S. E., Morimiya, A., Badve, S., & Nakshatri, H. (2007). NF-κB represses E-cadherin expression and enhances epithelial to mesenchymal transition of mammary epithelial cells: Potential involvement of ZEB-1 and ZEB-2. *Oncogene*, *26*(5), 711–724. https://doi.org/10.1038/sj.onc.1209808

Claesson-Welsh, L., Dejana, E., & McDonald, D. M. (2021). Permeability of the Endothelial Barrier: Identifying and Reconciling Controversies. In *Trends in Molecular Medicine* (Vol. 27, Issue 4, pp. 314–331). Elsevier Ltd. https://doi.org/10.1016/j.molmed.2020.11.006

Clark, E. R. (1918). Studies on the growth of blood-vessels in the tail of the frog larva—by observation and experiment on the living animal. *American Journal of Anatomy* , *23*(1), 37–88.

Cobos, E., Recalde, S., Anter, J., Hernandez-Sanchez, M., Barreales, C., Olavarrieta, L., Valverde, A., Suarez-Figueroa, M., Cruz, F., Abraldes, M., Pérez-Pérez, J., Fernández-Robredo, P., Arias, L., & García-Layana, A. (2018). Association between CFH, CFB, ARMS2, SERPINF1, VEGFR1 and VEGF polymorphisms and anatomical and functional response to ranibizumab treatment in neovascular age-related macular degeneration. *Acta Ophthalmologica*, *96*(2), e201–e212. https://doi.org/10.1111/aos.13519

Coll-Bonfill, N., Musri, M. M., Ivo, V., Barberà, J. A., & Tura-Ceide, O. (2015). Transdifferentiation of endothelial cells to smooth muscle cells play an important role in vascular remodelling. In *Am J Stem Cells* (Vol. 4, Issue 1). www.AJSC.us/ISSN:2160-4150/AJSC0003410

Corada, M., Morini, M. F., & Dejana, E. (2014). Signaling pathways in the specification of arteries and veins. In *Arteriosclerosis, Thrombosis, and Vascular Biology* (Vol. 34, Issue 11, pp. 2372–2377). Lippincott Williams and Wilkins. https://doi.org/10.1161/ATVBAHA.114.303218

Corada, M., Orsenigo, F., Morini, M. F., Pitulescu, M. E., Bhat, G., Nyqvist, D., Breviario, F., Conti, V., Briot, A., Iruela-Arispe, M. L., Adams, R. H., & Dejana, E. (2013). Sox17 is indispensable for acquisition and maintenance of arterial identity. *Nature Communications*, *4*. https://doi.org/10.1038/ncomms3609

Costantino, M. E., Stearman, R. P., Smith, G. E., & Darling, D. S. (2002). Cell-Specific Phosphorylation of Zfhep Transcription Factor. *Biochem Biophys Res Commun*, *296*(2), 368–373.

Couffinhal, T., Silver, M., Zheng, L. P., Kearney, M., Witzenbichler, B., & Isner, J. M. (1998). Mouse Model of Angiogenesis. In *American Journal ofPathology* (Vol. 152, Issue 6).

Coutelle, O., Hornig-Do, H. T., Witt, A., Andree, M., Schiffmann, L. M., Piekarek, M., Brinkmann, K., Seeger, J. M., Liwschitz, M., Miwa, S., Hallek, M., Krönke, M., Trifunovic, A., Eming, S. A., Wiesner, R. J., Hacker, U. T., & Kashkar, H. (2014). Embelin inhibits endothelial mitochondrial respiration and impairs neoangiogenesis during tumor growth and wound healing. *EMBO Molecular Medicine*, *6*(5), 624–639. https://doi.org/10.1002/emmm.201303016

Craene, B. De, & Berx, G. (2013). Regulatory networks defining EMT during cancer initiation and progression. In *Nature Reviews Cancer* (Vol. 13, Issue 2, pp. 97–110). https://doi.org/10.1038/nrc3447

Crist, A. M., Lee, A. R., Patel, N. R., Westhoff, D. E., & Meadows, S. M. (2018). Vascular deficiency of Smad4 causes arteriovenous malformations: a mouse model of Hereditary Hemorrhagic Telangiectasia. *Angiogenesis*, *21*(2), 363–380. https://doi.org/10.1007/s10456-018-9602-0

Daneman, R., & Prat, A. (2015). The blood–brain barrier. *Cold Spring Harbor Perspectives in Biology*, *7*(1). https://doi.org/10.1101/cshperspect.a020412

Daneman, R., Zhou, L., Kebede, A. A., & Barres, B. A. (2010). Pericytes are required for blood brain barrier integrity during embryogenesis. *Nature*, *468*(7323), 562–566. https://doi.org/10.1038/nature09513

Daniel, E., Toth, C. A., Grunwald, J. E., Jaffe, G. J., Martin, D. F., Fine, S. L., Huang, J., Ying, G. S., Hagstrom, S. A., Winter, K., & Maguire, M. G. (2014). Risk of scar in the comparison of Age-related Macular Degeneration Treatments Trials. *Ophthalmology*, *121*(3), 656–666. https://doi.org/10.1016/j.ophtha.2013.10.019

Datta, S., Cano, M., Ebrahimi, K., Wang, L., & Handa, J. T. (2017). The impact of oxidative stress and inflammation on RPE degeneration in non-neovascular AMD. In *Progress in Retinal and Eye Research* (Vol. 60, pp. 201–218). Elsevier Ltd. https://doi.org/10.1016/j.preteyeres.2017.03.002

Dauphinee, S. M., & Karsan, A. (2006). Lipopolysaccharide signaling in endothelial cells. In *Laboratory Investigation* (Vol. 86, Issue 1, pp. 9–22). https://doi.org/10.1038/labinvest.3700366

Dayang, E. Z., Plantinga, J., Ter Ellen, B., Van Meurs, M., Molema, G., & Moser, J. (2019). Identification of LPS-activated endothelial subpopulations with distinct

inflammatory phenotypes and regulatory signaling mechanisms. *Frontiers in Immunology*, *10*(MAY). https://doi.org/10.3389/fimmu.2019.01169

De Bock, K., Georgiadou, M., Schoors, S., Kuchnio, A., Wong, B. W., Cantelmo, A. R., Quaegebeur, A., Ghesquière, B., Cauwenberghs, S., Eelen, G., Phng, L. K., Betz, I., Tembuyser, B., Brepoels, K., Welti, J., Geudens, I., Segura, I., Cruys, B., Bifari, F., … Carmeliet, P. (2013). Role of PFKFB3-driven glycolysis in vessel sprouting. *Cell*, *154*(3). https://doi.org/10.1016/j.cell.2013.06.037

De Smet, F., Segura, I., De Bock, K., Hohensinner, P. J., & Carmeliet, P. (2009). Mechanisms of vessel branching: Filopodia on endothelial tip cells lead the way. In *Arteriosclerosis, Thrombosis, and Vascular Biology* (Vol. 29, Issue 5, pp. 639–649). https://doi.org/10.1161/ATVBAHA.109.185165

De Val, S., & Black, B. L. (2009). Transcriptional Control of Endothelial Cell Development. In *Developmental Cell* (Vol. 16, Issue 2, pp. 180–195). https://doi.org/10.1016/j.devcel.2009.01.014

De Val, S., Chi, N. C., Meadows, S. M., Minovitsky, S., Anderson, J. P., Harris, I. S., Ehlers, M. L., Agarwal, P., Visel, A., Xu, S. M., Pennacchio, L. A., Dubchak, I., Krieg, P. A., Stainier, D. Y. R., & Black, B. L. (2008). Combinatorial Regulation of Endothelial Gene Expression by Ets and Forkhead Transcription Factors. *Cell*, *135*(6), 1053–1064. https://doi.org/10.1016/j.cell.2008.10.049

De Vega, S., Iwamoto, T., & Yamada, Y. (2009). Fibulins: Multiple roles in matrix structures and tissue functions. In *Cellular and Molecular Life Sciences* (Vol. 66, Issues 11–12, pp. 1890–1902). https://doi.org/10.1007/s00018-009-8632-6

Del Toro, R., Prahst, C., Mathivet, T., Siegfried, G., Kaminker, J. S., Larrivee, B., Breant, C., Duarte, A., Takakura, N., Fukamizu, A., Penninger, J., & Eichmann, A. (2010). Identification and functional analysis of endothelial tip cell-enriched genes. *Blood*, *116*(19), 4025–4033. https://doi.org/10.1182/blood-2010-02-270819

Deng, Y., Qiao, L., Du, M., Qu, C., Wan, L., Li, J., & Huang, L. (2022). Age-related macular degeneration: Epidemiology, genetics, pathophysiology, diagnosis, and targeted therapy. In *Genes and Diseases* (Vol. 9, Issue 1, pp. 62–79). Chongqing University. https://doi.org/10.1016/j.gendis.2021.02.009

Dharaneeswaran, H., Abid, M. R., Yuan, L., Dupuis, D., Beeler, D., Spokes, K. C., Janes, L., Sciuto, T., Kang, P. M., Jaminet, S. C. S., Dvorak, A., Grant, M. A., Regan, E. R., & Aird, W. C. (2014). FOXO1-mediated activation of akt plays a critical role in vascular homeostasis. *Circulation Research*, *115*(2), 238–251. https://doi.org/10.1161/CIRCRESAHA.115.303227

Ding, K., Eaton, L., Bowley, D., Rieser, M., Chang, Q., Harris, M. C., Clabbers, A., Dong, F., Shen, J., Hackett, S. F., Touw, D. S., Bixby, J., Zhong, S., Benatuil, L., Bose, S., Grinnell, C., Preston, G. M., Iyer, R., Sadhukhan, R., … Gu, J. (2017). Generation and

characterization of ABBV642, a dual variable domain immunoglobulin molecule (DVD-Ig) that potently neutralizes VEGF and PDGF-BB and is designed for the treatment of exudative age-related macular degeneration. *MAbs*, *9*(2), 269–284. https://doi.org/10.1080/19420862.2016.1268305

DiPietro, L. A. (2016). Angiogenesis and wound repair: when enough is enough. *Journal of Leukocyte Biology*, *100*(5), 979–984. https://doi.org/10.1189/jlb.4mr0316-102r

Draoui, N., De Zeeuw, P., & Carmeliet, P. (2017). Angiogenesis revisited from a metabolic perspective: Role and therapeutic implications of endothelial cell metabolism. *Open Biology*, *7*(12). https://doi.org/10.1098/rsob.170219

Drápela, S., Bouchal, J., Jolly, M. K., Culig, Z., & Souček, K. (2020). ZEB1: A Critical Regulator of Cell Plasticity, DNA Damage Response, and Therapy Resistance. In *Frontiers in Molecular Biosciences* (Vol. 7). Frontiers Media S.A. https://doi.org/10.3389/fmolb.2020.00036

Dreyfuss, J. L., Giordano, R. J., & Regatieri, C. V. (2015). Ocular Angiogenesis. In *Journal of Ophthalmology* (Vol. 2015). Hindawi Publishing Corporation. https://doi.org/10.1155/2015/892043

Duan, L. J., Takeda, K., & Fong, G. H. (2014). Hypoxia inducible factor-2α regulates the development of retinal astrocytic network by maintaining adequate supply of astrocyte progenitors. *PLoS ONE*, *9*(1). https://doi.org/10.1371/journal.pone.0084736

Duan, L.-J., & Fong, G.-H. (2019). Developmental vascular pruning in neonatal mouse retinas is programmed by the astrocytic oxygen-sensing mechanism. *Development* , *146*(8), dev175117.

Dudley, A. C., & Griffioen, A. W. (2023). Pathological angiogenesis: mechanisms and therapeutic strategies. In *Angiogenesis*. Springer Science and Business Media B.V. https://doi.org/10.1007/s10456-023-09876-7

Durham, J. T., Surks, H. K., Dulmovits, B. M., & Herman, I. M. (2014). Pericyte contractility controls endothelial cell cycle progression and sprouting: insights into angiogenic switch mechanics. *Am J Physiol Cell Physiol*, *307*, 878–892. https://doi.org/10.1152/ajpcell.00185.2014.-Microvascular

Eelen, G., De Zeeuw, P., Treps, L., Harjes, U., Wong, B. W., & Carmeliet, P. (2018). ENDOTHELIAL CELL METABOLISM. *Physiol Rev*, *98*, 3–58. https://doi.org/10.1152/physrev.00001.2017.-Endothelial

Eelen, G., Treps, L., Li, X., & Carmeliet, P. (2020). Basic and Therapeutic Aspects of Angiogenesis Updated. In *Circulation Research* (Vol. 127, Issue 2, pp. 310–329). Lippincott Williams and Wilkins. https://doi.org/10.1161/CIRCRESAHA.120.316851

Eger, A., Aigner, K., Sonderegger, S., Dampier, B., Oehler, S., Schreiber, M., Berx, G., Cano, A., Beug, H., & Foisner, R. (2005). DeltaEF1 is a transcriptional repressor of E-cadherin and regulates epithelial plasticity in breast cancer cells. *Oncogene*, *24*(14), 2375–2385. https://doi.org/10.1038/sj.onc.1208429

Eilken, H. M., & Adams, R. H. (2010). Dynamics of endothelial cell behavior in sprouting angiogenesis. In *Current Opinion in Cell Biology* (Vol. 22, Issue 5, pp. 617–625). https://doi.org/10.1016/j.ceb.2010.08.010

Eilken, H. M., Diéguez-Hurtado, R., Schmidt, I., Nakayama, M., Jeong, H. W., Arf, H., Adams, S., Ferrara, N., & Adams, R. H. (2017). Pericytes regulate VEGF-induced endothelial sprouting through VEGFR1. *Nature Communications*, *8*(1). https://doi.org/10.1038/s41467-017-01738-3

Eisenberg, L. M., & Markwald, R. R. (1995). *Mini Review Molecular Regulation of Atrioventricular Valvuloseptal Morphogenesis*. http://ahajournals.org

Ejaz, S. (2008). Importance of pericytes and mechanisms of pericyte loss during diabetes retinopathy. *Diabetes, Obesity and Metabolism*, *10*(1), 53–63. https://doi.org/10.1111/j.1463-1326.2007.00795.x

Eklund, L., & Olsen, B. R. (2006). Tie receptors and their angiopoietin ligands are context-dependent regulators of vascular remodeling. In *Experimental Cell Research* (Vol. 312, Issue 5, pp. 630–641). Academic Press Inc. https://doi.org/10.1016/j.yexcr.2005.09.002

Eremina, V., Sood, M., Haigh, J., Nagy, A., Lajoie, G., Ferrara, N., Gerber, H. P., Kikkawa, Y., Miner, J. H., & Quaggin, S. E. (2003). Glomerular-specific alterations of VEGF-A expression lead to distinct congenital and acquired renal diseases. *Journal of Clinical Investigation*, *111*(5), 707–716. https://doi.org/10.1172/JCI17423

Espinosa-Heidmann, D. G., Marin-Castano, M. E., Pereira-Simon, S., Hernandez, E. P., Elliot, S., & Cousins, S. W. (2005). Gender and estrogen supplementation increases severity of experimental choroidal neovascularization. *Experimental Eye Research*, *80*(3), 413–423. https://doi.org/10.1016/j.exer.2004.10.008

Espinosa-Heidmann, D. G., Suner, I., Hernandez, E. P., Frazier, W. D., Csaky, K. G., & Cousins, S. W. (2002). Age as an Independent Risk Factor for Severity of Experimental Choroidal Neovascularization. *Invest Ophthalmol Vis Sci*, *43*(5), 1567–1573.

Espinosa-Heidmann, D. G., Suner, I. J., Hernandez, E. P., Monroy, D., Csaky, K. G., & Cousins, S. W. (2003). Macrophage depletion diminishes lesion size and severity in experimental choroidal neovascularization. *Investigative Ophthalmology and Visual Science*, *44*(8), 3586–3592. https://doi.org/10.1167/iovs.03-0038

Fadini, G. P., Albiero, M., Bonora, B. M., & Avogaro, A. (2019). Angiogenic Abnormalities in Diabetes Mellitus: Mechanistic and Clinical Aspects. In *Journal of Clinical Endocrinology and Metabolism* (Vol. 104, Issue 11, pp. 5431–5444). Endocrine Society. https://doi.org/10.1210/jc.2019-00980

Fang, J. S., Hultgren, N. W., & Hughes, C. C. W. (2021a). Regulation of Partial and Reversible Endothelial-to-Mesenchymal Transition in Angiogenesis. *Frontiers in Cell and Developmental Biology*, *9*. https://doi.org/10.3389/fcell.2021.702021

Fang, J. S., Hultgren, N. W., & Hughes, C. C. W. (2021b). Regulation of Partial and Reversible Endothelial-to-Mesenchymal Transition in Angiogenesis. *Frontiers in Cell and Developmental Biology*, *9*. https://doi.org/10.3389/fcell.2021.702021

Fantin, A. (2022). Quantifying and Characterizing Angiogenesis Using the Postnatal Mouse Retina. *N: Benest, A.V. (Eds) Angiogenesis. Methods in Molecular Biology*, *2441*(Humana, New York, NY), 63–73.

Fantin, A., Vieira, J. M., Gestri, G., Denti, L., Schwarz, Q., Prykhozhij, S., Peri, F., Wilson, S. W., & Ruhrberg, C. (2010). Tissue macrophages act as cellular chaperones for vascular anastomosis downstream of VEGF-mediated endothelial tip cell induction. *Blood*, *116*(5), 829–840. https://doi.org/10.1182/blood-2009-12-257832

Feldker, N., Ferrazzi, F., Schuhwerk, H., Widholz, S. A., Guenther, K., Frisch, I., Jakob, K., Kleemann, J., Riegel, D., Bönisch, U., Lukassen, S., Eccles, R. L., Schmidl, C., Stemmler, M. P., Brabletz, T., & Brabletz, S. (2020). Genome-wide cooperation of EMT transcription factor ZEB 1 with YAP and AP -1 in breast cancer . *The EMBO Journal*, *39*(17). https://doi.org/10.15252/embj.2019103209

Fernández-Klett, F., Offenhauser, N., Dirnagl, U., Priller, J., & Lindauer, U. (2010). Pericytes in capillaries are contractile in vivo, but arterioles mediate functional hyperemia in the mouse brain. *Proceedings of the National Academy of Sciences of the United States of America*, *107*(51), 22290–22295. https://doi.org/10.1073/pnas.1011321108

Fernández-Robredo, P., Sancho, A., Johnen, S., Recalde, S., Gama, N., Thumann, G., Groll, J., & García-Layana, A. (2014). Current treatment limitations in age-related macular degeneration and future approaches based on cell therapy and tissue engineering. *Journal of Ophthalmology*, *2014*. https://doi.org/10.1155/2014/510285

Fernández-Robredo, P., Selvam, S., Powner, M. B., Sim, D. A., & Fruttiger, M. (2017). Neuropilin 1 involvement in choroidal and retinal neovascularisation. *PLoS ONE*, *12*(1). https://doi.org/10.1371/journal.pone.0169865

Ferrara, N., Gerber, H.-P., & LeCouter, J. (2003). The biology of VEGF and its receptors. *Nature Medicine*, *9*, 669–676. http://www.nature.com/naturemedicine

Ferrara, N., & Henzel, W. J. (1989). Pituitary follicular cells secrete a novel heparin-binding growth factor specific for vascular endothelial cells. *Biochemical and Biophysical Research Communications* , *161*(2), 851–858.

Ferris, F. L., Wilkinson, C. P., Bird, A., Chakravarthy, U., Chew, E., Csaky, K., & Sadda, S. R. (2013). Clinical classification of age-related macular degeneration. *Ophthalmology*, *120*(4), 844–851. https://doi.org/10.1016/j.ophtha.2012.10.036

Fiedler, U., Reiss, Y., Scharpfenecker, M., Grunow, V., Koidl, S., Thurston, G., Gale, N. W., Witzenrath, M., Rosseau, S., Suttorp, N., Sobke, A., Herrmann, M., Preissner, K. T., Vajkoczy, P., & Augustin, H. G. (2006). Angiopoietin-2 sensitizes endothelial cells to TNF-α and has a crucial role in the induction of inflammation. *Nature Medicine*, *12*(2), 235–239. https://doi.org/10.1038/nm1351

Flomerfelt, F. A., & Gress, R. E. (2015). Analysis of cell proliferation and homeostasis using edu labeling. In *T-Cell Development: Methods and Protocols* (pp. 211–220). Springer New York. https://doi.org/10.1007/978-1-4939-2809-5_18

Fogli, S., Del Re, M., Rofi, E., Posarelli, C., Figus, M., & Danesi, R. (2018). Clinical pharmacology of intravitreal anti-VEGF drugs. In *Eye (Basingstoke)* (Vol. 32, Issue 6, pp. 1010–1020). Nature Publishing Group. https://doi.org/10.1038/s41433-018-0021-7

Fogo, A. B., & Kon, V. (2010). The glomerulus - a view from the inside - the endothelial cell. In *International Journal of Biochemistry and Cell Biology* (Vol. 42, Issue 9, pp. 1388–1397). Elsevier Ltd. https://doi.org/10.1016/j.biocel.2010.05.015

Folkman, J. (1971). Tumor angiogenesis: therapeutic implications. *The New England Journal of Medicine* , *1182*(6), 285–21.

Fong, G.-H., Rossant, J., Gertsenstein, M., & Breitman, M. L. (1995). Role of the Flt-1 receptor tyrosine kinase in regulating the assembly of vascular endothelium. *Nature*, *376*, 66–70.

Fontaine, M., Herkenne, S., Ek, O., Paquot, A., Boeckx, A., Paques, C., Nivelles, O., Thiry, M., & Struman, I. (2022). Extracellular vesicles mediate communication between endothelial and vascular smooth muscle cells. *International Journal of Molecular Sciences*, *23*(1). https://doi.org/10.3390/ijms23010331

Fortini, M. E., Lai, Z., & Rubin, G. M. (1991). The Drosophila zfh-1 and zfh-2 genes encode novel proteins containing both zinc-finger and homeodomain motifs. In *Mechanisms of Development* (Vol. 34).

Fowler, M. J. (2008). Microvascular and Macrovascular Complications of Diabetes. *Clinical Diabetes*, *26*(2), 77–82. http://clinical.diabetesjournals.org

Frausto, R. F., Chung, D. D., Boere, P. M., Swamy, V. S., Duong, H. N. V., Kao, L., Azimov, R., Zhang, W., Carrigan, L., Wong, D., Morselli, M., Zakharevich, M., Hanser, E. M.,

Kassels, A. C., Kurtz, I., Pellegrini, M., & Aldave, A. J. (2019). ZEB1 insufficiency causes corneal endothelial cell state transition and altered cellular processing. *PLoS ONE*, *14*(6). https://doi.org/10.1371/journal.pone.0218279

Frausto, R. F., Swamy, V. S., Peh, G. S. L., Boere, P. M., Hanser, E. M., Chung, D. D., George, B. L., Morselli, M., Kao, L., Azimov, R., Wu, J., Pellegrini, M., Kurtz, I., Mehta, J. S., & Aldave, A. J. (2020). Phenotypic and functional characterization of corneal endothelial cells during in vitro expansion. *Scientific Reports*, *10*(1). https://doi.org/10.1038/s41598-020-64311-x

Fruttiger, M. (2007). Development of the retinal vasculature. *Angiogenesis*, *10*(2), 77–88. https://doi.org/10.1007/s10456-007-9065-1

Fruttiger, M., & Calver, A. R. (1996). PDGF Mediates a Neuron-Astrocyte Interaction in the Developing Retina. *Neuron*, *17*, 1117–1131.

Fu, R., Li, Y., Jiang, N., Ren, B. X., Zang, C. Z., Liu, L. J., Lv, W. C., Li, H. M., Weiss, S., Li, Z. Y., Lu, T., & Wu, Z. Q. (2020). Inactivation of endothelial ZEB1 impedes tumor progression and sensitizes tumors to conventional therapies. *Journal of Clinical Investigation*, *130*(3), 1252–1270. https://doi.org/10.1172/JCI131507

Fu, R., Lv, W. C., Xu, Y., Gong, M. Y., Chen, X. J., Jiang, N., Xu, Y., Yao, Q. Q., Di, L., Lu, T., Wang, L. M., Mo, R., & Wu, Z. Q. (2020). Endothelial ZEB1 promotes angiogenesis-dependent bone formation and reverses osteoporosis. *Nature Communications*, *11*(1). https://doi.org/10.1038/s41467-019-14076-3

Funahashi, J., Sekido, R., Murai, K., Kamachi, Y., & Kondoh, H. (1993). Delta-crystallin enhancer binding protein delta EF1 is a zinc finger-homeodomain protein implicated in postgastrulation embryogenesis. *Development*, *119*(2), 433–446.

Funahashi, J.-I., Kamachi, Y., Goto+, K., & Kondoh, H. (1991). Identification of nuclear factor 6EF1 and its binding site essential for lens-specific activity of the 61-crystallin enhancer. *Nucleic Acids Research*, *19*(13), 3543–3547.

Gaengel, K., Genové, G., Armulik, A., & Betsholtz, C. (2009). Endothelial-mural cell signaling in vascular development and angiogenesis. In *Arteriosclerosis, Thrombosis, and Vascular Biology* (Vol. 29, Issue 5, pp. 630–638). https://doi.org/10.1161/ATVBAHA.107.161521

Galley, H. F., & Webster, N. R. (2004). Physiology of the endothelium. *British Journal of Anaesthesia*, *93*(1), 105–113. https://doi.org/10.1093/bja/aeh163

Gerhardt, H., Golding, M., Fruttiger, M., Ruhrberg, C., Lundkvist, A., Abramsson, A., Jeltsch, M., Mitchell, C., Alitalo, K., Shima, D., & Betsholtz, C. (2003). VEGF guides angiogenic sprouting utilizing endothelial tip cell filopodia. *Journal of Cell Biology*, *161*(6), 1163–1177. https://doi.org/10.1083/jcb.200302047

Gerhardt, H., Ruhrberg, C., Abramsson, A., Fujisawa, H., Shima, D., & Betsholtz, C. (2004). Neuropilin-1 is required for endothelial tip cell guidance in the developing central nervous system. *Developmental Dynamics*, *231*(3), 503–509. https://doi.org/10.1002/dvdy.20148

Ghasemi, M., Turnbull, T., Sebastian, S., & Kempson, I. (2021). The mtt assay: Utility, limitations, pitfalls, and interpretation in bulk and single-cell analysis. *International Journal of Molecular Sciences*, *22*(23). https://doi.org/10.3390/ijms222312827

Ghasemi Nasab, M. S., Niroomand-Oscuii, H., Bazmara, H., & Soltani, M. (2022). Morphogenetic Mechanisms of Endothelial Cells During Lumen Formation in Sprouting Angiogenesis. *Multidisciplinary Cancer Investigation*, *6*(2), 1–8. https://doi.org/10.30699/mci.6.2.523-1

Gimbrone, M. A., & García-Cardeña, G. (2016). Endothelial Cell Dysfunction and the Pathobiology of Atherosclerosis. *Circulation Research*, *118*(4), 620–636. https://doi.org/10.1161/CIRCRESAHA.115.306301

Gitter, A., Siegfried, Z., Klutstein, M., Fornes, O., Oliva, B., Simon, I., & Bar-Joseph, Z. (2009). Backup in gene regulatory networks explains differences between binding and knockout results. *Molecular Systems Biology*, *5*(1). https://doi.org/10.1038/msb.2009.33

Gong, Y., Li, J., Sun, Y., Fu, Z., Liu, C. H., Evans, L., Tian, K., Saba, N., Fredrick, T., Morss, P., Chen, J., & Smith, L. E. H. (2015). Optimization of an image-guided laser-induced choroidal neovascularization model in mice. *PLoS ONE*, *10*(7). https://doi.org/10.1371/journal.pone.0132643

Gorski, T., & De Bock, K. (2019). Metabolic regulation of exercise-induced angiogenesis. *Vascular Biology*, *1*(1), H1–H8. https://doi.org/10.1530/vb-19-0008

Green, K. R., Beazley-Long, N., Lynch, A. P., Allen, C. L., Bates, D. O., & Benest, A. V. (2022). Quantification of Angiogenesis in Laser Choroidal Neovascularization. In *Methods in Molecular Biology* (Vol. 2441, pp. 223–231). Humana Press Inc. https://doi.org/10.1007/978-1-0716-2059-5_17

Gu, X., Ma, Y., Liu, Y., & Wan, Q. (2021). Measurement of mitochondrial respiration in adherent cells by Seahorse XF96 Cell Mito Stress Test. *STAR Protocols*, *2*(1). https://doi.org/10.1016/j.xpro.2020.100245

Guo, Y., Lu, X., Chen, Y., Clark, G., Trent, J., Cuatrecasas, M., Emery, D., Song, Z. H., Chariker, J., Rouchka, E., Postigo, A., Liu, Y., & Dean, D. C. (2022). Opposing roles of ZEB1 in the cytoplasm and nucleus control cytoskeletal assembly and YAP1 activity. *Cell Reports*, *41*(1). https://doi.org/10.1016/j.celrep.2022.111452

Hackett, S. F., Wiegand, S., Yancopoulos, G., & Campochiaro, P. A. (2002). Angiopoietin-2 plays an important role in retinal angiogenesis. *Journal of Cellular Physiology*, *192*(2), 182–187. https://doi.org/10.1002/jcp.10128

Hamik, A., Lin, Z., Kumar, A., Balcells, M., Sinha, S., Katz, J., Feinberg, M. W., Gerszten, R. E., Edelman, E. R., & Jain, M. K. (2007). Kruppel-like factor 4 regulates endothelial inflammation. *Journal of Biological Chemistry*, *282*(18), 13769–13779. https://doi.org/10.1074/jbc.M700078200

Hanahan, D., & Folkman, J. (1996). Patterns and Emerging Mechanisms Review of the Angiogenic Switch during Tumorigenesis. In *Cell* (Vol. 86).

Hanahan, D., & Weinberg, R. A. (2011). Hallmarks of cancer: The next generation. In *Cell* (Vol. 144, Issue 5, pp. 646–674). https://doi.org/10.1016/j.cell.2011.02.013

Hartmann, D. A., Underly, R. G., Grant, R. I., Watson, A. N., Lindner, V., & Shih, A. Y. (2015). Pericyte structure and distribution in the cerebral cortex revealed by high-resolution imaging of transgenic mice. *Neurophotonics*, *2*(4), 041402. https://doi.org/10.1117/1.nph.2.4.041402

Hashiya, N., Jo, N., Aoki, M., Matsumoto, K., Nakamura, T., Sato, Y., Ogata, N., Ogihara, T., Kaneda, Y., & Morishita, R. (2004). In vivo evidence of angiogenesis induced by transcription factor ets-1: Ets-1 is located upstream of angiogenesis cascade. *Circulation*, *109*(24), 3035–3041. https://doi.org/10.1161/01.CIR.0000130643.41587.DB

Hashizume, H., Falcón, B. L., Kuroda, T., Baluk, P., Coxon, A., Yu, D., Bready, J. V., Oliner, J. D., & McDonald, D. M. (2010). Complementary actions of inhibitors of angiopoietin-2 and VEGF on tumor angiogenesis and growth. *Cancer Research*, *70*(6), 2213–2223. https://doi.org/10.1158/0008-5472.CAN-09-1977

Haynes, B. A., Yang, L. F., Huyck, R. W., Lehrer, E. J., Turner, J. M., Barabutis, N., Correll, V. L., Mathiesen, A., McPheat, W., Semmes, O. J., & Dobrian, A. D. (2019). Endothelial-to-mesenchymal transition in human adipose tissue vasculature alters the particulate secretome and induces endothelial dysfunction. *Arteriosclerosis, Thrombosis, and Vascular Biology*, *39*(10), 2168–2191. https://doi.org/10.1161/ATVBAHA.119.312826

Heier, J. S., Brown, D. M., Chong, V., Korobelnik, J. F., Kaiser, P. K., Nguyen, Q. D., Kirchhof, B., Ho, A., Ogura, Y., Yancopoulos, G. D., Stahl, N., Vitti, R., Berliner, A. J., Soo, Y., Anderesi, M., Groetzbach, G., Sommerauer, B., Sandbrink, R., Simader, C., & Schmidt-Erfurth, U. (2012). Intravitreal aflibercept (VEGF trap-eye) in wet age-related macular degeneration. *Ophthalmology*, *119*(12), 2537–2548. https://doi.org/10.1016/j.ophtha.2012.09.006

Hellste Ylva, H. B. (2014). Capillary growth in human skeletal muscle: physiological factors and the balance between pro-angiogenic and angiostatic factors. *Biochemical Society Transactions* , *42*(2), 1616–1622.

Hellström, M., Gerhardt, H., Kalén, M., Li, X., Eriksson, U., Wolburg, H., & Betsholtz, C. (2001). Lack of Pericytes Leads to Endothelial Hyperplasia and Abnormal Vascular Morphogenesis. In *The Journal of Cell Biology* (Vol. 153, Issue 3). http://www.jcb.org/cgi/content/full/153/3/543

Hellström, M., Kalén, M., Lindahl, P., Abramsson, A., & Betsholtz, C. (1999). Role of PDGF-B and PDGFR-beta in recruitment of vascular smooth muscle cells and pericytes during embryonic blood vessel formation in the mouse. *Development*, *126*(14), 3047–3055.

Hellström, M., Phng, L. K., Hofmann, J. J., Wallgard, E., Coultas, L., Lindblom, P., Alva, J., Nilsson, A. K., Karlsson, L., Gaiano, N., Yoon, K., Rossant, J., Iruela-Arispe, M. L., Kalén, M., Gerhardt, H., & Betsholtz, C. (2007). Dll4 signalling through Notch1 regulates formation of tip cells during angiogenesis. *Nature*, *445*(7129), 776–780. https://doi.org/10.1038/nature05571

Heo, S. H., Choi, Y. J., Ryoo, H. M., & Cho, J. Y. (2010). Expression profiling of ETS and MMP factors in VEGF-activated endothelial cells: Role of MMP-10 in VEGF-induced angiogenesis. *Journal of Cellular Physiology*, *224*(3), 734–742. https://doi.org/10.1002/jcp.22175

Hernández-Reséndiz, S., Muñoz-Vega, M., Contreras, W. E., Crespo-Avilan, G. E., Rodriguez-Montesinos, J., Arias-Carrión, O., Pérez-Méndez, O., Boisvert, W. A., Preissner, K. T., Cabrera-Fuentes, H. A., & Hector, C.-F. (2018). Responses of Endothelial Cells Towards Ischemic Conditioning Following Acute Myocardial Infarction HHS Public Access. *Cond Med*, *1*(5), 247–258.

Hill, R. A., Tong, L., Yuan, P., Murikinati, S., Gupta, S., & Grutzendler, J. (2015). Regional Blood Flow in the Normal and Ischemic Brain Is Controlled by Arteriolar Smooth Muscle Cell Contractility and Not by Capillary Pericytes. *Neuron*, *87*(1), 95–110. https://doi.org/10.1016/j.neuron.2015.06.001

Hiratsuka, S., Minowa, O., Kuno, J., Noda, T., & Shibuya, M. (1998). Flt-1 lacking the tyrosine kinase domain is sufficient for normal development and angiogenesis in mice. *PNAS*, *95*, 9349–9354. www.pnas.org.

Hodges, N. A., Suarez-Martinez, A. D., & Murfee, W. L. (2018). Understanding angiogenesis during aging: opportunities for discoveries and new models. *Journal of Applied Physiology* , *125*(6), 1843–1850.

Horiguchi, K., Sakamoto, K., Koinuma, D., Semba, K., Inoue, A., Inoue, S., Fujii, H., Yamaguchi, A., Miyazawa, K., Miyazono, K., & Saitoh, M. (2012a). TGF-B drives

epithelial-mesenchymal transition through EF1-mediated downregulation of ESRP. *Oncogene*, *31*(26), 3190–3201. https://doi.org/10.1038/onc.2011.493

Horiguchi, K., Sakamoto, K., Koinuma, D., Semba, K., Inoue, A., Inoue, S., Fujii, H., Yamaguchi, A., Miyazawa, K., Miyazono, K., & Saitoh, M. (2012b). TGF-B drives epithelial-mesenchymal transition through EF1-mediated downregulation of ESRP. *Oncogene*, *31*(26), 3190–3201. https://doi.org/10.1038/onc.2011.493

Hosaka, T., Biggs III, W. H., Tieu, D., Boyer, A. D., Varki, N. M., Cavenee, W. K., & Arden, K. C. (2004). *Disruption of forkhead transcription factor (FOXO) family members in mice reveals their functional diversification*. www.pnas.orgcgidoi10.1073pnas.0400093101

Houck, K. A., Leung, D. W., Rowland, A. M., Winer, J., & Ferrara, N. (1992). Dual regulation of vascular endothelial growth factor bioavailability by genetic and proteolytic mechanisms. *Journal of Biological Chemistry*, *267*(36), 26031–26037. https://doi.org/10.1016/s0021-9258(18)35712-0

Hu, Z., Killion, P. J., & Iyer, V. R. (2007). Genetic reconstruction of a functional transcriptional regulatory network. *Nature Genetics*, *39*(5), 683–687. https://doi.org/10.1038/ng2012

Huang, H., He, J., Johnson, D., Wei, Y., Liu, Y., Wang, S., Lutty, G. A., Duh, E. J., & Semba, R. D. (2015). Deletion of placental growth factor prevents diabetic retinopathy and is associated with akt activation and HIF1α-VEGF pathway inhibition. *Diabetes*, *64*(1), 200–212. https://doi.org/10.2337/db14-0016

Hughes, S., & Chan-Ling, T. (2000). Roles of endothelial cell migration and apoptosis in vascular remodeling during development of the central nervous system. *Microcirculation*, *7*(5), 317–333. https://doi.org/10.1111/j.1549-8719.2000.tb00131.x

Hultgren, N. W., Fang, J. S., Ziegler, M. E., Ramirez, R. N., Phan, D. T. T., Hatch, M. M. S., Welch-Reardon, K. M., Paniagua, A. E., Kim, L. S., Shon, N. N., Williams, D. S., Mortazavi, A., & Hughes, C. C. W. (2020). Slug regulates the Dll4-Notch-VEGFR2 axis to control endothelial cell activation and angiogenesis. *Nature Communications*, *11*(1). https://doi.org/10.1038/s41467-020-18633-z

Inuzuka, T., Tsuda, M., Tanaka, S., Kawaguchi, H., Higashi, Y., & Ohba, Y. (2009). Integral role of transcription factor 8 in the negative regulation of tumor angiogenesis. *Cancer Research*, *69*(4), 1678–1684. https://doi.org/10.1158/0008-5472.CAN-08-3620

Ishida, S., Yamashiro, K., Usui, T., Kaji, Y., Ogura, Y., Hida, T., Honda, Y., Oguchi, Y., & Adamis, A. (2003). Leukocytes mediate retinal vascular remodeling during development and vaso-obliteration in disease. *Nature Medicine*, *781*(8), 9–6.

Ivins, S., Chappell, J., Vernay, B., Suntharalingham, J., Martineau, A., Mohun, T. J., & Scambler, P. J. (2015). The CXCL12/CXCR4 Axis Plays a Critical Role in Coronary Artery Development. *Developmental Cell*, *33*(4), 455–468. https://doi.org/10.1016/j.devcel.2015.03.026

Iwasaka, C., Tanaka, K., Abe, M., & Sato, Y. (1996). Ets-1 regulates angiogenesis by inducing the expression of urokinase-type plasminogen activator and matrix metalloproteinase-1 and the migration of vascular endothelial cells. *Journal of Cellular Physiology*, *169*(3), 522–531. https://doi.org/10.1002/(SICI)1097-4652(199612)169:3<522::AID-JCP12>3.0.CO;2-7

Jakobsson, L., Franco, C. A., Bentley, K., Collins, R. T., Ponsioen, B., Aspalter, I. M., Rosewell, I., Busse, M., Thurston, G., Medvinsky, A., Schulte-Merker, S., & Gerhardt, H. (2010). Endothelial cells dynamically compete for the tip cell position during angiogenic sprouting. *Nature Cell Biology*, *12*(10), 943–953. https://doi.org/10.1038/ncb2103

Jang, J. J., Hoai-Ky, B. ;, Ho, V., Kwan, H. H., Luis, ;, Fajardo, F., & Cooke, J. P. (2000). *Angiogenesis Is Impaired by Hypercholesterolemia Role of Asymmetric Dimethylarginine*. http://www.circulationaha.org

Jia, T., Jacquet, T., Dalonneau, F., Coudert, P., Vaganay, E., Exbrayat-Héritier, C., Vollaire, J., Josserand, V., Ruggiero, F., Coll, J. L., & Eymin, B. (2021). FGF-2 promotes angiogenesis through a SRSF1/SRSF3/SRPK1-dependent axis that controls VEGFR1 splicing in endothelial cells. *BMC Biology*, *19*(1). https://doi.org/10.1186/s12915-021-01103-3

Jin, L., Zhang, Y., Liang, W., Lu, X., Piri, N., Wang, W., Kaplan, H. J., Dean, D. C., Zhang, L., & Liu, Y. (2020). Zeb1 promotes corneal neovascularization by regulation of vascular endothelial cell proliferation. *Communications Biology*, *3*(1). https://doi.org/10.1038/s42003-020-1069-z

Jonas, J. B., Tao, Y., Neumaier, M., & Findeisen, P. (2010). Monocyte Chemoattractant Protein 1, Intercellular Adhesion Molecule 1, and Vascular Cell Adhesion Molecule 1 in Exudative Age-Related Macular Degeneration. *Arch Ophthalmol*, *128*(10), 1281–1286. https://jamanetwork.com/

Joseph, J. V., Conroy, S., Tomar, T., Eggens-Meijer, E., Bhat, K., Copray, S., Walenkamp, A. M. E., Boddeke, E., Balasubramanyian, V., Wagemakers, M., Den Dunnen, W. F. A., & Kruyt, F. A. E. (2014). TGF-β is an inducer of ZEB1-dependent mesenchymal transdifferentiation in glioblastoma that is associated with tumor invasion. *Cell Death and Disease*, *5*(10). https://doi.org/10.1038/cddis.2014.395

Joukov, V., Pajusola, K., Kaipainen, A., Chilov, D., Lahtinen, I., Kukk, E., Sakselal, O., Kalkkinen2, N., Alitaio3, K., Alitalo, K., & Eriksson, U. (1996). A novel vascular

endothelial growth factor, VEGF-C, is a ligand for the Flt4 (VEGFR-3) and KDR (VEGFR-2) receptor tyrosine kinases. In *The EMBO Journal* (Vol. 15, Issue 2).

Kadry, H., Noorani, B., & Cucullo, L. (2020). A blood–brain barrier overview on structure, function, impairment, and biomarkers of integrity. In *Fluids and Barriers of the CNS* (Vol. 17, Issue 1). BioMed Central Ltd. https://doi.org/10.1186/s12987-020-00230-3

Kahlert, U. D., Maciaczyk, D., Doostkam, S., Orr, B. A., Simons, B., Bogiel, T., Reithmeier, T., Prinz, M., Schubert, J., Niedermann, G., Brabletz, T., Eberhart, C. G., Nikkhah, G., & Maciaczyk, J. (2012). Activation of canonical WNT/β-catenin signaling enhances in vitro motility of glioblastoma cells by activation of ZEB1 and other activators of epithelial-to-mesenchymal transition. *Cancer Letters*, *325*(1), 42–53. https://doi.org/10.1016/j.canlet.2012.05.024

Kaipatnen, A., Korhonen, J., Mustonen, T., Van Hinsberght, V. W. M., Fangt, G.-H., Dumontt, D., Breitmant, M., & Alitalo, K. (1995). Expression of the fms-like tyrosine kinase 4 gene becomes restricted to lymphatic endothelium during development. In *Medical Sciences* (Vol. 92).

Kalinowski, L., Janaszak-Jasiecka, A., Siekierzycka, A., Bartoszewska, S., Woźniak, M., Lejnowski, D., Collawn, J. F., & Bartoszewski, R. (2016). Posttranscriptional and transcriptional regulation of endothelial nitric-oxide synthase during hypoxia: The role of microRNAs. In *Cellular and Molecular Biology Letters* (Vol. 21, Issue 1). BioMed Central Ltd. https://doi.org/10.1186/s11658-016-0017-x

Kalluri, R., & Weinberg, R. A. (2009). The basics of epithelial-mesenchymal transition. In *Journal of Clinical Investigation* (Vol. 119, Issue 6, pp. 1420–1428). https://doi.org/10.1172/JCI39104

Kalucka, J., Bierhansl, L., Conchinha, N. V., Missiaen, R., Elia, I., Brüning, U., Scheinok, S., Treps, L., Cantelmo, A. R., Dubois, C., de Zeeuw, P., Goveia, J., Zecchin, A., Taverna, F., Morales-Rodriguez, F., Brajic, A., Conradi, L. C., Schoors, S., Harjes, U., … Carmeliet, P. (2018). Quiescent Endothelial Cells Upregulate Fatty Acid β-Oxidation for Vasculoprotection via Redox Homeostasis. *Cell Metabolism*, *28*(6), 881-894.e13. https://doi.org/10.1016/j.cmet.2018.07.016

Kalucka, J., de Rooij, L. P. M. H., Goveia, J., Rohlenova, K., Dumas, S. J., Meta, E., Conchinha, N. V., Taverna, F., Teuwen, L. A., Veys, K., García-Caballero, M., Khan, S., Geldhof, V., Sokol, L., Chen, R., Treps, L., Borri, M., de Zeeuw, P., Dubois, C., … Carmeliet, P. (2020). Single-Cell Transcriptome Atlas of Murine Endothelial Cells. *Cell*, *180*(4), 764-779.e20. https://doi.org/10.1016/j.cell.2020.01.015

Kanno, H., Yamamoto, I., Nishikawa, R., Matsutani, M., Wakabayashi, T., Yoshida, J., Shitara, N., Yamasaki, I., & Shuin, T. (2009). Spinal cord hemangioblastomas in von Hippel-Lindau disease. *Spinal Cord*, *47*(6), 447–452. https://doi.org/10.1038/sc.2008.151

Karaman, S., Paavonsalo, S., Heinolainen, K., Lackman, M. H., Ranta, A., Hemanthakumar, K. A., Kubota, Y., & Alitalo, K. (2022). Interplay of vascular endothelial growth factor receptors in organ-specific vessel maintenance. *Journal of Experimental Medicine*, *219*(3). https://doi.org/10.1084/jem.20210565

Kása, A., Csortos, C., & Verin, A. D. (2015). Cytoskeletal mechanisms regulating vascular endothelial barrier function in response to acute lung injury. In *Tissue Barriers* (Vol. 3, Issue 1). Taylor and Francis Inc. https://doi.org/10.4161/21688370.2014.974448

Kasahara, Y., Tuder, R. M., Taraseviciene-Stewart, L., Le Cras, T. D., Abman, S., Hirth, P. K., Waltenberger, J., & Voelkel, N. F. (2000). Inhibition of VEGF receptors causes lung cell apoptosis and emphysema. *Journal of Clinical Investigation*, *106*(11), 1311–1319. https://doi.org/10.1172/JCI10259

Kauppinen, A., Paterno, J. J., Blasiak, J., Salminen, A., & Kaarniranta, K. (2016). Inflammation and its role in age-related macular degeneration. In *Cellular and Molecular Life Sciences* (Vol. 73, Issue 9, pp. 1765–1786). Birkhauser Verlag AG. https://doi.org/10.1007/s00018-016-2147-8

Kavurma, M. M., Bursill, C., Stanley, C. P., Passam, F., Cartland, S. P., Patel, S., Loa, J., Figtree, G. A., Golledge, J., Aitken, S., & Robinson, D. A. (2022). Endothelial cell dysfunction: Implications for the pathogenesis of peripheral artery disease. *Frontiers in Cardiovascular Medicine* , *9*.

Kendall, R. L., & Thomas, K. A. (1993). Inhibition of vascular endothelial cell growth factor activity by an endogenously encoded soluble receptor (endothelial ceils/mitogenic inhibitor/alternative transcription/angiogenesis). In *Proc. Natl. Acad. Sci. USA* (Vol. 90).

Kim, J. (2018). MicroRNAs as critical regulators of the endothelial to mesenchymal transition in vascular biology. In *BMB Reports* (Vol. 51, Issue 2, pp. 65–72). The Biochemical Society of the Republic of Korea. https://doi.org/10.5483/BMBRep.2018.51.2.011

Kim, Y. H., Choi, J., Yang, M. J., Hong, S. P., Lee, C. kun, Kubota, Y., Lim, D. S., & Koh, G. Y. (2019). A MST1–FOXO1 cascade establishes endothelial tip cell polarity and facilitates sprouting angiogenesis. *Nature Communications*, *10*(1). https://doi.org/10.1038/s41467-019-08773-2

Kinsella, M. G., & Fitzharris, T. P. (1980). Origin of cushion tissue in the developing chick heart: Cinematographic recordings of in situ formation. *Science*, *207*(4437), 1359–1360. https://doi.org/10.1126/science.7355294

Kitchens, J. W., Kassem, N., Wood, W., Stone, T. W., Isernhagen, R., Wood, E., Hancock, B. A., Radovich, M., Waymire, J., Li, L., & Schneider, B. P. (2013). A pharmacogenetics study to predict outcome in patients receiving anti-VEGF

therapy in age related macular degeneration. *Clinical Ophthalmology*, *7*, 1987–1993. https://doi.org/10.2147/OPTH.S39635

Korn, C., & Augustin, H. G. (2015). Mechanisms of Vessel Pruning and Regression. In *Developmental Cell* (Vol. 34, Issue 1, pp. 5–17). Cell Press. https://doi.org/10.1016/j.devcel.2015.06.004

Korn, C., Scholz, B., Hu, J., Srivastava, K., Wojtarowicz, J., Arnsperger, T., Adams, R. H., Boutros, M., Augustin, H. G., & Augustin, I. (2014). Endothelial cell-derived non-canonical Wnt ligands control vascular pruning in angiogenesis. *Development (Cambridge)*, *141*(8), 1757–1766. https://doi.org/10.1242/dev.104422

Krafchak, C. M., Pawar, H., Moroi, S. E., Sugar, A., Lichter, P. R., Mackey, D. A., Mian, S., Nairus, T., Elner, V., Schteingart, M. T., Downs, C. A., Guckian Kijek, T., Johnson, J. M., Trager, E. H., Rozsa, F. W., Nawajes Ali Mandal, M., Epstein, M. P., Vollrath, D., Ayyagari, R., … Kellogg Eye Center, W. K. (2005). Mutations in TCF8 Cause Posterior Polymorphous Corneal Dystrophy and Ectopic Expression of COL4A3 by Corneal Endothelial Cells. In *Am. J. Hum. Genet* (Vol. 77).

Krebs, A. M., Mitschke, J., Losada, M. L., Schmalhofer, O., Boerries, M., Busch, H., Boettcher, M., Mougiakakos, Di., Reichardt, W., Bronsert, P., Brunton, V. G., Pilarsky, C., Winkler, T. H., Brabletz, S., Stemmler, M. P., & Brabletz, T. (2017). The EMT-activator Zeb1 is a key factor for cell plasticity and promotes metastasis in pancreatic cancer. *Nature Cell Biology*, *19*(5), 518–529. https://doi.org/10.1038/ncb3513

Krebs, I., Glittenberg, C., Ansari-Shahrezaei, S., Hagen, S., Steiner, I., & Binder, S. (2013). Non-responders to treatment with antagonists of vascular endothelial growth factor in age-related macular degeneration. *British Journal of Ophthalmology*, *97*(11), 1443–1446. https://doi.org/10.1136/bjophthalmol-2013-303513

Kretzschmar, K., & Watt, F. M. (2012). Lineage tracing. In *Cell* (Vol. 148, Issues 1–2, pp. 33–45). Elsevier B.V. https://doi.org/10.1016/j.cell.2012.01.002

Krishnamachary, B., Zagzag, D., Nagasawa, H., Rainey, K., Okuyama, H., Baek, J. H., & Semenza, G. L. (2006). Hypoxia-inducible factor-1-dependent repression of E-cadherin in von Hippel-Lindau tumor suppressor-null renal cell carcinoma mediated by TCF3, ZFHX1A, and ZFHX1B. *Cancer Research*, *66*(5), 2725–2731. https://doi.org/10.1158/0008-5472.CAN-05-3719

Krishnamoorthi, M. K., Thandavarayan, R. A., Youker, K. A., & Bhimaraj, A. (2022). An In Vitro Platform to Study Reversible Endothelial-to-Mesenchymal Transition. *Frontiers in Pharmacology*, *13*. https://doi.org/10.3389/fphar.2022.912660

Krock, B. L., Skuli, N., & Simon, M. C. (2011). Hypoxia-Induced Angiogenesis: Good and Evil. *Genes and Cancer*, *2*(12), 1117–1133. https://doi.org/10.1177/1947601911423654

Kubis, N., Besnard, S., Bastien Silvestre, J.-S. Â., Feletou, M., Huang, P. L., Le Â Vy, B. I., & Tedgui, A. (2002). Decreased arteriolar density in endothelial nitric oxide synthase knockout mice is due to hypertension, not to the constitutive defect in endothelial nitric oxide synthase enzyme. *Journal of Hypertension*, *20*(2), 273–280.

Kurz, H., Gärtner, T., Eggli, P. S., & Christ, B. (1996). First Blood Vessels in the Avian Neural Tube Are Formed by a Combination of Dorsal Angioblast Immigration and Ventral Sprouting of Endothelial Cells. In *DEVELOPMENTAL BIOLOGY* (Vol. 173).

Lambert, V., Lecomte, J., Hansen, S., Blacher, S., Gonzalez, M. L. A., Struman, I., Sounni, N. E., Rozet, E., De Tullio, P., Foidart, J. M., Rakic, J. M., & Noel, A. (2013). Laser-induced choroidal neovascularization model to study age-related macular degeneration in mice. *Nature Protocols*, *8*(11), 2197–2211. https://doi.org/10.1038/nprot.2013.135

Lawson, C., & Wolf, S. (2009). ICAM-1 signaling in endothelial cells. *Pharmacological Reports*, *61*(1), 22–32.

Lawson, N. D., Scheer, N., Pham, V. N., Kim, C., Chitnis, A. B., Campos-Ortega, J. A., & Weinstein, B. M. (2001). Notch signaling is required for arterial-venous differentiation during embryonic vascular development. *Development*, *128*(19), 3675–3683.

Leclech, C., Natale, C. F., & Barakat, A. I. (2021). The basement membrane as a structured surface – role in vascular health and disease. In *Journal of Cell Science* (Vol. 133, Issue 18). Company of Biologists Ltd. https://doi.org/10.1242/jcs.239889

Lee, H.-W., Adachi, T., Pak, B., Park, S., Hu, X., Choi, W., Kowalski, P. S., Chang, C. H., Clapham, K. R., Lee, A., Papangeli, I., Kim, J., Han, O., Park, J., Anderson, D. G., Simons, M., Jin, S.-W., & Chun, H. J. (2023). BMPR1A promotes ID2–ZEB1 interaction to suppress excessive endothelial to mesenchymal transition. *Cardiovascular Research*, *119*(3), 813–825. https://doi.org/10.1093/cvr/cvac159

Lee, H.-W., Adachi, T., Pak, B., Park, S., Hu, X., Choi, W., Kowalski, P. S., Chang, C.-H., Clapham, K. R., Lee, A., Papangeli, I., Kim, J., Han, O., Park, J., Anderson, D. G., Simons, M., Jin, S.-W., & Chun, H. J. (2022). BMPR1A promotes ID2–ZEB1 interaction to suppress excessive endothelial to mesenchymal transition. *Cardiovascular Research*. https://doi.org/10.1093/cvr/cvac159

Lee, S., Chen, T. T., Barber, C. L., Jordan, M. C., Murdock, J., Desai, S., Ferrara, N., Nagy, A., Roos, K. P., & Iruela-Arispe, M. L. (2007a). Autocrine VEGF Signaling Is Required for Vascular Homeostasis. *Cell*, *130*(4), 691–703. https://doi.org/10.1016/j.cell.2007.06.054

Lee, S., Chen, T. T., Barber, C. L., Jordan, M. C., Murdock, J., Desai, S., Ferrara, N., Nagy, A., Roos, K. P., & Iruela-Arispe, M. L. (2007b). Autocrine VEGF Signaling Is Required

for Vascular Homeostasis. *Cell*, *130*(4), 691–703. https://doi.org/10.1016/j.cell.2007.06.054

Lehmann, W., Mossmann, D., Kleemann, J., Mock, K., Meisinger, C., Brummer, T., Herr, R., Brabletz, S., Stemmler, M. P., & Brabletz, T. (2016). ZEB1 turns into a transcriptional activator by interacting with YAP1 in aggressive cancer types. *Nature Communications*, *7*. https://doi.org/10.1038/ncomms10498

Lenard, A., Ellertsdottir, E., Herwig, L., Krudewig, A., Sauteur, L., Belting, H. G., & Affolter, M. (2013). In vivo analysis reveals a highly stereotypic morphogenetic pathway of vascular anastomosis. *Developmental Cell*, *25*(5), 492–506. https://doi.org/10.1016/j.devcel.2013.05.010

Li, H., Wallerath, T., & Förstermann, U. (2002). Physiological mechanisms regulating the expression of endothelial-type NO synthase. *Nitric Oxide*, *7*(2), 132–147. www.academicpress.com

Li, J., Qu, X., & Bertram, J. F. (2009). Endothelial-myofibroblast transition contributes to the early development of diabetic renal interstitial fibrosis in streptozotocin-induced diabetic mice. *American Journal of Pathology*, *175*(4), 1380–1388. https://doi.org/10.2353/ajpath.2009.090096

Li, S., Zhang, H.-Y., Du, Z.-X., Li, C., An, M.-X., Zong, Z.-H., Liu, B.-Q., & Wang, H.-Q. (2016). Induction of epithelial-mesenchymal transition (EMT) by Beclin 1 knockdown via posttranscriptional upregulation of ZEB1 in thyroid cancer cells. *Oncotarget*, *7*(43), 70364–70377. www.impactjournals.com/oncotarget

Li, W., Liu, C., Burns, N., Hayashi, J., Yoshida, A., Sajja, A., González-Hernández, S., Gao, J. L., Murphy, P. M., Kubota, Y., Zou, Y. R., Nagasawa, T., & Mukouyama, Y. suke. (2021). Alterations in the spatiotemporal expression of the chemokine receptor CXCR4 in endothelial cells cause failure of hierarchical vascular branching. *Developmental Biology*, *477*, 70–84. https://doi.org/10.1016/j.ydbio.2021.05.008

Li, X., Sun, X., & Carmeliet, P. (2019). Hallmarks of Endothelial Cell Metabolism in Health and Disease. In *Cell Metabolism* (Vol. 30, Issue 3, pp. 414–433). Cell Press. https://doi.org/10.1016/j.cmet.2019.08.011

Li, Z., He, P., Xu, Y., Deng, Y., Gao, Y., & Chen, S.-L. (2022). In vivo evaluation of a lipopolysaccharide-induced ear vascular leakage model in mice using photoacoustic microscopy. *Biomedical Optics Express*, *13*(9), 4802. https://doi.org/10.1364/boe.471079

Libby, P., Buring, J. E., Badimon, L., Hansson, G. K., Deanfield, J., Bittencourt, M. S., Tokgözoğlu, L., & Lewis, E. F. (2019). Atherosclerosis. *Nature Reviews Disease Primers* , *5*(1), 56.

Liskova, P., Tuft, S. J., Gwilliam, R., Ebenezer, N. D., Jirsova, K., Prescott, Q., Martincova, R., Pretorius, M., Sinclair, N., Boase, D. L., Jeffrey, M. J., Deloukas, P., Hardcastle, A. J., Filipec, M., & Bhattacharya, S. S. (2007). Novel mutations in the ZEB1 gene identified in Czech and British patients with posterior polymorphous corneal dystrophy. *Human Mutation*, *28*(6), 638. https://doi.org/10.1002/humu.9495

Liu, L., Tong, Q., Liu, S., Cui, J., Zhang, Q., Sun, W., & Yang, S. (2016). ZEB1 upregulates VEGF expression and stimulates angiogenesis in breast cancer. *PLoS ONE*, *11*(2). https://doi.org/10.1371/journal.pone.0148774

Liu, Y., Cox, S. R., Morita T, & Kourembanas S. (1995). Hypoxia regulates vascular endothelial growth factor gene expression in endothelial cells. Identification of a 5' enhancer. *Circulation Research*, *77*(3), 638–643.

Liu, Y., El-Naggar, S., Darling, D. S., Higashi, Y., & Dean, D. C. (2008). ZEB1 Links Epithelial-Mesenchymal Transition and Cellular Senescence. *Development*, *135*(5), 579–588. http://www.upstate.com/misc/protocol

Liu, Y., Peng, X., Tan, J., Darling, D. S., Kaplan, H. J., & Dean, D. C. (2009). Zeb1 Mutant Mice as a Model of Posterior Corneal Dystrophy. *Invest Opthalmol Vis Sci*, *45*(9), 1843–1849. http://frodo.wi.mit.edu/cgi-bin/primer3/primer3.cgi

Liu, Y., Sánchez-Tilló, E., Lu, X., Huang, L., Clem, B., Telang, S., Jenson, A. B., Cuatrecasas, M., Chesney, J., Postigo, A., & Dean, D. C. (2014). The ZEB1 transcription factor acts in a negative feedback loop with miR200 downstream of ras and Rb1 to regulate Bmi1 expression. *Journal of Biological Chemistry*, *289*(7), 4116–4125. https://doi.org/10.1074/jbc.M113.533505

Liu, Z. L., Chen, H. H., Zheng, L. L., Sun, L. P., & Shi, L. (2023). Angiogenic signaling pathways and anti-angiogenic therapy for cancer. In *Signal Transduction and Targeted Therapy* (Vol. 8, Issue 1). Springer Nature. https://doi.org/10.1038/s41392-023-01460-1

Llorens, M. C., Lorenzatti, G., Cavallo, N. L., Vaglienti, M. V., Perrone, A. P., Carenbauer, A. L., Darling, D. S., & Cabanillas, A. M. (2016). Phosphorylation Regulates Functions of ZEB1 Transcription Factor. *Journal of Cellular Physiology*, *231*(10), 2205–2217. https://doi.org/10.1002/jcp.25338

Lobov, I. B., Renard, R. A., Papadopoulos, N., Gale, N. W., Thurston, G., Yancopoulos, G. D., & Wiegand, S. J. (2007). Delta-like ligand 4 (Dll4) is induced by VEGF as a negative regulator of angiogenic sprouting. *PNAS*, *104*(9), 3219–3224. www.pnas.orgcgidoi10.1073pnas.0611206104

Lolmède, K., Duffat, C., Zakaroff-Girard, A., & Bouloumié, A. (2011). Immune cells in adipose tissue: Key players in metabolic disorders. *Diabetes Metab*, *37*(4), 283–290.

Londesborough, A., Vaahtomeri, K., Tiainen, M., Katajisto, P., Ekman, N., Vallenius, T., & Mäkelä, T. P. (2008). LKB1 in endothelial cell is required for angiogenesis and TGFβ-mediated vascular smooth muscle cell recruitment. *Development*, *135*(13), 2331–2338. https://doi.org/10.1242/dev.017038

Lotfi, S., Patel, A. S., Mattock, K., Egginton, S., Smith, A., & Modarai, B. (2013). Towards a more relevant hind limb model of muscle ischaemia. In *Atherosclerosis* (Vol. 227, Issue 1, pp. 1–8). https://doi.org/10.1016/j.atherosclerosis.2012.10.060

Lu, J., Fei, F., Wu, C., Mei, J., Xu, J., & Lu, P. (2022). ZEB1: Catalyst of immune escape during tumor metastasis. In *Biomedicine and Pharmacotherapy* (Vol. 153). Elsevier Masson s.r.l. https://doi.org/10.1016/j.biopha.2022.113490

Maglione, D., Guerriero, V., Viglietto, G., Delli-Bovit, P., & Graziella Persico, M. (1991). Isolation of a human placenta cDNA coding for a protein related to the vascular permeability factor (growth factors/cancer/angiogenesis/protein proceing). In *Proc. Natl. Acad. Sci. USA* (Vol. 88). https://www.pnas.org

Maisonpierre, P. C., Suri, C., Jones, P. F., Bartunkova, S., Wiegand, S. J., Radziejewski, C., Compton, D., Mcclain, J., Aldrich, T. H., Papadopoulos, N., Daly, T. J., Davis, S., Sato, T. N., & Yancopoulos, G. D. (1997). Angiopoietin-2, a Natural Antagonist for Tie2 That Disrupts in vivo Angiogenesis. *Science*, *277*(5322), 55–60. https://www.science.org

Mammadzada, P., Corredoira, P. M., & André, H. (2020). The role of hypoxia-inducible factors in neovascular age-related macular degeneration: a gene therapy perspective. In *Cellular and Molecular Life Sciences* (Vol. 77, Issue 5, pp. 819–833). Springer. https://doi.org/10.1007/s00018-019-03422-9

Mani, S. A., Guo, W., Liao, M. J., Eaton, E. N., Ayyanan, A., Zhou, A. Y., Brooks, M., Reinhard, F., Zhang, C. C., Shipitsin, M., Campbell, L. L., Polyak, K., Brisken, C., Yang, J., & Weinberg, R. A. (2008). The Epithelial-Mesenchymal Transition Generates Cells with Properties of Stem Cells. *Cell*, *133*(4), 704–715. https://doi.org/10.1016/j.cell.2008.03.027

Manshouri, R., Coyaud, E., Kundu, S. T., Peng, D. H., Stratton, S. A., Alton, K., Bajaj, R., Fradette, J. J., Minelli, R., Peoples, M. D., Carugo, A., Chen, F., Bristow, C., Kovacs, J. J., Barton, M. C., Heffernan, T., Creighton, C. J., Raught, B., & Gibbons, D. L. (2019). ZEB1/NuRD complex suppresses TBC1D2b to stimulate E-cadherin internalization and promote metastasis in lung cancer. *Nature Communications*, *10*(1). https://doi.org/10.1038/s41467-019-12832-z

Martinez-Lemus, L. A. (2012). The dynamic structure of arterioles. In *Basic and Clinical Pharmacology and Toxicology* (Vol. 110, Issue 1, pp. 5–11). https://doi.org/10.1111/j.1742-7843.2011.00813.x

Maxwell, P. H., Wiesener, M. S., Chang, G., Clifford, S. C., Vaux, E. C., Cockman, M. E., Wykoff, C. C., Pugh, C. W., Maher, E. R., & Ratcliffe, P. J. (1999). The tumour suppressor protein VHL targets hypoxia-inducible factors for oxygen-dependent proteolysis. *Nature*, *399*, 271–275.

Mazzone, M., Dettori, D., Leite de Oliveira, R., Loges, S., Schmidt, T., Jonckx, B., Tian, Y. M., Lanahan, A. A., Pollard, P., Ruiz de Almodovar, C., De Smet, F., Vinckier, S., Aragonés, J., Debackere, K., Luttun, A., Wyns, S., Jordan, B., Pisacane, A., Gallez, B., … Carmeliet, P. (2009). Heterozygous Deficiency of PHD2 Restores Tumor Oxygenation and Inhibits Metastasis via Endothelial Normalization. *Cell*, *136*(5), 839–851. https://doi.org/10.1016/j.cell.2009.01.020

Mccormick, S. M., Eskin, S. G., Mcintire, L. V, Teng, C. L., Lu, C.-M., Russell, C. G., & Chittur, K. K. (2001). DNA microarray reveals changes in gene expression of shear stressed human umbilical vein endothelial cells. *Proc Natl Acad Sci USA*, *98*(16), 8955–8960. www.pnas.orgcgidoi10.1073pnas.171259298

McDonald, A. I., Shirali, A. S., Aragón, R., Ma, F., Hernandez, G., Vaughn, D. A., Mack, J. J., Lim, T. Y., Sunshine, H., Zhao, P., Kalinichenko, V., Hai, T., Pelegrini, M., Ardehali, R., & Iruela-Arispe, M. L. (2018). Endothelial Regeneration of Large Vessels Is a Biphasic Process Driven by Local Cells with Distinct Proliferative Capacities. *Cell Stem Cell*, *23*(2), 210-225.e6. https://doi.org/10.1016/j.stem.2018.07.011

Mcdonald, D. M., & Choyke, P. L. (2003). Imaging of angiogenesis: from microscope to clinic. *NATURE MEDICINE*, *9*(6). http://www.nature.com/naturemedicine

Mcleod, D. S., Grebe, R., Bhutto, I., Merges, C., Baba, T., & Lutty, G. A. (2009). Relationship between RPE and choriocapillaris in age-related macular degeneration. *Investigative Ophthalmology and Visual Science*, *50*(10), 4982–4991. https://doi.org/10.1167/iovs.09-3639

Mcleod, D. S., Lefer, D. J., Merges, C., & Lutty, G. A. (1995). Enhanced Expression of Intracellular Adhesion Molecule-1 and P-Selectin in the Diabetic Human Retina and Choroid. In *American Journal ofPathology* (Vol. 147, Issue 3).

Medina-Leyte, D. J., Domínguez-Pérez, M., Mercado, I., Villarreal-Molina, M. T., & Jacobo-Albavera, L. (2020). Use of human umbilical vein endothelial cells (HUVEC) as a model to study cardiovascular disease: A review. *Applied Sciences (Switzerland)*, *10*(3). https://doi.org/10.3390/app10030938

Mehrad, B., Keane, M. P., & Strieter, R. M. (2007). Chemokines as mediators of angiogenesis. *Thromb Haemost*, *97*(5), 755–762.

Meyer, M., Clauss, M., Lepple-Wienhues, A., Waltenberger, J., Augustin, H. G., Ziche, M., Lanz, C., Bü Ttner, M., Rziha, H.-J., & Dehio, C. (1999). A novel vascular endothelial growth factor encoded by Orf virus, VEGF-E, mediates angiogenesis via signalling through VEGFR-2 (KDR) but not VEGFR-1 (Flt-1) receptor tyrosine kinases. In *The*

EMBO Journal (Vol. 18, Issue 2). http://circinus.ebi.ac.uk:6543/~michele/java3/dev/contents.html

Miao, H., Tao, Y., & Li, X.-X. (2012). Inflammatory cytokines in aqueous humor of patients with choroidal neovascularization. *Molecular Vision*, *18*, 574–580. http://www.molvis.org/molvis/v18/a62

Milde, F., Lauw, S., Koumoutsakos, P., & Iruela-Arispe, M. L. (2013). The mouse retina in 3D: Quantification of vascular growth and remodeling. *Integrative Biology (United Kingdom)*, *5*(12), 1426–1438. https://doi.org/10.1039/c3ib40085a

Miller, H., Miller, B., Ishibashi, T., & Ryan, S. J. (1990). Pathogenesis of laser-induced choroidal subretinal neovascularization. *Ophthalmol Vis Sci*, *31*(5), 899–908.

Mizutani, K.-I., Kidoya, H., Nakayama, K., & Hattori, Y. (2022). The Multiple Roles of Pericytes in Vascular Formation and Microglial Functions in the Brain. *Life*, *12*(11), 1835. https://doi.org/10.3390/life

Montesano, R., Vassalli, J.-D., Bairdt, A., Guillemint, R., & Orci, L. (1986). Basic fibroblast growth factor induces angiogenesis in vitro (endothelial cells/collagen matrix/plasminogen activator/urokinase). In *Proc. Nati. Acad. Sci. USA* (Vol. 83).

Moon, Y. W., Rao, G., Kim, J. J., Shim, H. S., Park, K. S., An, S. S., Kim, B., Steeg, P. S., Sarfaraz, S., Changwoo Lee, L., Voeller, D., Choi, E. Y., Luo, J., Palmieri, D., Chung, H. C., Kim, J. H., Wang, Y., & Giaccone, G. (2015). LAMC2 enhances the metastatic potential of lung adenocarcinoma. *Cell Death and Differentiation*, *22*(8), 1341–1352. https://doi.org/10.1038/cdd.2014.228

Morita, Y., Fukuuchi1, Y., Koto1, A., Suzuki1, N., Isozumi1, K., Gotoh1, J., Shimizu1, T., Takao1, M., & Aoyama1, M. (1997). Rapid Changes in Pial Arterial Diameter and Cerebral Blood Flow Caused by Ipsilateral Carotid Artery Occlusion in Rats. *Keio J Med*, *46*(3), 120–127.

Morley, R. L., Sharma, A., Horsch, A. D., & Hinchliffe, R. J. (2018). Peripheral artery disease. *BMJ (Online)*, *360*. https://doi.org/10.1136/bmj.j5842

Mould, A. W., Greco, S. A., Cahill, M. M., Tonks, I. D., Bellomo, D., Patterson, C., Zournazi, A., Nash, A., Scotney, P., Hayward, N. K., & Kay, G. F. (2005). Transgenic overexpression of vascular endothelial growth factor-B isoforms by endothelial cells potentiates postnatal vessel growth in vivo and in vitro. *Circulation Research*, *97*(6). https://doi.org/10.1161/01.res.0000182631.33638.77

Murakami, M., Nguyen, L. T., Hatanaka, K., Schachterle, W., Chen, P. Y., Zhuang, Z. W., Black, B. L., & Simons, M. (2011). FGF-dependent regulation of VEGF receptor 2 expression in mice. *Journal of Clinical Investigation*, *121*(7), 2668–2678. https://doi.org/10.1172/JCI44762

Naqvi, S., Kim, S., Hoskens, H., Matthews, H. S., Spritz, R. A., Klein, O. D., Hallgrímsson, B., Swigut, T., Claes, P., Pritchard, J. K., & Wysocka, J. (2023). Precise modulation of transcription factor levels identifies features underlying dosage sensitivity. *Nature Genetics*, *55*(5), 841–851. https://doi.org/10.1038/s41588-023-01366-2

Ng, D. S., Yip, Y. W., Bakthavatsalam, M., Chen, L. J., Ng, T. K., Lai, T. Y., Pang, C. P., & Brelén, M. E. (2017). Elevated angiopoietin 2 in aqueous of patients with neovascular age related macular degeneration correlates with disease severity at presentation. *Scientific Reports*, *7*. https://doi.org/10.1038/srep45081

Nguyen, H. L., Lee, Y. J., Shin, J., Lee, E., Park, S. O., McCarty, J. H., & Oh, S. P. (2011). TGF-β signaling in endothelial cells, but not neuroepithelial cells, is essential for cerebral vascular development. *Laboratory Investigation*, *91*(11), 1554–1563. https://doi.org/10.1038/labinvest.2011.124

Nguyen, T., Zheng, M., Knapp, M., Sladojevic, N., Zhang, Q., Ai, L., Harrison, D., Chen, A., Sitikov, A., Shen, L., Gonzalez, F. J., Zhao, Q., Fang, Y., Liao, J. J. K., & Wu, R. (2021). Endothelial Aryl Hydrocarbon Receptor Nuclear Translocator Mediates the Angiogenic Response to Peripheral Ischemia in Mice With Type 2 Diabetes Mellitus. *Frontiers in Cell and Developmental Biology*, *9*. https://doi.org/10.3389/fcell.2021.691801

Nowak-Sliwinska, P., Alitalo, K., Allen, E., Anisimov, A., Aplin, A. C., Auerbach, R., Augustin, H. G., Bates, D. O., van Beijnum, J. R., Bender, R. H. F., Bergers, G., Bikfalvi, A., Bischoff, J., Böck, B. C., Brooks, P. C., Bussolino, F., Cakir, B., Carmeliet, P., Castranova, D., … Griffioen, A. W. (2018). Consensus guidelines for the use and interpretation of angiogenesis assays. In *Angiogenesis* (Vol. 21, Issue 3, pp. 425–532). Springer Netherlands. https://doi.org/10.1007/s10456-018-9613-x

Ohno-Matsui, K., Uetama, T., Yoshida, T., Hayano, M., Itoh, T., Morita, I., & Mochizuki, M. (2003). Reduced Retinal Angiogenesis in MMP-2 - Deficient Mice. *Investigative Ophthalmology and Visual Science*, *44*(12), 5370–5375. https://doi.org/10.1167/iovs.03-0249

Oliveira-Paula, G. H., Lacchini, R., & Tanus-Santos, J. E. (2016). Endothelial nitric oxide synthase: From biochemistry and gene structure to clinical implications of NOS3 polymorphisms. In *Gene* (Vol. 575, Issue 2, pp. 584–599). Elsevier B.V. https://doi.org/10.1016/j.gene.2015.09.061

Olofsson, B., Pajusolatt, K., Kaipainent, A., Von Euler, G., Joukovt, V., Saksela, O., Orpanat, A., Pettersson, R. F., Alitalott, K., & Eriksson, U. (1996). Vascular endothelial growth factor B, a novel growth factor for endothelial cells (angiogenesis/endothelium/mitosis). In *Cell Biology* (Vol. 93).

Onder, T. T., Gupta, P. B., Mani, S. A., Yang, J., Lander, E. S., & Weinberg, R. A. (2008). Loss of E-cadherin promotes metastasis via multiple downstream transcriptional

pathways. *Cancer Research*, *68*(10), 3645–3654. https://doi.org/10.1158/0008-5472.CAN-07-2938

Orsenigo, F., Giampietro, C., Ferrari, A., Corada, M., Galaup, A., Sigismund, S., Ristagno, G., Maddaluno, L., Koh, G. Y., Franco, D., Kurtcuoglu, V., Poulikakos, D., Baluk, P., McDonald, D., Grazia Lampugnani, M., & Dejana, E. (2012). Phosphorylation of VE-cadherin is modulated by haemodynamic forces and contributes to the regulation of vascular permeability in vivo. *Nature Communications*, *3*, 1208. https://doi.org/10.1038/ncomms2199

O'Sullivan, M. L., Puñal, V. M., Kerstein, P. C., Brzezinski, J. A., Glaser, T., Wright, K. M., & Kay, J. N. (2017). Astrocytes follow ganglion cell axons to establish an angiogenic template during retinal development. *GLIA*, *65*(10), 1697–1716. https://doi.org/10.1002/glia.23189

Otsuji, T., Nagai, Y., Sho, K., Tsumura, A., Koike, N., Tsuda, M., Nishimura, T., & Takahashi, K. (2013). Initial non-responders to ranibizumabin the treatment of age-related macular degeneration (AMD). *Clinical Ophthalmology*, *7*, 1487–1490. https://doi.org/10.2147/OPTH.S46317

Ouriel, K. (2001). Peripheral arterial disease. *The Lancet*, *358*(9289), 1257–1264.

Padget, R. L., Mohite, S. S., Hoog, T. G., Justis, B. S., Green, B. E., & Udan, R. S. (2019). Hemodynamic force is required for vascular smooth muscle cell recruitment to blood vessels during mouse embryonic development. *Mechanisms of Development*, *156*, 8–19. https://doi.org/10.1016/j.mod.2019.02.002

Panos, G. D., Lakshmanan, A., Dadoukis, P., Ripa, M., Motta, L., & Amoaku, W. M. (2023). Faricimab: Transforming the Future of Macular Diseases Treatment-A Comprehensive Review of Clinical Studies. In *Drug Design, Development and Therapy* (Vol. 17, pp. 2861–2873). Dove Medical Press Ltd. https://doi.org/10.2147/DDDT.S427416

Papadopoulou, V., Postigo, A., Sánchez-Tilló, E., Porter, A. C. G., & Wagner, S. D. (2010). ZEB1 and CtBP form a repressive complex at a distal promoter element of the BCL6 locus. *The Biochemical Journal* , *427*(3), 541–550.

Papapetropoulos, A., Fulton, D., Mahboubi, K., Kalb, R. G., O'Connor, D. S., Li, F., Altieri, D. C., & Sessa, W. C. (2000). Angiopoietin-1 inhibits endothelial cell apoptosis via the Akt/survivin pathway. *Journal of Biological Chemistry*, *275*(13), 9102–9105. https://doi.org/10.1074/jbc.275.13.9102

Parikh, S. M., Mammoto, T., Schultz, A., Yuan, H. T., Christiani, D., Karumanchi, S. A., & Sukhatme, V. P. (2006). Excess circulating angiopoietin-2 may contribute to pulmonary vascular leak in sepsis in humans. *PLoS Medicine*, *3*(3), 356–370. https://doi.org/10.1371/journal.pmed.0030046

Park, J. A., Kim, D. Y., Kim, Y. M., Lee, I. K., & Kwon, Y. G. (2015). Endothelial Snail Regulates Capillary Branching Morphogenesis via Vascular Endothelial Growth Factor Receptor 3 Expression. *PLoS Genetics*, *11*(7). https://doi.org/10.1371/journal.pgen.1005324

Park, J. E., Keller, G.-A., & Ferrara, N. (1993). The Vascular Endothelial Growth Factor (VEGF) Isoforms: Differential Deposition into the Subepithelial Extracellular Matrix and Bioactivity of Extracellular Matrix-bound VEGF. In *Molecular Biology of the Cell* (Vol. 4).

Park, J. S., Kim, I. K., Han, S., Park, I., Kim, C., Bae, J., Oh, S. J., Lee, S., Kim, J. H., Woo, D. C., He, Y., Augustin, H. G., Kim, I., Lee, D., & Koh, G. Y. (2016). Normalization of Tumor Vessels by Tie2 Activation and Ang2 Inhibition Enhances Drug Delivery and Produces a Favorable Tumor Microenvironment. *Cancer Cell*, *30*(6), 953–967. https://doi.org/10.1016/j.ccell.2016.10.018

Park, M. K., Lee, H., & Lee, C. H. (2022). Post-Translational Modification of ZEB Family Members in Cancer Progression. In *International Journal of Molecular Sciences* (Vol. 23, Issue 23). MDPI. https://doi.org/10.3390/ijms232315127

Park, S. O., Jae Lee, Y., Seki, T., Hong, K.-H., Fliess, N., Jiang, Z., Park, A., Wu, X., Kaartinen, V., Roman, B. L., & Paul Oh, S. (2008). *ALK5-and TGFBR2-independent role of ALK1 in the pathogenesis of hereditary hemorrhagic telangiectasia type 2*. https://doi.org/10.1182/blood-2007-08

Payne, S., Val, S. De, & Neal, A. (2018). Endothelial-specific cre mouse models is your cre CREdibile? *Arteriosclerosis, Thrombosis, and Vascular Biology*, *38*(11), 2550–2561. https://doi.org/10.1161/ATVBAHA.118.309669

Peng, Q., Shan, D., Cui, K., Li, K., Zhu, B., Wu, H., Wang, B., Wong, S., Norton, V., Dong, Y., Lu, Y. W., Zhou, C., & Chen, H. (2022). The Role of Endothelial-to-Mesenchymal Transition in Cardiovascular Disease. In *Cells* (Vol. 11, Issue 11). MDPI. https://doi.org/10.3390/cells11111834

Peng, X., Xiao, H., Tang, M., Zhan, Z., Yang, Y., Sun, L., Luo, X., Zhang, A., & Ding, X. (2018). Mechanism of fibrosis inhibition in laser induced choroidal neovascularization by doxycycline. *Experimental Eye Research*, *176*, 88–97. https://doi.org/10.1016/j.exer.2018.06.030

Phng, L. K., Potente, M., Leslie, J. D., Babbage, J., Nyqvist, D., Lobov, I., Ondr, J. K., Rao, S., Lang, R. A., Thurston, G., & Gerhardt, H. (2009). Nrarp Coordinates Endothelial Notch and Wnt Signaling to Control Vessel Density in Angiogenesis. *Developmental Cell*, *16*(1), 70–82. https://doi.org/10.1016/j.devcel.2008.12.009

Phng, L. K., Stanchi, F., & Gerhardt, H. (2013). Filopodia are dispensable for endothelial tip cell guidance. *Development (Cambridge)*, *140*(19), 4031–4040. https://doi.org/10.1242/dev.097352

Piera-Velazquez, S., & Jimenez, S. A. (2012). Molecular mechanisms of endothelial to mesenchymal cell transition (EndoMT) in experimentally induced fibrotic diseases. *Fibrogenesis & Tissue Repair*, *5*, S7. http://www.fibrogenesis.com/content/5/S1/S7

Piera-Velazquez, S., & Jimenez, S. A. (2019). ENDOTHELIAL TO MESENCHYMAL TRANSITION: ROLE IN PHYSIOLOGY AND IN THE PATHOGENESIS OF HUMAN DISEASES. *Physiol Rev*, *99*, 1281–1324. https://doi.org/10.1152/physrev.00021.2018.-Numer

Pipp, F., Boehm, S., Cai, W. J., Adili, F., Ziegler, B., Karanovic, G., Ritter, R., Balzer, J., Scheler, C., Schaper, W., & Schmitz-Rixen, T. (2004). Elevated fluid shear stress enhances postocclusive collateral artery growth and gene expression in the pig hind limb. *Arteriosclerosis, Thrombosis, and Vascular Biology*, *24*(9), 1664–1668. https://doi.org/10.1161/01.ATV.0000138028.14390.e4

Platel, V., Faure, S., Corre, I., & Clere, N. (2019). Endothelial-to-Mesenchymal Transition (EndoMT): Roles in Tumorigenesis, Metastatic Extravasation and Therapy Resistance. In *Journal of Oncology* (Vol. 2019). Hindawi Limited. https://doi.org/10.1155/2019/8361945

Pontes-Quero, S., Fernández-Chacón, M., Luo, W., Lunella, F. F., Casquero-Garcia, V., Garcia-Gonzalez, I., Hermoso, A., Rocha, S. F., Bansal, M., & Benedito, R. (2019). High mitogenic stimulation arrests angiogenesis. *Nature Communications*, *10*(1). https://doi.org/10.1038/s41467-019-09875-7

Postigo, A. A., & Dean, D. C. (1999). ZEB represses transcription through interaction with the corepressor CtBP. *PNAS*, *96*(12), 6683–6688. www.pnas.org.

Postigo, A. A., Depp, J. L., Taylor, J. J., & Kroll, K. L. (2003). Regulation of Smad signaling through a differential recruitment of coactivators and corepressors by ZEB proteins. *EMBO Journal*, *22*(10), 2453–2462. https://doi.org/10.1093/emboj/cdg226

Potente, M., Gerhardt, H., & Carmeliet, P. (2011). Basic and therapeutic aspects of angiogenesis. In *Cell* (Vol. 146, Issue 6, pp. 873–887). Elsevier B.V. https://doi.org/10.1016/j.cell.2011.08.039

Preca, B. T., Bajdak, K., Mock, K., Sundararajan, V., Pfannstiel, J., Maurer, J., Wellner, U., Hopt, U. T., Brummer, T., Brabletz, S., Brabletz, T., & Stemmler, M. P. (2015). A self-enforcing CD44s/ZEB1 feedback loop maintains EMT and stemness properties in cancer cells. *International Journal of Cancer*, *137*(11), 2566–2577. https://doi.org/10.1002/ijc.29642

Pries, A. R., Secomb, T. W., & Gaehtgens, P. (2000). The endothelial surface layer. In *Pflugers Archiv European Journal of Physiology* (Vol. 440, Issue 5, pp. 653–666). Springer Verlag. https://doi.org/10.1007/s004240000307

Pugh, C. W., & Ratcliffe, P. J. (2003). Regulation of angiogenesis by hypoxia: role of the HIF system ANGIOGENESIS FOCUS. In *NATURE MEDICINE* (Vol. 9, Issue 6). http://www.nature.com/naturemedicine

Rajendran, P., Rengarajan, T., Thangavel, J., Nishigaki, Y., Sakthisekaran, D., Sethi, G., & Nishigaki, I. (2013). The vascular endothelium and human diseases. In *International Journal of Biological Sciences* (Vol. 9, Issue 10, pp. 1057–1069). Ivyspring International Publisher. https://doi.org/10.7150/ijbs.7502

Ramjaun, A. R., & Hodivala-Dilke, K. (2009). The role of cell adhesion pathways in angiogenesis. In *International Journal of Biochemistry and Cell Biology* (Vol. 41, Issue 3, pp. 521–530). https://doi.org/10.1016/j.biocel.2008.05.030

Ranchoux, B., Antigny, F., Rucker-Martin, C., Hautefort, A., Péchoux, C., Bogaard, H. J., Dorfmüller, P., Remy, S., Lecerf, F., Planté, S., Chat, S., Fadel, E., Houssaini, A., Anegon, I., Adnot, S., Simonneau, G., Humbert, M., Cohen-Kaminsky, S., & Perros, F. (2015). Endothelial-to-mesenchymal transition in pulmonary hypertension. *Circulation*, *131*(11), 1006–1018. https://doi.org/10.1161/CIRCULATIONAHA.114.008750

Rao, S., Lobov, I. B., Vallance, J. E., Tsujikawa, K., Shiojima, I., Akunuru, S., Walsh, K., Benjamin, L. E., & Lang, R. A. (2007). Obligatory participation of macrophages in an angiopoietin 2-mediated cell death switch. *Development*, *134*(24), 4449–4458. https://doi.org/10.1242/dev.012187

Rashbrook, V. S., Brash, J. T., & Ruhrberg, C. (2022). Cre toxicity in mouse models of cardiovascular physiology and disease. *Nature Cardiovascular Research*, *1*(9), 806–816. https://doi.org/10.1038/s44161-022-00125-6

Reglero-Real, N., Colom, B., Bodkin, J. V., & Nourshargh, S. (2016). Endothelial cell junctional adhesion molecules. *Arteriosclerosis, Thrombosis, and Vascular Biology*, *36*(10), 2048–2057. https://doi.org/10.1161/ATVBAHA.116.307610

Reine, T. M., Vuong, T. T., Rutkovskiy, A., Meen, A. J., Vaage, J., Jenssen, T. G., & Kolset, S. O. (2015). Serglycin in quiescent and proliferating primary endothelial cells. *PLoS ONE*, *10*(12). https://doi.org/10.1371/journal.pone.0145584

Rezzola, S., Di Somma, M., Corsini, M., Leali, D., Ravelli, C., Polli, V. A. B., Grillo, E., Presta, M., & Mitola, S. (2019). VEGFR2 activation mediates the pro-angiogenic activity of BMP4. *Angiogenesis*, *22*(4), 521–533. https://doi.org/10.1007/s10456-019-09676-y

Ribatti, D., & Crivellato, E. (2009). Immune cells and angiogenesis. In *Journal of Cellular and Molecular Medicine* (Vol. 13, Issue 9 A, pp. 2822–2833). https://doi.org/10.1111/j.1582-4934.2009.00810.x

Ricard, N., Bailly, S., Guignabert, C., & Simons, M. (2021a). The quiescent endothelium: signalling pathways regulating organ-specific endothelial normalcy. In *Nature*

Reviews Cardiology (Vol. 18, Issue 8, pp. 565–580). Nature Research. https://doi.org/10.1038/s41569-021-00517-4

Ricard, N., Bailly, S., Guignabert, C., & Simons, M. (2021b). The quiescent endothelium: signalling pathways regulating organ-specific endothelial normalcy. In *Nature Reviews Cardiology* (Vol. 18, Issue 8, pp. 565–580). Nature Research. https://doi.org/10.1038/s41569-021-00517-4

Ricard, N., Scott, R. P., Booth, C. J., Velazquez, H., Cilfone, N. A., Baylon, J. L., Gulcher, J. R., Quaggin, S. E., Chittenden, T. W., & Simons, M. (2019). Endothelial ERK1/2 signaling maintains integrity of the quiescent endothelium. *Journal of Experimental Medicine*, *216*(8), 1874–1890. https://doi.org/10.1084/jem.20182151

Risau, W., & Flamme, L. (1995). VASCULOGENESIS. *Annual Review of Cell and Developmental Biology*, *11*, 73–91. www.annualreviews.org

Rocha, S. F., Schiller, M., Jing, D., Li, H., Butz, S., Vestweber, D., Biljes, D., Drexler, H. C. A., Nieminen-Kelhä, M., Vajkoczy, P., Adams, S., Benedito, R., & Adams, R. H. (2014). Esm1 modulates endothelial tip cell behavior and vascular permeability by enhancing VEGF bioavailability. *Circulation Research*, *115*(6), 581–590. https://doi.org/10.1161/CIRCRESAHA.115.304718

Romagnani, P., Annunziato, F., Lasagni, L., Lazzeri, E., Beltrame, C., Francalanci, M., Uguccioni, M., Galli, G., Cosmi, L., Maurenzig, L., Baggiolini, M., Maggi, E., Romagnani, S., & Serio, M. (2001). Cell cycle-dependent expression of CXC chemokine receptor 3 by endothelial cells mediates angiostatic activity. *Journal of Clinical Investigation*, *107*(1), 53–63. https://doi.org/10.1172/JCI9775

Rosmaninho, P., Mükusch, S., Piscopo, V., Teixeira, V., Raposo, A. A., Warta, R., Bennewitz, R., Tang, Y., Herold-Mende, C., Stifani, S., Momma, S., & Castro, D. S. (2018). Zeb1 potentiates genome-wide gene transcription with Lef1 to promote glioblastoma cell invasion. *The EMBO Journal*, *37*(15). https://doi.org/10.15252/embj.201797115

Ross, M., Kargl, C. K., Ferguson, R., Gavin, T. P., & Hellsten, Y. (2023). Exercise-induced skeletal muscle angiogenesis: impact of age, sex, angiocrines and cellular mediators. In *European Journal of Applied Physiology* (Vol. 123, Issue 7, pp. 1415–1432). Springer Science and Business Media Deutschland GmbH. https://doi.org/10.1007/s00421-022-05128-6

Roth, L., Prahst, C., Ruckdeschel, T., Savant, S., Weström, † Simone, Fantin, A., Riedel, M., Héroult, M., Ruhrberg, C., & Augustin, H. G. (2016). Neuropilin-1 mediates vascular permeability independently of vascular endothelial growth factor receptor-2 activation. *Science Signalling*, *9*(425), ra42. www.SCIENCESIGNALING.org

Rothhammer, T., Bataille, F., Spruss, T., Eissner, G., & Bosserhoff, A. K. (2007). Functional implication of BMP4 expression on angiogenesis in malignant melanoma. *Oncogene*, *26*(28), 4158–4170. https://doi.org/10.1038/sj.onc.1210182

Rouget, C. (1874). Note sur le development de la tunique contractile des vaisseaux. *Compt. Rend. Acad. Sci.*, *59*, 559–562.

Ruhrberg, C., Gerhardt, H., Golding, M., Watson, R., Ioannidou, S., Fujisawa, H., Betsholtz, C., & Shima, D. T. (2002). Spatially restricted patterning cues provided by heparin-binding VEGF-A control blood vessel branching morphogenesis. *Genes and Development*, *16*(20), 2684–2698. https://doi.org/10.1101/gad.242002

Rust, R., Grönnert, L., Dogançay, B., & Schwab, M. E. (2019). A Revised View on Growth and Remodeling in the Retinal Vasculature. *Scientific Reports*, *9*(1). https://doi.org/10.1038/s41598-019-40135-2

Ryan, S. J. (1979). The development of an experimental model of subretinal neovascularization in disciform macular degeneration. *Trans Am Ophthalmol Soc*, *77*, 707–745.

Sakurai, Y., Ohgimoto, K., Kataoka, Y., Yoshida, N., & Shibuya, M. (2005). Essential role of Flk-1 (VEGF receptor 2) tyrosine residue 1173 in vasculogenesis in mice. *PNAS*, *102*(4), 1076–1081. www.pnas.orgcgidoi10.1073pnas.0404984102

Sánchez-Tilló, E., Fanlo, L., Siles, L., Montes-Moreno, S., Moros, A., Chiva-Blanch, G., Estruch, R., Martinez, A., Colomer, D., Gyrffy, B., Roué, G., & Postigo, A. (2014). The EMT activator ZEB1 promotes tumor growth and determines differential response to chemotherapy in mantle cell lymphoma. *Cell Death and Differentiation*, *21*(2), 247–257. https://doi.org/10.1038/cdd.2013.123

Sánchez-Tilló, E., Lázaro, A., Torrent, R., Cuatrecasas, M., Vaquero, E. C., Castells, A., Engel, P., & Postigo, A. (2010). ZEB1 represses E-cadherin and induces an EMT by recruiting the SWI/SNF chromatin-remodeling protein BRG1. *Oncogene*, *29*(24), 3490–3500. https://doi.org/10.1038/onc.2010.102

Sánchez-Tilló, E., Liu, Y., De Barrios, O., Siles, L., Fanlo, L., Cuatrecasas, M., Darling, D. S., Dean, D. C., Castells, A., & Postigo, A. (2012). EMT-activating transcription factors in cancer: Beyond EMT and tumor invasiveness. In *Cellular and Molecular Life Sciences* (Vol. 69, Issue 20, pp. 3429–3456). https://doi.org/10.1007/s00018-012-1122-2

Sato, H., Oyanagi, J., Komiya, E., Ogawa, T., Higashi, S., & Miyazaki, K. (2014). Amino-terminal fragments of laminin γ2 chain retract vascular endothelial cells and increase vascular permeability. *Cancer Science*, *105*(2), 168–175. https://doi.org/10.1111/cas.12323

Sawano, A., Takahashi, T., Yamaguchi, S., & Shibuya, M. (1996). Flt-1 but not KDR/Flk-1 tyrosine kinase is a receptor for placenta growth factor, which is related to vascular endothelial growth factor. *Cell Growth and Differentiation*, *7*(2), 213–221.

Schlereth, K., Weichenhan, D., Bauer, T., Heumann, T., Giannakouri, E., Lipka, D., Jaeger, S., Schlesner, M., Aloy, P., Eils, R., Plass, C., & Augustin, H. G. (2018). The transcriptomic and epigenetic map of vascular quiescence in the continuous lung endothelium. *ELife*, *7*. https://doi.org/10.7554/eLife.34423.001

Schoggins, J. W. (2025). Interferon-Stimulated Genes: What Do They All Do? *Annual Review of Virology*, *22*(1). https://doi.org/10.1146/annurev-virology-092818

Scholz, D., Cai, W. J., & Schaper, W. (2001). Arteriogenesis, a new concept of vascular adaptation in occlusive disease. *Angiogenesis* , *4*(4), 247–257.

Schoors, S., Bruning, U., Missiaen, R., Queiroz, K. C. S., Borgers, G., Elia, I., Zecchin, A., Cantelmo, A. R., Christen, S., Goveia, J., Heggermont, W., Goddé, L., Vinckier, S., Van Veldhoven, P. P., Eelen, G., Schoonjans, L., Gerhardt, H., Dewerchin, M., Baes, M., … Carmeliet, P. (2015). Fatty acid carbon is essential for dNTP synthesis in endothelial cells. *Nature*, *520*(7546), 192–197. https://doi.org/10.1038/nature14362

Schoors, S., De Bock, K., Cantelmo, A. R., Georgiadou, M., Ghesquière, B., Cauwenberghs, S., Kuchnio, A., Wong, B. W., Quaegebeur, A., Goveia, J., Bifari, F., Wang, X., Blanco, R., Tembuyser, B., Cornelissen, I., Bouché, A., Vinckier, S., Diaz-Moralli, S., Gerhardt, H., … Carmeliet, P. (2014). Partial and transient reduction of glycolysis by PFKFB3 blockade reduces pathological angiogenesis. *Cell Metabolism*, *19*(1), 37–48. https://doi.org/10.1016/j.cmet.2013.11.008

Scott, A., Powner, M. B., Gandhi, P., Clarkin, C., Gutmann, D. H., Johnson, R. S., Ferrara, N., & Fruttiger, M. (2010). Astrocyte-derived vascular endothelial growth factor stabilizes vessels in the developing retinal vasculature. *PLoS ONE*, *5*(7). https://doi.org/10.1371/journal.pone.0011863

Seaman, S., Stevens, J., Young Yang, M., Logsdon, D., Graff-Cherry, C., & St Croix, B. (2007). Genes that Distinguish Physiological and Pathological Angiogenesis. In *Cancer Cell* (Vol. 11, Issue 6).

Seemann, S., Zohles, F., & Lupp, A. (2017). Comprehensive comparison of three different animal models for systemic inflammation. *Journal of Biomedical Science*, *24*(1). https://doi.org/10.1186/s12929-017-0370-8

Seghezzi, G., Patel, S., Ren, C. J., Gualandris, A., Pintucci, G., Robbins, E. S., Shapiro, R. L., Galloway, A. C., Rifkin, D. B., & Mignatti, P. (1998). Fibroblast Growth Factor-2 (FGF-2) Induces Vascular Endothelial Growth Factor (VEGF) Expression in the Endothelial Cells of Forming Capillaries: An Autocrine Mechanism Contributing to Angiogenesis. In *The Journal of Cell Biology* (Vol. 141, Issue 7). http://www.jcb.org

Seidman, J. G., & Seidman, C. (2002). Transcription factor haploinsufficiency: when half a loaf is not enough. *Journal of Clinical Investigation*, *109*(4), 451–455. https://doi.org/10.1172/jci200215043

Senger, D. E., Galli, S. J., Dvorak A M, Perruzzi C A, Harvery, V. S., & Dvorak, H. F. (1983). Tumor cells secrete a vascular permeability factor that promotes accumulation of ascites fluid. *Science*, *219*(4587), 983–985.

Senger, D. R., Connolly, D. T., Van de Water, L., Feder, J., & Dvorak H F. (1990). Purification and NH2-terminal amino acid sequence of guinea pig tumor-secreted vascular permeability factor. *Cancer Research*, *50*(6), 1774–1778.

Shah, A. V., Birdsey, G. M., Peghaire, C., Pitulescu, M. E., Dufton, N. P., Yang, Y., Weinberg, I., Osuna Almagro, L., Payne, L., Mason, J. C., Gerhardt, H., Adams, R. H., & Randi, A. M. (2017). The endothelial transcription factor ERG mediates Angiopoietin-1-dependent control of Notch signalling and vascular stability. *Nature Communications*, *8*. https://doi.org/10.1038/ncomms16002

Shah, A. V., Birdsey, G. M., & Randi, A. M. (2016). Regulation of endothelial homeostasis, vascular development and angiogenesis by the transcription factor ERG. In *Vascular Pharmacology* (Vol. 86, pp. 3–13). Elsevier Inc. https://doi.org/10.1016/j.vph.2016.05.003

Shen, J., Frye, M., Lee, B. L., Reinardy, J. L., McClung, J. M., Ding, K., Kojima, M., Xia, H., Seidel, C., Lima E Silva, R., Dong, A., Hackett, S. F., Wang, J., Howard, B. W., Vestweber, D., Kontos, C. D., Peters, K. G., & Campochiaro, P. A. (2014). Targeting VE-PTP activates TIE2 and stabilizes the ocular vasculature. *Journal of Clinical Investigation*, *124*(10), 4564–4576. https://doi.org/10.1172/JCI74527

Shibuya, M. (2006). Differential roles of vascular endothelial growth factor receptor-1 and receptor-2 in angiogenesis. *The Journal of Biochemistry and Molecular Biology*, *39*(5), 469–478.

Silvestre, J. S., Mallat, Z., Tedgui, A., & Lévy, B. I. (2008). Post-ischaemic neovascularization and inflammation. In *Cardiovascular Research* (Vol. 78, Issue 2, pp. 242–249). https://doi.org/10.1093/cvr/cvn027

Simons, M., Gordon, E., & Claesson-Welsh, L. (2016). Mechanisms and regulation of endothelial VEGF receptor signalling. In *Nature Reviews Molecular Cell Biology* (Vol. 17, Issue 10, pp. 611–625). Nature Publishing Group. https://doi.org/10.1038/nrm.2016.87

Sissaoui, S., Yu, J., Yan, A., Li, R., Yukselen, O., Kucukural, A., Zhu, L. J., & Lawson, N. D. (2020). Genomic Characterization of Endothelial Enhancers Reveals a Multifunctional Role for NR2F2 in Regulation of Arteriovenous Gene Expression. *Circulation Research*, *126*(7), 875–888. https://doi.org/10.1161/CIRCRESAHA.119.316075

Sörensen, I., Adams, R. H., & Gossler, A. (2009). DLL1-mediated Notch activation regulates endothelial identity in mouse fetal arteries. *Blood*, *113*(22), 5680–5688. https://doi.org/10.1182/blood-2008-08-174508

Sorokin, V., Vickneson, K., Kofidis, T., Woo, C. C., Lin, X. Y., Foo, R., & Shanahan, C. M. (2020). Role of Vascular Smooth Muscle Cell Plasticity and Interactions in Vessel Wall Inflammation. In *Frontiers in Immunology* (Vol. 11). Frontiers Media S.A. https://doi.org/10.3389/fimmu.2020.599415

Spaderna, S., Schmalhofer, O., Wahlbuhl, M., Dimmler, A., Bauer, K., Sultan, A., Hlubek, F., Jung, A., Strand, D., Eger, A., Kirchner, T., Behrens, J., & Brabletz, T. (2008). The transcriptional repressor ZEB1 promotes metastasis and loss of cell polarity in cancer. *Cancer Research*, *68*(2), 537–544. https://doi.org/10.1158/0008-5472.CAN-07-5682

Spadoni, I., Zagato, E., Bertocchi, A., Paolinelli, R., Hot, E., Di Sabatino, A., Caprioli, F., Bottiglieri, L., Oldani, A., Viale, G., Penna, G., Dejana, E., & Rescigno, M. (2015). A gut-vascular barrier controls the systemic dissemination of bacteria. *Science*, *350*(6262), 830–834. https://doi.org/10.1126/science.aab3145

Sperone, A., Dryden, N. H., Birdsey, G. M., Madden, L., Johns, M., Evans, P. C., Mason, J. C., Haskard, D. O., Boyle, J. J., Paleolog, E. M., & Randi, A. M. (2011). The transcription factor erg inhibits vascular inflammation by repressing NF-κB activation and proinflammatory gene expression in endothelial cells. *Arteriosclerosis, Thrombosis, and Vascular Biology*, *31*(1), 142–150. https://doi.org/10.1161/ATVBAHA.110.216473

Sprague, A. H., & Khalil, R. A. (2009). Inflammatory cytokines in vascular dysfunction and vascular disease. In *Biochemical Pharmacology* (Vol. 78, Issue 6, pp. 539–552). Elsevier Inc. https://doi.org/10.1016/j.bcp.2009.04.029

Stahl, A., Connor, K. M., Sapieha, P., Chen, J., Dennison, R. J., Krah, N. M., Seaward, M. R., Willett, K. L., Aderman, C. M., Guerin, K. I., Hua, J., Löfqvist, C., Hellström, A., & Smith, L. E. H. (2010). The mouse retina as an angiogenesis model. In *Investigative Ophthalmology and Visual Science* (Vol. 51, Issue 6, pp. 2813–2826). https://doi.org/10.1167/iovs.10-5176

Stone, J., Itin, A., Alon, T., Pe'er, J., Gnessin, H., Chan-Ling, T., & Keshet', E. (1995). Development of Retinal Vasculature Is Mediated by Hypoxia-Induced Vascular Endothelial Growth Factor (VEGF) Expression by Neuroglia. In *The Journal of Neuroscience* (Vol. 15, Issue 7).

Strasser, G. A., Kaminker, J. S., & Tessier-Lavigne, M. (2010). Microarray analysis of retinal endothelial tip cells identifies CXCR4 as a mediator of tip cell morphology and branching. *Blood*, *115*(24), 5102–5110. https://doi.org/10.1182/blood-2009-07-230284

Straub, A. C., Zeigler, A. C., & Isakson, B. E. (2014). The myoendothelial junction: Connections that deliver the message. In *Physiology* (Vol. 29, Issue 4, pp. 242–249). American Physiological Society. https://doi.org/10.1152/physiol.00042.2013

Strauss, O. (2005). The Retinal Pigment Epithelium in Visual Function. *Physiol Rev*, *85*, 845–881. https://doi.org/10.1152/physrev.00021.2004.-Located

Suchting, S., Freitas, C., le Noble, F., Benedito, R., Bré ant, C., Duarte, A., & Eichmann, A. (2007). The Notch ligand Delta-like 4 negatively regulates endothelial tip cell formation and vessel branching. *PNAS*, *104*(9), 3225–3230. www.pnas.org/cgi/content/full/

Suri, C., Jones, P. F., Patan, S., Bartunkova, S., Maisonpierre, P. C., Davis, S., Sato, T. N., & Yancopoulos, G. D. (1996). Requisite role of angiopoietin-1, a ligand for the TIE2 receptor, during embryonic angiogenesis. *Cell*, *87*(7), 1171–1180. https://doi.org/10.1016/S0092-8674(00)81813-9

Suzuki, M., Nagai, N., Izumi-Nagai, K., Shinoda, H., Koto, T., Uchida, A., Mochimaru, H., Yuki, K., Sasaki, M., Tsubota, K., & Ozawa, Y. (2014). Predictive factors for non-response to intravitreal ranibizumab treatment in age-related macular degeneration. *British Journal of Ophthalmology*, *98*(9), 1186–1191. https://doi.org/10.1136/bjophthalmol-2013-304670

Swahn, H., Li, K., Duffy, T., Olmer, M., D'Lima, D. D., Mondala, T. S., Natarajan, P., Head, S. R., & Lotz, M. K. (2023). Senescent cell population with ZEB1 transcription factor as its main regulator promotes osteoarthritis in cartilage and meniscus. *Annals of the Rheumatic Diseases*, *82*(3), 403–425.

Tachibana, K., Hirota, S., Iizasa, H., Yoshida, H., Kawabata, K., Kataoka, Y., Kitamura, Y., Matsushima, K., Yoshida, N., Nishikawa, S., Kishimoto, T., & Nagasawa, T. (1998). The chemokine receptor CXCR4 is essential for vascularization of the gastrointestinal tract. *Nature*, *393*, 591–594.

Taddei, A., Giampietro, C., Conti, A., Orsenigo, F., Breviario, F., Pirazzoli, V., Potente, M., Daly, C., Dimmeler, S., & Dejana, E. (2008). Endothelial adherens junctions control tight junctions by VE-cadherin-mediated upregulation of claudin-5. *Nature Cell Biology*, *10*(8), 923–934. https://doi.org/10.1038/ncb1752

Takagi, T., Moribe, H., Kondoh, H., & Higashi, Y. (1998). DeltaEF1, a zinc finger and homeodomain transcription factor, is required for skeleton patterning in multiple lineages. *Development*, *125*(1), 21–31.

Takeshita, S., Zheng, L. P., Brogi, E., Kearney, M., Pu, L.-Q., Bunting, S., Ferrara, N., Symes, J. F., & Isner, J. M. (1994). Therapeutic Angiogenesis A Single Intraarterial Bolus of Vascular Endothelial Growth Factor Augments Revascularization in a Rabbit Ischemic Hind Limb Model. *Journal of Clinical Investigation*, *93*(2), 662–670.

Tammela, T., Zarkada, G., Wallgard, E., Murtomäki, A., Suchting, S., Wirzenius, M., Waltari, M., Hellström, M., Schomber, T., Peltonen, R., Freitas, C., Duarte, A., Isoniemi, H., Laakkonen, P., Christofori, G., Ylä-Herttuala, S., Shibuya, M., Pytowski, B., Eichmann, A., … Alitalo, K. (2008). Blocking VEGFR-3 suppresses angiogenic sprouting and vascular network formation. *Nature*, *454*(7204), 656–660. https://doi.org/10.1038/nature07083

Tao, C., & Zhang, X. (2014). Development of astrocytes in the vertebrate eye. In *Developmental Dynamics* (Vol. 243, Issue 12, pp. 1501–1510). John Wiley and Sons Inc. https://doi.org/10.1002/dvdy.24190

Tao, C., & Zhang, X. (2016). Retinal Proteoglycans Act as Cellular Receptors for Basement Membrane Assembly to Control Astrocyte Migration and Angiogenesis. *Cell Reports*, *17*(7), 1832–1844. https://doi.org/10.1016/j.celrep.2016.10.035

Tisch, N., Freire-Valls, A., Yerbes, R., Paredes, I., Porta, S. La, Wang, X., Martín-Pérez, R., Castro, L., Wong, W. W. L., Coultas, L., Strilic, B., Gröne, H. J., Hielscher, T., Mogler, C., Adams, R. H., Heiduschka, P., Claesson-Welsh, L., Mazzone, M., López-Rivas, A., … De Almodovar, C. R. (2019). Caspase-8 modulates physiological and pathological angiogenesis during retina development. *Journal of Clinical Investigation*, *129*(12), 5092–5107. https://doi.org/10.1172/JCI122767

Tobe, T., Ortega, S., Luna, J. D., Ozaki, H., Okamoto, N., Derevjanik, N. L., Vinores, S. A., Basilico, C., & Campochiaro, P. A. (1998). Animal Model Targeted Disruption of the FGF2 Gene Does Not Prevent Choroidal Neovascularization in a Murine Model. In *American Journal of Pathology* (Vol. 153, Issue 5).

Tornavaca, O., Chia, M., Dufton, N., Almagro, L. O., Conway, D. E., Randi, A. M., Schwartz, M. A., Matter, K., & Balda, M. S. (2015). ZO-1 controls endothelial adherens junctions, cell-cell tension, angiogenesis, and barrier formation. *Journal of Cell Biology*, *208*(6), 821–838. https://doi.org/10.1083/jcb.201404140

Tosi, G. M., Caldi, E., Neri, G., Nuti, E., Marigliani, D., Baiocchi, S., Traversi, C., Cevenini, G., Tarantello, A., Fusco, F., Nardi, F., Orlandini, M., & Galvagni, F. (2017). HTRA1 and TGF-β1 concentrations in the aqueous humor of patients with neovascular age-related macular degeneration. *Investigative Ophthalmology and Visual Science*, *58*(1), 162–167. https://doi.org/10.1167/iovs.16-20922

Tual-Chalot, S., Allinson, K. R., Fruttiger, M., & Arthur, H. M. (2013). Whole Mount Immunofluorescent Staining of the Neonatal Mouse Retina to Investigate Angiogenesis In vivo *Journal of Visualized Experiments*, *77*. https://doi.org/10.3791/50546

Valiron, O., Chevrier, V., Usson, Y., Breviario, F., Job, D., & Dejana, E. (1996). Desmoplakin expression and organization at human umbilical vein endothelial cell-to-cell junctions. *Journal of Cell Science*, *109*(8), 2141–2149.

Vallier, L., Mancip, J., Markossian, S., Lukaszewicz, A., Dehay, C., Metzger, D., Chambon, P., Samarut, J., & Savatier, P. (2001). An efficient system for conditional gene expression in embryonic stem cells and in their in vitro and in vivo differentiated derivatives. *PNAS*, *98*(5), 2467–2472. www.pnas.orgcgidoi10.1073pnas.041617198

Van Royen, N., Piek, J. J., Buschmann, I., Hoefer, I., Voskuil, M., & Schaper, W. (2001). Stimulation of arteriogenesis; a new concept for the treatment of arterial occlusive disease. In *Cardiovascular Research* (Vol. 49). www.elsevier.com/locate/cardioreswww.elsevier.nl/locate/cardiores

Vandewalle, C., Van Roy, F., & Berx, G. (2009). The role of the ZEB family of transcription factors in development and disease. In *Cellular and Molecular Life Sciences* (Vol. 66, Issue 5, pp. 773–787). https://doi.org/10.1007/s00018-008-8465-8

Vannier, C., Mock, K., Brabletz, T., & Driever, W. (2013). Zeb1 regulates E-cadherin and Epcam (epithelial cell adhesion molecule) expression to control cell behavior in early zebrafish development. *Journal of Biological Chemistry*, *288*(26), 18643–18659. https://doi.org/10.1074/jbc.M113.467787

Verschueren, K., Remacle, J. E., Collart, C., Kraft, H., Baker, B. S., Tylzanowski, P., Nelles, L., Wuytens, G., Su, M. T., Bodmer, R., Smith, J. C., & Huylebroeck, D. (1999). SIP1, a novel zinc finger/homeodomain repressor, interacts with Smad proteins and binds to 5'-CACCT sequences in candidate target genes. *Journal of Biological Chemistry*, *274*(29), 20489–20498. https://doi.org/10.1074/jbc.274.29.20489

Virani, S. S., Alonso, A., Aparicio, H. J., Benjamin, E. J., Bittencourt, M. S., Callaway, C. W., Carson, A. P., Chamberlain, A. M., Cheng, S., Delling, F. N., Elkind, M. S. V., Evenson, K. R., Ferguson, J. F., Gupta, D. K., Khan, S. S., Kissela, B. M., Knutson, K. L., Lee, C. D., Lewis, T. T., … Tsao, C. W. (2021). Heart Disease and Stroke Statistics - 2021 Update: A Report From the American Heart Association. In *Circulation* (Vol. 143, Issue 8, pp. E254–E743). Lippincott Williams and Wilkins. https://doi.org/10.1161/CIR.0000000000000950

Vitullo, J. C., Penn, M. S., Rakusan, K., & Wicker, P. (1993). Effects of Hypertension and Aging on Coronary Artery Density. *Hypertension*, *21*(4), 406–414. http://ahajournals.org

Von Gise, A., & Pu, W. T. (2012). Endocardial and epicardial epithelial to mesenchymal transitions in heart development and disease. *Circulation Research*, *110*(12), 1628–1645. https://doi.org/10.1161/CIRCRESAHA.111.259960

Wagman, O. L., Julie, C. N., Müller, M., Bross, P., Magalhaes Novais, S., Rohlena, J., Rohlenova, K., Frye, M., Fenton, R., Wu, Q., Paludan, S. R., Fendt, S. M., & Kalucka, J. M. (2022). Endothelial IRF3-activation links inflammation and phenotypic changes. *International Vascular Biology Meeting* .

Walker, A. M. N., Warmke, N., Mercer, B., Watt, N. T., Mughal, R., Smith, J., Galloway, S., Haywood, N. J., Soomro, T., Griffin, K. J., Wheatcroft, S. B., Yuldasheva, N. Y., Beech, D. J., Carmeliet, P., Kearney, M. T., & Cubbon, R. M. (2021). Endothelial insulin receptors promote vegf-a signaling via erk1/2 and sprouting angiogenesis. *Endocrinology (United States)*, *162*(8). https://doi.org/10.1210/endocr/bqab104

Wang, H., & Hartnett, E. M. (2016). Regulation of signaling events involved in the pathophysiology of neovascular AMD. *Molecular Vision*, *22*, 189–202.

Wang, H., Wang, X., Li, M., Wang, S., Chen, Q., & Lu, S. (2022). Identification of key sex-specific pathways and genes in the subcutaneous adipose tissue from pigs using WGCNA method. *BMC Genomic Data*, *23*(1). https://doi.org/10.1186/s12863-022-01054-w

Wang, J., & Zhang, S. (2020). Fluid shear stress modulates endothelial inflammation by targeting LIMS2. *Experimental Biology and Medicine*, *245*(18), 1656–1663. https://doi.org/10.1177/1535370220943837

Wang, W., & Lo, A. C. Y. (2018). Diabetic retinopathy: Pathophysiology and treatments. In *International Journal of Molecular Sciences* (Vol. 19, Issue 6). MDPI AG. https://doi.org/10.3390/ijms19061816

Wang, X., & Khalil, R. A. (2018). Matrix Metalloproteinases, Vascular Remodeling, and Vascular Disease. In *Advances in Pharmacology* (Vol. 81, pp. 241–330). Academic Press Inc. https://doi.org/10.1016/bs.apha.2017.08.002

Wang, X., Ma, W., Han, S., Meng, Z., Zhao, L., Yin, Y., Wang, Y., & Li, J. (2017). TGF-β participates choroid neovascularization through Smad2/3-VEGF/TNF-α signaling in mice with Laser-induced wet age-related macular degeneration. *Scientific Reports*, *7*(1). https://doi.org/10.1038/s41598-017-10124-4

Watson, E. C., Koenig, M. N., Grant, Z. L., Whitehead, L., Trounson, E., Dewson, G., & Coultas, L. (2016). Apoptosis regulates endothelial cell number and capillary vessel diameter but not vessel regression during retinal angiogenesis. *Development (Cambridge)*, *143*(16), 2973–2982. https://doi.org/10.1242/dev.137513

Weber, C., Fraemohs, L., & Dejana, E. (2007). The role of junctional adhesion molecules in vascular inflammation. In *Nature Reviews Immunology* (Vol. 7, Issue 6, pp. 467–477). https://doi.org/10.1038/nri2096

Wei, G., Srinivasan, R., Cantemir-Stone, C. Z., Sharma, S. M., Santhanam, R., Weinstein, M., Muthusamy, N., Man, A. K., Oshima, R. G., Leone, G., & Ostrowski, M. C. (2009). Ets1 and Ets2 are required for endothelial cell survival during embryonic angiogenesis. *Blood*, *114*(5), 1123–1130. https://doi.org/10.1182/blood-2009-03-211391

Weinstein, N., Mendoza, L., & Álvarez-Buylla, E. R. (2020). A Computational Model of the Endothelial to Mesenchymal Transition. *Frontiers in Genetics*, *11*. https://doi.org/10.3389/fgene.2020.00040

Welch-Reardon, K. M., Ehsan, S. M., Wang, K., Wu, N., Newman, A. C., Romero-Lopez, M., Fong, A. H., George, S. C., Edwards, R. A., & Hughes, C. C. W. (2014). Angiogenic sprouting is regulated by endothelial cell expression of Slug. *Journal of Cell Science*, *127*(9), 2017–2028. https://doi.org/10.1242/jcs.143420

Welch-Reardon, K. M., Wu, N., & Hughes, C. C. W. (2015). A role for partial endothelial-mesenchymal transitions in angiogenesis? *Arteriosclerosis, Thrombosis, and Vascular Biology*, *35*(2), 303–308. https://doi.org/10.1161/ATVBAHA.114.303220

Wessel, F., Winderlich, M., Holm, M., Frye, M., Rivera-Galdos, R., Vockel, M., Linnepe, R., Ipe, U., Stadtmann, A., Zarbock, A., Nottebaum, A. F., & Vestweber, D. (2014). Leukocyte extravasation and vascular permeability are each controlled in vivo by different tyrosine residues of VE-cadherin. *Nature Immunology*, *15*(3), 223–230. https://doi.org/10.1038/ni.2824

Wilhelm, K., Happel, K., Eelen, G., Schoors, S., Oellerich, M. F., Lim, R., Zimmermann, B., Aspalter, I. M., Franco, C. A., Boettger, T., Braun, T., Fruttiger, M., Rajewsky, K., Keller, C., Brüning, J. C., Gerhardt, H., Carmeliet, P., & Potente, M. (2016). FOXO1 couples metabolic activity and growth state in the vascular endothelium. *Nature*, *529*(7585), 216–220. https://doi.org/10.1038/nature16498

Williams, C. K., Li, J., Murga, M., Harris, A. L., & Toasto, G. (2006). Up-regulation of the Notch ligand Delta-like 4 inhibits VEGF-induced endothelial cell function. *Blood*, *107*(3), 931–939.

Wolf, A. T., Harris, A., Oddone, F., Siesky, B., Verticchio Vercellin, A., & Ciulla, T. A. (2022). Disease progression pathways of wet AMD: opportunities for new target discovery. *Expert Opinion on Therapeutic Targets*, *26*(1), 5–12. https://doi.org/10.1080/14728222.2022.2030706

Wong, A. L., Haroon, Z. A., Werner S, Dewhirst, M. W., Greenberg, C. S., & Peters, K. G. (1997). Tie2 Expression and Phosphorylation in Angiogenic and Quiescent Adult Tissues. *Circulation Research*, *81*(4), 567–574.

Wong, W. L., Su, X., Li, X., Cheung, C. M. G., Klein, R., Cheng, C. Y., & Wong, T. Y. (2014). Global prevalence of age-related macular degeneration and disease burden projection for 2020 and 2040: A systematic review and meta-analysis. *The Lancet Global Health*, *2*(2). https://doi.org/10.1016/S2214-109X(13)70145-1

Wu, H. T., Zhong, H. T., Li, G. W., Shen, J. X., Ye, Q. Q., Zhang, M. L., & Liu, J. (2020). Oncogenic functions of the EMT-related transcription factor ZEB1 in breast cancer. In *Journal of Translational Medicine* (Vol. 18, Issue 1). BioMed Central Ltd. https://doi.org/10.1186/s12967-020-02240-z

Wu, W. S., & Lai, F. J. (2015). Functional redundancy of transcription factors explains why most binding targets of a transcription factor are not affected when the transcription factor is knocked out. *BMC Systems Biology*, *9*(6). https://doi.org/10.1186/1752-0509-9-S6-S2

Wynn, T. A., & Vannella, K. M. (2016). Macrophages in Tissue Repair, Regeneration, and Fibrosis. In *Immunity* (Vol. 44, Issue 3, pp. 450–462). Cell Press. https://doi.org/10.1016/j.immuni.2016.02.015

Xie, N., Li, Z., Adesanya, T. M., Guo, W., Liu, Y., Fu, M., Kilic, A., Tan, T., Zhu, H., & Xie, X. (2016). Transplantation of placenta-derived mesenchymal stem cells enhances angiogenesis after ischemic limb injury in mice. *Journal of Cellular and Molecular Medicine*, *20*(1), 29–37. https://doi.org/10.1111/jcmm.12489

Xing, D., Nozell, S., Chen, Y. F., Hage, F., & Oparil, S. (2009). Estrogen and mechanisms of vascular protection. *Arteriosclerosis, Thrombosis, and Vascular Biology*, *29*(3), 289–295. https://doi.org/10.1161/ATVBAHA.108.182279

Xu, J., Zhu, D., Sonoda, S., He, S., Spee, C., Ryan, S. J., & Hinton, D. R. (2012). Over-expression of BMP4 inhibits experimental choroidal neovascularization by modulating VEGF and MMP-9. *Angiogenesis*, *15*(2), 213–227. https://doi.org/10.1007/s10456-012-9254-4

Yan, J., Tie, G., Park, B., Yan, Y., Nowicki, P. T., & Messina, L. M. (2009). Recovery from hind limb ischemia is less effective in type 2 than in type 1 diabetic mice: Roles of endothelial nitric oxide synthase and endothelial progenitor cells. *Journal of Vascular Surgery*, *50*(6), 1412–1422. https://doi.org/10.1016/j.jvs.2009.08.007

Yang, Y., Liu, F., Tang, M., Yuan, M., Hu, A., Zhan, Z., Li, Z., Li, J., Ding, X., & Lu, L. (2016). Macrophage polarization in experimental and clinical choroidal neovascularization. *Scientific Reports*, *6*. https://doi.org/10.1038/srep30933

Yeo, N. J. Y., Chan, E. J. J., & Cheung, C. (2019). Choroidal neovascularization: Mechanisms of endothelial dysfunction. In *Frontiers in Pharmacology* (Vol. 10). Frontiers Media S.A. https://doi.org/10.3389/fphar.2019.01363

You, L., Lin, F., Tee, C. T., DeMayo, F. J., Tsai, M., & Tsai, S. Y. (2005). Suppression of Notch signalling by the COUP-TFII transcription factor regulates vein identity. *Nature*, *435*, 98–104.

Yu, Q. C., Geng, A., Preusch, C. B., Chen, Y., Peng, G., Xu, Y., Jia, Y., Miao, Y., Xue, H., Gao, D., Bao, L., Pan, W., Chen, J., Garcia, K. C., Cheung, T. H., & Zeng, Y. A. (2022). Activation of Wnt/β-catenin signaling by Zeb1 in endothelial progenitors induces vascular quiescence entry. *Cell Reports*, *41*(8). https://doi.org/10.1016/j.celrep.2022.111694

Yuan, L., Le Bras, A., Sacharidou, A., Itagaki, K., Zhan, Y., Kondo, M., Carman, C. V., Davis, G. E., Aird, W. C., & Oettgen, P. (2012). ETS-related gene (ERG) controls endothelial cell permeability via transcriptional regulation of the claudin 5 (CLDN5) gene. *Journal of Biological Chemistry*, *287*(9), 6582–6591. https://doi.org/10.1074/jbc.M111.300236

Zarkada, G., Howard, J. P., Xiao, X., Park, H., Bizou, M., Leclerc, S., Künzel, S. E., Boisseau, B., Li, J., Cagnone, G., Joyal, J. S., Andelfinger, G., Eichmann, A., & Dubrac, A. (2021). Specialized endothelial tip cells guide neuroretina vascularization and blood-retina-barrier formation. *Developmental Cell*, *56*(15), 2237-2251.e6. https://doi.org/10.1016/j.devcel.2021.06.021

Zeisberg, E. M., Potenta, S. E., Sugimoto, H., Zeisberg, M., & Kalluri, R. (2008). Fibroblasts in kidney fibrosis emerge via endothelial-to-mesenchymal transition. *Journal of the American Society of Nephrology*, *19*(12), 2282–2287. https://doi.org/10.1681/ASN.2008050513

Zeisberg, E. M., Potenta, S., Xie, L., Zeisberg, M., & Kalluri, R. (2007). Discovery of endothelial to mesenchymal transition as a source for carcinoma-associated fibroblasts. *Cancer Research*, *67*(21), 10123–10128. https://doi.org/10.1158/0008-5472.CAN-07-3127

Zeisberg, E. M., Tarnavski, O., Zeisberg, M., Dorfman, A. L., McMullen, J. R., Gustafsson, E., Chandraker, A., Yuan, X., Pu, W. T., Roberts, A. B., Neilson, E. G., Sayegh, M. H., Izumo, S., & Kalluri, R. (2007). Endothelial-to-mesenchymal transition contributes to cardiac fibrosis. *Nature Medicine*, *13*(8), 952–961. https://doi.org/10.1038/nm1613

Zeisberg, M., & Neilson, E. G. (2009). Biomarkers for epithelial-mesenchymal transitions. In *Journal of Clinical Investigation* (Vol. 119, Issue 6, pp. 1429–1437). https://doi.org/10.1172/JCI36183

Zhang, J., Lu, T., Lu, S., Ma, S., Han, D., Zhang, K., Xu, C., Liu, S., Gan, L., Wu, X., Yang, F., Wen, W., & Qin, W. (2023). Single-cell analysis of multiple cancer types reveals differences in endothelial cells between tumors and normal tissues. *Computational and Structural Biotechnology Journal*, *21*, 665–676. https://doi.org/10.1016/j.csbj.2022.12.049

Zhang, P., Sun, Y., & Ma, L. (2015). ZEB1: At the crossroads of epithelial-mesenchymal transition, metastasis and therapy resistance. In *Cell Cycle* (Vol. 14, Issue 4, pp. 481–487). Landes Bioscience. https://doi.org/10.1080/15384101.2015.1006048

Zheng, X., Zhang, W., & Hu, X. (2018). Different concentrations of lipopolysaccharide regulate barrier function through the PI3K/Akt signalling pathway in human pulmonary microvascular endothelial cells. *Scientific Reports*, *8*(1). https://doi.org/10.1038/s41598-018-28089-3

Zhou, H., Zhao, X., Yuan, M., & Chen, Y. (2020). Comparison of cytokine levels in the aqueous humor of polypoidal choroidal vasculopathy and neovascular age-related macular degeneration patients. *BMC Ophthalmology*, *20*(1). https://doi.org/10.1186/s12886-019-1278-8

Zhu, P., Huang, L., Ge, X., Yan, F., Wu, R., & Ao, Q. (2006). Transdifferentiation of pulmonary arteriolar endothelial cells into smooth muscle-like cells regulated by myocardin involved in hypoxia-induced pulmonary vascular remodelling. *International Journal of Experimental Pathology*, *87*(6), 463–474. https://doi.org/10.1111/j.1365-2613.2006.00503.x

Zimmermann, K. W. (1923). Der feinere bau der blutcapillaren. *Für Anat. Und Entwickl*, *68*, 29–109.